POLYMERIC NANOSPHERES FOR SKIN PENETRATION ENHANCEMENT: *IN VITRO* AND *IN VIVO* ASSESSMENT IN SKIN MODELS

by

PRIYA B BATHEJA

A Dissertation submitted to the

Graduate School-New Brunswick

Rutgers, The State University of New Jersey

in partial fulfillment of the requirements

for the degree of

Doctor of Philosophy

Graduate Program in Pharmaceutical Sciences

written under the direction of

Professor Bozena Michniak-Kohn, Ph.D.

and approved by

_____

_____

_____

_____

New Brunswick, New Jersey

January 2010

ABSTRACT OF THE DISSERTATION

POLYMERIC NANOSPHERES FOR SKIN PENETRATION ENHANCEMENT: *IN VITRO* AND *IN VIVO* ASSESSMENT IN SKIN MODELS

By PRIYA B BATHEJA

Dissertation Director:

Professor Bozena Michniak-Kohn, Ph.D.

Research and development in the field of topical and transdermal delivery has been particularly challenging due to the tough penetration barrier provided by the stratum corneum, the superficial skin layer. Nano-sized vesicles can potentially act as carriers to skin layers without causing the toxicity and irritation associated with chemical and physical skin penetration enhancers. In this study we have characterized the skin penetration potential of polymeric nanospheres made from amphiphilic ABA-triblock co-polymers that are biocompatible, biodegradable and bind efficiently to hydrophobic molecules. We evaluated the delivery of hydrophobic and poorly water soluble compounds via these nanospheres into different skin layers and found significant enhancement in their delivery to the

epidermal-dermal junction and to the dermis. Thus, these nanospheres have tremendous potential for targeting diseases such as acne, psoriasis and eczema that have their origins in these layers. Formulation of the nanospheres in hydrophilic gels, alone and in combination with a chemical skin penetration enhancer significantly increased the penetration of complexed molecules *in vitro* in human skin and *in vivo* in porcine skin. We also evaluated the delivery profiles of these nanospheres in a bioengineered Human Skin Equivalent (HSE). The full thickness HSE was developed from a combination of human derived cells and extra-cellular components and cultured with a novel media cocktail to strengthen the permeability barrier. The HSE was characterized for the permeability profiles of agents with differing physiochemical properties and was found to be more permeable than human skin, but similar to the commercially available skin equivalent EpidermFT®. The HSE also served as an effective model for evaluation of phototoxicity of topically applied agents, and was able to correctly predict the phototoxic potential of compounds when evaluated against a validated *in vitro* cell-based method. When used for evaluation of the skin delivery potential of nanosphere formulations, the penetration enhancement ratios in the HSE were similar to those obtained in human skin and porcine skin, although the amount and depth of skin penetration of compounds was different. Thus, despite a weaker permeability barrier, the HSE can serve as a reproducible model for pre-screening of the skin delivery properties of formulations.

Acknowledgement

I would like to thank everyone who has inspired me during this exciting journey.

First and foremost, I would like to thank my advisor, Dr. Bozena Michniak-Kohn, who has been a wonderful mentor to me during my graduate study. Dr. Michniak was an excellent teacher, patiently imparting her knowledge while nurturing my curiosity and creativity. Her insight in the field of skin delivery, infectious enthusiasm and continuous support during my graduate study kept me focused and motivated toward achieving my goals. My interactions with Dr. Michniak have played a great role in my professional and personal development over the years and I have come to have high regard for her organizational skills, promptness and her personable nature.

I would also like to thank all members of my thesis advisory committee. Dr. Tamara Minko and Dr. Goufeng You have provided me with expert guidance during classes and during several stages of my research. I have also learned tremendously from Dr. Nava Dayan, with whom I collaborated on various industry projects. My interactions with her have broadened my span of knowledge in various facets of skin delivery. Working with Dr. Dayan has been a great pleasure, especially due to her contagious optimism and her energy.

I express my gratitude to all my colleagues at the Laboratory for Drug Delivery for their inputs during my research and for being very supportive friends. I would also like to thank members of the New Jersey Center for Biomaterials, especially Dr. Joachim Kohn and Dr. Larisa Sheihet, for providing me with the opportunity of working with the polymers synthesized in their laboratory. I also appreciate the support of our dean, Dr. Christopher Molloy, all faculty, students and staff of the Ernest Mario School of Pharmacy and the graduate school at Rutgers University, NJ.

I thank all members of the Pharmaceutical R&D dept. at Novartis Pharmaceuticals where I pursued a summer internship. My experience at Novartis has helped broaden my perspective on the practical aspects of pharmaceutical sciences in the industry.

Most importantly, this thesis would not have been possible without the patience, support and encouragement of my family and friends. I am indebted to my family for their unflagging love and for having faith in me every step of the way. Their confidence in me has imparted me with the resilience I needed to overcome all obstacles during my journey over the years. I am ever grateful to be on the receiving end of their unconditional love and support.

Table of Contents

Abstract of the Dissertation ii

Acknowledgement iv

List of Tables xii

List of Figures xiv

Abbreviations xix

1 Introduction 1

2 Background and Significance 8

2.1 Structure of skin 8

2.2 Epidermis 8

2.3 Dermis 10

2.4 Hypodermis 11

2.5 Skin penetration barrier and routes of permeation 11

2.6 Enhancement of skin permeation: chemical and physical methods 14

2.7 Nanoparticles for enhancement of dermal delivery 15

2.8 Topical formulation development of polymeric nanospheres 18

2.9 Human skin equivalent (HSE) models 21

2.10 Phototoxicity 24

3 Specific Aims 28

4 Preparation and evaluation of tyrosine-derived nanospheres for enhanced topical delivery 32

4.1 Introduction 32

4.2 Materials 34
4.3 Methods 35
4.3.1 Polymer synthesis and characterization 35
4.3.2 Preparation of NSP-compound complexes 35
4.3.3 Characterization of NSP and NSP- compound complexes 36
4.3.4 *In vitro* skin penetration of NR and DAF via NSP 39
4.3.5 Statistical analysis 42
4.4 Results and Discussion 42
4.4.1 Characterization of NSP and NSP-compound complexes 42
4.4.2 HPLC validation of NR and DAF 43
4.4.3 Binding efficiency and release of NR from NSP 44
4.4.4 Skin penetration- 24 h 45
4.4.5 Skin penetration- Time based kinetic experiments 47
4.5 Conclusion 50
5 Formulation development for delivery of polymeric nanospheres to skin layers 52
5.1 Introduction 52
5.2 Materials 56
5.3 Methods 56
5.3.1 Preparation and characterization of nanosphere formulations 56
5.3.2 Gel preparation 57
5.3.3 Content of Diclofenac Sodium (DS) in the hydrophilic gels 58
5.3.4 HPLC methods for determination of DS and NR 58

5.3.5 *In vitro* gel release studies 59
5.3.6 Viscosity of the gels 60
5.3.7 Preparation, characterization and optimization of NSP in gel formulations 60
5.3.8 *In vitro* skin penetration studies 61
5.3.9 *In vivo* skin penetration studies 64
5.3.10 *In vitro* cellular and tissue cytotoxicity 66
5.4 Results and Discussion 68
5.4.1 HPLC validation of DS and NR 68
5.4.2 Morphology and dispersion of NSP in hydrophilic gels 69
5.4.3 Gel content and *in vitro* release of diclofenac sodium from gels 71
5.4.4 Viscosity of the gels 74
5.4.5 *In vitro* skin permeation of NR via NSP-gels 76
5.4.6 *In vivo* skin permeation of NR via NSP-gels 79
5.4.7 Cytotoxicity of NR-NSP formulations and Azone 80
5.5 Conclusion 82
6 Human Skin Equivalent as an *in vitro* model for permeability testing - culture optimization and characterization 85
6.1 Introduction 85
6.2 Materials and Methods 88
6.2.1 Cell Culture 88
6.2.2 Preparation of the Dermal Layer 89
6.2.3 Preparation of the Full Thickness HSE Model 89

6.2.4 Optimization of attachment of the keratinocytes to the dermal matrix 90
6.2.5 Visualization of the Cell Dynamics in the HSE 92
6.2.6 Characterization of HSE - Morphology and Immunohistochemistry 93
6.2.7 Characterization of HSE- *In Vitro* Permeability Studies..... 95
6.2.8 HPLC Methods and Data Analysis 96
6.2.9 Reproducibility of HSE 97
6.2.10 Mechanical testing 97
6.2.11 Statistical Analysis 99
6.3 Results and discussion..... 99
6.3.1 Macroscopic, histological and ultrastructural features of HSE 99
6.3.2 Involucrin localization and protein expression in HSE..... 101
6.3.3 Distribution and Attachment of Cells in the SE Matrix 103
6.3.4 Epidermal–dermal attachment and integrity in the HSE..... 104
6.3.5 Permeability of the HSE to Model Drugs..... 105
6.3.6 Reproducibility of the HSE 110
6.3.7 Evaluation of mechanical strength 110
6.4 Conclusion 111
7 Phototoxicity evaluation of Hydroxycinnamic acid using the *in vitro* 3T3 NRU assay and three-dimensional Human Skin Equivalents..... 114
7.1 Introduction 114
7.2 Materials..... 117

7.3 Methods 118
7.3.1 Phototoxicity evaluation in Balb/c 3T3 fibroblasts (Figure 7.2 (A)) 118
7.3.2 Phototoxicity evaluation using the HSE 122
7.4 Results and Discussion 125
7.4.1 Validation of the irradiation equipment 125
7.4.2 UVA sensitivity of Balb/c 3T3 fibroblasts 126
7.4.3 Phototoxicity evaluation of HCA in Balb/c 3T3 fibroblasts 126
7.4.4 UVA sensitivity and phototoxicity evaluation of CPZ in HSE tissues 128
7.4.5 Phototoxicity evaluation of HCA in HSE tissues 129
7.5 Conclusion 130
8 Application of the Human Skin Equivalent (HSE) for prediction of functional properties of multicomponent formulations 132
8.1 Introduction 132
8.2 Methods 136
8.2.1 Evaluation of barrier properties of SERPACWA in human skin ... 136
8.2.2 Evaluation of barrier properties of SERPACWA in HSE 137
8.2.3 HPLC of paraoxon and data analysis 138
8.2.4 Skin delivery of NR via the Nanosphere formulations in the Human Skin Equivalent model 139
8.2.5 HPLC analysis of Nile Red 141
8.3 Results and discussion 142

8.3.1 Barrier properties of SERPACWA in human skin (Table 15)..... 142
8.3.2 Barrier properties of SERPACWA in the HSE..... 143
8.3.3 Skin delivery of NR via the Nanosphere formulations in the HSE144
8.4 Conclusions..... 146
9 Future work 149
10 Tables..... 151
11 Figures 168
12 Structures..... 229
13 Bibliography..... 237
14 Appendix 248
15 Curriculum Vita..... 260

List of Tables

Table 1: HPLC parameters for Nile Red (NR) and 5-Dodecanoylaminofluorescein (DAF) using the Waters 2695 HPLC system. 151

Table 2: HPLC parameters for Nile Red (NR) and Diclofenac sodium (DS) using the Agilent 1100 system. 152

Table 3: Release rates and cumulative amount of Diclofenac sodium (DS) released from HPMC (HydroxyPropyl Methyl Cellulose) gels. 153

Table 4: *In vitro* skin penetration effect of key NR-NSP formulations..... 154

Table 5: *In vivo* skin penetration effect of key NR-NSP formulations in the domestic pig. 155

Table 6: Lipid composition of Human Skin Equivalent (HSE) treated with 300 μM of clofibrate in conjunction with ascorbic acid (100 μg/ml) and external lipids. . 156

Table 7: Ceramides composition of HSE treated with 300 μM of clofibrate in conjunction with ascorbic acid (100 μg/ml) and external lipids. 157

Table 8: Development and validation of HPLC methods for model compounds used for permeability evaluation of HSE..... 158

Table 9: Permeability parameters of model agents in the dermal matrix of the HSE. 159

Table 10: Permeation parameters for six agents after 24 h *in vitro* permeation experiments with three skin models: HSE, EpidermFT® and Human Skin 160

Table 11: Reproducibility of the HSE with caffeine as a model drug. 161

Table 12: EC_{50} values and Photo-Irritancy Factor (PIF) for Hydroxycinnamic acid (HCA) and Chlorpromazine (CPZ) in the presence (UVA (+)) and absence (UVA (-)) of UVA irradiation – Range Finder 3T3 NRU Experiment. 162

Table 13: EC_{50} values and Photo-Irritancy Factor (PIF) for Hydroxycinnamic acid (HCA) and Chlorpromazine (CPZ) in the presence (UVA (+)) and absence (UVA (-)) of UVA irradiation – Main 3T3 NRU experiment. 163

Table 14: Viability of HSE tissues after treatment with Chlorpromazine (CPZ) and Hydroxycinnamic acid (HCA) in the presence (UVA (+)) and absence (UVA (-)) of UVA irradiation. 164

Table 15: *In vitro* skin penetration (A) and skin accumulation (B) of paraoxon through human cadaver skin after 6 hours of treatment in the presence and absence of SERPACWA and DEET. 165

Table 16: *In vitro* skin penetration (A) and skin accumulation (B) of paraoxon through HSE after 6 hours of treatment in the presence and absence of SERPACWA and DEET. 166

Table 17: Total Penetration Effect (Mean ± S.E.) of NR in the Human Skin Equivalent after treatment with various NR formulations for 24 h. 167

List of Figures

Figure 2.1: Structure of Skin..……168

Figure 2.2: Cross-section of the epidermis depicting the epidermal layers of human skin and the composition of the stratum corneum barrier..……..169

Figure 4.1: Concentration profiles of OMC (Octyl Methoxycinnamate) in porcine stratum corneum following delivery from an emulsion and from poly(ε - caprolactone) nanoparticles……..….170

Figure 4.2: Diagrammatic representation and actual image of a vertical static Franz diffusion cell…….....…171

Figure 4.3: Transmission electron microscopy (TEM) images of Nanospheres (NSP) made from tyrosine based polymers in aqueous solution…….172

Figure 4.4: Size distribution of solute-nanosphere formulations as measured by dynamic light scattering…….....173

Figure 4.5: Release of Nile Red (NR) from tyrosine based polymeric nanospheres…….174

Figure 4.6: Cross-sectional images obtained following 24 h of passive permeation of dyes via NSP through human skin *in vitro*……..175

Figure 4.7: Schematic representation and H&E staining of cryo-sectioned human skin…….....176

Figure 4.8: Cross-sectional images obtained following 1, 3 and 6 h of passive permeation of dyes via NSP through human skin in vitro……..177

Figure 5.1: *In vivo* skin penetration study for evaluation of skin delivery of NSP in the female domestic pig…….....178

Figure 5.2: TEM images of polymeric NSP at various concentrations in hydrophilic gels in the presence and absence of chemical enhancers……179

Figure 5.3: TEM images of HPMC and carbopol gels after negative staining..180

Figure 5.4: TEM and cryo-SEM images of carbopol gels depicting the nature of their network……..181

Figure 5.5: Images of 1% w/v HPMC and carbopol 981 NF gels with Diclofenac sodium (DS) 1% and 2.5% w/v..…….....182

Figure 5.6: Effect of polymer type and drug loading on *in vitro* release of Diclofenac Sodium (DS) from formulations.....183

Figure 5.7: Release of Diclofenac Sodium (DS) from HPMC 1% w/v gel follows Fickian diffusion.....184

Figure 5.8: Release of Diclofenac Sodium (DS) from three concentrations of HPMC gels.....185

Figure 5.9: *In vitro* skin permeation of NR via NSP in HPMC gel and aqueous formulations through human skin.....186

Figure 5.10: Quantitative determination of *in vitro* skin permeation of NR via NSP in HPMC gel and aqueous formulations through human cadaver skin.....187-188

Figure 5.11: *In vivo* skin permeation of NR via NSP in HPMC gel and aqueous formulations.....189

Figure 5.12: Quantitative determination of i*n vivo* skin permeation of NR via NSP in HPMC gel and aqueous formulations in the stratum corneum and epidermis of the domestic pig.....190

Figure 5.13: Cytotoxicity determination of NR formulations in human dermal fibroblasts.....191

Figure 5.14: Cytotoxicity determination of NR formulations in neonatal keratinocytes.....192

Figure 5.15: Scanning Electron Microscopy (SEM) images of skin surface and skin cross-section treated with various aqueous and gel formulations of Nanospheres for 24 h.....193-195

Figure 6.1: Preparation of the Human Skin Equivalent (HSE).....196

Figure 6.2: Schematic representation and images of the inflation device used for mechanical testing of the HSE and EpidermFT® tissues.....197

Figure 6.3: Contraction of dermal layers over 7 days of incubation at 10% CO_2 at 37℃ in a humidified incubator.....198

Figure 6.4: Histology of human skin and of HSE at 7 days after exposure to ALI.....199

Figure 6.5: Vertical (cross-section) and horizontal (looking down from stratum corneum surface) histology of HSE at 21 days after exposure to ALI.....200

Figure 6.6: Involucrin expression in HSE and in human skin.....201

Figure 6.7: Changes in protein expression in HSE after culture at 7 days at ALI and 19 days at ALI detected by 2 D Gel Electrophoresis.....202

Figure 6.8: Dermal layers made with GFP expressing fibroblasts.....203

Figure 6.9: Keratinocytes labeled with 7.5 μM Calcein AM post 3 h of adhesion.....204

Figure 6.10: Attachment of Calcein labeled keratinocytes on protein coated surfaces (analysis by calcein fluorescence).....205

Figure 6.11: Attachment of Calcein labeled keratinocytes on protein coated surfaces (analysis by MTS assay).....206

Figure 6.12: Permeation of caffeine, hydrocortisone and ketoprofen through the full thickness HSE and its dermal component.....207

Figure 6.13: Permeability profiles of agents through HSE-OP, EpidermFT® and Human Skin.....208-210

Figure 7.1: UVA irradiation source for the Phototoxicity experiment.....211

Figure 7.2: Schematic representation of evaluation of phototoxicity potential of agents in fibroblasts and in a skin equivalent model.....212

Figure 7.3: UVA sensitivity of Balb/c 3T3 fibroblasts.....213

Figure 7.4: Dose Response Curves of Hydroxycinnamic Acid (HCA) and Chlorpromazine (CPZ) from the range finder 3T3 NRU assay.....214

Figure 7.5: Neutral Red Extracted from 3T3 fibroblasts after treatment with Chlorpromazine (CPZ) and Hydroxycinnamic Acid (HCA) in the absence and presence of UVA light (Main Experiment).....215

Figure 7.6: Dose Response Curves of Chlorpromazine (CPZ) and Hydroxycinnamic Acid (HCA) from main 3T3 NRU assay.....216

Figure 7.7: Phase contrast images of Balb/c 3T3 cells after treatment with Hydroxycinnamic Acid (HCA) or Chlorpromazine (CPZ) and UVA irradiation...217

Figure 7.8: UVA sensitivity of HSE tissues.....218

Figure 7.9: HSE after 3 h of incubation with MTS reagent post treatment with Chlorpromazine and UVA irradiation. 219

Figure 7.10: Quantitation of HSE viability after 3 h of incubation with MTS reagent post treatment with Chlorpromazine and UVA irradiation.....220

Figure 7.11: Evaluation of Phototoxicity of HCA in the HSE model.....221

Figure 8.1: Transwell® inserts with cultured HSE mounted on vertical Franz diffusion cells (5.1 ml) for evaluating the skin penetration potential of nanosphere formulations.....222

Figure 8.2: Mean cumulative amount (± S.E) of paraoxon permeated per cm^2 of human skin in the presence and absence of SERPACWA.....223

Figure 8.3: Mean cumulative amount (± S.E) of paraoxon permeated per cm^2 of human skin in the presence and absence of SERPACWA and DEET.....224

Figure 8.4: Mean cumulative amount (± S.E) of paraoxon permeated per cm^2 of HSE in the presence and absence of SERPACWA 225

Figure 8.5: Mean cumulative amount (± S.E) of paraoxon permeated per cm^2 of HSE in the presence and absence of SERPACWA and DEET 226

Figure 8.6: *In vitro* skin permeation of NR via NSP in HPMC gel and aqueous formulations through the Human Skin Equivalent.....227

Figure 8.7: Quantitative determination of *in vitro* skin permeation of NR via NSP in HPMC gel and aqueous formulations through the Human Skin Equivalent...228

Abbreviations

TDDS: Transdermal Drug Delivery System/systems

SC: Stratum Corneum

NSP: Nanosphere/Nanospheres

PLGA: Poly (Lactide-Co-Glycolide)

SLN: Solid Lipid Nanoparticle/ Nanoparticles

NLC: Nanostructured Lipid Carrier/Carriers

HPMC: HydroxyPropyl Methyl Cellulose

HSE: Human Skin Equivalent/ Equivalents

SE: Skin Equivalent/ Equivalents

ALI: Air-Liquid Interface

NR: Nile Red

DAF: 5-DodecanoylAminoFluorescein

DS: Diclofenac Sodium

HPLC: High Performance Liquid Chromatography

PBS: Phosphate Buffered Saline

TEM: Transmission Electron Microscopy

SEM: Scanning Electron Microscopy

DLS: Dynamic Light Scattering

RT: Room Temperature

h: hour/hours

mins: minutes

NRU: Neutral Red Uptake

HCA: Hydroxycinnamic acid

CPZ: Chlorpromazine

DEET: N,N-Diethyl-m-toluamide

SERPACWA: Skin Exposure Reduction Paste Against Chemical Warfare Agents

1 Introduction

Transdermal drug delivery systems (TDDS) have offered several clinical advantages over oral drug delivery since their inception more than 25 years ago, and have been gaining momentum in the past decade due to their ability to provide controlled release of molecules, avoidance of first pass metabolism, reduced side effects and increased patient compliance. This has led to the development of several novel delivery devices that utilize the skin as a port for systemic delivery of agents. A report by Adhesives Research, Inc. reveals that since the approval of the first transdermal patch by FDA in 1981, the transdermal delivery systems market has grown into a $2 billion market in USA, with 35 approved products.(1) According to estimates, more than one billion transdermal patches are currently manufactured each year and one transdermal delivery system was approved every 7.5 months in the years 2003-2007. A report by Jain PharmaBiotech estimated the value of the global transdermal delivery market at $12.7 billion in the year 2005 and predicts an increase to $21.5 billion in the year 2010 and $31.5 billion in the year 2015.(2) The successful TDDS target various therapeutic areas such as pain relief (fentanyl), motion sickness (scopolamine), local pain control (lidocaine), contraception (estradiol and its combinations), hypogonadism (testosterone), depression (selegiline), Attention Deficit Hyperactivity Disorder (ADHD) (methylphenidate) and many others.

In addition to transdermal delivery, skin is the site of application of various topical products that aim for localized effects at the site of application or specific delivery to skin layers by virtue of drug penetration through the superficial skin barrier. Topical skin applications can be targeted to various skin diseases such as acne, psoriasis, eczema, melanoma, microbial skin infections or for use in the personal care industry, such as cosmetics, skin care products and sunscreens. Formulations for topical application are multifaceted and can range from aqueous solutions and suspensions to semisolids such as gels, emulsions and ointments, and also solid systems such as powders and patches.

Despite continued research and development efforts, the field of transdermal and targeted epidermal/dermal delivery has been restricted by the rigid skin barrier, contributed primarily by the stratum corneum, the topmost skin layer. The nature of this barrier restricts the skin penetration of most compounds and necessitates the potential candidate to possess certain physiochemical properties, thereby limiting successful product development to about 13 molecules till date. Compounds with moderate lipophilicity (oil-water partition coefficients between 1-3), low melting point (<200 ^{0}C), molecular weight < 500 daltons and high potency (dose < 50 mg/day, preferably <10 mg/day) are favorable molecules for transdermal permeation.(3) The use of chemical and physical enhancement efforts have succeeded in overcoming the skin penetration barrier, but are limited in their scope due to skin irritation and pain potential (chemical and physical enhancers) and the feasibility and cost of development (physical enhancers).

One of the methods of enhancing skin delivery of agents entails the use of vesicle-containing formulations. Vesicles have been used on skin for transdermal drug delivery or for their localizing effects for targeted delivery to the skin. However, the extent of permeation enhancement or targeted delivery provided by vesicles has been a controversial area, with some groups demonstrating that intact vesicles can penetrate skin, while others have disputed this phenomenon. Nevertheless, these carriers possess great potential due to their ability to deliver molecules to skin, thereby overcoming the skin's tough barrier without causing skin irritation. Vesicular structures for skin delivery include lipid based colloidal systems such as conventional liposomes and similar carriers such as ethosomes, niosomes, transfersomes, Solid Lipid Nanoparticles (SLN) or Nanostructured Lipid Carriers (NLC). While lipid based skin delivery systems have been extensively researched, their successful development and commercialization has been limited to a few products such as Pevaryl Lipogel (1% econazole in liposomes, introduced by Cilag A.G. in Switzerland in 1998) and Diractin® (ketoprofen in transfersome carriers, currently in Phase III development by IDEA A.G.). One of the primary concerns about these products has been the interaction of the lipids and the potent surfactants with healthy/diseased skin, their effect on the permeability barrier and resulting toxicity. Apart from safety issues, lack of translation of *in vitro* results into biological responses *in vivo* has stumped further research of these delivery systems. In the recent years, the use of polymeric/biomaterial based carriers for skin delivery has been gaining increasing momentum. A select group of polymers including poly (ε-

caprolactone) and poly (Lactide-co-Glycolide) (PLGA) have been used to prepare nanocarriers with varying chemical compositions and designs that can be used for dermal delivery or for transdermal permeation.

In this study, we hope to create novel formulations containing biodegradable, biocompatible polymeric nanoparticles for effective delivery to specific skin layers without the toxic profiles associated with other vesicular delivery systems or chemical/physical enhancers. These nanoparticles are made from patented tyrosine-based biocompatible amphiphilic ABA-triblock copolymers that self assemble to form dynamic nanospheres (NSP). These NSP form strong complexes with lipophilic agents while retaining their activity. The versatility of the polymeric architecture of these NSP enables effective binding and delivery of a vast array of hydrophobic and poorly water soluble agents.(4) Previous studies have established their lack of toxicity in KB cervical carcinoma cells and after injection in mice.(5) For efficient skin application, skin contact and delivery, these nanoparticles were formulated in hydrophilic gels that provide a stable environment for the polymers and for the encapsulated agents while facilitating their controlled release. The gels will also provide suitable consistency and viscosity for topical application, resulting in maximization of skin contact and increased effectiveness. We have increased the uniqueness of this formulation system by incorporating a chemical skin penetration enhancer, which in combination with the nanospheres can increase the effectiveness and extent of skin delivery. We propose that the gel formulation will provide a stable

environment for co-existence of the nanospheres and the enhancer, while the action of the enhancer on the skin lipids may open up pathways for enhanced nanosphere permeation into skin.

The second phase of our study entails the evaluation of *in vitro* and *in vivo* skin penetration of agents via the nanosphere delivery system. Though we will evaluate the delivery profiles of agents from these carriers in human cadaver skin *in vitro*, human skin specimens obtained from tissue banks are expensive and difficult to procure and have shown to result in large standard deviations in data due to variations between the skin of different donors or different body sites. In order to test our delivery systems in reproducible models, we have developed in our laboratory an *in vitro* bioengineered full thickness Human Skin Equivalent (HSE). Though the penetration barrier of the HSE is not at par with that of human skin *in vivo*, we have optimized the HSE to serve as a reproducible model with morphology and barrier properties that are close to that of human skin, and compare to the leading commercial skin equivalent, EpidermFT® (MatTek, Ashland, MA). In order to characterize and validate the physical and the biochemical properties of the epidermis and the stratum corneum, the most critical part of the penetration barrier, we have evaluated the HSE for three different applications:

(i) as a reproducible model for evaluation of *in vitro* permeability of formulations containing agents with differing physiochemical properties.

(ii) its ability to serve as an effective model for evaluation of phototoxicity, an area of increasing concern for topical and transdermal formulations.

(iii) its ability to serve as a model for evaluation of functional efficacy of multicomponent formulations, such as skin penetration retardants (barrier creams) and skin penetration enhancers (chemical enhancers and nanospheres).

We believe that this study will have major impact on the pharmaceutical and personal care drug delivery sector due to two key achievements:

- The development, optimization and validation of an *in vitro* HSE will provide a reproducible skin model for evaluation of permeability profiles and phototoxicity of topical and transdermal formulations. Supported by further validation with a large library of agents, the HSE can potentially be used for screening various delivery systems.
- The development and validation of the polymeric nanosphere formulations will provide a stable and effective delivery system that can be used to target different skin layers for diseases residing within, such as psoriasis, eczema and acne, without the toxic profiles of currently available skin penetration enhancement methods. This formulation could potentially serve as a dynamic system, where the extent and rate of delivery can be controlled by variation of the formulation components, such as the chemical properties of the triblock co-polymer, the

concentration of nanospheres and the hydrophilic gels, and the amount of the incorporated chemical enhancer.

2 Background and Significance

2.1 Structure of skin

Skin is the largest organ of the body and accounts for 3 to 4 kilograms in weight and 2 sq. m. of the human body. It performs several vital functions such as protection of the body from mechanical, thermal, and environmental impact, regulation of body temperature, prevention of water loss and formation of a crucial barrier to the entry of exogenous elements (such as chemicals, microorganisms and harmful UV and radioactive rays). The skin structure can be divided into three primary layers: the epidermis, dermis and the hypodermis (Figure 2.1), where each layer is composed of elements that contribute to different aspects of skin functions.

2.2 Epidermis

The epidermis consists of four distinct layers: stratum germinativum (or stratum basale), stratum spinosum, stratum granulosum and the stratum corneum (Figure 2.2). Sometimes the lower layers of the stratum corneum are described as a different layer, called stratum lucidum.

Stratum basale, also called as the stratum germinativum, is the metabolically active basal layer of skin, where the keratinocytes undergo cell division by

mitosis. This layer is also connected to the basement membrane or the dermo-epidermal junction by hemidesmosomes that act as anchors for the cells in the basal layer. In addition to the keratinocytes, the basal layer also contains melanocytes (responsible for producing the pigment melanin) and langerhans cells (antigen producing cells). In some areas of the body, such as the lips, the basal layer contains a specialized type of cell, called the Merkel cell that are associated with nerve endings and play a role in cutaneous sensation.

Stratum spinosum (spinous layer or prickle cell layer) rests on top of the basal layer and consist of 2-6 rows of keratinocytes that graduate from columnar to polyhedral cells towards the top layers. The keratinocytes in this layer have prominent nuclei and begin to differentiate and synthesize keratins. The keratins aggregate to form tonofilaments that eventually form desmosomes, special proteins that connect the cell membranes of adjacent keratinocytes.

Stratum granulosum (granular layer) consists of 1-3 layers of increasingly differentiating and flattening cells. The cells contain enzymes that begin degradation of the viable components such as nuclei and organelles and begin to acquire granular structures. Keratohyalin granules and membrane coating granules are synthesized and eventually extruded into intercellular spaces as cells approach the upper layers. These lamellar granules are precursors for the intercellular lipid lamellae.

Stratum lucidum is a transitionary layer where the cell nucleus disintegrates and cells undergo increased keratinization and flattening.

Stratum corneum (horny layer) is the topmost layer of the skin and the final product of epidermal differentiation. It is around 10 to 14 µm thick and consists of 10 to 15 layers of flattened, dead and anucleated cells called corneocytes. These corneocytes contain keratin and are intercalated with SC lipids, forming the 'brick (corneocytes) and mortar (lipids)' model that forms the primary barrier to skin penetration (Figure 2.2).

2.3 Dermis

The dermis lies below the epidermis, is about 3-5 mm thick and is composed of connective tissues (primarily collagen fibrils that provide support) and elastic tissue (provide strength and flexibility) that are embedded in a mucopolysaccharide gel. It contains numerous fibroblasts and is supplied with a network of blood and lymphatic vessels, nerve endings and various appendages. The primary appendages that lie in the dermis are the pilosebaceous units (hair follicles and sebaceous glands) and sweat glands (eccrine and apocrine glands). While this layer provides little barrier against hydrophilic drugs, it significantly restricts the passage of lipophilic molecules.

2.4 Hypodermis

The hypodermis or subcutaneous fat layer lies below the dermis and connects it to the underlying tissues. It is usually several millimeters thick and is composed of adipose tissue, which serves to insulate the body and provide mechanical protection against shock.

2.5 Skin penetration barrier and routes of permeation

The skin's permeability barrier is localized in the Stratum Corneum (SC), where the 'brick and mortar' structure of the corneocytes and the intercellular lipids provide tough resistance to the passage of molecules. This barrier depends on the unique and critical SC contents; protein (75-80%), lipids (5-15%) and other unidentified components (5-10%) (calculated on a dry weight basis).(6, 7) The 'bricks' of the SC are made of flattened corneocytes that contain insoluble protein (mostly keratin and filaggrin) and are connected by corneodesmosomes. These proteinaceous corneocytes are surrounded by the cornified cell envelope (CE), a tough protein-lipid structure formed just below the cytoplasmic membrane of the cells.(8) The CE consists of two parts: a protein envelope and a lipid envelope. The protein envelope contributes to the biomechanical properties of the CE and consists of specialized cross-linked structural proteins (such as involucrin, loricrin, trichohyalin). The protein envelope is surrounded by a covalently bound lipid envelope that also interdigitates with the intercellular lipid lamellae surrounding the corneocytes and serve as scaffolds for these lipid lamellae.

The primary contribution to the permeability barrier in the SC is provided by the combination of SC lipids, unique in its composition due to the lack of phospholipids, present in most other biological membranes. The SC lipids consist of ceramides (41%), cholesterol (27%), free fatty acids (9%), cholesteryl ester (10%), and cholesterol sulfate (2%).(9) The intercellular lipids are formed during the differentiation process of keratinocytes and are eventually stacked as highly organized crystalline lipid lamellae that are aligned parallel to the surface of the SC and form a continuous lipid phase. Thus, the presence of proteinaceous corneocytes, the rigid corneocyte envelope and the hydrophobic matrix consisting of the non-polar lipids surrounding the corneocytes form a highly resistant barrier to permeation of compounds.

Drugs that permeate skin can traverse skin layers through one or a combination of three pathways: the transcellular pathway (across the corneocytes and the lipid matrix), the intercellular pathway (through the lipid domains between the corneocytes) or the shunt pathway (via skin appendages). Because the skin appendages occupy only about 0.1-1% of the skin surface, the contribution of this pathway to skin penetration is limited. The permeation of most compounds through skin is thought to occur via the intercellular pathway, though very hydrophilic compounds can permeate through both the intercellular and the transcellular route.

The diffusion of a permeant through skin is a passive kinetic process along a concentration gradient and is commonly described by Fick's first law. The steady state flux of a compound through skin is given by:

$$J_{ss} = \frac{DKCv}{h} \qquad \text{(Equation 1)}$$

where J_{ss} (µg/cm^2/h) is the steady state flux, D (cm^2/h) is the diffusion coefficient, Cv is the concentration gradient of the permeant between the vehicle and the receiver side, K is the partition coefficient of the permeant between the stratum corneum and the vehicle, h (cm) is the diffusional path length.

Equation 1 can be further modified to define the permeability coefficient of a compound through skin, given as:

$$K_p = \frac{DK}{h} \qquad \text{(Equation 2)}$$

$$\text{Thus, } J_{ss} = K_p.Cv \qquad \text{(Equation 3)}$$

Where K_p (cm/h) is the permeability coefficient of the permeant in the stratum corneum.

2.6 Enhancement of skin permeation: chemical and physical methods

In order to overcome the skin penetration barrier and enhance permeation, a number of chemical and physical enhancement techniques have been developed either alone or in combination. Chemical enhancers have been widely studied over the years and they work to increase the drug flux by one or a combination of the following mechanisms: i) disruption of the lipid structure in the stratum corneum, ii) opening up the dense protein structure in the corneocytes or iii) altering the chemical environment in the stratum corneum, thereby increasing the partitioning of a second active agent into skin.(10) However, the type and amount of chemical enhancers that can be used in transdermal applications is restricted by their skin irritation potential.(11) In fact, most chemical enhancers have been found to be cytotoxic at various concentrations, and only a few classes of enhancers, like Terpenes, have been classified as Generally Regarded As Safe (GRAS) by the Food and Drug Administration (FDA).(12) Physical enhancement methods constitute electrically assisted methods (iontophoresis, electroporation), mechanical methods (microneedles), velocity-based techniques such as jet-propulsion, or other methods such as ultrasound, laser and photomechanical waves. (13) Limitations of physical enhancement devices include their bulkiness, cost of the dosage form and their potential to cause pain and irritation.

2.7 Nanoparticles for enhancement of dermal delivery

Vesicular systems have been extensively researched over the years for their potential for topical and transdermal delivery of compounds. Their use in transdermal delivery has been limited due to inadequate data about penetration of intact vesicles through all skin layers and the subsequent systemic delivery of compounds. However, they have demonstrated moderate success for their localizing effects in skin layers. Different types of vesicles that have been studied over the years are liposomes (lipid based vesicles that can range typically from 0.02 to 10 µm in diameter and enclose an aqueous phase),(14) transfersomes (ultradeformable liposomes made from phospholipids, water and a surface edge activator),(15) ethosomes (made from phospholipids, water and a high concentration (20-40%) of ethanol)(16) and niosomes (non-ionic surfactant vesicles formed from amphiphiles and aqueous solvents and sometimes excipients such as cholesterol).(17) In the last decade, a significant amount of research has been conducted in the development and evaluation of nano-size carriers for dermal delivery. These include Solid Lipid Nanoparticles (SLN),(18) Nanostructured Lipid Carriers (NLC),(19) nanocapsules(20) and polymeric nanoparticles.(21) SLN and NLC have gained increased popularity over the years and currently are being actively researched by more than 20 groups.(22) SLN range from 40 to 1000 nm in size and are composed of 0.1% (w/w) to 30% (w/w) lipids that are solid at Room Temperature (RT) and body temperature, dispersed in an aqueous medium, and may be stabilized with a surfactant 0.5% (w/w) to 5% (w/w). NLC contain a blend of solid and liquid lipids in ratios from

70:30 upto 99.9:0.1, where the final blend is solid at body temperature. SLN and NLC have been evaluated for their application in pharmaceuticals and cosmetics, such as sunscreens and topical Vitamin A formulations.(22) These carriers have predominantly been used to target the upper skin layers and have been postulated to deposit the encapsulated agents in the upper layers by fusion of their lipid components with skin lipids and by way of occlusion.(23)

Polymeric nanoparticles on the other hand have been shown to transport the drug to deeper skin layers and also deliver the drug transdermally.(21) Polymeric nanoparticles for skin delivery have been prepared in the past from poly (ε-caprolactone),(24) polystyrene,(25) Poly(Lactide-co-Glycolide) (PLGA,)(26) hyaluronan,(27) chitosan(28) and a combination of chitosan and poly-gamma-glutamic acid (gamma-PGA).(29) Based on the great potential of nanocarriers for dermal drug delivery and the market growth for topical and transdermal delivery systems, we decided to investigate the potential of nanospheres made from tyrosine derived polymers for drug delivery to skin. These nanospheres are made from patented tyrosine derived amphiphilic ABA block co-polymers that consist of hydrophilic A blocks of poly(ethylene glycol) and hydrophobic B-blocks of desaminotyrosyl-tyrosine alkyl esters (DTR) and diacids.(30) This group of biomaterials constitutes a library of triblock copolymers that possess great versatility in their architecture, such that variations in the chemical composition of the blocks and the pendant chain “R”, molecular weight, block length ratio and polarity lead to subsets of polymers with varying drug binding abilities and

cellular behavior. At low critical aggregation concentrations, these polymers self-assemble in aqueous solutions to form nanospheres with hydrodynamic diameters between 40 and 70 nm that are stable systems and do not dissociate even under chromatographic and ultracentrifugation conditions. Previous studies have characterized the nanospheres to be biocompatible, biodegradable and non toxic to KB human carcinoma cells.(4) In addition, these polymeric nanospheres have been shown to form strong complexes with hydrophobic molecules such as paclitaxel in a manner that ensures good binding affinity as well as efficient drug delivery. Generally, the skin penetration of very lipophilic molecules is restricted to the stratum corneum and the upper epidermis, where the molecules stay trapped in the lipid domains and are not able to traverse into the more hydrophilic dermis. The ability of the nanospheres to bind and release lipophilic agents makes them advantageous for dermal delivery as they can act as carriers for these agents to the deeper skin layers, such as the upper and lower dermal regions. Also, the high lipophilicity of these molecules hinders their formulation in aqueous vehicles and necessitates the use of harsher solvent systems that may be irritating or toxic to skin. We propose that the size, dynamic structure and their binding capacity to hydrophobic molecules will enable these nanocarriers to overcome the skin penetration barrier and lead to enhanced delivery of lipophilic and poorly water soluble molecules to deeper skin layers, where several diseases such as psoriasis, acne and eczema originate.

2.8 Topical formulation development of polymeric nanospheres

Topical drug delivery systems constitute formulations that are applied to skin to treat cutaneous disorders, where the delivery of drug is intended to be confined to the surface of the skin or within the skin in its various layers. Topical delivery systems increase the effectiveness of the drug as they provide localized delivery, resulting in decrease in the required dose and in systemic side effects. While topical delivery systems are widely used for delivery of drugs, the personal care industry (sunscreens, cosmetics, etc.) also contributes significantly to this market. Most commonly used topical formulations are gels, ointments, creams, lotions (emulsions and suspensions), sprays, foams, medicated powders and medicated adhesive systems. Topical drug delivery systems should serve to optimize the delivery of the agent to specific areas and increase the efficacy of the drug, while providing an inert environment that is non toxic to skin. Also, they are required to produce zero or minimal transdermal permeation of the molecule to avoid any systemic side effects. In addition, the formulations have to be physically and chemically stable and aesthetically acceptable. Also, topical formulations are required to work in completely uncontrolled environments post skin application as they are exposed to evaporation, running-off and physical changes that occur during the patient's routine activities.

It has been established that the formulation components and the vehicle used in skin delivery systems have a distinctive effect on the dermal delivery of active ingredients. Gels are one of the most commonly used delivery systems for topical formulations and are also used widely as drug reservoirs in transdermal drug

delivery systems (patches).(31, 32) One of the principal advantages of gels is their ability to quickly rub into the skin and to provide an extended time of contact for the agent with the skin. The flow properties and the spreadability of the gels can be easily altered to achieve the desired contact time with skin. Gels formulated for drug delivery to skin can also provide controlled release of the agent, since the release of drugs from gels is a factor of their concentration and the resulting viscosity. Though gels have been traditionally used for formulating drugs and personal care agents, they have also been researched over the recent years for their ability to serve as an effective formulation for polymeric/non-polymeric drug carriers such as liposomes, microemulsions and nanoparticles. Most studies in this area have evaluated different types of hydrogels, which are three-dimensional, hydrophilic, polymeric networks capable of imbibing and retaining large amounts of water or biological fluids while remaining insoluble in aqueous solutions and retaining their shapes. Hydrogel networks are composed of homopolymers or copolymers, and are insoluble due to the presence of chemical or physical cross-links which provide the network structure and physical integrity. These hydrogels exhibit a thermodynamic compatibility with water which allows them to swell in aqueous media and absorb and retain a large amount of water. Hydrogels exhibit many unique physicochemical properties that make them advantageous for biomedical applications including drug delivery. They are also are excellent candidates for encapsulating biomacromolecules including proteins and peptides due to their aqueous environment and their lack of hydrophobic interactions which can denature these fragile species. (33) Also, the

conditions for fabricating hydrogels are relatively mild, with gel formation occurring at ambient temperature and moderate use of organic solvents. Besides clinical advantages, hydrogels have also been well received aesthetically as they form clear to semi-opaque gels.

We believe that simple hydrophilic gels will provide effective, inert and aesthetic vehicles for formulating the polymeric nanospheres. The formulation of these nanocarriers in gels will provide uniform and stable dispersions of these carriers and will increase the contact time of these carriers with the skin, thereby increasing the efficacy of skin penetration. Also, many hydrophilic gels can facilitate the development of multicomponent formulations, such as a combination of a skin penetration enhancer and the nanospheres. The presence of a skin penetration enhancer in the gel formulation can manipulate the skin lipids and open up pathways to facilitate the penetration of the nanospheres and thereby lead to enhanced delivery of the complexed agent. In addition, the use of a carrier and a penetration enhancer can result in usage of lower non-toxic doses of the chemical enhancer. Also, variation in the amount of enhancers in the combined formulation can serve to manipulate the extent or depth of skin penetration of these nanospheres. The final formulation will thereby consist of a hydrophilic gel containing nanocarriers and a chemical enhancer that can deliver the drugs to a desired site/depth in skin.

Various polymers, natural, semi-synthetic and synthetic, have been used in formulation of topical gels of which HPMC (HydroxyPropyl Methyl cellulose) and carbopols (carbomers) have been most extensively investigated. These polymers have been used for thickening, gelling, modification of viscosity, consistency and for gel stabilization. We will investigate both these polymers for their ability to serve as an optimal formulation for skin delivery of the nanospheres.

2.9 Human skin equivalent (HSE) models

One of the primary factors in development of transdermal and topical drug delivery systems is the assessment of the percutaneous absorption and skin deposition of the agents from transdermal/topical formulations and devices. Traditionally, excised human cadaver or animal skin from rat, hairless mouse, guinea pig, snake and others has been used extensively for permeability testing of formulations.(34) Though the data collected from human skin studies would most reflect *in vivo* performance, its advantages are offset by high data variability between skin tissues obtained from different donors or different sites of the body, increasing difficulties in procurement and high cost. Animal skin is easily procured as compared to human skin, but differs from human skin in terms of the morphological characteristics, water content and the lipid composition of the stratum corneum, which is essential to the maintenance of the skin's barrier properties.(35) The need for a suitable model for permeability testing has necessitated the development and evaluation of several tissue-cultured *in vitro*

skin models, frequently known as bioengineered skin substitutes or Skin Equivalents (SE). SE have been developed and researched over the past years for various applications, mainly as skin replacements in burns or wounds,(36, 37) for skin biology research,(38) for cutaneous irritation and toxicity testing,(39, 40) and as models for permeability testing of agents and formulations.(39, 41) These skin substitutes are cultured in a controlled environment, thus increasing reproducibility and reducing scope for larger standard deviations normally encountered with human skin data. Today, reconstructed models are commercially available and have a well defined architecture and lipid composition but are more frequently being used for irritation and toxicity testing(42) and to a lesser extent for evaluation of cutaneous absorption. This application is nevertheless being increasingly evaluated in recent years and has received a boost due to the acceptance of SE models by the OECD guidelines 431 for corrosivity testing,(43) while the test procedure for cutaneous absorption based on reconstructed models is still open for discussion and subject to the equivalence of the permeability data obtained from the SE to that obtained with human skin. Because the unique combination of skin barrier lipids is formed as a result of the keratinocyte differentiation process, the normalization of the epidermal differentiation process and the subsequent accumulation of lipids are crucial to the formation of permeability barrier in the reconstructed skin models. Though the synthesis of intercellular lipids *in vitro* and their subsequent organization into lipid lamellae have been established in the skin models, and the intercorneocyte route has been confirmed as the main route of permeation,(44)

the lipid content and profile of SE differ from that of human SC and has been suggested as the cause of the weaker permeability barrier.(45) The permeability of tested SE in literature has been found to be several fold higher to various tested compounds when compared to human skin.(46, 47) However, alterations of culture conditions of the SE, especially the culture media constitution can lead to alterations in the differentiation process and the lipid profiles of the SE. We have cultured in our laboratory a Human Skin Equivalent (HSE) and have attempted to create an *in vitro* skin model with barrier properties that resemble that of human skin *in vivo*. In order to create a model for *in vitro* permeability testing, we decided to focus our efforts on the epidermal permeability barrier and hence designed a system with a matrix consisting of human-derived skin cells and collagen. This mixture of dermal fibroblasts, collagen and epidermal keratinocytes would result in a model that would be close to human skin at a physiological or cellular level. In order to create a strong permeability barrier, we cultured the HSE with a unique mixture of media constituents, the combination of which has not been described elsewhere in literature to date (to our knowledge). Each of these media constituents, ascorbic acid, external fatty acids and a PPAR-α agonist, has been shown to individually contribute to the normalization of the epidermal differentiation process. We hypothesize that culture with a combination of these constituents will lead to generation of the required proportion of barrier lipids and development of a strong permeability barrier in the HSE.

2.10 Phototoxicity

Phototoxicity is defined as a response from a substance applied to the body which is either elicited or increased (mostly at lower dose levels) after subsequent exposure to UV light or that is induced by skin irradiation after systemic administration of a substance (OECD guidelines 432 for testing of chemicals).(48) Phototoxicity occurs due to a combined effect of a substance and UV light and is capable of producing adverse effects on skin that resemble exaggerated 'sunburns' on areas exposed to light. More severe phototoxic reactions can lead to acute erythema, edema, blistering, hyperpigmentation and over chronic periods, photocarcinogenicity. Use of phototoxic compounds in everyday 'innocuous' products such as topical formulations or personal care products can lead to undesirable adverse effects. Many chemicals have been shown to absorb light energy in the UV range and thus are all potentially phototoxic. Several of these are extensively used drugs such as quinolone antibiotics (ciprofloxacin), tetracyclines, NSAIDs (Non Steroidal Anti-Inflamatory Drugs), diuretics (bumetanide), antifungals, oral contraceptives, retinoids, and also personal care agents such as sunscreens and fragrances. Absorption of light energy by these molecules results in the formation of free radicals, which eventually bind to cellular proteins and DNA and result in cell damage and phototoxic reactions.

Evaluation of *in vitro* phototoxicity has received tremendous attention in recent years due to the emergence of *in vitro* cell-based tests as substitutes for animal

testing for personal care products. The replacement of animal testing was initiated by the EU (European Union) as part of the EU Directive (86/609/EEC) (1986) for protection of animals used for experimental and other scientific purposes. They encouraged the use of the 3 **R**s:

– Refinement (decrease in the incidence or severity of procedures on animals)

– **R**eduction (decrease in the number of animals used to obtain information for a given amount of precision)

– Replacement (the substitution of conscious living vertebrates by other models)

To develop and coordinate the validation of alternative test methods at the European Union level, the EU set up a special center called ECVAM (European Centre for the Validation of Alternative Methods, established in 1991). In addition, the EU and Colipa (the European Cosmetics, Toiletry and Perfumery Association) announced bans on animal testing in the context of the Cosmetics Directive (76/768/ECC) with target dates of 2009 and 2013 for various endpoints for phasing out animal testing for cosmetic ingredients and finished products. The recent emergence of REACH (Registration, Evaluation, Authorization, and Restriction of CHemicals), an EU regulation, has further boosted the development of *in vitro* alternative methods for safety testing of chemicals. REACH requires that safety information must be provided on all chemicals that are either sold, manufactured or imported into the EU in a quantity greater than or equal to one ton per year. This has been estimated to affect at least 30,000 chemicals that belong to a vast array of industries, including pharmaceuticals and personal care. Since some of the primary aims of REACH are to improve the

protection of human health and the environment from the risks that can be posed by chemicals, the REACH regulation has mandated that *in vitro* alternatives be used to replace animal testing whenever possible.

Since phototoxicity has been rapidly evolving as a required test for many topically applied compounds, several alternative *in vitro* methods have been researched for its evaluation. The EU in collaboration with COLIPA and ZEBET (Germany) has chosen the *in vitro* ***3T3 NRU*** (Neutral Red Uptake) test as a standard method for phototoxicity evaluation and has validated the test on Balb/c 3T3 fibroblasts. This method is now widely recommended as the primary method of choice for phototoxicity testing.(49) However, the monolayer culture of fibroblasts provides a simple and basic system as compared to *in vitro* skin equivalents, which have a 3-dimensional matrix, a better representation of skin *in vivo*. Due to this reason, 3-dimensional SE have also been evaluated over the years as models for phototoxicity evaluation. Using SE for phototoxicity can also account for the bioavailability of chemicals after passing through the skin barrier and the metabolism of compounds in skin. In addition, SE provide a better alternative for testing compounds that are insoluble/sparingly soluble in aqueous media and also for finished formulations (creams, perfumes, sunscreens) which cannot be evaluated by the 3T3 NRU assay. Some of the SE models that have been used for phototoxicity evaluation are Epiderm® (MatTek, Ashland, MA), SkinEthic® (SkinEthic laboratories, France) and Episkin® (L'Oreal, France). The Epiderm® model is currently being evaluated for the phototoxicity assay by the EU

Validation Centre, ECVAM. Though all skin models that have been evaluated for phototoxicity are 'epidermis only' models, we predict that our full thickness collagen based Human Skin Equivalent (HSE) will also serve as a suitable model for phototoxicity evaluation. Therefore we decided to evaluate our HSE for phototoxicity testing of a topical formulation and compare its performance with results obtained with the validated method, 3T3 NRU testing in mouse fibroblasts.

3 Specific Aims

The objective of this study is to create an effective and stable nanosphere formulation for delivery of hydrophobic and poorly soluble compounds to specific skin layers. These nanoparticles are made from tyrosine based polymers that are biocompatible, biodegradable and have shown to bind effectively to lipophilic molecules. Also, they have been shown to be non-toxic *in vitro* in KB cell lines and after injection in mice. We hypothesize that these nano-sized carriers will permeate the skin due to their small size and dynamic architecture and lead to enhanced dermal delivery of poorly water soluble molecules with high lipophilicity, that are usually difficult to formulate and deliver through skin. In addition, the nanospheres will also serve as a safe and non-toxic method of skin penetration enhancement when compared to the many adverse effects associated with current chemical and physical enhancement methods, such as pain, irritation and high cellular cytotoxicity.

We will evaluate the nanosphere delivery system *in vitro* in human cadaver skin, in a Human Skin Equivalent (HSE) and *in vivo* in domestic pigs. The HSE is an *in vitro* tissue engineered skin model that will be cultured from start to finish in our laboratory under optimized conditions for generation of a penetration barrier that resembles native human skin. This HSE will be validated for its morphology, biochemical properties and barrier properties to several compounds and also its potential for phototoxicity evaluation. This model will then be compared to human skin and the leading commercially available full thickness skin equivalent. The HSE can then be used as a consistent and reproducible model for permeability

testing, providing more reliable data and lesser deviations than obtained by using human skin as a model.

The Specific Aims of the study are:

1. Development and characterization of triblock ABA co-polymer nanospheres for delivery to skin layers.

The synthesis of the polymer and its chemical characterization will be conducted at the NJ Center for Biomaterials, Rutgers University, NJ. The characterization of the nanospheres will involve assessment of their morphology and size distribution by Transmission Electron Microscopy and Dynamic Light Scattering respectively. Their potential for skin penetration enhancement will be evaluated *in vitro* in human skin by studying the depth and extent of skin penetration of fluorescent lipophilic compounds bound to the nanospheres.

2. Development and characterization of a suitable formulation for skin delivery of agents via nanospheres.

Two types of hydrophilic gels, HPMC and Carbopol 981NF in different concentrations will be evaluated for their drug release and viscosity profiles. The gel with high solute release and an optimal viscosity for topical/transdermal application will be used for nanosphere dispersion and the final formulation will be characterized and evaluated for the skin delivery efficiency of nanospheres *in vitro* in human skin and *in vivo* in a domestic pig. In addition, a combined

formulation of the nanospheres and the chemical penetration enhancer Azone in the hydrophilic gels will be evaluated for enhancement in skin delivery.

3. Development and characterization of a bioengineered full thickness Human Skin Equivalent (HSE).

The dermal matrix of the HSE will be made from an optimized mixture of dermal fibroblasts and type I collagen. A full thickness differentiated HSE will then be cultured after proliferation and differentiation of keratinocytes on the dermal matrix. The viability, attachment and proliferation of the cells inside the matrix and at the dermal-epidermal junction will be studied by using fluorescently labeled cells during culture. Throughout culture at the Air-Liquid Interface, the HSE will be cultured in strictly controlled conditions with media containing combinations of various growth additives that will serve to normalize the differentiation process and improve the generation of essential lipids and the resulting permeability barrier. The final HSE will then be evaluated for its morphology, immunohistochemistry, permeability properties and mechanical strength.

4. Validation of the HSE as an *in vitro* skin model for evaluation of the permeability of agents and formulations.

The permeability profiles of six agents differing in their physiochemical properties through the HSE will be evaluated with the aid of *in vitro* diffusion setups and compared to human skin and the leading commercial full thickness skin

equivalent EpidermFT®. In addition, the reproducibility of the HSE for permeability studies will be assessed.

5. *In vitro* phototoxicity evaluation of a personal care agent Hydroxycinnamic Acid (HCA) in cell lines and in the HSE.

The Balb/c 3T3 mouse fibroblast cell lines will be used for evaluation of the phototoxicity of HCA, an antioxidant and skin brightening agent, using the NRU (Neutral Red Uptake) assay. The cells will be exposed to HCA in the presence and absence of UVA light, and the difference in viability will be assessed by their capacity to take up a vital dye Neutral Red. Subsequently, the HSE will be evaluated for its ability to evaluate the phototoxic potential of HCA and compared to the results from the 3T3 NRU assay.

6. Evaluation of the HSE as a model for assessment of the skin permeation of multicomponent formulations.

The skin delivery potential of the polymeric nanospheres and the functional properties of the barrier cream SERPACWA (Skin Exposure Reduction Paste to Chemical Warfare Agents) will be assessed in the HSE model. The enhancement and retardation effects of these formulations in the HSE will be compared to similar data obtained from experiments in human skin.

4 Preparation and evaluation of tyrosine-derived nanospheres for enhanced topical delivery

Published in: International Journal of Pharmaceutics 350 (2008), p:312–319.

Patent: Kohn, J., Michniak, B., Devore, D., Sheihet, L., Chandra, P., **Batheja, P.,** "Controlled release of actives in skin" (US Patent Application No. 60/887,553)

4.1 Introduction

Vesicular based skin delivery systems can enhance the dermal and transdermal penetration of compounds without the toxic profiles and irritation/pain potential of chemical and physical enhancers. Nano-sized vesicular systems have been well researched in the past years, especially for specific delivery to the superficial or deeper skin layers. Most of these delivery systems have consisted of lipid derived materials such as Solid Lipid Nanoparticles and Nanostructured Lipid Carriers. A few polymeric nanocarriers have also been evaluated for dermal delivery and have been fabricated from commonly used polymers such as poly (Lactide-co-Glycolide), poly (ε-caprolactone), chitosan and others. Nanoparticles made from poly (ε-caprolactone) were found to result in a 3.4 fold increase in the deposition of the encapsulated lipophilic agent octyl methoxycinnamate in the stratum corneum and deeper epidermal layers as compared to an equivalent emulsion (Figure 4.1).(25)

We hypothesize that polymeric nanospheres made from patented tyrosine based triblock co-polymers that are synthesized at the New Jersey Center for Biomaterials (Rutgers University, Piscataway, NJ) can serve as potential carriers for delivery of hydrophobic compounds to skin layers. These amphiphilic triblock co-polymers consist of hydrophilic blocks of poly (ethylene glycol) and hydrophobic blocks of desaminotyrosyl-tyrosine alkyl esters (DTR) and diacids. The general chemical structure of the tyrosine-based triblock co-polymer is illustrated in Structure 1. For dermal delivery studies, we chose ABA-triblock co-polymers that consist of hydrophilic A-blocks of PEG (Mw=5000) and hydrophobic B-blocks of desaminotyrosyl-tyrosine octyl esters (where R = octyl) and suberic acid. These co-polymers self-assemble in aqueous solution to form very stable amphiphilic nanospheres that do not dissociate under chromatographic and ultracentrifugation conditions. Drug binding studies have shown that these nanospheres bind preferentially and strongly to hydrophobic molecules.(4) If the nanospheres can overcome the rigid SC barrier, they can act as effective carriers for hydrophobic and poorly water soluble molecules, the delivery of which is usually restricted to the upper layers of skin, and eventually transport them to deeper skin layers. Thus, they have great potential to serve as biocompatible and biodegradable skin penetration enhancers without any irritation and sensitivity.

In order to visualize the skin penetration effects of these nanospheres and elucidate their mechanism, we created complexes of the nanospheres with lipophilic and fluorescent dyes, Nile Red (NR) and 5-dodecanoylaminofluorescein

(DAF) and determined their binding efficiency. The morphology and size distribution of the nanospheres and the nanosphere-dye complexes were determined using Transmission Electron Microscopy and Dynamic Light Scattering. After studying the release of dyes from the nanospheres, the *in vitro* skin penetration of the dyes via the nanospheres were determined with the aid of Franz diffusion cells and cryosectioning techniques. For the purpose of convenience, nanospheres will be abbreviated as NSP through this and the following chapters.

4.2 Materials

Suberic acid, propylene glycol (PG), poly(ethylene glycol) monomethyl ether (Mw 5000) and Dulbecco's phosphate buffered saline (PBS, pH 7.4) were purchased from Aldrich Chemical Co. (Milwaukee, WI). Methylene chloride (HPLC grade), methanol (HPLC grade), 2-propanol and optimal cutting temperature compound (OCT) were purchased from Fisher Scientific, (Pittsburgh, PA). Diisopropylcarbodiimide (DIPC) was purchased from Tanabe Chemicals (San Diego, CA). *N,N*-dimethylformamide (DMF) and tetrahydrofuran (THF) were obtained from Merck (EM Science, Darmstadt, Germany) and dimethyl sulfoxide (DMSO) was obtained from Sigma. 5-Dodecanoylaminofluorescein (DAF) and Nile Red (NR) were obtained from Molecular Probes (Eugene, OR).

4.3 Methods

4.3.1 Polymer synthesis and characterization

Synthesis of the triblock co-polymer was conducted in a one-pot reaction at 20˚C using *in situ* carbodiimide coupling of the poly(ethylene glycol) monomethyl ether, PEG, and oligo (DTO-SA). ^{1}H NMR (*d*6-DMSO, Varian Unity 300 spectrophotometer, Palo Alto, CA) was used to confirm the chemical structure and purity of the copolymer. The molecular weight and the molecular number (Mn and Mw) were determined using gel permeation chromatography (PL-gel columns, pore size 10^5 and 10^4 A°, Perkin-Elmer, Shelton, CT; Waters 410 RI detector) using THF at a flow rate of 1 ml/min. Polystyrene was used as standards for Mw markers.

4.3.2 Preparation of NSP-compound complexes

NSP were made with and without complexation with the model compounds NR and DAF. NSP-compound complexes were prepared by combining 60 mg of triblock copolymer with 600 µg of either DAF or NR in 600 µl of DMF followed by drop wise additions of these solutions to 14.4 ml of deionized water with constant stirring. This led to formation of turbid aqueous dispersions containing self assembled NSP that were purified by a series of steps. First, the NSP-solute suspensions were filtered through 0.22 µm PVDF syringe filters (Millipore, Bedford, MA) in order to remove particles greater than 220 nm in diameter. The

purified NSP were then isolated by ultracentrifugation at 65,000 rpm (290,000×*g*) for 3 h at 25°C (Beckman L8-70M ultracentrifuge, Beckman Coulter, Fullerton, CA). After removal of the supernatant, the pelleted NSP were washed twice with PBS, and re-suspended with gentle agitation in 1 ml of PBS at 25°C, which was later increased to 3 ml and filter-sterilized through 0.22 µm filters.

4.3.3 Characterization of NSP and NSP- compound complexes

4.3.3.1 Morphology and size distribution

The morphology of NSP was determined using Transmission Electron Microscopy (TEM). TEM is a microscopy technique that transmits a beam of electrons through an ultra thin specimen. The electrons interact with the specimen as they pass through, and the image formed as a result of this interaction is magnified and focused onto an imaging device, such as a fluorescent screen, a photographic film, or a CCD camera. In order to obtain contrast between the sample and the surroundings, the preparation is negatively stained, usually with heavy metal salts. The high atomic weight of metals deflects electrons and gives the area surrounding the specimen increased electron opacity while the specimen itself remains more translucent. For negative staining of the polymeric NSP, a drop of the NSP dispersion was allowed to settle on a Formvar/Carbon pre-coated grid for 1 min. The excess sample was removed by gentle blotting with filter paper followed by addition of a drop of staining solution

(2% uranyl acetate) for 1 min. Then, the excess stain was removed carefully with a filter paper. For the Pt/C shadow method experiments, a drop of NSP was applied onto a copper Formvar/Carbon coated grid for 1 min, and the excess fluid was removed by gently blotting the grid with a piece of filter paper. The grids were air-dried and shadowed with 2.5 nm Pt/C (30°C) using High Vacuum Freeze-Etch unit BAF 300 (Balzers, Elgin, IL). Electron micrographs were taken on a model JEM 100CX Transmission Electron Microscope (JEOL LTD, Peabody, MA).

The hydrodynamic diameter of the nanospheres was obtained using Dynamic Light Scattering (DLS) at q=90◦, λ = 523 nm and T = 298K using cumulant fit analysis (Lexel argon ion laser, Fremont, CA; Brookhaven Instruments goniometer and correlator BI-2030; Holtsville, NY). DLS is used to measure the size distribution of small particles in colloidal solutions. If the particles are small compared to the incident wavelength (< 250 nm), the light scatters in all directions (Rayleigh scattering). The particles in solution, due to their small size undergo Brownian motion, with the distance between them constantly changing over time. This time-dependent fluctuation in the scattering intensity can be observed with the aid of a monochromatic light source such as a laser, which undergoes constructive or destructive interference by the surrounding particles and is captured at the detector plane. The resulting information is used to calculate the hydrodynamic radius of the particles.

4.3.3.2 Binding efficiency of nanospheres

To determine the binding efficiency of nanospheres, a predetermined aliquot of the purified NSP-dye complex was freeze-dried and the dry residue was accurately weighed. The amount of dye in this aliquot was determined by extraction with methanol (for NR) and ethanol (for DAF) for 1 h by shaking. The dye amount was detected by sensitive and validated HPLC methods. The binding efficiency was calculated by the ratio:

Binding efficiency (%) = mass of dye in the nanospheres/ mass of initial dye used.

An equivalent concentration of all dyes in propylene glycol (PG) was prepared for use as controls during the experiments.

4.3.3.3 HPLC methods for NR and DAF

The dye concentrations were determined using High Performance Liquid Chromatography (HPLC) assays using a Waters 2695 HPLC system equipped with UV–Vis detector (Waters 2487, Dual I Absorbance Detector) and a RP-C18 column (Perkin- Elmer Brownlee Analytical C-18 column, 33mm×4.6 mm). The mobile phase was a mixture of water (0.1% TFA)/acetonitrile (0.1% TFA) with the ratio of 35/65 (v/v) for DAF and 40/60 (v/v) for NR. The detection wavelengths were 550 and 270 nm for NR and DAF respectively. The methods were validated on the system and the linearity of the calibration curve, the intra- and inter-day precision and accuracy and the lower limits of detection were evaluated.

4.3.3.4 Release of NR from NSP

Release of NR from NSP was measured with the aid of dialysis cassettes. The Slide-A-Lyzer Dialysis Cassette (10,000 MWCO; 0.5 – 3 ml Capacity, Pierce, Rockford, IL) were hydrated in PBS before use for 1-2 minutes. 2 ml of purified NSP–NR complex (40 µg of NR/ml of preparation) was injected into dialysis cassettes (n=3) with the aid of a needle and syringe. The cassette was then immersed in 150 ml of 0.1 M PBS (pH 7.4) with 0.1 w/v % Tween 80, maintained at 37˚C with gentle agitation. Samples (20 ml) were withdrawn at pre-determined time points and replaced with fresh media. All withdrawn samples were then lyophilized, and the NR was extracted in 1 ml of methanol and the content analyzed by HPLC after filtration through 0.45 µm filters.

4.3.4 *In vitro* skin penetration of NR and DAF via NSP

4.3.4.1 Preparation of human skin

Split thickness human skin dermatomed to (~500 µm) derived from the abdominal regions of female Caucasian cadavers was obtained from AlloSource (Englewood, CO) and stored at -80^0C. Just before each experiment, the skin was thawed at room temperature and used immediately in studies. For all *in vitro* studies, the thawed skin was cut into small pieces of equal size (approximately 1 sq. inch area) and used for the diffusion experiments. The skin from the same donor was used for test and control experiments for each formulation.

4.3.4.2 Skin penetration studies

Skin transport of the dyes via NSP was determined using vertical Franz diffusion cells (Figure 4.2) (PermeGear, Bethlehem, PA). Pieces of dermatomed human skin were mounted on the diffusion cells (cell volume: 5.1 ml, diffusion area: 0.64 cm^2) and clamped between the receptor and the donor compartments. The skin was hydrated for 1 h with the receptor fluid (Phosphate Buffered Saline, PBS, pH 7.4) which was maintained at 37^0C and constantly stirred at 600 rpm. 300 µl of the NSP-dye formulations (NR or DAF) were added on top of the skin in the donor compartments and allowed to remain for 24 h or for 1, 3, 6 h in case of NR time-dependency permeation experiments. The donor compartments and the sampling ports of the cells were covered with Parafilm® and the set up was covered with aluminum foil to prevent bleaching of the dyes.

The following formulations were evaluated:

- NSP-dye complexes
- Equivalent amounts of dye in PG
- NSP alone
- PBS alone

The no. of replicates were n=6 for the 24 h experiments or n=4 for the time-based permeation experiments.

At the end of the permeation experiment, the excess formulation was removed from the skin surface, the skin sections were removed from the diffusion cells,

washed three times with PBS, and dried gently with Kimwipes®. The skin pieces were then frozen on dry ice and 0.2 cm × 0.5 cm pieces were cut out from the from the central treated area. The cut skin pieces were then embedded in optimal cutting temperature compound (OCT) and skin cross sections (20 µm thickness) were obtained with the aid of a cryostat (Leica Cryostat CM 3050S, Wetzlar, Germany). The cross sections (about nine to twelve for every sample) were then stored at 4^0C until analysis by fluorescence microscopy.

For evaluation of transdermal permeation, samples from the receptor solutions were taken at the end of each experiment, lyophilized overnight and the amount of dye in the sample was extracted by shaking with methanol/ethanol for 1 h followed by evaluation of dye content by HPLC analysis.

4.3.4.3 Fluorescence microscopy

The skin sections were analyzed by both fluorescent and phase-contrast microscopy using an Olympus CK40 microscope equipped with a UV source and filters for fluorescent measurement. The amount of NR and DAF in different skin layers were evaluated at excitation and emission wavelengths of 546 and 585 nm for NR and 485 and 520 nm for DAF, respectively. The same parameters were used for imaging all samples and skin auto fluorescence was taken into account. An Olympus Microsuite TM B35V program was used for Image capture and analysis. Quantitation of the fluorescence was conducted using the Image J software, (v1.36, NIH) (50) and the integration of pixel brightness in arbitrary

units (ABU) was translated to the relative dye content. Each selected image was a representative image chosen from an average of 30–40 replicates of skin sections. For determination of the relative presence of dyes in skin layers, the layers of human skin were identified and demarcated by Hematoxylin and Eosin (H&E) staining (Figure 4.7).

4.3.5 Statistical analysis

Data was analyzed using ANOVA and expressed as the mean value ± S.E. (standard error of mean); $p < 0.05$ was considered to be statistically significant.

4.4 Results and Discussion

4.4.1 Characterization of NSP and NSP-compound complexes

The co-polymers used for making the NSP were found to possess narrow molecular weight distributions centered around 25 kDA. The NSP demonstrated a spherical morphology and were found to be uniformly dispersed in the TEM studies (Figure 4.3). The spherical morphology of the NSP may be due to the low glass transition temperature (Tg =294 K) of the middle block consisting of oligo (DTO suberate), which confers upon the polymer an ability to be flexible and to self-assemble into a dynamic and non-frozen structure.

The NSP demonstrated a relatively narrow size distribution centered around 55 nm, obtained by DLS. The binding of the nanospheres with the dyes of differing hydrophobicities (NR and DAF) did not create changes in the morphology or the size distribution of the NSP-dye complexes, as seen in the size distribution chart in Figure 4.4. However, from the TEM images, their size distribution appears to be ranging from 30 to 200 nm in diameter, larger than observed by DLS. We suspect that this is most probably an artifact that occurred due to drying of the specimens prior to electron microscopy (leading to morphological changes and changes in size). The small nano-scale size and the flexible and dynamic nature of these vesicles are the primary properties of these NSP that will enable them to penetrate skin layers and enhance the delivery of agents.

4.4.2 HPLC validation of NR and DAF

The HPLC validation parameters for NR and DAF are reported in Table 1. HPLC detection methods for both compounds were highly reproducible with good inter and intra-day precision (better than 10%). The HPLC methods for these fluorophores were also validated in the presence of the pure polymer, NSP and processing variables such as drug lyophilization. No peak interference or shifts were observed and drug recovery was high (> 85 %). Linearity of the calibration curves with and without the presence of NSP was >0.99.

4.4.3 Binding efficiency and release of NR from NSP

The binding efficiency of NSP to NR was found to be ~ 65%, with similar results obtained with the other model compound, DAF. However, in order to exert a physiological action in the skin, the NSP should act as carriers and be able to release the bound compounds within skin layers. The release pattern of the lipophilic dye NR from NSP was determined using dialysis cassettes with a molecular weight cut off of 10,000, to allow transmembrane diffusion of all the unassociated NR (MW=318.4), but not of the polymer (MW=25,000 daltons). The release profiles of the NSP over 24 h and 66 h are shown in Figure 4.5. The detection of NR at time zero indicates no lag time for release and a possible burst release phenomenon. About 5% of NR was released during the initial burst release, followed by ~45 % release in 24 h and ~67% release in 66 h. The burst release of NR can be associated with the superficially bound drug molecules that may be associated with the NSP corona or the interface between the corona and the NSP core and may be released easily due to gentle agitation. The remaining drug was released at a fast rate for the first 24 h and at a sustained rate for the remaining time. The relatively fast rate of drug release may be a factor of the low *T*g of the hydrophobic core in the copolymer, which has been shown to be indicative of a dynamic polymeric matrix that enables easy diffusion of small molecules.(51) The more sustained release after 24 h may be due to tightly bound molecules in the matrix or the decrease in the concentration gradient of NR.

4.4.4 Skin penetration- 24 h

In order to evaluate the ability of the NSP to enhance topical or transdermal penetration, the skin penetration of the dyes NR and DAF via the NSP were compared to the penetration of the dyes from the corresponding solutions in PG. We chose PG as a control for this study based on its ability to act as a strong solvent for the lipophilic dyes, its neutral nature and also previous use in various studies of similar nature.(25) The role of PG itself in skin penetration is widely debated, with some groups proclaiming it to be a mild enhancer, (52) while others state that it retards the skin penetration of compounds.(53) However, we believe that the effect of PG depends on the drug in question and its effect on the thermodynamic properties of the formulation. In this study, we believe that PG serves the role of a suitable solvent for the lipophilic dyes without irritating the skin or significantly altering its barrier properties.

HPLC analysis of the receptor solutions from below the skin samples treated with the NSP-dye complexes or the dye solutions in PG for 24 h showed an absence of the dyes in all samples indicating lack of transdermal permeation of these molecules through human skin. It may also be possible that the amount of penetrated dyes was negligible and below the limit of detection by HPLC. The lack of transdermal permeation has also been observed with other polymeric nanoparticles in published reports, where encapsulation of agents in poly(ε-caprolactone) nanoparticles increased the residence time in the stratum corneum, but did not facilitate transdermal permeation.(25)

The vertical cross-section images of skin treated with NSP only or with PBS showed negligible auto fluorescence, which was nevertheless accounted for during the process of imaging. The 24 h application of the dyes NR and DAF in polymeric NSP to skin showed a clear and significant increase in the skin penetration of both these dyes as compared to their respective controls in PG. Figure 4.6 demonstrates the representative skin sections treated with NR and DAF bound to NSP, where the NSP appear to have significantly enhanced the penetration of these dyes in the epidermis and the deeper skin layers (dermis). It is apparent that the dyes in PG are predominantly present on the surface and the superficial skin layers, with very little penetration into deeper skin layers. On the other hand, when NR and DAF were complexed with NSP, their concentration on the skin surface and superficial skin layers was minimal, but the dyes showed higher and more uniform distribution in the epidermis and the superficial and lower dermis. Quantitative analysis of dye penetration was obtained with the aid of Image J software by evaluation of the pixel intensities derived from fluorescence intensity measurements of the skin sections. The fluorescence intensities of DAF and NR in different skin layers are expressed in arbitrary units (ABU) as Penetration Effect (P.E) ± S.E. (Figures 4.6, (E and F)). The skin section was divided into three regions for quantitative fluorescence analysis using the H&E stained skin sections (Figure 4.7) as reference; the stratum corneum and the viable epidermis (~115 µm), the superficial dermis (SD, the region measuring ~ 100 µm below the viable epidermis) and the lower dermis (LD, the remaining portion of the skin below the superficial dermis, measuring ~

350 µm). The fluorescence intensity in the superficial dermis of skin samples treated with NSP-DAF complexes (Figure 4.6, B) was 2 times higher than for PG-DAF formulations (Figure 4.6, A), while that of NSP-NR complexes (Figure 4.6, D) was 10 times higher than PG-NR formulations (Figure 4.6, C) ($p<0.05$). Similarly in the lower dermis, the distribution of dyes delivered via NSP resulted in about 2.5-fold and 9-fold increase ($p < 0.05$) for DAF and NR, respectively. For NR, the amount of dye deposited in the superficial dermis via the NSP was significantly higher than that in the lower dermis, while this difference was less significant with DAF.

4.4.5 Skin penetration- Time based kinetic experiments

Because NR demonstrated a more significant effect, qualitatively and quantitatively, in the 24 h skin permeation experiments, we chose this dye to study the time based skin penetration profile via NSP. The penetration kinetics of NR delivered via NSP and PG are represented in Figure 4.8. Qualitative observations of the skin cross-sections show an increased time based skin penetration of the dye when delivered via NSP. A significant difference ($p < 0.05$) in the fluorescence intensity was detected in all skin layers after 1 h of exposure to NSP-NR complexes (Figure 4.8, B-1), as compared to PG-NR (Figure 4.8, A-1). The resulting P.E. values in the superficial dermis were 6.5±0.2 and 9.5±0.3 for PG-NR and NSP-NR, respectively (Figure 4.8, C). This difference was more significant in the lower dermis, with P.E values of 7.6±0.4 for PG-NR and

13.6±1.2 for NSP-NR (Figure 4.8, D). Thus, penetration of NR via NSP into lower dermis was faster and about 45% higher than the control formulation in PG. Also, the fluorescent intensity of NR at 3 h (from NR-NSP) increased by about 70% (SD) and 67% (LD) from the 1 h time point. The difference in intensity between the 3 h and 1 h penetration of NR from the corresponding solution in PG was not significant.

At 6 h of treatment, there was a further increase in NR penetration via both nanospheres and PG, but the enhancement due to NSP (Figure 4.8, B-6) was about 45% higher as compared to PG (Figure 4.8, A-6). The time based increase in dye permeation via NSP at 6h was more significant in the SD (40% increase from 3 h) as compared to the LD (7% increase from 3 h). This may be due to a decrease in the concentration gradient due to significant deposition of dye in the LD at 3 h. These results show that the NSP can potentially accumulate an agent in the upper or superficial dermis strata by serving as carriers for agents and by-passing the tough SC penetration barrier.

The greater extent of skin penetration of NSP-dye formulations can be attributed primarily to the nano-scale size of the vesicle, their dynamic and flexible structure or a synergy of both. Various nano-sized carriers, such as solid lipid nanoparticles are postulated to improve skin penetration due to their small size.(54) Also, the presence of surfactants in polymeric vesicles, such as Transfersomes®, have shown to confer upon it a degree of deformability that can enable the vesicles to squeeze through water channels in the SC and result in enhanced skin delivery of the encapsulated agent.(55) Similarly, we believe that

our NSP, owing to their small size (~55 nm) and the dynamic structure of NSP-dye complexes, may traverse through the transepidermal hydrophilic pathways (water evaporation pathways that are in the order of 0.4 nm), the intercorneocyte spaces (100 nm) or the intercluster pathway that may be a result of structural irregularities within the intercellular lipid lamellae.(56, 57) A critical contribution to increased penetration by the NSP may be provided by the polymer composition, specially the presence of PEG in the nanosphere corona, which could lead to superior hydration of the skin, a phenomenon commonly known to enhance skin permeation of compounds. Also, in line with thermodynamic principles, these polymeric vesicles may be considered as a supersaturated system of an agent, thus possessing higher thermodynamic activity than the respected solutions in PG and thereby increasing skin partitioning. In addition, the amphiphilic nature of the polymer may also be an important factor in the skin penetration of these NSP and may be specially be responsible for their ability to target the superficial dermis. We know that lipophilic agents can traverse the skin through the paracellular route by partitioning into skin lipids of the SC but have limited diffusion into the more hydrophilic epidermis and dermis. The ability of the NSP to surpass the SC barrier is further complemented by its hydrophilic corona which may enable it to reach and target the hydrophilic dermis. Thus the NSP can serve as excellent carriers for highly lipophilic and poorly water soluble drugs that may not otherwise reach and accumulate in the dermis.

4.5 Conclusion

The tyrosine-derived NSP were shown to significantly enhance skin penetration of lipophilic model compounds (DAF and Nile Red) in human cadaver skin as compared to the respective solution of the dyes in PG. Although no transdermal permeation of these dyes was detected, these carriers enhanced the delivery of the agents to all skin layers, especially the superficial dermis, where the dyes accumulated. These systems thus have tremendous potential for targeting the delivery of drugs to specific skin layers, such as the dermo-epidermal junction which is the site of occurrence of prominent diseases such as psoriasis, and the superficial dermis. Also, these NSP would be ideal as delivery systems for topical administration of lipophilic agents, such as retinoids, other Vitamin A derivates, Vitamin D, personal care agents (sunscreens) or steroids (glucocorticoids). The lack of transdermal delivery by these NSP can actually be an advantage in topical delivery where systemic absorption could present toxicity concerns.

The permeation enhancement effects of these NSP can further be increased by delivering them as a formulation that will encourage their prolonged contact with skin and prevent the formulation 'run-off' experienced with the aqueous dispersion. A significant advantage of these biocompatible NSP over other methods of skin penetration enhancement is their potential lack of toxicity, which will be evaluated and compared to a commonly researched chemical enhancer. The next chapter focuses on the creation of a stable and effective formulation for these NSP that will increase their effectiveness and subsequent skin delivery.

Note: *The authors would sincerely like to thank Prof. Joachim Kohn and Dr. Larisa Sheihet from the NJ Center for Biomaterials, NJ for their expert guidance, discussions, synthesis of the tyrosine based polymers and assistance with the nanospheres.*

5 Formulation development for delivery of polymeric nanospheres to skin layers

5.1 Introduction

Tyrosine-derived nanospheres composed of amphiphilic ABA-triblock co-polymers are biodegradable and biocompatible carriers that have been shown to efficiently encapsulate lipophilic compounds.(4) These NSP have hydrodynamic diameters between 40 and 70 nm and were shown to significantly enhance skin penetration of highly lipophilic model compounds (DAF and Nile Red) in human cadaver skin (chapter 4).(58) Aqueous NSP formulations were shown to deliver 9 and 2.5 times more Nile Red (NR) and DAF (5-dodecanoylaminofluorescein) respectively to the lower dermis of human skin than respective control formulations in propylene glycol (PG). While the NSP themselves enhanced skin permeation of these lipophilic agents, these carriers may function even more effectively when used in combination with a chemical penetration enhancer. It is known that the primary mechanism of chemical enhancers involves the manipulation and fluidization of skin barrier lipids. This alteration of the skin lipids can open up pathways in the skin layers for better penetration of the nanocarriers and subsequent delivery of the associated compound. Thus, we decided to create a novel combination formulation of the nanospheres and the potent skin penetration enhancer Azone (1-dodecylazacycloheptan-2-one, laurocapram).

When formulated as aqueous suspensions, the NSP can stay in contact with skin only when they are confined to the donor compartment of diffusion cells used for *in vitro* permeation testing. However, these suspensions may 'run-off' when applied as a formulation *in vivo* on animals or for future use in humans, leading to insufficient contact time and inaccurate dosing thereby decreasing the effectiveness of skin delivery. We postulated that a dispersion of NSP in hydrophilic gels will produce a uniform and stable formulation with an adequate viscosity and consistency to maximize skin contact time and hence delivery to deeper skin layers. Similar gel dispersions of vesicles such as nanocapsules,(20, 24) liposomes,(59) solid lipid nanoparticles(60) and microemulsions(61) have been explored in recent years.

Gels have been used extensively in topical and transdermal delivery and can be used to develop stable formulations with suitable viscosity for topical application and good aesthetic appeal. The viscosity, release rates and spreadability of gels are usually a fraction of their concentration and drug loading, which can be easily altered to provide controlled release of the agent to the skin. We chose hydrophilic gels because they provide stable and inert environments and the conditions for their fabrication are relatively mild. These gels can also accommodate added ingredients or excipients, such as chemical skin penetration enhancers, for development of multicomponent formulations.

We hypothesize that an optimal dispersion of our polymeric NSP in a gel will provide a stable and uniform formulation with a suitable viscosity for topical or

transdermal application. Hence, we created novel gel formulations consisting of a combination of the polymeric NSP and the skin penetration enhancer Azone dispersed in hydrophilic gels. We are basing the effectiveness of these unique gel formulations on two probable phenomenons:

1) The gels, due to their inert environment will provide a stable environment and a uniform dispersion for the polymeric NSP. Higher viscosity of the gels will improve the contact of the NSP with skin, thus facilitating their permeation into skin and hence their effectiveness of skin delivery. The consistency of the gels will also aid in the application of the formulation to skin.
2) Due to its lipophilicity, Azone (structure 7) is insoluble in water and separates out in aqueous formulations. However, it may form a uniform dispersion in a gel made in the solvent base of PG:Water. The dispersion of Azone in the gel network may control its release and reduce the skin irritation caused by it, at the same time creating channels in skin for easier penetration of NSP.

We decided to evaluate two types of gels for NSP dispersion: cellulose derivatives and carbopols (carbomers), both commonly used in topical and transdermal formulations and shown to form stable gels. HydroxyPropyl MethylCellulose (HPMC), a semi-synthethic cellulose derivative, is a non-ionic, hydrophilic polymer used as an emulsifier, thickening agent, stabilizer, gelling and suspending agent. It is often preferred over other cellulose derivatives due to

its ability to form clear gels and its compatibility with salts and preservatives such as parabens.(62) The polymeric structure of HPMC is depicted in structure 4. Carbopols (structure 5) are carboxyvinyl polymers (synthetic high molecular weight polymers of acrylic acid) that are cross-linked with either allyl sucrose (divinyl glycol) or allyl ethers of pentaerythritol (polyalkenyl ethers). When dispersed in water, the tightly coiled carbopol powders hydrate and uncoil partially exposing the acidic groups. These acidic molecules are then neutralized by addition of an amine (triethanolamine) or an inorganic base (sodium hydroxide). The neutralization ionizes the polymer, generates negative charges along the backbone leading to electrostatic repulsion and formation of a three dimensional structure (structure 6).

In order to choose a suitable formulation for NSP dispersion, we evaluated different concentrations of these polymers for their solute-release rates and viscosity profiles. Diclofenac Sodium (DS, structure 8) was chosen as the drug for these studies due to its lipophilicity (log P=4.7, log D=1.2, ACD labs software), lower cost and easy availability. The morphology and dispersion uniformity of the NSP in the gels were evaluated by TEM. The final gel formulation was then used to prepare the NSP-Nile Red dispersion and the *in vitro* and *in vivo* skin permeation was determined and compared to aqueous NSP formulations.

5.2 Materials

Propylene glycol (PG) was purchased from Aldrich Chemical Co. (Milwaukee, WI). Methanol, acetonitrile and water (all HPLC grade) and optimal cutting temperature compound (OCT) were purchased from Fisher Scientific. Dimethyl sulfoxide (DMSO), Phosphate Buffered Saline (PBS, pH 7.4) and Diclofenac Sodium were obtained from Sigma (St. Louis, MO). Nile Red (NR) was obtained from Molecular Probes (Eugene, OR). Carbopol 981 NF was obtained from Lubrizol (Ohio, USA) and HPMC (METHOCEL™ K15M Premium CR Grade) was obtained from Colorcon, (West Point, PA).

5.3 Methods

5.3.1 Preparation and characterization of nanosphere formulations

Triblock co-polymer NSP were prepared from ABA triblock co-polymer that was synthesized in a one-pot reaction at 20°C using *in situ* carbodiimide coupling of the poly(ethylene glycol) monomethyl ether, PEG, and oligo(DTO-SA) as described before in Chapter 4. ^{1}H NMR was used to confirm the chemical structure and purity, and the molecular weights (Mn and Mw) were determined using gel permeation chromatography, GPC (PL-gel columns, pore size 10^5 and 10^4 A° , Perkin-Elmer, Shelton, CT; Waters 410 RI detector). NSP alone were prepared by dissolving 120 mg of polymer in 1 ml of DMF and adding this solution drop-wise to 28.8 ml of PBS with constant stirring. NR loaded NSP were

prepared by combining 240 mg of polymer in 1.6 ml of DMF with 2.4 mg of NR in 0.8 ml of DMF and then adding this solution drop-wise to 57.6 ml of PBS with constant stirring. The drop-wise addition of polymer solutions to PBS resulted in formation of turbid dispersions containing self assembled nanospheres, which were purified by filtering through 0.22 µm PVDF syringe filters (Millipore, Bedford, MA) and isolated by ultracentrifugation at 65,000 rpm (290,000×*g*) for 3 h at 25˚C (Beckman L8-70M ultracentrifuge, Beckman Coulter, Fullerton, CA). After removal of the supernatant, the NSP pellet was washed twice with PBS, and re-suspended with gentle agitation in PBS. Finally, the solutions were filter-sterilized (0.22 µm) and used for preparing subsequent formulations or alone in studies.

5.3.2 Gel preparation

The gels were prepared with either diclofenac sodium (for determination of optimum polymer type, concentration and viscosity) or with NR (for evaluation of the extent of delivery to skin layers by fluorescence quantitation).

HPMC gels were made by adding the polymer to a solution of drug/dye in PG:Water (80:20 v/v) and stirring the mixture with a magnetic stirrer until complete gel formation. Thereafter, the gel was allowed to stabilize at room temperature for 48 h before being used for any studies. Carbopol 981 NF gels were prepared by adding the required amount of polymer to solutions of the drug/dye in a mixture of PG:Water (80:20 v/v) while constantly stirring with the aid of a mixer until gel formation. The gel was allowed to stand on the lab bench

for 24 h, and subsequently neutralized by drop-wise addition of triethanolamine (pH 7.0). The final preparation was allowed to stabilize at room temperature for 48 h before being used for any studies.

When the enhancer Azone was incorporated in the hydrogels, NR and Azone 0.2 M were dissolved separately in mixtures of PG:Water (80:20 v/v). After the two solutions were combined, HPMC was added and mixed slowly at room temperature until gel formation.

5.3.3 Content of Diclofenac Sodium (DS) in the hydrophilic gels

For analysis of gel content and the stability of DS in the gel, ~ 1 g of the HPMC gels containing DS was weighed in volumetric flasks and the amount of DS was extracted by shaking overnight with 100 ml of methanol. An aliquot was then filtered through 0.45 µm PFTE filters and the amount of DS was determined by HPLC analysis. The experiment was conducted in triplicate.

5.3.4 HPLC methods for determination of DS and NR

An Agilent 1100 system (Agilent Technologies, USA) was used for the HPLC detection of DS and NR in samples. Samples were run through an Agilent C18 RP column (Eclipse XDB-C18, 4.6 X 150 mm, 5µm) (Agilent Technologies, USA) with mobile phase constitutions of water: acetonitrile (40: 60 v/v) for NR and methanol:water (0.1% TFA) (80:20 v/v) for DS. The flow rate and detection wavelength for NR and DS were 1.75 ml/min, 550 nm and 1ml/min, 280 nm

respectively. Both methods were validated for linearity of the calibration curves, limits of detection and intra- and inter-day variability. All parameters are reported in Table 2. The drug peaks were also calibrated in the presence of pure triblock polymer, polymeric nanospheres, HPMC and carbopol 981 NF to ensure the lack of interference from these components and to evaluate any possible interactions.

5.3.5 *In vitro* gel release studies

Release of DS from HPMC and carbopol 981 NF gels was measured using regenerated cellulose membranes (MWCO: 10,000 Dalton, Spectrum Laboratories, USA). After washing and equilibration with PBS, the membranes were mounted on static vertical Franz diffusion cells (receptor volume 5.1ml, permeation area 0.64 cm^2) by clamping them between the donor and receptor compartments. The receptor compartments were filled with isotonic PBS (pH 7.4) which was maintained at 37 ± 0.5 °C and constantly stirred at 600 rpm. 0.5 ml of the prepared formulations (n=3) were added to the donor compartment with a graduated 1 ml syringe and the donor and the sampling ports were covered with Parafilm® to prevent any external interference. Samples were collected from the receptor fluid at pre-determined time points and replaced with an equivalent amount of buffer. The drug content in samples was analyzed by HPLC. Initially, release studies were conducted with similar polymer concentrations of carbopol and HPMC gels with the same drug loading, in order to determine the differences in their release characteristics. Thereafter, three different concentrations of the

chosen gel formulation were evaluated for *in vitro* release in order to determine the optimum polymer concentration for drug release.

5.3.6 Viscosity of the gels

In order to characterize the rheological characteristics of the gel formulations, we measured the viscosity of the gels using a Bohlin Gemini HR nano Rheometer (Bob and Cup type Rheometer, Malvern Instruments, Malvern, Worcestershire, UK). Steady shear measurements were conducted at 25^0C using a controlled rate mode with increasing shear rates that represent typical pharmaceutical operations such as pouring from a bottle and spreading of the formulation on skin(63). The resulting viscosity (Pa.s) was analyzed using a Bohlin Instruments Gemini Advanced software system.

5.3.7 Preparation, characterization and optimization of NSP in gel formulations

NSP with and without NR were dispersed in the gels after they had been allowed to stabilize at room temperature for 48 h, to achieve a final concentration (HPMC or carbopol) of 1 % w/v. The NSP-gel dispersions were mixed slowly for 4 h in order to obtain a uniform dispersion and subsequently allowed to stabilize at room temperature for 24 h.

The content of NR in the NSP-NR-gel formulation was determined by measuring accurately ~ 1 g of the nanosphere-gel formulation and extracting the NR by

shaking with 100 ml of methanol in a volumetric flask overnight. An aliquot was then filtered through 0.45 µm PFTE filters and the amount of NR was determined by HPLC analysis.

The morphology, size and uniformity of dispersion of the nanospheres in the gel formulation were characterized by Transmission Electron Microscopy (TEM), as per procedure described earlier in chapter 4. Briefly, Formvar pre-coated grids were treated with a drop of the NSP-gel dispersion for 1 min, followed by negative staining with 1% uranyl acetate for 1 min. Thereafter, electron micrographs were taken using the TEM (JEOL LTD, Peabody, MA). Various NSP concentrations, mixing times and dispersion procedures of the NSP in the gels were evaluated in order to determine the optimum dispersion. In addition, the morphology of the plain gels (without NSP) was also studied by TEM using the procedure described above.

5.3.8 *In vitro* skin penetration studies

Human Cadaver skin obtained from NYFF (New York Firefighters Association, NY) was used to evaluate the *in vitro* skin permeation of the dye NR via NSP dispersed in the gel and aqueous formulations. Skin obtained from the tissue bank was stored at -80 ^{0}C and thawed at room temp before the experiment. After 1 h of pre-hydration with PBS, the skin pieces were mounted on Franz diffusion cells (receptor volume 5.1ml, permeation area 0.64 cm^2) in between the donor and the receptor compartment. The receptor solution consisted of PBS (pH 7.4)

that was constantly stirred at 600 rpm and maintained at 37 ± 0.5^{0}C. Thereafter 6 pieces of skin were pre-treated with 100 µl of 0.2 M Azone for 1 hour. After 1 hour, the excess Azone was removed with a Q tip and the skin surface was wiped with another Q tip. Thereafter, 800 µl of the prepared formulations were added to the donor compartment of the diffusion cells with the aid of a 1 ml syringe. Formulations with the following compositions were evaluated (n = replicates):

No.	**Formulation**	**Description**	**Solvent base**	**n**
1	NR-NSP	Aqueous dispersion	PBS	6
2	NR-NSP-gel	NR-NSP dispersed in 1 % w/v HPMC gel	PG:Water 80: 20 v/v	6
3	NR-NSP in gel + enhancer pre-treatment	Pre-treatment with 0.2 M Azone followed by treatment with NR- NSP dispersed in 1 % w/v HPMC gel	PG:Water 80: 20 v/v	6
4	NSP alone	Aqueous dispersion of NSP	PBS	3
5	NR solution (control)	Aqueous solution of NR	PG:Water 80: 20 v/v	6
6	NR solution + enhancer pre-treatment (control)	Pre-treatment with 0.2 M Azone followed by treatment with aqueous solution of NR	PG:Water 80: 20 v/v	6

After 24 h, 1 ml of the receptor sample was withdrawn and lyophilized overnight, followed by extraction of NR in the sample by shaking with methanol for 1 h and determination of NR content by HPLC. The excess formulation on top of the skin in the donor compartment was removed and the skin pieces were demounted, washed 3 times in PBS and the skin surface was wiped lightly with a Kimwipe®. Thereafter rectangular small skin pieces (~ 4 mm X 8 mm) were cut out from the center of the treated skin and embedded in moulds with the aid of OCT (Optimal Cutting Temperature), an embedding compound for frozen tissues. 20 µm thick cross-sections (al least 6 per sample) of each treated skin sample were cut with the aid of a Leica CM 1850 cryostat (Leica systems, Germany). The NR in the skin sections was visualized using fluorescence microscopy with a Zeiss Axio Observer D1 microscope (Germany) with excitation and emission wavelength for NR (546 nm and 585 nm respectively). Quantitation of the NR fluorescence in different skin layers was conducted with the Image J software (NIH, USA) in terms of pixel intensities after adjusting the instrument for skin auto fluorescence. For quantitation, the skin was histologically divided into sections with various phase contrast pictures as reference, and the quantitation of fluorescence in each of these sections was conducted. Statistical evaluation (ANOVA) ($p<0.05$) was conducted with the aid of Kaleida Graph 4.0, (Synergy Software, Reading, PA).

5.3.9 *In vivo* skin penetration studies

In vivo studies were conducted in a female domestic pig maintained at Stony brook University, Department of Emergency Medicine, NY. The female pig (age: 3 months) was anesthetized and the hair was shaved off the back with the help of an electric shaver. The formulations were applied to the back of the female pig with the aid of Hill Top chambers, patented occlusive patch test systems (Hill Top Research, Miamiville, OH, USA). The Hill Top Chamber is a flexible plastic chamber that consists of an outer ring and an inner, flexible flange, that aid in conforming to skin contours and increasing occlusivity.(64) Hill Top chambers containing ~ 200 µl of the formulations were glued on to the back of the pig with the help of crazy glue (Figure 5.1). In case of aqueous dispersions, the empty Hill Top chamber was glued on the pig back first and the aqueous dispersions were injected into the chamber with a syringe and needle. For the gel formulations, ~ 200 µl of the formulations was added to the Hill Top chamber first with a syringe, glue was applied onto the edges of the chamber and the chamber was then quickly inverted onto the pig back and glued on. The application of formulation replicates was randomized to different areas on the back to eliminate any site-specific bias.

1. The following formulations were evaluated in replicates indicated:
    1. NR-NSP aqueous dispersion in PBS (n=6)
    2. NR-NSP containing 0.2 M Azone aqueous dispersion in PBS (n=6)
    3. NR-NSP in 1 % w/v HPMC gel (solvent base: PG:Water, 80:20 v/v) (n=6)

4. NR–NSP in 1 % w/v HPMC gel containing 0.2 M Azone (solvent base: PG:Water, 80:20 v/v) (n=6)

Controls

5. NR in PG:water (80:20 v/v) (n=6)
6. NR in 1 % w/v HPMC gel (solvent base: PG:Water, 80:20 v/v) (n=6)
7. NR in 1 % w/v HPMC gel containing 0.2 M Azone (solvent base: PG:Water, 80:20 v/v) (n=6)
8. NSP aqueous dispersion (n=2)
9. PG:Water, 80:20 v/v (n=2)
10. 1 % w/v HPMC gel (solvent base: PG:Water, 80:20 v/v) (n=2)

After formulation application, the Hill Top chambers were covered with a layer of Tegaderm and subsequently a layer of gauze and crepe bandage were wrapped around the back and belly of the animal to help keep the chambers in place and to prevent the pig movements from disturbing the applied formulations. After 24 h, the crepe bandage, gauze and the Tegaderm were removed carefully, and the chambers were peeled off. The site of formulation application was wiped with wet gauzes, and 8 mm biopsies of the central treated area were taken with a biopsy punch. The biopsies were rinsed thrice with PBS, wiped dry, frozen on dry ice and stored for further analysis. Rectangular small skin pieces (~ 4 mm X 8 mm) were cut out from the center of the skin biopsies and embedded in moulds with

the aid of OCT (Optimal Cutting Temperature). 20 µm thick cross-sections (at least 6 per sample) of the porcine skin samples were then cut with the aid of a Leica CM 1850 cryostat (Leica systems, Germany). The NR in the skin sections was visualized by fluorescence microscopy as described in "*in vitro* skin penetration studies." Quantitation of the NR fluorescence was conducted with the Image J software (NIH, USA) in terms of pixel intensities after adjusting the instrument for skin auto fluorescence. For quantitation, the skin was histologically divided into three vertical sections: a) 110 µm depth from top of skin: represents the stratum corneum and the viable epidermis b) 100 µm depth from the epidermis: represents the upper dermis and c) the remaining dermis. Statistical evaluation (ANOVA) ($p<0.05$ was conducted with the aid of Kaleida Graph 4.0, (Synergy Software, Reading, PA).

5.3.10 *In vitro* cellular and tissue cytotoxicity

In order to evaluate the toxic potential of the formulations and its individual components, we conducted *in vitro* toxicity studies of the formulations at a cellular level (cytotoxicity in dermal fibroblasts and keratinocytes) and also in tissues (SEM of treated human skin). Cytotoxicity studies utilized the MTS (3-(4,5-dimethylthiazol-2-yl)-5-(3-carboxymethoxyphenyl)-2-(4-sulfophenyl)-2H-tetrazolium) assays (Promega CellTiter 96 AQueous One Solution Cell Proliferation Assay, Promega, Madison, WI). MTS in the presence of phenazine methosulfate (PMS) is reduced to a water-soluble formazan product by the

reductase enzymes in the mitochondria of viable/living cells. This soluble product has an absorbance maximum at 490-500 nm that can be measured in a plate reader and is a measure of the viability or the lack of cytotoxicity of cells.

Primary dermal fibroblasts and epidermal keratinocytes were obtained from Invitrogen Corp., (Carlsbad, CA) and cultured *in vitro* in 75 cc tissue culture flasks. Secondary cultures of fibroblasts were established with media containing Dulbecco's Modified Eagles Medium (DMEM) (Gibco-Invitrogen Corporation, Carlsbad, CA) supplemented with 10% fetal bovine serum (FBS) (Sigma, St. Louis, MO). Secondary cultures of keratinocytes were established with supplemented Epilife® medium (Invitrogen Corp., Carlsbad, CA) containing 0.06 mM calcium chloride, bovine pituitary extract (0.2% v/v), bovine insulin (5 μg/ml), hydrocortisone (0.18 μg/ml), bovine transferrin (5 μg/ml), and human epidermal growth factor (0.2 ng/ml).

Human skin cells (fibroblasts or keratinocytes) were seeded in wells of 96-well plates at a density of 7000 cells/well. After 24 h, the cells were incubated with varying concentrations of Azone and the NSP formulations in respective media for 24 h at 37^0C. A mixture of PG:Water 80:20 v/v used as a solvent for the formulations was used as negative control. After 24 h of treatment, the formulations were removed, and the cells were washed with PBS and supplemented with fresh medium containing MTS solution. The plates were incubated at 37^0C for 3 h and the intensity of the purple formazan end-product was measured in a plate reader at 490 m.

Toxicity evaluation in skin tissues was conducted by Scanning Electron Microscopy (SEM). Human skin was treated with the formulations as described under "*In vitro* skin permeation studies" for 24 h and sectioned partially with a cryostat in order to create a smooth and uniform surface across the vertical section. The skin pieces were then fixed with 5% glutaraldehyde solution at 4℃ for 2 h and washed with water. The fixed skin was then dehydrated with 25%, 50%, 75%, and 95% ethanol for 1 h each at room temperature, followed by two changes of 100% ethanol for 1 h each. Finally the skin was dried with a critical-point drying machine and sputter coated with gold-palladium. The skin surface (top layer) and the vertical cross section along the side were then visualized with a Scanning Electron Microscope (AMRAY 1830) after mounting them on aluminum stubs. Spectra were obtained with a 300-MHz Varian Mercury spectrometer (Palo Alto, CA).

5.4 Results and Discussion

5.4.1 HPLC validation of DS and NR

Both DS and NR were accurately and reproducibly detected by HPLC analysis with high inter- and intra-day precision. All HPLC validation parameters are reported in Table 2. The presence of the pure tyrosine derived polymer, NSP, gel polymers and also processing variables such as drug lyophilization did not create

any interference or peak shifts and drug recovery was > 85 %. Linearity of the calibration curves with and without the presence of NSP was >0.99.

5.4.2 Morphology and dispersion of NSP in hydrophilic gels

In order to visualize the NSP in gel formulations, we prepared NSP dispersions at various concentrations in 1% w/v HPMC and carbopol 981 NF gels and observed them with the aid of a TEM. Dispersion of the NSP in the gels did not create any morphological changes and their average size in the gels (~ 35 nm diameter) was synonymous with their size in aqueous solution.

NSP-HPMC gel dispersions at concentrations of 10 mg/ml or greater (of NSP) appeared to be associated in large groups (Figure 5.2, A) and could not be dissociated by shaking or brief sonication. NSP dispersions in the carbopol gels appeared to be significantly more clumped together than those in the HPMC gel (Figure 5.2, B). When the concentration of NSP in the dispersions were reduced to 3-6 mg/ml, most NSP were found to be uniformly and individually dispersed in 1% w/v HPMC gels, and few were present in the form of very small groups (Figure 5.2, E). Again, the NSP dispersions at low concentrations in the 1% w/v carbopol gels appeared to be associated in groups to a significantly greater extent than the corresponding HPMC gels (Figure 5.2, F). We believe that this phenomenon occurs due to the anionic nature of the carbopol polymer chains that may lead to interactions between the polymer chains and the NSP. To

evaluate the possibility of this phenomenon, we tried to observe the structure of the swollen polymer networks by TEM. While the carbopol gels could not be observed by TEM, the HPMC gels showed presence of uniform polymer networks, but did not provide any conclusive information about the NSP dispersability (Figure 5.3, A, B). However, after observation of TEM and cryo-SEM images of the carbopol family of polymers in literature (Figure 5.4, A, B), it appears that the swollen carbopol gels have a very intricate honey-comb like structure that may interfere with uniform dispersion of polymeric nanoparticles. The TEM studies and the literature research indicate that the non-ionic HPMC gel network may provide a more inert environment to the NSP as compared to carbopol.

The presence of 0.2 M Azone in the HPMC gel did not affect the morphology or the NSP size (Figure 5.2, C). Similar results were obtained with menthone 2%, a chemical enhancer belonging to the ‘terpene’ class (Figure 5.2, D). Since the presence of these two potent enhancers did not affect the NSP dynamics when dispersed in gels, it is safe to conclude that similar results will be obtained with most other chemical enhancers. Thus, NSP and chemical enhancers can be used concurrently as components of gel formulations.

5.4.3 Gel content and *in vitro* release of diclofenac sodium from gels

To determine the effect of drug solubility and loading on the physical properties of the gel, we prepared 1% w/v HPMC and carbopol 981 NF gels with 1% and 2.5% w/v DS in PG:Water (80:20 v/v) as the base, chosen due to its ability to act as a suitable solvent for Azone. The resulting HPMC gels (with 1 and 2.5% w/v DS) were clear and remained stable for 48 h at room temperature (Figure 5.5, A, B). On the other hand, carbopol gels could only be prepared with low drug content (1% DS w/v), as incorporation of DS at 2.5% w/v led to high precipitation of the drug/polymer (Figure 5.5, C, D). This may have occurred due to solubility limitations of DS and the carbopol polymer in the PG:Water mixture or due to the conversion of DS to its base form (diclofenac) leading to its precipitation.

We compared the *in vitro* release of 1 % DS from 1% w/v HPMC and carbopol gels through regenerated cellulose membranes. The cumulative release of DS at the end of 24 h from the HPMC gel (Q_{24}=5198 ± 156 µg/cm^2) was ~3 times that from the carbopol gel (Q_{24}=1699 ± 216 µg/cm^2) (Figure 5.6, A). Similarly, the rate of release (flux) of DS from the 1% w/v HPMC gel (flux= 686.6 ± 74 µg/cm^2/h) was ~ 2.9 times that of the carbopol 1% w/v ((flux= 239 ± 14 µg/cm^2/h). Thus, the amount and the rate of DS release from the HPMC gels were significantly higher than from carbopol 981 NF. The release of DS from the HPMC gels increased with increased drug loading, though the increase was not proportional, as seen by the comparison of release of 1 and 2.5% w/v DS from 1% HPMC gels (Figure 5.6, B). Also, the DS release from 1% HPMC gel was very similar to its release

from an aqueous suspension in PG:Water (80:20 v/v) (Figure 5.6, C). This result was contrary to our expectations, as some studies have shown that the release of drugs from gels is lesser and at a more controlled rate than that of an aqueous suspension. This increased diffusion could be a result of high porosity of the specific type of HPMC polymer (Methocel K15) and its low concentration (1% w/v).

Analysis of gel content showed that the HPMC gel formulations were found to contain between 97-105% of DS. Also, the drug was found to be stable in this gel network, since HPLC assay of DS post extraction from the HPMC gel reservoir showed no additional peaks and did not affect the retention time of the drug.

Based on the drug loading limitations of carbopol 981NF, the un-uniform dispersion of the NSP in this gel (TEM studies), the lower and slower drug release of DS from its gel matrix and its low viscosity (studies reported below), we chose the HPMC gel for further formulation studies. In order to chose a suitable concentration of the HPMC gel for NSP dispersion and release, we evaluated the release of DS from three concentrations of HPMC (0.5, 1, 1.5 % w/v) through regenerated cellulose membranes. A plot of the cumulative amount of DS released from all three HPMC gels (0.5, 1 and 1.5 % w/v) against the square root of time ($h^{1/2}$) was found to be linear (R^2, regression coefficient = 0.99), indicating a direct relationship between these two factors (Figure 5.7). This

shows that the drug was released form the HPMC gel matrices by passive (fickian) diffusion according to the Higuchi diffusion mechanism (65) given by:

$Q/A = 2\ C_0\ C_s\ (D\ t/\pi)^{1/2}$ (Equation 4)

Where Q = amount of drug released during time t

A= surface area

D= Diffusion coefficient (cm^2/s)

C_s = Solubility of the drug in the gel

C_0 = initial loading of the drug in the gel

For drugs that are soluble in the polymer matrix, the equation becomes:

$Q/A = 2\ C_0\ (D\ t/\pi)^{1/2}$ (Equation 5)

The cumulative amount of DS released from these three gels and the corresponding steady state fluxes are depicted in Figure 5.8 and Table 3. The cumulative amount of DS released and its flux from 0.5 % w/v HPMC (Q_{10}= 9291 ± 367 µg/cm^2, J_{ss} = 1499 ± 76 µg/cm^2/h) were very similar to that of 1 % w/v HPMC (Q_{10}= 9110 ± 180 µg/cm^2, J_{ss} = 1444 ± 18 µg/cm^2/h). However, the Q_{10} and the J_{ss} of DS when released from the 1.5 % w/v HPMC gel was significantly lesser, indicating a lower release of DS due to higher complexity of the polymer network and a longer diffusion pathway. This decrease in release could also be

due to a significant increase in gel viscosity at this concentration (discussed below).

5.4.4 Viscosity of the gels

Rheology of gels is an important aspect for skin contact and spreadability. An ideal gel should be a non-Newtonian system, and should demonstrate shear-thinning behavior. This assures that when the gel is applied to the skin surface and spread by use of force, the gel network breaks to achieve a certain spreadability and contact with the skin surface leading to a decrease in viscosity. After removal of the force, the gel network viscosity again increases thereby forming a layer to increase skin contact for longer periods of time. Rheology of topical formulations also have a profound effect on the storage stability and the drug release, as the gel viscosity is a function of the amount and molecular weight of the polymer, factors that also affect the drug release from the gel network. We determined the viscosity of three concentrations of the DS-HPMC gels evaluated earlier for their drug release, using a rheometer (Table 3). The 0.5 % w/v HPMC formulation demonstrated low viscosity and behaved more like a Newtonian fluid. The 1.0 % and 1.5% w/v HPMC gels demonstrated non-Newtonian behavior and exhibited shear thinning properties (pseudoplastic fluids). However, the viscosity of the 1.5% w/v HPMC gels increased significantly and disproportionately and was found to be ~ 9.5 times higher than that of the 1 % w/v HPMC gel. This increase in viscosity could be due to an abnormal

increase in the cross-link of the polymer network at this particular concentration of HPMC (1.5% w/v). Similar observations were made by Ramachandran et al. where they found that HPC (HydroxyPropylCellulose) gels became increasingly non-Newtonian due to increase in polymer concentration.(63) They suggested that a very high non-Newtonian index or behavior of the gel may make it unsuitable for manufacture process and subsequent topical application.

In order to determine any significant viscosity changes in the HPMC gel formulation after dispersion of the NSP and NR, we evaluated the viscosity of 1% w/v HPMC gel formulation with and without the NR-NSP dispersion and Azone. The instantaneous viscosity (Pa.S) of the NR-NSP loaded HPMC gel was found to be ~ 7.5 times of the HPMC gel alone. In addition, the incorporation of 0.2 M Azone in the NR-NSP loaded HPMC gel increased the viscosity to ~ 18.8 fold of the HPMC gel alone. Although this change in viscosity was unexpected, this finding facilitated the choice of the appropriate gel concentration for the final formulation. Based on the results of DS release and the viscosity profiles of the HPMC gels, we chose the HPMC 1% w/v gel as the optimal gel for NSP formulation. The HPMC polymer at this concentration did not significantly retard the rate and amount of drug release. In addition, the further increase in viscosity of the formulation after addition of the NR-NSP dispersion made the NR-NSP-1% w/v HPMC gel formulation optimal for storage and topical application. For further skin penetration studies, NR loaded NSP were dispersed at optimal concentrations determined by TEM (3-6mg/ml) in HPMC 1% w/v gel formulations

made in a solvent base of PG:Water (80:20 v/v) as described under “Preparation, characterization and optimization of NSP in gel formulations”.

5.4.5 *In vitro* skin permeation of NR via NSP-gels

In order to determine the skin penetration effects of NR–NSP in the HPMC gel formulation, we cryo-sectioned the treated human skin post 24 h *in vitro* studies and determined the amount of NR fluorescence in specific skin layers and the corresponding depth of NR penetration. Figure 5.9 shows the vertical cross-section images depicting the NR fluorescence in layers of human skin. Figures 5.9 (A and B) depict a representation of the phase contrast pictures that were used as a guide to demarcate the skin section into four different layers: a) 10 µm depth from top of skin: represents the stratum corneum b) 100 µm from the SC: represents the viable epidermis c) 100 µm depth from the viable epidermis: represents the upper dermis d) 100 µm depth from the upper dermis: represents the lower dermis.

It can be seen that the NSP themselves did not show any fluorescence (Figure 5.9, C). The penetration of NR from its solution in the PG:Water mixture seems restricted to the superficial epidermal layers, predominantly the SC (Figure 5.9, D). Complexation of the NR with the polymeric NSP enhanced the penetration of NR (Figure 5.9, E, F) to all skin layers as compared to its solution in PG:Water. The NR deposited in the epidermis, upper dermis and lower dermis via the NSP

was ~ 5, 7 and 3.5 fold higher than the amount of NR deposited from a solution in PG:Water (Figure 5.10, A, Table 4). Similar results were obtained with the proof of concept studies conducted earlier in Chapter 4. NR complexed NSP dispersed in the HPMC gel formulation delivered similar amounts of NR to the SC and the epidermis when compared to the respective aqueous formulation in PBS. However, the amount of NR deposited in the upper and lower dermis from the gel formulation of NSP was 1.4 and 1.8 times higher (significant difference, $p< 0.05$) when compared to the aqueous formulation (Figure 5.9, I, J, 5.10, B). This confirms our hypothesis that the HPLC gel system is a better formulation for the NSP than its aqueous dispersion. Formulating the NSP in a gel significantly increased the viscosity of the formulation, and the improved consistency was evident visually and was also confirmed during application to skin in the *in vitro* studies. At the end of the experiment, when the donor compartments were removed from the diffusion set up, it was observed that the gel formulation remained in contact with the skin even after 24 h, while the aqueous formulations demonstrated a 'run-off' effect. This improved contact with the skin may have increased the efficacy of the NSP by providing them more time and opportunity to penetrate skin. We also believe that the HPMC gels contributed to superior occlusion and hydration of the skin, factors that have been shown to open up skin penetration pathways and lead to penetration enhancement. It appears that the low concentration of the polymer used in the gels (1% HPMC w/v gels) did not significantly retard the release of NSP from the gel matrix, consistent with our

release study of DS from this gel. Any minimal retardation that existed was most probably offset by the improved formulation characteristics.

Pre-treatment of the skin with 0.2 M Azone enhanced the NR penetration via NR-NSP gel formulation by 1.2, 1.8 and 2.7 fold in the epidermis, upper dermis and lower dermis (Figure 5.10, C). This increase was significantly apparent in the vertical skin sections where the sections pre-treated with Azone showed the presence of bright red fluorescence through all the skin layers (Figure 5.8, K, L). Thus, the combined effect of the NSP and Azone significantly enhanced the skin penetration of NR. We chose Azone because it has shown to be a potent skin enhancer, has been studied widely and its mechanism of action has been researched and confirmed in literature. Azone has been shown to enhance skin penetration of compounds by fluidization of the skin lipids.(13) This action of opening up the barrier pathways between the corneocytes may have created channels for the NSP to surpass the SC barrier and permeate deeper and faster into the epidermis and dermis. The effect of Azone in enhancement of skin delivery of NR from the aqueous formulation of NSP (Figure 5.8, G, H) was less significant than the corresponding HPMC gel formulation. As observed in previous studies, the NSP did not deliver NR transdermally, even when formulated as a gel and combined with Azone.

5.4.6 *In vivo* skin permeation of NR via NSP-gels

The *in vivo* skin penetration studies were conducted in the domestic pig, and the skin sections after 24 h of treatment were processed similar to the *in vitro* diffusion study. Images of the vertical skin cross-sections are presented in Figure 5.11. The qualitative analysis reveals that the NSP deliver higher amounts of NR to the porcine SC/epidermis than the equivalent formulations of NR in PG: Water 80:20 v/v or NR in HPMC gel. The fluorescence quantification (Figure 5.12) confirmed 2.3 fold ($p < 0.05$) and 1.6 fold ($p < 0.05$) higher amount of NR in the SC/epidermis deposited via NSP (aqueous) than the NR solution in PG: water and HPMC gel, respectively. The HPMC gel formulation of NR-NSP was found to deposit 1.4 and 2.3 fold higher amount of NR in the SC/Epidermis than the aqueous NR-NSP and NR-HPMC gel, respectively ($p<0.05$). The penetration enhancing effects of the NR-NSP gel formulation (P.E.: 121.3 ± 22.7) could also partly result from the presence of PG: Water 80:20 v/v (P.E.: 37.5 ± 6.06) added as solubilizing agents to the gel (Figure 5.12 C, Table 5). Further, it is important to note that the gel formulations demonstrated more suitable viscosity for topical application in the *in vivo* study as they did not leak out of Hill Top chambers as opposed to the aqueous formulations, and appeared to stay in close contact with the skin. Also, incorporation of Azone in aqueous NSP formulation lead to the Azone separating out as droplets, while its addition to the gel formulation resulted in a more uniform product, with slight change in color and haziness, but no distinct phase separation.

The presence of the skin penetration enhancer Azone (0.2M) in the gel formulation increased the skin deposition of NR via NSP by 1.4 fold of the equivalent formulation without Azone. This is in agreement with the synergistic effects of Azone and NSP in the *in vitro* study. This combined formulation demonstrated the highest skin penetration of NR (Figure 5.12, H), a 4.5 fold higher deposition than non-particulate formulation of the NR in PG:Water alone. The skin delivery effects of this formulation can be further enhanced by alteration of the concentrations of the components (HPMC, NSP, NR and Azone) thereby customizing the formulation to target specific and desired skin layers.

5.4.7 Cytotoxicity of NR-NSP formulations and Azone

We evaluated the cytotoxicity of select NR formulations and a series of Azone concentrations in human skin cell lines (MTS assay) and in human skin (SEM). The viability of the fibroblasts and keratinocytes decreased significantly with increasing concentrations of Azone (Figure 5.13 and 5.14). Cell viability with Azone was seen only at concentrations under 0.00002 M, which is 10,000 times lower than the concentration frequently used in skin penetration enhancement studies (0.2 M). Treatment of the cells with NR 8-13 µg/ml, HPMC 1% w/v, PG:Water (80:20 v/v) did not reduce the cell viability below 80% of control (untreated cells). NSP alone (3.5 -11.5 µg/ml) and when complexed with NR (NSP-NR, 8-13 µg/ml) in aqueous suspension and HPMC gels, were found to be non-cytotoxic to the cells with viability post 24 h treatment always ~ 100%.

SEM was used to study the cytotoxicity to skin tissues after 24 h of treatment with the formulations. Surface and cross-sectional SEM images of human skin treated with NR-NSP (Figure 5.15, C, D) shows flattened SC corneocytes tightly interconnected and the SC and epidermal layers stacked together similar to untreated human skin (Figure 5.15, A, B). Treatment with NR in PG:Water (80:20 v/v) lead to 'lifting up' of corneocytes from the surface and minimal 'ballooning' of the epidermis (Figure 5.15, E, F), possibly due to the hydration effects of the PG:Water mixture. Also, PG has also reported to be a mild skin penetration enhancer, although this effect has been disputed by some groups. The 'lifting up' and 'ballooning' effect of skin cells and layers was more enhanced when skin tissues were treated with NR-NSP in HPMC gel (Figure 5.15, G, H), an effect that probably occurred due to the prolonged contact of the gel with skin and the resulting occlusion and hydration. Treatment with NR-NSP in HPMC gel with 0.2 M Azone had pronounced effect on the skin cells (Figure 5.15, I, J, K, L, M, N, O). The skin surface appeared undulated and many corneocytes were seen sloughing off the skin surface. The cross section SEM images showed intense ballooning and separation of the SC layers with occasional disappearance of the intercorneocyte connections. This effect, which is a result of the action of Azone on the intercorneocyte lipids leading to their partial dissolution, is possibly the reason for the penetration enhancement effect of Azone as well as its toxicity.

5.5 Conclusion

The enhanced penetration of NR via the polymeric NSP to the deeper skin layers confirmed our results from chapter 4, demonstrating that these NSP are capable of significant penetration enhancement of lipophilic compounds to skin layers. The dispersion of the NR-NSP in 1% w/v HPMC produced a formulation with a uniform and stable dispersion of NR-NSP and Azone, increased viscosity for topical application and better and longer contact with the skin surface. I*n vitro* skin penetration studies showed that the deposition of NR via the NR-NSP-HPMC gel in the upper and lower dermis was 1.4 and 1.8 times the amount of NR deposited from the aqueous NR-NSP formulation. The NR-NSP-HPMC gel formulation also significantly enhanced the permeation of NR to the porcine epidermis *in vivo,* depositing 1.4 fold higher amount of NR in the SC/Epidermis than the aqueous NR-NSP formulation. We used the domestic pig as an *in vivo* model because the stratum corneum of the domestic pig has been found to be most similar to human stratum corneum in terms of lipid composition. However, the thickness of porcine and human SC differs considerably, where porcine skin has been reported to be considerably thicker than human skin. The permeation of NR from the gel and aqueous formulations was lower in the porcine skin *in vivo* than human skin *in vitro*. Apart from the physical and biochemical differences in human and porcine skin, this reduced permeation in porcine skin could also be due to the lower amount of applied formulations (~200 µl) in the *in vivo* study as compared to 800 µl in the *in vitro* study. Lower amounts of the formulation were used *in vivo* due to the volume limitations of the Hill Top

chambers used. Also to be noted is the fact that the formulations applied on the pig were subject to any disturbances that could have arose due to random and uncontrollable movements of the animal for 24 h. Nevertheless, the NSP-gel formulations demonstrated better efficacy and consistency for topical application both in the *in vitro* and *in vivo* studies.

The combined formulation of the chemical enhancer Azone 0.2 M and the NSP in the HPMC gel base produced the highest amount of skin penetration of NR in the *in vitro* and *in vivo* studies. This confirms our hypothesis that the fluidization action of Azone on the intercellular skin lipids aids the NSP to overcome the SC barrier and penetrate better into deeper skin layers. However, Azone was found to be cytotoxic to skin cells and the skin tissues, unlike the NSP, which did not change the cell viability *in vitro* and the tissue characteristics of skin. Thus the NSP-HPMC gel formulation can be considered as a biocompatible and non-cytotoxic skin penetration enhancing formulation for lipophilic compounds. Nevertheless, chemical enhancers like Azone can be added to this formulation in non-cytotoxic concentrations to create synergistic effects with NSP for skin permeation. Variation of Azone concentration and the concentrations of drug, NSP and the gel polymer can produce customized formulations that can be used to control the amount and the depth of skin penetration and subsequently the deposition of the complexed drug.

Note:

The authors would sincerely like to thank Prof. Joachim Kohn, Dr. Larisa Sheihet and Dr. Stefan Saloman from the NJ Center for Biomaterials, NJ for their expert guidance, discussions, synthesis of the tyrosine based polymers and assistance in the in vivo studies. We would also like to thank members of the department of Emergency Medicine, Stony Brook University and Medical Center, NY for their help with the in vivo studies in the domestic pig. We would like to acknowledge assistance by Mihaela Jitianu for the rheology studies and Valentin Starovoytov for the SEM analysis.

6 Human Skin Equivalent as an *in vitro* model for permeability testing - culture optimization and characterization

Published as: "Effects of Growth Conditions on the Barrier Properties of a Human Skin"

Priya Batheja, Yifan Song, Philip Wertz and Bozena Michniak-Kohn

Pharmaceutical Research, 26(7) (2009), p:1689-1700

6.1 Introduction

The enormous growth and potential of transdermal and topical delivery systems necessitates the use of reliable models that aid in the evaluation of skin permeation of compounds and their subsequent screening and formulation development. In order to obtain reliable permeability data, the skin models should possess a permeability barrier that reflects the barrier provided by human skin. Though several Skin Equivalents (SE) have been developed for this purpose, all of these SE, including the leading commercially available SE, Epiderm® (MatTek, Ashland, VA) possess weak permeability barriers, with several fold higher permeability to agents when compared to human skin. The weaker permeability of the SE has been postulated to be a function of the difference in composition of the barrier lipids in the SC, which is the rate limiting step in skin permeation. Therefore, we decided to culture our HSE with media components that would

lead to production of these essential lipids and hence a normalized permeability barrier.

The full thickness Human Skin equivalent (HSE) bioengineered *in vitro* in our laboratory was cultured with a media formulated with a combination of external lipids, ascorbic acid and the PPAR-α agonist clofibrate. Preliminary lipid composition studies of the HSE cultured in our laboratory with this media combination have shown an increase in the production of essential skin barrier lipids (Tables 6 and 7). Media supplemented with external lipids has been shown to induce the synthesis of lipid precursors and formation of lamellar bodies in serum free SE culture.(66) Also, the presence of ascorbic acid in cultures has been shown to markedly improve the lipid profile and the barrier formation in reconstructed skin.(67) Pasonen-Seppanen et al. have shown that culture of an organotypic keratinocyte culture with 40 µg/ml of ascorbic acid for 3 weeks reduced the TEWL (TransEpidermal Water Loss) by approximately 50%.(68) The effect of PPAR agonists on skin homeostasis has been studied by some groups since the 1990s. The PPAR receptor subtypes (α, β, γ) are expressed in man and have shown to heterodimerize with Retinoid X Receptors (RXRs) and play an important role in lipid metabolism. All three PPAR subtypes are expressed in human epidermal keratinocytes and the expression of PPAR (α, and γ) has been found to increase during the course of keratinocyte differentiation.(69) PPAR-α agonists such as clofibrate have also been shown to play a role in the stimulation of epidermal lipid synthesis, increase in lamellar body secretion, acceleration of

extracellular lipid processing, all eventually leading to improvement in epidermal permeability barrier homeostasis.(70)

The HSE was constructed predominantly from human derived components, in order to closely resemble human skin *in vivo*. After complete culture, the HSE was characterized for its morphology, immunohistochemistry, cellular and extracellular dynamics and its permeability barrier to six agents with differing physiochemical properties. The HSE permeability profiles were compared to human skin and also to the leading commercially available full thickness SE, EpidermFT®. The reproducibility of the permeability barrier of the HSE was evaluated by determination of its intra-batch and inter-batch permeability profiles to the model drug caffeine.

We also found that the HSE epidermis was easily detached from the dermal matrix during processing for morphology, immunohistochemistry, or sometimes even during permeability experiments and simple handling. This phenomenon has been reported by various groups and has been attributed to the lack of a normally formed basement membrane, which is responsible for establishing adhesion between the epidermis and the dermis and also for regulation of the proliferation and differentiation of the epidermis.(71, 72) In order to improve the attachment of keratinocytes to the dermis, we studied the effect of extracellular matrix ECM proteins (fibronectin, collagen I and IV, laminin) and a coating matrix kit (combination of collagen I and IV) on keratinocyte attachment. Lastly, due to

observed fragility of the HSE model, we evaluated the mechanical strength of the dermal layer of the HSE by an inflation-based biaxial failure testing device and compared it to the corresponding dermal component of EpidermFT®.

6.2 Materials and Methods

6.2.1 Cell Culture

Human dermal fibroblasts and human keratinocytes were obtained from Invitrogen Corp., (Carlsbad, CA) or were isolated from the epidermal and dermal fragments of neonatal foreskins obtained during routine circumcisions from the Department of Pediatrics, University Hospital, University of Medicine and Dentistry, Newark, NJ. Secondary cultures of fibroblasts were established with media containing Dulbecco's Modified Eagles Medium (DMEM) (Gibco-Invitrogen Corporation, Carlsbad, CA) supplemented with 10% fetal bovine serum (FBS) (Sigma, St. Louis, MO). Secondary cultures of keratinocytes were established with supplemented Epilife® medium (Invitrogen Corp., Carlsbad, CA) containing 0.06 mM calcium chloride, bovine pituitary extract (0.2% v/v), bovine insulin (5 µg/ml), hydrocortisone (0.18 µg/ml), bovine transferrin (5 µg/ml), and human epidermal growth factor (0.2 ng/ml).

6.2.2 Preparation of the Dermal Layer

The human skin equivalents were made in two stages, the preparation of the dermal layer followed by seeding of the keratinocytes on the dermal layer and their subsequent proliferation and differentiation (Figure 6.1). The dermal layer was made by mixing in a 60 mm Petri dish an aliquot of 2X DMEM (1.6 ml), FBS (1.6 ml), 0.1 N NaOH (0.2 ml), bovine type I collagen (2.0 ml) (Inamed, Santa Barbara, CA), and fibroblasts in 1.0 ml of DMEM. In order to optimize the final diameter of the dermal layer and to study the contraction process, we investigated the formation of dermal layer with three concentrations of fibroblasts: 0, 220,000 and 440,000 cells in each layer. The mixture of the fibroblasts and the collagen was then incubated for 7 days in 10% CO_2 at 37℃ in a humidified incubator, to allow for contraction of this matrix to a tissue like scaffold. This contracted collagen scaffold was transferred to a Transwell® insert (12 mm diameter, pore size=0.4 μm, Corning Costar Corporation, Cambridge, MA) placed in 12 well plates (Corning Costar Corporation, Cambridge, MA).

6.2.3 Preparation of the Full Thickness HSE Model

Seven hundred thousand keratinocytes (passage 2–3) were seeded on the top of the dermal layers in 75 μl of the media and allowed to attach for 3 h in an incubator at 37^0C. The attachment media consisted of supplemented Epilife® with 1.2 mM calcium chloride to enhance the attachment of keratinocytes to the dermal scaffold. DMEM (without serum) was then added to the wells from the

bottom and the skin cultures were submerged in Epilife® and cultured submerged for 6 days (0.06 mM calcium) at 37℃, 10% CO2 and 75% RH. During the 4 last days of the submerged culture, the feeding media was supplemented with an external free fatty acids/lipids mixture (25 µM palmitic acid, 15 µM linoleic acid, 25 µM oleic acid, 7 µM arachidonic acid, and 24 µM bovine serum albumin).(66) Thereafter, the skin cultures were only fed from the bottom and the surface was exposed to air to promote the differentiation of the epidermis *in vitro*. The skin equivalents were cultured at the Air–Liquid Interface (ALI) for 21 days to allow full differentiation of keratinocytes and fed with media two or three times a week. The feeding media at this stage was supplemented with lipids (25 µM palmitic acid, 15 µM linoleic acid, 25 µM oleic acid, 7 µM arachidonic acid, and 24 µM bovine serum albumin), ascorbic acid (100 µg/ml) and clofibrate (300 µM) . All lipids and ascorbic acid were purchased from Sigma, St. Louis, MA, and clofibrate was purchased from Calbiochem, San Diego, CA.

6.2.4 Optimization of attachment of the keratinocytes to the dermal matrix

To improve the attachment of keratinocytes to the dermal matrix, we studied the effect of extracellular matrix ECM proteins (fibronectin, collagen I and IV, laminin, and a coating matrix containing a mixture of collagen I and collagen IV proteins) on keratinocyte attachment. In order to visualize the keratinocytes, we utilized the Vybrant cell adhesion assay kit (Molecular Probes, Invitrogen, Carlsbad, CA) that primarily consists of the dye Calcein AM, a non-fluorescent molecule that when

loaded into cells, is cleaved by the endogenous esterases to produce the highly fluorescent Calcein. Calcein is a cytoplasmic cell marker that interferes minimally with the cell adhesion process and can be used with fluorescent plate readers. An optimal and non-toxic concentration of Calcein AM (7.5 µm) was used to label the keratinocytes in suspension, as per the manufacturer's instructions. Four ECM proteins, Fibronectin (human natural), Collagen Type IV (mouse), Laminin (mouse) and collagen Type I (rat tail) were obtained from BD Biosciences (San Jose, CA), diluted as per manufacturer's instructions, and stored at the specified conditions until use. The coating matrix was obtained from Invitrogen (Carlsbad, CA). 50 µl of the proteins (n=3) at different concentrations (fibronectin, collagen I and IV, laminin in concentrations of 0, 1, 0.3, 0.1, 0.03, 0.01 µg/ml) and the coating matrix was used to coat the wells of two duplicate 96 well plates. The coated 96-well plates were allowed to remain in the hood for 1.5 h, after which the excess protein solution was removed and the plates were stored overnight at 4^0C. Calcein labeled keratinocytes were seeded in the coated wells of one 96 well plate at a concentration of 5000 cells/well. Immediately after addition, the total initial fluorescence in each of the wells was read with the aid of a fluorescent plate reader (470 nm and 530 nm absorption and emission respectively) and images of the added cells were taken with a fluorescent microscope. In the second plate, unlabeled keratinocytes were added to the wells at similar concentrations (5000/well). After 3 h of attachment at 37^0C, the media in both plates was removed, the wells were washed with PBS, and the number of attached cells in the wells was evaluated by fluorescence quantitation and

microscopy (plate 1) and MTS assay (plate 2). For the MTS assay, 100 µl of MTS reagent was added to each well and the plate was incubated for 3 h at 37^0C. After 3 h, the absorbance of the formazan end product was read in a plate reader at 490 nm.

6.2.5 Visualization of the Cell Dynamics in the HSE

In order to visualize the cell dynamics within the collagen based scaffolds of the HSE, rat neonatal GFP-expressing fibroblasts were used to prepare the dermal scaffold instead of the regular human dermal fibroblasts. The dermal matrices were made as described under “Preparation of the dermal layer” and the layers were observed under a fluorescent microscope (Nikon Eclipse TE2000-E) during the 1st, 4th and 6th day of contraction. To visualize the attachment and distribution of keratinocytes, the nuclei of the human neonatal keratinocytes in suspension were labeled with Hoechst 33342 dye (component B of Image-iT Live Plasma Membrane and Nuclear Labeling Kit, Molecular Probes, Invitrogen Detection Technologies, Eugene, OR). All labeling procedures were conducted as per manufacturer’s instructions. The labeled keratinocytes in suspension were then seeded on top of dermal layers prepared from unlabeled human dermal fibroblasts and bovine collagen as per the procedure described in “Preparation of the dermal layer”. The dermal layers were fed with media, and stored in the humidified incubator at 37℃ and 10% CO_2. On the subsequent day and on the 4th day after seeding, the layers were observed under a fluorescence

microscope (350/461 nm) for attachment of the keratinocytes to the dermal layers and their distribution.

6.2.6 Characterization of HSE - Morphology and Immunohistochemistry

After complete culture for 21 days at the ALI, the HSE were characterized for their morphology, immunohistochemistry (Involucrin content) and expression of other proteins. Also, skin thickness of the HSE post 21 days of ALI culture was measured with the aid of a micrometer (Mitutoyo, Japan) and reconfirmed by microscopy.

For morphological analysis, HSE cultures were fixed in 1% paraformaldehyde - 0.1% glutaraldehyde solution overnight and then processed (by dehydration) for embedding in paraffin. Sections (6 µm) were obtained with the aid of a microtome and stained with Hematoxylin and Eosin (H &E). Stained samples were analyzed by light microscopy.

The expression of Involucrin was detected by an immunohistochemistry method utilizing an Involucrin immuno-kit (Biomedical Technologies, Inc., Stoughton, MA). Paraffin embedded sections of HSE (6 µm) were rehydrated by incubation for 2 min each in xylene (twice), 100% ethanol (twice), 95% ethanol, 70% ethanol and Tris-saline (0.15M NaCl - 0.05 M Tris, pH 7.6). The endogenous

peroxidase activity was reduced by incubation of slides in Tris-saline containing 0.3% H_2O_2 for 30 min. After rinsing in Tris-saline, the slides were incubated with normal goat serum for 30 min to block non-specific binding followed by rinsing in Tris-saline again. Then the sections were incubated with 100 µl of rabbit anti-human involucrin serum for 30 min followed by rinsing in Tris-saline. The sections were then incubated with 100 µl goat anti-rabbit IgG horseradish peroxidase (HRP) for 30 min followed by rinsing in Tris buffer (1 M Tris-Cl, pH 7.6). The slides were incubated for 10 minutes to desired color development with 3,3-diaminobenzidine HCl (0.6 mg/ml) - H_2O_2 (0.3) in Tris buffer. The slides were then cover-slipped and observed under a light microscope.

For the preliminary determination of the proteins expressed in the HSE, aliquots of HSE collected at day 7 (ALI-7) and day 19 (ALI-19) after being raised to the ALI were subjected to (i) sectioning and Hematoxylin and Eosin (H&E) staining and (ii) protein extraction. The total protein and RNA extracted from ALI-7 and ALI-19 were subject to 2D gel analyses and RT-PCR with primers that are specific for basal and spinous / granular stage specific expression of keratins i.e. Keratin 14 and Keratin 10. The 2 D gel electrophoresis was conducted using the ZOOM IPGRunner system (Invitrogen). Briefly, 50 mg of tissue was homogenized in 950 µl lysis buffer (Invitrogen) and sonicated on ice. The extracts were cross-linked with 5 µl 99% N,N'-Dimethylacrylamide (DMA), quenched with 10 µl 2M DTT and centrifuged to yield supernatants with protein concentrations of 8-10 µg/ml. Strips (ZOOM Strip, Invitrogen) of acrylamide with non linear pH

gradients ranging from pH 3 to pH 10 (pH 3-10 NL, Invitrogen) were equilibrated with 12 µl of each protein supernatant and electrophoresed in the first dimension in the ZOOM IPGRunner Cassette and Mini-Cell (Invitrogen) at 1200-4200 Vh (Invitrogen). The electrophoresed strips were extracted from the cassettes, equilibrated with NuPAGE Novex Running buffer and co-electrophoresed with molecular weight markers in the second dimension through 4-12% Bis-Tris ZOOM Gels. Gels were stained with silver stain (SilverSnap, Pierce), air dried and scanned.

6.2.7 Characterization of HSE- *In Vitro* Permeability Studies

The cultured HSE were tested for their barrier properties, evaluated by comparison of their permeability to model agents as compared to split thickness human cadaver skin (obtained dermatomed to ~500 µm, Allosource, Cincinnati, OH) and a commercially available SE model EpidermFT® (MatTek Corporation, Ashland, MA). EpidermFT® is a full thickness skin model developed and marketed by MatTek Corp. and is shipped on medium supplemented agarose gels at 4°C. On receipt, the tissue wells were supplemented with the provided medium and equilibrated at 37°C, 5% CO_2 overnight. All tissues were used within 1–2 days of the equilibration for permeability studies. Human skin equivalents cultured in house for 21 days at the ALI were used for the same permeability studies. The skin equivalents (HSE or EpidermFT®) were transferred to jacketed vertical Franz diffusion cells (volume 4.1 ml, diffusion area 0.196 cm^2)

(PermeGear Inc., Bethlehem, PA) containing Phosphate Buffered Saline (PBS, pH 7.4) as the receptor solution being continuously stirred at 600 rpm. Smaller size diffusion cells were used to accommodate the smaller diameters (~1.2 cm) of the skin equivalents. The diffusion cells were maintained at 37℃ with the help of a thermostatic water pump (Haake DC10, Karlsruhe, Germany) leading to skin temperatures of 32±0.5℃. Saturated suspensions of drug agents in propylene glycol (5 µl) were added to the donor compartments, which was covered with Parafilm®. Samples (300 µl) were withdrawn from the receptor over 24 h and replaced with an equivalent volume of the buffer. Results were compared to data obtained from similar experiments with human skin. In order to determine the contribution of the dermal matrices to the permeability barrier of the HSE, we compared the permeability of model agents through the full thickness HSE to their permeability profiles through the dermal matrices (without the epidermal layer). Dermal layer permeability studies were conducted as per procedure described for full thickness HSE, but immediately after desired contraction of the dermal layers.

6.2.8 HPLC Methods and Data Analysis

Analysis for drug content was conducted on an Agilent 1100 HPLC system (Agilent Technologies, USA) with an Agilent C18 RP column (Eclipse XDB-C18, 4.6×150 mm, 5 µm) (Agilent Technologies, USA). All methods were validated for linearity of the calibration curves, limits of detection and intra- and inter-day

variability. All parameters are reported in Table 8. For evaluation of permeability parameters, the cumulative amounts of drug per area (μg/cm^2) were plotted against time, and the steady state flux (Jss, μg/cm^2/h) was calculated as the slope of linear portion of the plot using linear regression (Microsoft Excel). Lag time (h) was obtained as the x-axis intercept of this linear part of the plot. Thereafter, the permeability coefficient (K_p, cm/h) was calculated as the ratio of the steady state flux to the concentration of the drug in the vehicle/formulation (C_o, mg/ml).

6.2.9 Reproducibility of HSE

The intra-batch (within a batch) and the inter-batch (different batches) variation in permeation parameters of the HSE model were assessed by *in vitro* permeability testing as described earlier. While the intra-batch variability was evaluated for different agents, the inter-batch variability was evaluated by keeping the drug constant (caffeine) and evaluating its permeation parameters through two/three pieces of each HSE batch produced over time.

6.2.10 Mechanical testing

The mechanical strength of the dermal components of the HSE and EpidermFT® were determined by inflation testing with the aid of a customized inflation device. To accommodate the dimensions of the inflation device, we constructed dermal matrices with larger diameters (~2.2 cm) by doubling the content of fibroblasts

and collagen and seeding the mixture in larger Petri dishes. The contracted dermal layers and similarly sized EpidermFT® tissues were sent for mechanical testing to Dr. K. L. Billiar (Worcester Polytechnic Institute, Worcester, Massachusetts). Upon receipt, EpidermFT® was separated into its epidermal and dermal components, and the latter was used for mechanical testing.

A schematic representation and an image of the inflation device(73, 74) is depicted in Figure 6.2. The biaxial failure testing of cultured tissues was conducted by clamping the tissues in the devices with the aid of an O-ring. A pressure load (measured by a transducer) was then applied to the tissue, and the clamped sample was inflated with isotonic PBS using a syringe pump. The resulting displacement and radius of curvature of the central region of the inflated sample was measured using Labview (National Instruments, Austin, TX). Load pressure was applied to all samples until they ruptured at or close to its center. Thereafter, the maximum membrane tension, *T* (N/m), a measure of structural strength, was calculated from the differential pressure, *P*, between the inside and outside of an inflated membrane and the local radius of curvature, *R*, using the Young-Laplace equation for a spherical membrane:

$$T = \tfrac{1}{2} PR \qquad \text{(Equation 6)}$$

The ultimate tensile strength (UTS, kPa), a commonly used measure of intrinsic strength of a material, was calculated by

$$UTS = T/t \quad \text{(Equation 7)}$$

where *t* is the initial thickness of the specimen before inflation.

6.2.11 Statistical Analysis

All data was analyzed with the aid of Microsoft Excel and Kaleida Graphs 4.02, (Synergy Software, Reading, PA). ANOVA ($p<0.05$) was used to determine statistical significance of data.

6.3 Results and discussion

6.3.1 Macroscopic, histological and ultrastructural features of HSE

The dermal layers made from collagen and fibroblasts contracted gradually over 6 days to tissue diameters that were proportional to the number of fibroblasts added to the matrix (Figure 6.3). While the matrices containing no fibroblasts did not contract at all, those containing 440,000 fibroblasts contracted fast, unevenly and presented an undulated surface. The dermal matrix containing 220,000 fibroblasts contracted gradually over 7 days to a smooth and even-surfaced tissue about 1 to 1.2 cm in diameter. Since this is the approximate diameter of a Transwell® insert to be used for culture of the full thickness HSE, the fibroblast cell number of 220,000/dermal matrix was used to culture the HSE in all

experiments. These results also confirm that the fibroblasts drive the dermal contraction of the matrix, as reported in literature by groups.(75)

After contraction, the dermal matrices were seeded with keratinocytes from the top, with a media containing increased calcium (1.2 mM) to facilitate the attachment of keratinocytes by promoting the formation of hemidesmosomes. After keratinocyte attachment, the HSE were cultured submerged in low calcium media (0.06 mM) to encourage the keratinocyte proliferation on the dermal matrix. Culture of keratinocytes in low calcium media (0.05-0.1 mM) has been shown to accelerate the proliferation of these cells with high growth fractions, while discouraging formation of desmosomes, stratification and maintaining the phenotype.(76) When the cultures were exposed to the ALI, the calcium concentration was increased to 1.2 mM to encourage the stratification of keratinocytes and formation of desmosomes.(76, 77)

Macroscopic observation of the surface of the skin equivalents post exposure to the ALI showed a transformation from wet and shiny surfaces to dry and matte yellowish surfaces 2–3 days post exposure to air, indicating the formation and differentiation of an epidermal layer. The HSE cultures were ~1,000 μm thick, and histological analysis after 7 and 21 days of culture showed an epithelial architecture resembling native epidermis with formation of a multilayered and differentiated epidermis, including the basal, spinous, and granular layers and a flattened stratum corneum (Figure 6.4 (A, B) and 6.5 (A)). Large amount of

keratohyalin granules were present in HSE in the granular layers (Figure 6.5 A). Keratohyalin granules are cytoplasmic granules that originate in the granular layer and contain profilagrrin and loricrin among other constituents that serve as precursors for the formation of the insoluble keratin bundles in the corneocytes.(78) Thus, these granules serve as prominent morphological hallmarks of differentiation in the epidermis and their presence indicates a normalized differentiation process. The normalized differentiation process was also validated by the presence of flat anucleated corneocytes in the 21 day culture of the HSE, seen by imaging a horizontal top-down H & E stained section (Figure 6.5 (B)) .

6.3.2 Involucrin localization and protein expression in HSE

Involucrin is a soluble protein that serves as a preferred substrate of transglutaminase, a major enzyme that catalyzes the formation of the cornified envelope by cross-linking involucrin and other membrane proteins of the stratum corneum. It is expressed relatively early in keratinocyte differentiation in epidermal layers that are 3-4 layers above the basement membrane and is later also expressed in the spinous layers (Figure 6.6 (B).(79, 80) In *in vitro* culture, the regulation of involucrin does not correspond with that of natural epithelia. In most SE, involucrin has been found to be expressed in the suprabasal layers and sometimes even extends into the basal layers.(81) (82) Involucrin and transglutaminase however form important markers of the keratinocyte terminal

differentiation process and are also indicators of the permeability barrier in SE.(83) We conducted preliminary studies to detect the expression of involucrin in the HSE model with the aid of an involucrin antibody kit. Involucrin expression was observed in HSE in the upper basal layers and the spinous and granular layer of the epidermis as seen in Figure 6.6 (A), which validates the presence of this important marker in the epidermal differentiation process.

Analysis of protein content in the HSE showed four clear patterns of qualitative and quantitative changes between protein species from ALI-7 (7 days of culture at ALI) (Figure 6.7, A) and ALI-19 (19 days of culture at ALI) (Figure 6.7, B). First, neither relative ratios of doublets nor abundance of single bands of protein species 1 to 6 show significant differences between ALI-7 and ALI-19. These serve as controls for sample loading. However, the abundance of either individual or groups of protein species 5a, 5b, 5c and 6 – 14 is evident in ALI-19 relative to ALI-7. The relative abundance of the group of protein species (box 14) suggests that they might be keratins which are known to be upregulated during the development of the epithelial layer. Finally, a third group of protein species 15 to 24 that is entirely absent in ALI-7 appears at varied abundance in ALI-19. Also, the doublet protein species 25 is less abundant in ALI-19 than in ALI-7 and therefore it is down regulated. The identity of the protein content of differentiating HSE and therefore the nature of the protein changes will require further analyses of total protein species by Liquid Chromatography–Mass Spectrometry/Mass Spectrometry (LC-MS/MS) and specific proteins excised from 2D gels by Matrix

Assisted Laser Desorption / Ionization-Time of Flight coupled Mass Spectrometry (MALDI-TOF-MS).

6.3.3 Distribution and Attachment of Cells in the SE Matrix

In order to visualize the distribution and viability of fibroblasts in the skin equivalent matrix, we used rat neonatal GFP-expressing fibroblasts to make the dermal equivalents and observed the matrices over 6 days of contraction under a fluorescent microscope. On the 1st day, the fluorescent cells were found to be uniformly dispersed throughout the matrix and exhibited a circular shape with a circularity index of 0.86 (SD: 0.04) (Figure 6.8, A). On day 4, and more so on day 6, the fibroblasts looked increasingly fibrous, displayed a uniform dispersion throughout the matrix and appeared to be growing well and proliferating in the collagen matrix (Day 4 circularity index: 0.43 (SD: 0.12) (Figure 6.8, B), day 6 circularity index: 0.22 (SD: 0.07) (Figure 6.8, C)). The circularity indices obtained for cells on day 4 and 6 were significantly different from that of day 1 ($p<0.05$). The health and homogeneity of the cells corresponded to the gradual contraction of the collagen matrix over 6 days to a dermal tissue.

In order to determine the attachment of keratinocytes on the surface of the collagen matrix and their homogeneity when attached, we labeled the nucleus of keratinocytes in suspension with Hoechst 33342 dye and seeded them on dermal matrices made with type I collagen and unlabeled dermal fibroblasts. When

viewed under a microscope one day after seeding, the keratinocytes had attached to the surface of the matrix and appeared to be uniformly distributed throughout the surface of the dermal layer (Figure 6.8, D).

6.3.4 Epidermal–dermal attachment and integrity in the HSE

The epidermal–dermal adhesion, contributed to a large extent by the presence of a basement membrane, is important for the integrity of a full thickness HSE during testing. Although the keratinocytes and fibroblasts produce basement membrane components in cultured skin equivalents, only traces of basement membrane formation have been observed in SE *in vitro*. Conjugation of extracellular matrix (ECM) proteins through passive adsorption on the dermal matrix can enhance the attachment and the subsequent proliferation of keratinocytes.(84, 85) We studied the effect of ECM proteins (fibronectin, collagen I and IV, laminin and a coating matrix kit consisting of collagen I and IV) on keratinocyte attachment to the dermal matrix with the aid of a Calcein fluorescence assay (Figure 6.9) and the MTS assay. All proteins significantly increased the keratinocyte adhesion to the wells of the polycarbonate plates. All individual proteins (fibronectin, collagen I and collagen IV) except for laminin increased the keratinocyte adhesion to the wells after 3 h of attachment, as seen in the results of the fluorescence assay (Figure 6.10, (A)) and confirmed by the MTS assay (Figure 6.11, (A)). However, the combination of collagen I and IV (Coating Matrix, CM) resulted in the highest percentage attachment in the

fluorescence assay (~68%) and also the highest cell absorbance in the MTS assay (Figure 6.10 (B) and 6.11 (B)). The coating matrix was also more economical than other proteins, and hence this combination was selected to be used in the HSE model. During future HSE culture, the CM was used to coat the surface of the dermal layers for 0.5 h at room temperature just before seeding the keratinocytes.

6.3.5 Permeability of the HSE to Model Drugs

We cultured HSE in serum-free conditions in the presence of external fatty acids/lipids (25 µM palmitic acid, 15 µM linoleic acid, 25 µM oleic acid, 7 µM arachidonic acid), ascorbic acid (100 µg/ml) and a PPAR-α agonist clofibrate (300 µM). This HSE cultured with the unique combination of additives (HSE-OP) was then evaluated for its permeability profiles of six model agents by *in vitro* diffusion studies and HPLC analysis. Validation of the HPLC methods for the agents resulted in robust methods with low high inter- and intra-day precision. All HPLC parameters are reported in Table 8.

In order to verify the location of the HSE permeability barrier, we compared the permeability profiles of three agents (caffeine, hydrocortisone and ketoprofen) through the full thickness HSE-OP and the dermal component of the HSE. The permeability profiles (Figure 6.12, Table 9) indicate that the penetration barrier of the HSE resides in the epidermis, evident from the significantly higher

permeation of compounds through the dermis. The cumulative permeation of caffeine, hydrocortisone and ketoprofen at the end of 24 h through the dermis was 3.4, 5.2 and 2.2 fold of their permeated amounts through the full thickness HSE-OP with high corresponding flux values. Thus, the histology and the permeation profiles both show that the HSE-OP epidermis undergoes normalized differentiation in order to produce the epidermal barrier lipids. However, the significantly higher permeation of ketoprofen through the dermal component (as compared to caffeine and hydrocortisone) suggests that the physiochemical properties of the compound affect the dermal permeability too, which in turn may contribute, although not to a great extent, to the permeation of agents through full thickness skin.

For evaluation of the permeability barrier of the HSE, we chose compounds differing in their physiochemical properties and their therapeutic potential. Caffeine (stimulant) (log P: –0.13± 0.37, MW: 194.12), hydrocortisone (steroid hormone) (log P: 1.42±0.47, MW: 362.47), DEET (insect repellant) (log P: 1.95 ±0.23, MW: 191.27), malathion (organophosphate insecticide) (log P: 2.92±0.34, MW: 330.4), paraoxon (organophosphate insecticide) (log P: 2.30±0.30, MW: 275.22), and ketoprofen (non-steroidal anti-inflammatory drug) (log P: 2.81±0.32, MW: 254.3) were all evaluated for their permeability through HSE, EpidermFT® and human cadaver skin. Although the HSE-OP demonstrated very similar permeation profiles for most agents when compared to EpidermFT® (Figure 6.13), a significant difference was observed between these models for caffeine

permeation (Figure 6.13 (A)), where the permeation parameters for HSE-OP (Q_{24}: 118.56 μg/cm^2, J: 9.46 μg/cm^2/h) were significantly lower than EpidermFT® (Q_{24}: 504.56 μg/cm^2, J: 38.53 μg/cm^2/h) ($p<0.05$). The cumulative amount of drug permeated, the steady state flux and permeability coefficient of all agents though the skin models are listed in Table 10. The lower permeability of the HSE-OP to the hydrophilic low molecular weight drug caffeine (MW: 194.19) may indicate intact structures of the lipid bilayers and the corneocytes in the epidermis of the HSE-OP which may provide a high barrier to diffusion for hydrophilic compounds. However, as no difference between HSE-OP and EpidermFT® was observed with other compounds of varying lipophilicities, further studies on the permeation pathways in reconstructed skin models and penetration profiles of other low molecular weight hydrophilic solutes will have to be intensively evaluated in order to derive significant conclusions. Differences in the permeability barrier of SE to hydrophilic and hydrophobic agents have also been observed by other research groups. Schmook et al.(47) found that Graftskin® LSE (Living Skin Equivalent, Organogenesis, Canton, MA) and HRE® (Human Reconstructed Epidermis, Skinethic, Nice, France) both provided an adequate barrier to the hydrophilic salicylic acid, but were very permeable to more hydrophobic compounds.

Overall, both reconstructed models, HSE and EpidermFT® depicted significantly higher permeability to all agents as compared to human skin. While permeabilities of caffeine, malathion and hydrocortisone were approximately 2, 3, 4 fold respectively of human skin, permeability of ketoprofen and DEET with

HSE-OP was ~5 and 7 times that of human skin (Figure 6.13). The overestimation of permeability by reconstructed skin models has been observed by several groups in literature.(41, 47, 86-88) In a skin absorption German prevalidation study, Schäfer-Korting et al. found that Epiderm®, Episkin® and SkinEthic® were 4, 46 and 60 fold permeable to caffeine as compared to human epidermis.(87)

A high difference in the permeability of HSE to paraoxon (MW: 275.19) was observed in our study (~25 fold higher permeability with HSE-OP as compared to human skin), with EpidermFT® mirroring the same permeability trend. The high permeability obtained for paraoxon with the skin equivalents could be a result of an underestimation of paraoxon permeability through human skin due to its decomposition during the extensive epidermal passage of native human skin.(89) Also, the human dermis has been postulated to exhibit a depot for moderately lipophilic compounds *in vitro*(90) and the dermatomed split thickness skin used in the experiments could have lead to increased diffusion and retention of this agent in the deeper skin layers thereby decreasing the transdermal permeation.

We attribute the generation of the permeability barrier in the HSE to the production of essential epidermal lipids due to a combined contribution by the added growth additives, all of which individually have been shown to be responsible for improvement in barrier lipid production. PPAR-α receptor agonists like clofibrate have been shown to significantly improve keratinocyte

differentiation and lead to production of a multilayered SC, mature lamellar membranes and a competent barrier.(91, 92) The presence of external fatty acids in the growth media probably enhanced the barrier by three probable mechanisms: i) naturally occurring fatty acids are known potent activators of PPAR-α, and their action has also been shown to generate epidermal homeostasis and accelerate barrier development, ii) the absence of essential fatty acids, such as linoleic acid has been shown to be responsible for epidermal abnormalities related to cutaneous essential fatty acid (EFA) deficiency. In skin, EFA deficiency is manifested as severe dryness and presence of scaly lesions, chronic epidermal hyperproliferation, abnormal differentiation and increased transepidermal water loss(93, 94), iii) the combination of palmitic acid, linoleic acid, oleic acid and arachidonic acid were postulated to induce the formation of precursors of barrier lipids (acylglucosylceramides) and induce the formation of lamellar bodies in a cultured skin substitute.(66) Lastly, ascorbic acid has been shown to induce the formation of the key ceramides responsible for barrier function. The presence of ascorbic acid in skin cultures was shown to elevate the ceramide and glucosylceramide synthesis, especially the α- and ω-hydroxylated species. This action can be attributed to the ascorbic acid led stimulation in the activity of ceramide synthase, a key enzyme in epidermal sphingolipid metabolism and generation of hydroxylated and non-hydroxylated ceramides.(95)

6.3.6 Reproducibility of the HSE

The average intra-batch reproducibility of the HSE was higher than its inter-batch reproducibility, a phenomenon that was observed in similar studies conducted with Epiderm®, Episkin® and SkinEthic®.(96) Although the average standard deviation produced by HSE within each batch was higher than that of EpidermFT® (Table 11), the overall % CV (Coefficient of Variation) for inter-batch testing (8 batches, % CV= 27%) was comparable to and sometimes even lower than that reported in literature(87) with SE models (Epiderm®= 55%, SkinEthic®=52%, Episkin®=25%).

6.3.7 Evaluation of mechanical strength

Because the dermal component provides for the mechanical strength in skin, we evaluated the mechanical strength of the dermal matrix used for our HSE in comparison to the corresponding dermal component of EpidermFT®. The mechanical strength for the HSE-OP dermis could not be recorded in the inflation machine as the force required for the inflation and subsequent rupture of the sample was below the noise range of the transducer. The strength of the dermal component of EpidermFT® was found to be 81 +/- 33 kPa. Although, both the dermal components of the SE (HSE and EpidermFT®) were mechanically weak, the dermal component of EpidermFT® was found to be stronger than HSE-OP.

6.4 Conclusion

A full thickness HSE was bio-engineered with mostly human cellular components and cultured in controlled environments with a unique combination of external free fatty acid mixtures, ascorbic acid and the PPAR-α agonist clofibrate (HSE-OP). The morphological analysis and immunohistochemistry studies showed that the HSE-OP possesses all epidermal skin layers, including the terminally differentiated SC. The presence of involucrin, a key marker of epidermal homeostasis, keratohyalin granules and the expression of several other proteins during the ALI culture shows that the HSE-OP epidermis undergoes normalized differentiation that subsequently leads to production of essential SC lipids, the critical components of the permeability barrier. This production of barrier lipids in the HSE-OP was a function of the unique combination of growth additives that was used during culture.

Despite the generation of a three-dimensional fully differentiated SE, the permeability of the HSE-OP to agents was higher as compared to human skin. Barring the case of paraoxon, the HSE-OP overestimated the permeability of agents by ~2 to 7 fold, and similar results were obtained with the commercially available model, EpidermFT®. The permeability overestimation of the HSE-OP is smaller than that reported in literature for other SE models, all of which have shown a large overestimation of permeability. A significant difference ($p<0.05$) in permeability between the HSE-OP and EpidermFT® was observed for the model drug caffeine, where the HSE-OP estimated lower permeability than

EpidermFT®. This indicates that the HSE-OP develops a good barrier for hydrophilic low molecular weight compounds. However, the behavior of skin models to permeability of compounds with various physiochemical properties can only be validated with a large library of compounds with differing properties.

The HSE-OP also showed good reproducibility with low variability in results, but was lacking in mechanical strength. In order to improve the mechanical strength of the HSE, we are currently investigating the incorporation of biocompatible tyrosine based polymers into the dermal matrix of HSE. This will increase the mechanical properties of the HSE and will also prolong its stability and culture life.

We conclude that the development and testing of the HSE-OP, along with its future validation represents an important step toward the use of these skin equivalents as reproducible and accessible skin models for permeation testing. The primary drawback of the HSE-OP, its overestimation of permeability, will be the focus of further research and attempts to further improve the lipid profile in the epidermis could result in their universal use for formulation testing and also in drug delivery. In the next chapters, we have evaluated the HSE for its ability to serve as a skin model for prediction of phototoxicity of topical and transdermal formulations and for evaluation of functional properties of multicomponent formulations.

Note: *We would like to acknowledge funding by U.S. Army Medical Research Institute of Chemical Defense (USAMRICD) and Center for Military Biomaterials Research (CEMBR). The authors would also like to thank Dr. Prafulla Chandra for his suggestions during culture experiments of the Human Skin Equivalent and Dr. Ferez Nallaseth for his contribution to the protein expression study.*

7 Phototoxicity evaluation of Hydroxycinnamic acid using the *in vitro* 3T3 NRU assay and three-dimensional Human Skin Equivalents

7.1 Introduction

Phototoxicity is an abnormal cutaneous response that occurs due to a combination of a chemical and UV light. Typical phototoxic reactions include redness, erythema, edema, desquamation and hyperpigmentation, but severe cases can lead to photocarcinogenicity. Evaluation of phototoxicity of topical formulations has received increasing attention in recent years, in line with the current wave of replacement of animal testing with validated *in vitro* cell based studies. Also, it has been discovered over the past years that many commonly used compounds that appear innocuous may actually possess phototoxic potential depending on their ability to absorb light in the UV range. Examples of such compounds are vitamin A derivatives, tetracyclines (doxycycline, tetracycline), NSAIDs (ibuprofen, ketoprofen) and ingredients used in personal care products such as sunscreens. One category of increasingly used personal care products today are skin brightening agents, used worldwide for the treatment of irregular pigmentation such as age spots, creation of a more even skin tone and for enhancement of overall beauty. Hydroxycinnamic acid (HCA) is one such recently launched skin lightening agent that in the past couple of years has come to be used in a wide range of topical skin care formulations such as

sunscreens, moisturizing lotions, cleansers and body washes. It acts as a skin brightening agent and an antioxidant, due to its tyrosinase inhibition properties and radical scavenging activities respectively. However, little is known about its phototoxic and cytotoxic effects upon exposure to UV radiation.

While all UV radiation is harmful, UVC rays (<280 nm) are absorbed by the ozone layer and do not usually reach the earth's surface. UVA and UVB on the other hand are responsible for the most harmful effects to human skin on exposure to sunlight. While UVB rays (280 - 320 nm) can only reach the outer skin layer (epidermis), UVA rays (320 - 400 nm) can penetrate the epidermis and the dermis and can act on the connective tissue and collagen in the skin. In addition, most phototoxic reactions are activated in the UVA range, because many compounds, including HCA, absorb light in this range. Thus although HCA and its derivatives are plant based phenolic acids, they may be potentially phototoxic and need to be evaluated for their skin irritation potential upon topical application.

The validated method for evaluation of phototoxicity *in vitro* involves testing the substances for their phototoxic potential in fibroblast cell lines. The European Union (EU) represented by ECVAM (the European Centre for the Validation of Alternative Methods), in collaboration with European Cosmetic Toiletry and Perfumery Association (COLIPA) and ZEBET (Germany) has validated the *in vitro 3T3 NRU* (Neutral Red Uptake) test for *in vitro* testing. This test is

conducted on Balb/c 3T3 fibroblasts and is widely recommended as the primary method of choice for phototoxicity testing.(49) The phototoxicity is measured as an inhibition of the capacity of the cell cultures to take up a vital dye, Neutral Red, one day after treatment (treatment involves application of a test article to the cells in the presence and the absence of a non cytotoxic dose of UVA light).

The use of a cell monolayer for the test provides a rapid, inexpensive, simple and reproducible method as common problems of animal/human testing such as variability in skin source, thickness and pigmentation are avoided. However, testing with the Balb/c 3T3 fibroblasts may not be reflective of a phototoxic reaction *in vivo*. For this reason, Skin Equivalent (SE) models have also been evaluated over the years for phototoxicity testing. The SE can account for the bioavailability of chemicals after passing through the skin barrier and also the metabolism of compounds in skin and thus offer significant advantages over cell monolayers. Also, the cell lines cannot be used for testing compounds that are insoluble/sparingly soluble in aqueous media or for finished formulations (creams, perfumes, sunscreens). Lastly, while the test on cell lines involves only one type of cells (fibroblasts), the SE models reflect a three-dimensional *in vivo* environment with multiple cell lines (keratinocytes and fibroblasts) and extracellular matrix. Some of the SE models evaluated for phototoxicity are Epiderm® (MatTek, VA, USA), SkinEthic® (SkinEthic laboratories, France) and Episkin® (L'Oreal, France). The Epiderm® model is currently being validated for phototoxicity testing by the EU Validation Centre, ECVAM. Though all the skin

models that have been evaluated for phototoxicity are ‘epidermis only’ models, we predict that our full thickness collagen based Human Skin Equivalent (HSE) will also serve as a suitable model for this application.

This chapter involves the evaluation of phototoxic potential of HCA by the 3T3 NRU assay and the three-dimensional HSE. Both models were evaluated for their potential to discriminate correctly between phototoxic and non-phototoxic compounds and later used to determine the phototoxicity potential of HCA.

7.2 Materials

Hydroxycinnamic acid (HCA) was provided by Lipo chemicals, Inc. Balb/c 3T3 cells, clone A31 were obtained from ATCC (Manassas, VA). Dulbecco’s modified Eagles medium (DMEM), calf serum, DMSO for molecular biology, Hanks Balanced Salt Solution (HBSS) and Chlorpromazine were obtained from Sigma Aldrich (St. Louis, MO). The SOL 500 lamp and the UV meter (type 16501) were procured from Hönle, (Martinsried, Germany).

7.3 Methods

7.3.1 Phototoxicity evaluation in Balb/c 3T3 fibroblasts (Figure 7.2 (A))

7.3.1.1 Cell culture

Balb/c 3T3 cells (Passage 63) obtained from ATCC were grown and expanded from the initial stock and cryo-preserved at -80^{0}C until use. Four days before each experiment, the cells were thawed and cultured in T-75 cc flasks with Dulbecco's modified Eagle's medium (with 4 mM L-glutamine, 4.5 g/l glucose, 1.5 g/l sodium bicarbonate, 10% calf serum, 100 IU/ml penicillin, 100 µg/ml streptomycin). This medium is referred to as complete culture medium. The cells were grown until 80% confluence and then subcultured and used for the *in vitro* experiments.

7.3.1.2 Irradiation equipment and procedure

The UV light source used was Hönle SOL 500 lamp (Martinsried, Germany) equipped with a H-1 filter (Dr. Hönle, Martinsried Germany) that produces a spectrum almost devoid of UVB light (<320 nm). This solar simulator was mounted inverted on a customized lamp docking equipment constructed in our laboratory (Figure 7.1). This docking equipment has adjustable levels that allow the lamp to move vertically in order to modify the distance from the light source (lamp) and the sample. The irradiation incident on the sample is a factor of this distance of the light source from the sample, which was adjusted to achieve an

irradiance of 1.7 J/cm^2, the recommended intensity. The incident irradiation was measured with the aid of a UVA meter (type 1650, Hönle, Germany). The entire lamp equipment was covered with a thick black cloth to focus the incident UVA irradiation on the sample.

7.3.1.3 Preparation of cultures in 96 well plates

On day one of the experiment, Balb/c 3T3 fibroblasts were seeded in the wells of two 96 well plates (one for determination of phototoxicity (+UVA) and another for cytotoxicity (-UVA)) at a density of 1X10^4 cells/well. To do this, a cell suspension of 1X10^5 cells/ml was prepared in the complete culture medium and 100 µl of the cell suspension was seeded into the center 60 wells of the plate using a multi-channel pipette. In the peripheral wells of the 96-well plate, 100 µl of the complete culture medium only was added (blank). The plates were incubated overnight at 37^{o}C, 5% CO_2 to allow a half-confluent monolayer to form.

7.3.1.4 Treatment of cells with test articles and UVA irradiation (day two)

Range finder experiment: Test articles were prepared in 8 concentrations, made by geometric dilution with a factor of 3.16, to encompass a broad range of concentrations for HCA and the positive control Chlorpromazine (CPZ). The concentrations were prepared by making stock solutions in DMSO and diluting with HBSS to achieve final concentrations of: 1000, 316, 100, 31.6, 10, 3.16, 1, 0.316 µg/ml. The final amount of DMSO in all concentrations was 1 %.

Main Experiment: A narrow range of concentrations centered around the EC_{50} values obtained from the range finder experiment was used for the main experiment. A small dilution factor (1.47) was used to attain a narrow concentration range, which was targeted to include at least three cytotoxic concentrations between 10% and 90%. The final amount of DMSO in all concentrations was 1 %.

The next day after cell seeding, the cells were observed to ensure the formation of half confluent monolayers. The culture medium in the wells was decanted and excessive media was removed. 100 µl of the HCA and CPZ concentrations were added to the wells in replicates of three. Two lines of wells, one each on the right and left were treated with the negative control (HBSS with 1% DMSO). After addition of the treatment solutions, the plates were incubated for 60 minutes at 37^{o}C and 5% $CO_{2.}$ To perform the (+UVA) part of the assay, the (+UVA) plates were exposed to the irradiation from the SOL 500 lamp for 50 minutes at a dose of 1.7 mW/cm^2 through the plate lid, leading to a cumulative dosage of 5 J/cm^2. The irradiation dose incident on the plate was measured using the calibrated UVA meter. The duplicate plate (-UVA plate) was kept at room temperature in a dark box for 50 min (equals the +UVA exposure time). After irradiation, the test solution was decanted from the wells and the cells were washed once with 150 µl HBSS. The HBSS was then replaced with complete culture medium and the plates were incubated at 37℃ and 5% CO_2 overnight (18-24 h).

7.3.1.5 Neutral Red Uptake

On day three of the experiment, the cells were observed under a phase contrast microscope to evaluate the cytotoxic effects of the test chemical, and changes in morphology were recorded. The culture medium was removed and 100 µl Neutral Red medium (50 µg/ml) was added to each well and the plates were incubated at 37^{o}C in a humidified atmosphere of 5% CO_2 for 3 hours. After 3 hours the Neutral Red medium was removed completely and the cells were washed once with 150 µl HBSS followed by careful decantion. 150 µl of Neutral Red extractant solution (50% ethanol, 49% water, 1% Glacial Acetic Acid) was added to each well and the plates were shaken on a microtiter plate shaker for one hour or until a homogenous extract was observed. The absorbance of the resulting solution at 540 nm was measured in a plate reader using the mean of the outer wells (blanks) as a reference.

7.3.1.6 UVA sensitivity

In order to be used for the phototoxicity assay, the Balb/c 3T3 cells should not be sensitive to UVA light, since the measure of phototoxicity involves a combination of the test sample and UVA light. The UVA sensitivity of the cells were measured by treating half confluent 3T3 cells in 96 well plates with the negative controls (HBSS and 1% DMSO) and exposing the cells to different doses of UVA irradiation ranging from 1J/cm^2 to 9J/cm^2 keeping a second plate as unexposed

control. The Neutral Red uptake of all treated cells was measured as described above in 'Neutral Red Uptake" and % viability of cells was calculated.

7.3.1.7 Data analysis

For the range finder experiment, percentage of cell viability obtained from absorbance data was plotted against concentrations of HCA/CPZ to derive the dose response curves and the corresponding EC_{50} values, both with and without UVA exposure (EC_{50} UVA(+) and EC_{50} UVA(-) respectively). EC_{50} was defined as the concentration responsible for 50% cytotoxicity. Photo-Irritancy Factor (PIF) where applicable, was derived as a ratio of EC_{50} UVA (-) / EC_{50} UVA (+) and was used to determine the phototoxic potential of compounds.

For the main experiment, the EC_{50} UVA(+) and EC_{50} UVA(-) and the PIF were calculated with the aid of Phototox version 2.0 (ZEBET, Germany), a software developed especially for calculation of phototoxicity parameters.

7.3.2 Phototoxicity evaluation using the HSE

7.3.2.1 Culture of HSE

The HSE was cultured as described in Chapter 6: "Preparation of the Full Thickness HSE Model". Briefly, the matrix of the HSE was constructed from

dermal fibroblasts, type I collagen and epidermal keratinocytes. A full thickness HSE was obtained after complete differentiation of the epidermis when exposed to the Air-Liquid Interface (ALI) to produce all epidermal layers including the stratum corneum. During culture at ALI, the HSE was supplemented with a unique combination of media additives including external fatty acids, ascorbic acid (100 µg/ml) and clofibrate (300 µM). The exact composition of the media additives and their functions are described in detail in chapter 6. HSE cultures at 21 days of exposure to the ALI were used for the phototoxicity studies.

7.3.2.2 Proof of concept experiment with CPZ

In order to determine the capability of the HSE tissues to evaluate the phototoxic potential of CPZ, a preliminary experiment was conducted by treatment of HSE tissues with two concentrations of CPZ (50 µg/ml and 150 µg/ml, n=2 for each). Two other tissues were treated with negative control (PBS + 1% DMSO). 100 µl of the CPZ concentrations/negative control was added from the top (stratum corneum surface) to the tissues while they were cultured in maintenance media (Epilife® 50% and DMEM 50%) from the bottom (Figure 7.2 (B)). Duplicate plates with the HSE tissues were treated with the CPZ concentrations for 18 h at 37^0C, 10% CO_2 at 75%RH. After treatment, excess treatment solution was removed and one plate (n=6 tissues) was exposed to UVA irradiation at an intensity of 1.7 mW/cm^2 for 50 min through the plate lid leading to a cumulative dosage of 5 J/cm^2 with the aid of an SOL 500 lamp and a calibrated UVA meter. The

duplicate plate was kept at room temperature in a dark box for 50 min (= +UVA exposure time). After UVA exposure, the plates were transferred back to the incubator and allowed to remain for 2 h (latent period). After 2 h, the tissues were washed twice with 500 µl PBS and supplemented with 500 µl maintenance media (50% DMEM + 50% Epilife®) from the bottom and incubated at 37^0C for 18-20 h. After overnight incubation, the maintenance media was removed and replaced with 500 µl of 1 mg/ml MTS solution in plain DMEM for 3 h at 37^0C. After 3 h, an aliquot of 100 µl was withdrawn from the wells and the absorbance was measured with a plate reader at 490 nm. In addition, the MTS solution in the HSE tissues was extracted by shaking with 1.5 ml of Isopropanol for 2 h. The absorbance of the extracted MTS solution was measured with a plate reader at 490 nm.

7.3.2.3 UVA sensitivity

In order to confirm that the HSE tissues were not UVA sensitive, they were exposed to a range of UVA irradiation from 1J/cm^2 to 9J/cm^2 after treatment with PBS + 1% DMSO. Two tissues were used for each radiation dose, while two tissues were kept in a dark environment as negative controls. Tissues were irradiated as described earlier and evaluated for viability using the MTS assay.

7.3.2.4 Evaluation of phototoxic potential of HCA with the HSE

HSE tissues cultured until 21 of the ALI exposure were treated with four concentrations each of CPZ and HCA (n=4 for each concentration) and the negative control (PBS + 1% DMSO) for 18 h at 37^0C, 10% CO_2 at 75% RH. The irradiation and measurement of tissue viability was conducted as described earlier in: “Proof of concept experiment with CPZ”.

7.3.2.5 Data analysis

Cell viability (%) obtained from absorbance data in the presence and absence of UVA light was plotted against concentration of HCA/CPZ to derive the dose response plots, and compared to the cell viability of the negative control.

7.4 Results and Discussion

7.4.1 Validation of the irradiation equipment

The distance between the lamp source and the sample was adjusted with the aid of the adjustable docking equipment. The distance to achieve an irradiation intensity of 1.7 mW/cm^2 was found to be ~39 inches. Before the beginning of each experiment, this distance was fine-tuned to achieve the desired intensity.

7.4.2 UVA sensitivity of Balb/c 3T3 fibroblasts

This experiment was conducted to assess the sensitivity of the cells to UVA light and to ascertain that any phototoxic reaction in the experiments would occur only due to a combination of the chemical and UVA light and not due to UVA light alone. Cell cultures are considered to not be sensitive to UVA light, if the viability after irradiation with a UVA dose of 5J/cm^2 is at least 80% of non-irradiated cells, and after irradiation with a UVA dose of 9J/cm^2 is at least 50% of non-irradiated cells. As seen in Figure 7.3, the % viability of the fibroblasts after irradiation at 1 and 5J/cm^2 was ~ 100 % and at 9J/cm^2 was ~ 60% of controls. Thus, the Balb/c 3T3 fibroblasts were not found to be sensitive to the doses of UVA light used in the phototoxicity experiments.

7.4.3 Phototoxicity evaluation of HCA in Balb/c 3T3 fibroblasts

According to the European Center for Validation of Alternative Methods (ECVAM) and the OECD (Organization for Economic Co-operation and Development) test guidelines – TG 432, a test substance with a Photo-Irritancy Factor (PIF) < 5 predicts: “no phototoxicity” and PIF > 5 predicts: “phototoxicity”. The dose response curves and the EC_{50} values of HCA and CPZ from the range finder experiment are depicted in Figure 7.4 and Table 12. EC_{50} values obtained from the ‘percentage viability vs. concentration curves’ for HCA and CPZ were found to be lower for the cells that were exposed to UVA irradiation (EC_{50} UVA (+)). Both EC_{50} values (UVA (+) and UVA (-)) for HCA were much higher than those

for CPZ indicating the low cytotoxicity potential of HCA. The PIF value for CPZ from the range finder expt. was found to be 28.46 which indicates that CPZ is a phototoxic compound and also served as an effective positive control. The corresponding PIF value for HCA was found to be 4.06, which demonstrates the non-phototoxic potential of HCA as the PIF was < 5. Microscopic observations of the cells post-treatment demonstrated cytotoxic effects of CPZ on the cells, especially in the presence of UVA irradiation where severely fragmented cells were observed. Cells treated with HCA did not exhibit signs of cytotoxicity and appeared healthy even after UVA irradiation.

The lack of phototoxicity of HCA was confirmed from the main experiment (the neutral red uptake endpoint and the dose-response curve are shown in Figures 7.5 and 7.6). Vast difference between the neutral red uptake and the corresponding dose response curves of CPZ (in the absence and presence of UVA light) indicate the significant difference in viability of the UVA treated (EC_{50}= 1.46 µg/ml) and untreated (EC_{50}= 26.15 µg/ml) cells. The PIF ratio for CPZ from the main expt. was found to be 17.9, confirming its phototoxicity (PIF >>> 5). Also, CPZ consistently served as a good positive control in all experiments with EC_{50} UVA (+) ranging from 0.7-1.5 µg/ml and EC_{50} UVA (-) ranging from 21-27 µg/ml. OECD requirements for the effective functioning of CPZ as a positive control are: EC_{50} values in the ranges of 0.2-2.0 µg/ml for UVA (+) and 7.0-90 µg/ml for UVA (-), with a PIF > 6.(97)

The UVA (+) and UVA (-) dose response curves of HCA from the main expt. were almost overlapping, indicating that there was negligible difference in the viability of the UVA treated (EC_{50}= 676.25 µg/ml) and untreated (EC_{50}= 722.69 µg/ml) cells. The PIF for HCA was 1.08 with a toxicity probability of 0.0 (Phototox Software 2.0), thus classifying HCA as a non-phototoxic compound. The lack of toxicity of HCA on the cells was also confirmed from microscopic observations (Figure 7.7) post-treatment with HCA and UVA light, where the cells appeared healthy. On the other hand, cells treated with the combination of UVA light and CPZ were manifested as unhealthy, fragmented cells, confirming the harmful phototoxic effects of CPZ on the fibroblasts.

7.4.4 UVA sensitivity and phototoxicity evaluation of CPZ in HSE tissues

The insignificant decrease in the viability of HSE tissues treated with different doses of UVA light (Figure 7.8) indicate that these tissues are not UVA sensitive. The phototoxicity of CPZ in the HSE tissues was evaluated by treating the tissues topically with CPZ and a non-cytotoxic dose of UVA light and measuring the decrease in viability of the cells in the lower epidermal layers of the HSE by the MTS assay. The MTS tetrazolium compound is reduced in viable cells into a colored formazan compound (purple) which is soluble in tissue culture media. This conversion occurs via dehydrogenase enzymes which are present in live cells. Thus, the quantity of formazan produced when measured by absorbance at 490 nm is directly proportional to the number of viable cells in culture. The

phototoxic effects of CPZ on the HSE tissues were obvious from the qualitative results (Figure 7.9) where the treated tissues and the corresponding media in the wells have turned to a deep purple color in the absence of UVA light. In the presence of UVA light, the negative controls show a high viability, while the CPZ treated tissue demonstrate low viability and hence a phototoxic effect. The quantitative determination of HSE viability (Figure 7.10) confirmed the qualitative observations of the phototoxic effects of CPZ on these tissues. Both the quantitative methods, MTS solution taken from the wells and extraction of MTS from the HSE tissues demonstrated phototoxic effects of CPZ on tissues. However, the differences in the effect of the concentrations were more pronounced with the solubilized MTS solution taken from the bottom of the wells. Hence, this method was used for the evaluation of phototoxicity of HCA in HSE.

7.4.5 Phototoxicity evaluation of HCA in HSE tissues

A progressive decrease in the viability of HSE tissues was observed with the combination of UVA irradiation and increasing doses of CPZ (Figure 7.11). At the same time, the viability of the UVA (-) tissues did not decrease correspondingly, indicating that CPZ was toxic to the tissues in the presence of UVA light. The % viability for CPZ in presence of UVA light decreased by 22-61% of the UVA (-) tissues, for the four different concentrations of CPZ (Table 14). Research groups that have utilized SE for phototoxicity testing have defined a compound as phototoxic if one or more test concentrations induced a decrease in cell viability

exceeding 25% as compared to cell viability without UVA exposure for the identical test concentrations.(98) By this definition, it can be confirmed that CPZ was clearly phototoxic to the HSE tissues. On the other hand, treatment of the tissues with different concentrations of HCA and UVA light did not reduce the viability by greater than 3% of untreated controls for any tested concentration (Table 14 and Figure 7.11), indicating that HCA was not phototoxic.

7.5 Conclusion

The 3T3 fibroblasts and the HSE both were able to clearly distinguish between phototoxic compounds (CPZ) and non-phototoxic compounds (HCA). In the 3T3 NRU uptake assay, the PIF of HCA was always < 5, thus classifying this compound as non-phototoxic. This was confirmed by the HSE assay, where the viability of the tissues did not decrease by > 3% when treated with a combination of different concentrations of HCA and UVA light as compared to the unexposed controls. HCA can thus be used in topical formulations without concerns of phototoxicity. The ability of the HSE tissues to accurately discriminate between phototoxic and non-phototoxic agents establishes the possible application of this model for phototoxicity evaluation. Since the phototoxicity reaction takes place in the lower epidermal layers, this study also validates the formation of a uniform epidermis in the HSE and the applicability of the MTS assay to this method. All studies conducted for phototoxicity evaluation in SE have used the traditional MTT assay, where the purple formazan crystals are extracted from the skin by

dissolution in appropriate solvents. The MTS assay used in our studies produces a soluble end-product that permeates from the epidermis into the media below the Transwell® inserts, and can be easily collected and evaluated for its absorbance in a plate reader. Also, all SE used for this application have been restricted to epidermis only models. Our studies confirm that the full-thickness HSE can be used for phototoxicity evaluation with the aid of the MTS assay, which eliminates the need for a key extraction step in the process, thereby possibly reducing the variability in the results.

Research groups that have evaluated SE for phototoxicity determination have so far not established a factor for correlation of results between the SE model and the *in vitro* 3T3 NRU assay. Both models have served to complement each other and confirm the potential or the lack of phototoxicity of compounds. The utilization of our HSE for this assay confirms its normalized *in vitro* development as a three-dimensional tissue that can also be used for cytotoxicity evaluation in addition to its intended application for permeability screening.

Note: *The authors would like to thank Dr. Nava Dayan and Dr. Rajarajeswari Sivalenka from Lipo Chemicals Inc. (Paterson, NJ) for providing us with the opportunity and funding for this project. The authors would also like to acknowledge the contribution provided by John Khan for construction of the lamp docking equipment.*

8 Application of the Human Skin Equivalent (HSE) for prediction of functional properties of multicomponent formulations

8.1 Introduction

Human skin equivalents or reconstructed skin alternatives have been evaluated over the last decades for their application as models for skin irritation and permeability testing, as skin transplants in wounds and burns and as models for study of skin pharmacology, biochemistry and diseases. Of the various explored applications for these bioengineered models, these skin alternatives today are used primarily for skin transplants and as *in vitro* skin irritation models. The recent wave of regulations that call for replacement of animal testing for analysis of many topically applied products and actives has created a renewed interest and a thrust in the development and validation of these skin models, with special focus on their application for safety and efficacy evaluation of products. The Skin Equivalents (SE) have recently, after successful validation, received approval for their use as alternatives for safety/corrosivity testing of topical/transdermal formulations by ECVAM (European Centre for the Validation of Alternative Methods) – the EU validation committee for alternative testing models. However, their use for permeability/absorption testing has not been universally accepted due to their weak permeability barrier and the subsequent overestimation of

permeability of agents as compared to human skin *in vivo*. Several of the commercially available SE models have been evaluated for their permeability characteristics, but have demonstrated several fold higher permeability as compared to human skin (Epiderm® :2 to 8 fold, Episkin® : 4-10 fold, Skin Ethic® : 2.5 to 30 fold higher than human skin).(99) Despite their overestimation of permeability, these SE correctly estimate the rank-order of agents according to their permeability profiles. Thus, they can be used for the initial high-throughput screening of agents for narrowing down the library of lead compounds based on their permeability characteristics. Most permeability testing studies conducted in the SE has however been restricted to simple solutions of a drug/agent, with fewer studies conducted on the permeability of agents when incorporated in multicomponent formulations.(100, 101)

We have developed a full thickness HSE in our laboratory that is bioengineered *in vitro* with human derived cells and an extracellular matrix containing bovine collagen, and exhibits all histological layers present in human skin *in vivo*. The HSE was cultured with a unique combination of media additives that served to normalize the epidermal differentiation process and increase the generation and deposition of essential skin barrier lipids, thereby reducing its permeability to compounds. The culture, optimization, characterization and permeability profiles of this model have been detailed in chapters 6 and 7. Though this HSE model overestimated the permeability of the tested agents, its permeability profiles were similar to the leading commercial SE EpidermFT®, and in fact were significantly

better for caffeine, a hydrophilic low molecular weight agent. In conjunction with studies focused on bolstering the permeability barrier of the HSE, we also studied the application of the HSE as a model for evaluation of the *in vitro* functional properties of multicomponent formulations. For this purpose, we selected two formulations with varying functions: (i) a barrier cream for retardation of skin penetration of compounds and (ii) a novel polymeric nanocarrier formulation for enhancement of skin penetration of compounds.

The barrier cream, SERPACWA (Skin Exposure Reduction Paste Against Chemical Warfare Agents) is a topical protectant developed by the U.S. Army Medical Research Institute of Chemical Defense (USAMRICD) and was approved by the FDA in 2000.(102) It is recommended to be used in conjunction with Mission Orientated Protective Posture (MOPP) gear to reduce or delay the absorption of chemical warfare agents through the skin. SERPACWA is a viscous white paste containing 50:50 mixture of perfluoroalkylpolyether and polytetrafluorethylene (PTFE). Its efficacy has not been demonstrated beyond 5 hours of use and it is indicated to be applied to skin before exposure to toxic agents. The efficacy of SERPACWA has been evaluated extensively *in vivo* with the help of a clipped rabbit model, where the barrier cream showed a significant decrease in the size of HD (sulfur mustard) induced skin lesions relative to unprotected controls. The USAMRICD has already developed newer formulation alternatives to the original SERPACWA cream, with the newer generation of barrier creams consisting of a combination of physical and chemical protection as

compared to just physical protection provided by SERPACWA. Such development efforts frequently require the assessment of the functional efficacy of these formulations, primarily their protectant effect against skin penetration of toxic chemical warfare agents and their simulants. This testing cannot be conducted *in vivo* in humans and animals due to safety reasons and the extensive scope of animal cruelty. In addition, the large variation in data and difficulties in procurement of human skin from tissue banks makes the *in vitro* skin equivalent model a perfect alternative for the evaluation of these barrier creams. We used our optimized HSE for evaluation of the barrier properties of SERPACWA by studying its retardation effect on skin permeation of paraoxon, a pesticide and chemical warfare agent simulant. In order to evaluate the efficacy of the HSE as a suitable skin model for this application, results obtained from the HSE studies were compared to similar data obtained from experiments with human cadaver skin.

The second multicomponent formulation evaluated on the HSE was the topical delivery system containing polymeric nanospheres (NSP) in gel or aqueous forms, with and without the skin penetration enhancer Azone. These NSP have been developed, characterized and evaluated in our laboratory for their ability to deliver lipophilic agents to deeper skin layers (studies described in detail in Chapters 4 and 5). We have tested these formulations in human cadaver skin *in vitro* and in the domestic pig *in vivo*, where the NSP-containing formulations have been shown to deliver significantly higher amounts of the lipophilic dye Nile Red

(NR) to the epidermis and the dermis as compared to the solutions of NR in propylene glycol. Our studies have shown these NSP formulations to serve as biocompatible, non-toxic skin penetration enhancement carrier systems for delivery of hydrophobic and poorly water soluble compounds. We evaluated the skin delivery of NR via these NSP formulations to the skin layers of the HSE model. These studies have enabled us to compare the formulation efficacy of the NSP formulations in three different skin models: human skin *in vitro*, animal model *in vivo* and human skin alternative *in vitro.*

8.2 Methods

8.2.1 Evaluation of barrier properties of SERPACWA in human skin

Human skin was obtained from a tissue bank (New York Fire Fighters, NY) and stored at -80^{0}C until use. The skin was thawed at room temperature before each experiment and cut into one inch square pieces for mounting on diffusion cells. The skin pieces were then allowed to hydrate for 1 h with PBS (Phosphate Buffer Saline) and mounted on vertical Franz diffusion cells (0.64 cm^2, 5.1 ml) with PBS (pH = 7.4) in the receptor compartment, continuously stirred at 600 rpm (total n=18) . In six diffusion cells, 20 µl of DEET was added on top of the skin and allowed to remain for 1 h. ~50 µl of the barrier cream (SERPACWA) was then applied to the dorsal surface of the skin with a syringe (n=12, including 6 cells with pre-applied DEET), spread with a glass rod and allowed to remain for 1 h. The quantity of the applied SERPACWA was adjusted to achieve thickness of ~

0.3 mm on top of the skin. Paraoxon (50 µl) was then added to the donor compartments of all the diffusion cells (n=18, including 6 cells for control - no SERPACWA application) and the donor compartments and the sampling ports were covered with Parafilm®. Receptor compartment samples (300 µl) were taken at 0, 1, 2, 3, 4, 5 and 6 h and replaced with an equivalent amount of fresh buffer. After 6 h, the covering Parafilm®, the donor and 2 Q-tip swabs from the skin surface were added to wells of a 6 well plate, washed with 5 ml of ethanol:water (50:50) and shaken slowly on a shaker for 2 hrs. The skin was removed and added to vials containing 5 ml of ethanol:water (50:50) and shaken rapidly on a shaker overnight. The donor and the skin samples were filtered and all samples were analyzed by HPLC for paraoxon content. The amount of paraoxon permeated through human skin over 6 h and the amount retained in the skin, in the presence and absence of SERPACWA was determined. The effect of concurrent application of DEET, a commonly used insect repellant in the battlefield on the barrier properties of SERPACWA was also determined in this experiment.

8.2.2 Evaluation of barrier properties of SERPACWA in HSE

HSE was cultured *in vitro* with unique growth media additives using the procedure described earlier in Chapter 6. After 21 days of culture at the Air-Liquid Interface (ALI), the HSE pieces were mounted on Franz diffusion cells (0.196 cm^2, 4.1 ml) with PBS (pH = 7.4) in the receptor phase. Three treatments:

(a) paraoxon 5 µl (control) (b) paraoxon 5 µl + SERPACWA (15 µl) added on top on the center portion of the HSE (c) paraoxon 5 µl + SERPACWA (15 µl) + DEET (5 µl) were evaluated. The application of SERPACWA, DEET and paraoxon to the HSE was similar to the procedure described in the human skin experiments. Receptor compartment samples (300 µl) were taken at 0, 1, 2, 3, 4, 5 and 6 h and replaced with an equivalent amount of fresh buffer. After 6 h, the covering Parafilm®, the donor and one Q tip swab from the skin surface were added to wells of a 6 well plate, washed with 5 ml of ethanol:water (50:50) and shaken slowly on a shaker for 2 hrs. The HSE pieces were removed and added to vials containing 5 ml of ethanol:water (50:50) and shaken on a shaker overnight. The washings from the donors and the treated skin samples were filtered and all samples were analyzed by HPLC for paraoxon content.

8.2.3 HPLC of paraoxon and data analysis

HPLC analysis for detection of paraoxon was conducted on an Agilent 1100 HPLC system (Agilent Technologies, USA). Samples (20 µl) were run on an Agilent C18 reverse phase column (Eclipse XDB-C18, 4.6 X 150 mm, 5 µm) with Tetrahydrofuran (THF): Acetonitrile (ACN): 0.01M sodium phosphate buffer pH 7.4 (12:25:63 v / v / v) as the mobile phase at a flow rate of 1 ml/min. Paraoxon was detected at 280 nm. All results were analyzed with the aid of Microsoft excel, and ANOVA ($p<0.05$) was used for statistical analysis (Kaleida Graphs 4.02, Synergy Software). The cumulative amount of paraoxon permeated through the

skin models at the end of 6 h (Q_6), steady state flux (J_{ss}) and lag time were determined. The penetration modification (enhancement/retardation) factor after various treatments was determined as:

$$\text{Penetration Modification} = \frac{\text{Cumulative permeation after SERPACWA treatment}}{\text{Cumulative permeation in control (no treatment)}}$$

The penetration modification obtained for the two skin models, human skin and HSE, were compared in order to determine the efficacy of the HSE as a skin model for estimation of the functional properties of SERPACWA.

8.2.4 Skin delivery of NR via the Nanosphere formulations in the Human Skin Equivalent model

HSE was cultured *in vitro* with unique growth media additives as per procedure described earlier in chapter 6. NR-NSP aqueous and gel formulations with and without Azone (0.2 M) were prepared as described in chapter 5. After 21 days of culture at the Air-Liquid Interface, the permeation of NR via various formulations was evaluated with the aid of *in vitro* diffusion experiments in Franz diffusion cells followed by cryo-sectioning to visualize the NR in the skin layers. Since the HSE are fragile and are destroyed after mounting on the diffusion cells in between the donor and receptor, it was not possible to obtain undamaged samples for cyrosectioning. Hence the HSE in their respective culture inserts were mounted directly on the Franz cells (Figure 8.1). Silicone grease was used to hold the inserts firmly on the Franz cell receptors and the formulations were added on top

of the HSE while they remained in the inserts. The polycarbonate membrane at the bottom of the inserts (pore size 0.4 µm) does not interfere with the permeation of molecules and has been frequently used as a support film for SE in permeation studies.

The receptor solution in the diffusion cells consisted of PBS (pH 7.4) that was constantly stirred at 600 rpm and maintained at 37 ± 0.5^0C. ~ 800 µl of the prepared formulations were added to the HSE in the Transwell® inserts with the aid of a 1 ml syringe.

The following formulations were evaluated:

- NR-NSP aqueous dispersion (n=4)
- NR-NSP containing 0.2 M Azone aqueous dispersion (n=4)
- NR-NSP in 1 % w/v HPMC gel (solvent base: PG:Water, 80:20 v/v) (n=4)
- NR–NSP in 1 % w/v HPMC gel containing 0.2 M Azone (solvent base: PG:Water, 80:20 v/v) (n=4)

Controls included NSP only, NR in PG:Water and NR in 1 % w/v HPMC gel with and without 0.2 M Azone. After 24 h, 1 ml of the receptor sample was withdrawn and lyophilized overnight, followed by extraction of NR from the sample by shaking with methanol for 1 h and determination of NR content by HPLC. The Transwell® inserts were detached from the diffusion cells and the HSE specimens were removed carefully and placed on a Petri dish. The excess formulation on the HSE surface was removed by rinsing with PBS followed by gentle blotting of the surface with a Kimwipe®. Thereafter the HSE was frozen on

dry ice and rectangular small skin pieces from the central treated area were cut, embedded in moulds with the aid of OCT (Optimal Cutting Temperature) and sectioned with a Leica CM 1850 cryostat (Leica Systems, Germany). The NR in the skin sections was visualized using fluorescence microscopy with a Zeiss Axio Observer D1 microscope (Germany) with excitation and emission wavelength for NR (546 nm and 585 nm respectively) and quantified by Image J software (NIH, USA) in terms of pixel intensities. Statistical evaluation (ANOVA) ($p<0.05$) was conducted with the aid of Kaleida Graph 4.0, Synergy Software. The NR penetration into the HSE layers from various formulations was then compared to the penetration profiles of these formulations in human skin *in vitro* and porcine skin *in vivo*.

8.2.5 HPLC analysis of Nile Red

Transdermal permeation of NR through the HSE into the receptor compartments was analyzed by HPLC. HPLC analysis was conducted on an Agilent 1100 HPLC system (Agilent Technologies, USA). Samples (20 µl) were run on an Agilent C18 reverse phase column (Eclipse XDB-C18, 4.6 X 150 mm, 5 µm) with acetonitrile:water (60:40 v/v) as the mobile phase at a flow rate of 1.75 ml/min. Nile Red was detected at 550 nm at an approximate retention time of 7.9 minutes. All results were analyzed with the aid of Microsoft excel.

8.3 Results and discussion

8.3.1 Barrier properties of SERPACWA in human skin (Table 15)

Permeation of paraoxon through human skin in the presence of SERPACWA was reduced by a factor of 0.28 (retardation factor) ($p<0.05$) (Figure 8.2) confirming that SERPACWA provides a good barrier to the penetration of paraoxon. Experiments that examined the effect of pre-applied DEET on the barrier properties of SERPACWA showed that the presence of DEET on the skin nullified the barrier properties of SERPACWA (Figure 8.3). In fact, DEET acted as a mild penetration enhancer for the permeation of paraoxon through skin (Enhancement factor: 1.2) despite the presence of SERPACWA. The receptor permeation of paraoxon when DEET was used in conjunction with SERPACWA was higher than the receptor permeation of paraoxon when applied to the skin alone. The skin retention of paraoxon in the presence of SERPACWA was several fold lower (retardation factor of 0.047) than the control (paraoxon only). When DEET was used in conjunction with SERPACWA, the skin retention of paraoxon was reduced only by a factor of 0.28 as compared to the control (paraoxon only). Thus, DEET reduced the ability of SERPACWA to prevent the penetration and subsequent accumulation of paraoxon in skin.

These results indicate that SERPACWA significantly reduced the penetration of paraoxon through human skin ($p<0.05$). However, in the presence of DEET, the penetration of paraoxon into the receptor was enhanced when compared to the

control, even in the presence of SERPACWA. This indicates that DEET application may lead to more systemic absorption of paraoxon despite the presence of SERPACWA, a finding that is significant to soldiers who tend to use insect repellants containing DEET together with the barrier cream.

8.3.2 Barrier properties of SERPACWA in the HSE

Permeation of paraoxon through HSE in the presence of SERPACWA was reduced by a factor of 0.36 (retardation factor) (Figure 8.4). This was comparable ($p<0.05$) to the retardation properties of SERPACWA in human skin (retardation factor of 0.28). The HSE model also simulated the effect of DEET on the barrier properties of SERPACWA, leading to an enhancement factor of 1.39 in the HSE (Figure 8.5), which is again comparable to the enhancement ratio of 1.2 observed in human cadaver skin. Though the enhancement/retardation ratios were comparable between the two skin models, the values of cumulative amount permeated and the flux of paraoxon were much higher in the HSE as compared to human skin (Table 16). This occurs due to the stronger penetration barrier of human skin to paraoxon and also due to the possible hydrolytic decomposition of paraoxon during passage through human skin. These aspects of skin permeability barrier have been discussed in detail in chapter 5.

8.3.3 Skin delivery of NR via the Nanosphere formulations in the HSE

The experimental design for evaluation of the skin delivery potential of the nanosphere formulations in the HSE model was modified in two ways:

a) Transwell® inserts used for HSE culture were used as donor compartments instead of the donor equivalents of the vertical Franz diffusion cells;
b) Treated HSE were rinsed with PBS, just like the skin sections in the human cadaver skin studies and in the porcine skin model. However, owing to the fragility of the HSE, the specimens were not wiped with a Kimwipe® as in the case of human and porcine skin.

The total penetration of NR into skin layers of the HSE was significantly higher with the nanosphere formulations of NR when compared with the respective control (NR in PG:Water) (Table 17). However, the rank order of the formulations according to their penetration effect (P.E) predicted by the HSE cultures was in agreement with the rank order predicted earlier in the human and pig skin experiments (Figure 8.6 and Figure 8.7) . The total deposition of NR from four key formulations into the HSE, from the highest to the lowest deposition was as follows:

NR Nanospheres in HPMC gel + 0.2 M Azone > NR Nanospheres in HPMC gel > NR Nanospheres > NR in PG.

Thus, the nanospheres acted as suitable carriers for enhanced skin penetration of NR into the HSE. The penetration of NR from the nanospheres in the HSE was 2.7 times its penetration from its solution in PG:Water. The penetration

enhancement effect of the nanocarriers in the HSE is similar to that observed in human skin *in vitro* (3.4 fold) and in pig skin *in vivo* (2.2 fold). Similarly, formulation of the NSP in the HPMC gel increased its HSE penetration by 1.1 fold as compared to its aqueous formulation, validating similar effects observed in human skin (1.2 fold enhancement) and in pig skin (1.3 fold enhancement). The combined formulation of NR-Nanospheres and 0.2 M Azone in the HPMC gel produced the highest deposition of NR in the skin layers with a ~ 1.4 fold increase as compared to the NR-NSP formulations in HPMC gel and in PBS, and a 3.6 fold increase when compared to the NR solution in PG. Similar observations were made earlier in the human skin studies with the addition of Azone to the gel formulation of the NSP (~ 1.4 fold increase as compared to the NR-NSP formulations in HPMC gel and in PBS and a 5.3 fold increase when compared to the NR solution in PG) and also in pig skin (~ 1.4 fold increase as compared to the NR-NSP formulations in HPMC gel, ~ 2 fold increase as compared to the NR-NSP aqueous dispersion, and a 4.2 fold increase when compared to the NR solution in PG).

Despite the similarities in trends of permeation, there was a difference in the specific skin layers where NR was preferentially deposited from the NSP in the HSE model, when compared to human skin *in vitro*. A more significant deposition of NR (when delivered via NSP) was observed in the SC and the epidermis of the HSE than in the dermis. The NR deposition from the NSP in the SC, epidermis, upper dermis and lower dermis was 2.6, 3.8, 2.2 and 1.9 fold of its deposition

from NR-PG. Unlike the HSE, the human skin penetration of NR from NSP in the SC, epidermis, upper dermis and lower dermis was 2.5, 5.1, 7.3 and 3.4 fold of its deposition from NR-PG. The lower penetration enhancement via the NSP in the upper and the lower dermis of the HSE could be due to the following reasons:

- It evident from earlier *in vitro* permeability studies with the HSE that the permeability barrier of the HSE is weaker than that of human skin. Because of this weaker barrier, especially to lipophilic compounds like NR, it is possible that the HSE model was not sensitive enough to accurately distinguish between the NR formulations. Assuming a significantly higher penetration and the faster diffusion of the dye through the HSE layers, the difference between the dye deposition from different formulations in the dermis could be less distinct.
- Although the HSE model is similar in cellular morphology to human skin, it does not possess the appendages that exist in human skin. This shunt route of skin permeation has been cited as a possible mechanism for vesicles and carrier based delivery systems.(103, 104) Thus, the shunt route may be a contributing factor for NR penetration in human skin and its absence in the HSE may have led to lower dye deposition in the dermis.

8.4 Conclusions

The HSE was evaluated for its ability to predict the functional properties of multicomponent formulations. The first formulation, SERPACWA, is a barrier

cream designed to protect the warfighters against absorption of toxic agents through skin. Evaluation of SERPACWA efficacy in the HSE resulted in a retardation factor of 0.36 against penetration of paraoxon, which was not significantly different ($p<0.05$) than that predicted in human cadaver skin (0.28). The HSE also closely predicted the ability of DEET to nullify the barrier property of SERPACWA and enhance the skin penetration of agents. Similar observations of interference of DEET with the function of applied barrier creams have been briefly reported.(102) The validity of the HSE as a skin model for testing the efficacy of SERPCWA offers a suitable alternative to the use of *in vivo* models for testing the barrier properties of formulations against extremely toxic agents. Our studies demonstrate that the HSE can be used as an accessible and reproducible model to predict the retardation properties of barrier formulations and can serve as a valuable tool for screening of developmental formulations in preliminary studies.

The HSE was also used to evaluate the skin delivery potential of the tyrosine based NSP formulations. Enhancement of NR penetration into the HSE layers via the NSP aqueous and gel formulations was not significantly different from the enhancement ratios obtained in the *in vitro* human skin studies and the *in vivo* study in the porcine model. In addition, the rank order of the formulations (evaluated based on the penetration effect (P.E) of NR) estimated by the HSE model was in conjunction with the rank order that was predicted by the *in vitro* human cadaver skin model and the *in vivo* pig skin model. However, due to the

weaker barrier properties of the HSE and also the lack of several skin appendages in the HSE model, the differences in the amount and depth of penetration of NR from various formulations was less drastic than that observed in the human and pig skin models. Thus, the HSE in its current optimized stage is suitable for rank ordering the formulations and for initial pre-screening of a range of formulations. The reproducibility and the easy availability of the HSE make it an accessible and reliable model that can be used for routine testing. However, the final quantitation of skin penetration and the pharmacological evaluation of formulations would require the use of suitable *in vivo* models or human skin.

9 Future work

Tyrosine derived Nanospheres: The NSP have been repeatedly shown to act as carriers for lipophilic molecules and increase the depth and the extent of skin penetration of the complexed agents. Future studies with these NSP will significantly benefit from a detailed understanding of the mechanism of penetration of the NSP in the skin and the elucidation of the exact time and place of release of the agents from the NSP when present in the skin. For these studies, a polymeric component of the NSP can be tagged with a fluorescent compound that absorbs at a different wavelength than the compound encapsulated in the NSP. Skin penetration studies with the NSP, followed by sectioning and visualization of both fluorescent compounds in different skin layers will help us understand the location of the NSP and of the dye after certain hours of skin treatment. Finally, the NSP can be used to encapsulate drugs and subsequently be evaluated for their ability to effectively penetrate diseased skin as compared to healthy skin and for aiding the pharmacological action of the complexed molecules.

Human Skin Equivalent: Difference in the packing of the SC lipids has been cited as one of the primary reasons for the weaker permeability barrier of the reconstructed skin models.(105) Hence, investigation of the SC lipids by Transmission Electron Microscopy (TEM) would aid in understanding the current packing of the lipids in the HSE and possible future methods to improve their organization. This will aid to strengthen the permeability barrier of the HSE, one

of the primary objectives for development of a suitable permeability model comparable to human skin. One of the methods to improve the permeability barrier could involve culture of the HSE with additional agents that normalize the lipid production and packing, and act by different mechanisms than the currently evaluated PPAR agonists. Also, studies are already underway in our laboratory for improvement of the mechanical properties of the HSE by incorporation of an electrospun polymer scaffold. Evaluation of the barrier properties of this polymer incorporated HSE will require extensive permeability studies with a large library of agents with different physiochemical properties. Also, reproducibility and the scale up validation of this HSE will have to be assessed before using this model for the routine screening of formulations.

10 Tables

Table 1: HPLC parameters for Nile Red (NR) and 5-Dodecanoylaminofluorescein (DAF) using the Waters 2695 HPLC system.

Drug	**Mobile Phase**	**Flow Rate (ml/min)**	**Detection wavelength (nm), retention time (mins)**	**Intra- and inter-day variability, Limit of detection**
DAF	Acetonitrile:Water (0.1 % TFA) (65:35 v/v)	1	270, 6.5	0.1, 0.1 0.07 µg/ml
NR	Acetonitrile:Water (0.1 % TFA) (60:40 v/v)	1.75	550, 7	0.1, 0.1 0.04 µg/ml

Table 2: HPLC parameters for Nile Red (NR) and Diclofenac sodium (DS) using the Agilent 1100 system.

Drug	**Mobile Phase**	**Flow Rate (ml/min)**	**Detection wavelength (nm), retention time (mins)**	**Intra- and inter-day variability, Limit of detection**
DS	Methanol:Water (0.1% TFA) 80:20 v/v	1	280, 3.6	0.06, 1.2 0.1 µg/ml
NR	Acetonitrile:Water (60:40 v/v)	1.75	550, 7.9	0.2, 1.4 0.05 µg/ml

Table 3: Release rates and cumulative amount of Diclofenac sodium (DS) released from HPMC (HydroxyPropyl Methyl Cellulose) gels.

The viscosity of the gels at 25^0C is given in Pa.s.

HPMC concentration	**Cumulative amount of DS released, Q_{10} ($\mu g/cm^2$) ± SE**	**Steady state Flux ($\mu g/cm^2/h$) ± S.E.**	**Viscosity (Pa.s)**
0.5 % W/V	9291 ± 367	1499 ± 76	0.09
1 % W/V	9110 ± 180	1444 ± 18	1.14
1.5 % W/V	8240 ± 431	1300 ± 57	10.89

Table 4: *In vitro* skin penetration effect of key NR-NSP formulations.

Note: SC: Stratum Corneum, E: Epidermis, UD: Upper Dermis, LD: Lower Dermis. NSP: Nanospheres, NR: Nile Red, HPMC: HydroxyPropyl Methyl Cellulose.

Formulation	**Average Penetration effect P.E. ± S.E.**				
	SC	**E**	**UD**	**LD**	**Total**
NR in PG:Water	34.5 ± 1.9	14.7 ± 1	4.05 ± 0.2	3.4 ± 0.1	56.55 ± 2.7
NR-NSP in PBS	84.5 ± 0.1	72.4 ± 2.4	29.9 ± 2.1	11.7 ± 0.5	198.22 ± 4.3
NR-NSP in HPMC gel	84.67 ± 0.1	72.8 ± 2.2	42.9 ± 3.7	21.8 ± 1.6	222.7 ± 7.1
NR- NSP + 0.2 M Azone	84.1 ± 0.4	76.7 ± 1.8	33.8 ± 1.9	15.4 ± 0.9	210.22 ± 1.8
NR-NSP in HPMC gel + 0.2 M Azone	84.89 ± 0.1	85 ± 2.3	77.4 ± 3.8	60.1 ± 1.7	307.48 ± 4.4

Table 5: *In vivo* skin penetration effect of key NR-NSP formulations in the domestic pig.

Note: SC: Stratum Corneum, E: Epidermis.

NSP: Nanospheres, NR: Nile Red, HPMC: HydroxyPropyl Methyl Cellulose.

Formulation	**Average Penetration effect P.E. ± S.E.**		
	SC + E	**Dermis**	**Total**
NR in PG:Water	37.59 ± 6	6.85 ± 0.2	44.44 ± 5.9
NR-NSP in PBS	86.79 ± 14.3	9.86 ± 1.1	96.65 ± 14.8
NR-NSP in HPMC gel	121.31 ± 22.7	11.16 ± 1.5	132.47 ± 23.5
NR- NSP + 0.2 M Azone	99.64 ± 6	10.07 ± 1.4	109.71 ± 7.3
NR-NSP in HPMC gel + 0.2 M Azone	168.82 ± 25	17.29 ± 4.2	186.11 ± 29.9

Table 6: Lipid composition of Human Skin Equivalent (HSE) treated with 300 μM of clofibrate in conjunction with ascorbic acid (100 μg/ml) and external lipids.

Note: HSE Control was cultured with no added clofibrate, ascorbic acid and external lipids.

Data generated in our laboratory by Yifan Song. Ref: (106).

Lipid Class	**HSE Control**	**HSE-OP cultured with clofibrate 300μM, ascorbic acid (100 μg/ml) and external lipids**	**Human cadaver skin**
Phospholipids	19.5 ± 3.8	23.8 ± 2.1	39.2 ± 2.1
Glucosylceramides	1.0 ± 0.3	5.3 ± 0.3	4.8 ± 0.7
Acylglucosylceramides	0.2 ± 0.1	0.6 ± 0.1	Trace
Ceramides	8.6 ± 1.4	14.1 ± 0.5	12.2 ± 2.2
Cholesterol	25.9 ± 3.6	25.3 ± 3.1	19.4 ± 2.9
Fatty acids	6.7 ± 0.6	10.1 ± 0.5	8.1 ± 0.6
Triglycerides	33.5 ± 3.1	15.5 ± 1.6	9.2 ± 0.9
Cholesterol esters	4.6 ± 0.8	5.3 ± 1.2	7.1 ± 0.5

Table 7: Ceramides composition of HSE treated with 300 μM of clofibrate in conjunction with ascorbic acid (100 μg/ml) and external lipids.

Note: Control HSE was cultured with no added clofibrate, ascorbic acid and external lipids.

Data generated in our laboratory by Yifan Song. Ref: (106).

Ceramides	HSE Control	HSE-OP cultured with clofibrate 300 μM, ascorbic acid (100 μg/ml) and lipids	Human cadaver skin
1	16.9 ± 2.3	14.8 ± 0.9	10.2 ± 1.8
2	49.8 ± 2.9	26.2 ± 2.3	22.1 ± 0.2
3	23.2 ± 3.1	19.6 ± 2.2	21.9 ± 1.6
4	5.2 ± 1.0	10.7 ± 1.8	6.9 ± 1.3
5	3.7 ± 0.8	15.8 ± 1.3	16.7 ± 1.6
6	1.1 ± 0.0	5.4 ± 0.7	7.5 ± 1.5
7	0.1 ± 0.0	7.5 ± 1.7	14.7 ± 0.8

Table 8: Development and validation of HPLC methods for model compounds used for permeability evaluation of HSE.

Note: The correlation coefficient of linearity for all methods was >0.99.

Drug	Mobile Phase	Flow Rate (ml/min)	Detection wavelength (nm), retention time (mins)	Intra and inter-day variability, Limit of detection
Caffeine	Acetonitrile: Water: Methanol (10:70:20 v/v/v)	1	270, 3.2	0.06, 0.81 0.5 µg/ml
Hydrocortisone	Acetonitrile:Water (40:60 v/v)	1	242, 2.90	0.23, 2.78 0.5 µg/ml
Ketoprofen	Acetonitrile:Water (0.1%TFA) (80:20 v/v)	1	264, 1.82	0.08, 1.31 0.05 µg/ml
DEET	Methanol: water (80:20 v/v)	0.7	240, 3.08	0.45, 0.48 0.5 µg/ml
Paraoxon	THF: Acetonitrile: sodium phosphate buffer (pH 7.4) (12:25:63 v/v/v)	1	280, 7.2	0.07, 1.67 0.5 µg/ml
Malathion	Acetonitrile: water (70:30)	1.25	215, 3.1	0.23, 1.78 0.1 µg/ml

Table 9: Permeability parameters of model agents in the dermal matrix of the HSE.

Note: Q_{24} is the cumulative amount permeated through skin in 24 h.

Drug	**Flux ± S.E. (μg/cm^2/h)**	**Q_{24} ± S.E. (μg/cm^2)**
Caffeine	268.8 ± 28.1	403.1 ± 10.9
Hydrocortisone	268.7 ± 32	502.5 ± 9.67
Ketoprofen	400.9 ± 35	5480.0 ± 214

Table 10: Permeation parameters for six agents after 24 h *in vitro* permeation experiments with three skin models: HSE, EpidermFT® and Human Skin

Co: concentration of the solute in the donor solution (mg/ml); Q_{24}: Cumulative amount of solute permeated after 24 h (µg/cm^2); Jss: steady state flux (µg/cm^2/h); Kp: Permeability Coefficient (cm/h).

Cumulative amounts of drug per square cm. of skin area was plotted against time, and the steady state flux (Jss) was calculated as the slope of linear portion of the plot. The permeability coefficient (Kp) was obtained as the ratio of the steady state flux and the solute concentration in the donor solution.

		HSE			**EpidermFT®**			**Human Skin**		
Agent	**Co**	**Q_{24}**	**Jss**	**Kp * 10^{-5}**	**Q_{24}**	**Jss**	**Kp * 10^{-5}**	**Q_{24}**	**Jss**	**Kp * 10^{-5}**
Caffeine	12.87	118.5 ±18.6	9.4 ±1.2	73.5 ±9.5	504.5 ±47.3	38.5 ±10.3	299.3 ±80.5	65.6 ±48.8	2.2 ±1.5	17.4 ±11.7
Hydrocortisone	19.64	96.7 ±10.1	7.9 ±0.4	40.5 ±2.1	111.8 ±29.7	6.4 ±1.9	32.9 ±9.8	28.6 ±31.7	2.0 ±2	10.3 ±11
Ketoprofen	54.32	2432.5 ±1153	140.5 ±41.5	258.7 ±76.4	3051.9 ±1185	166.4 ±40.8	306.4 ±75.2	561.7 ±376	19.3 ±17.5	35.5 ±32.2
DEET	295.26	15030.5 ±1253	837.9 ±57.3	283.7 ±19.4	15088.8 ±355.12	942.5 ±54.3	319.2 ±18.4	2076.5 ±458.4	100.7 ±33.9	34.1 ±11.5
Malathion	145.60	195.6 ±34.2	8.4 ±1.2	5.7 ±0.8	200 ±8.2	11.6 ±3	7.5 ±2.1	76.2 ±23.5	5.5 ±1.3	3.8 ±0.9
Paraoxon	25.39	2811.4 ±45.6	115.9 ±2.5	456.8 ±9.8	2964.9 ±691	123.6 ±18.7	487.1 ±123	94.4 ±4.0	4.54 ±0.1	17.9 ±0.2

Table 11: Reproducibility of the HSE with caffeine as a model drug.

Skin Model	# Batches	Replicates	Mean Q_{24} ($\mu g/cm^2$)	SD (Q_{24})	Mean Flux ($\mu g/cm^2/h$)	SD (flux)
HSE	8	2-4	298.78	81.73	51.74	13.63
EpidermFT®	1	3	513.86	53.32	38.53	10.36

Table 12: EC_{50} values and Photo-Irritancy Factor (PIF) for Hydroxycinnamic acid (HCA) and Chlorpromazine (CPZ) in the presence (UVA (+)) and absence (UVA (-)) of UVA irradiation – Range Finder 3T3 NRU Experiment.

(Results obtained with the aid of Microsoft Excel and Linear Regression).

Compound	**EC_{50} UVA (+)**	**EC_{50} UVA (-)**	**PIF**	**Phototoxic potential**
CPZ	0.73 µg/ml	20.78 µg/ml	28.46	Yes
HCA	127.11 µg/ml	516.22 µg/ml	4.06	No

Table 13: EC_{50} values and Photo-Irritancy Factor (PIF) for Hydroxycinnamic acid (HCA) and Chlorpromazine (CPZ) in the presence (UVA (+)) and absence (UVA (-)) of UVA irradiation – Main 3T3 NRU experiment.

(Results obtained with the aid of Phototox Software Version 2.0, ZEBET, Germany).

Compound	**EC_{50} UVA (+)**	**EC_{50} UVA (-)**	**PIF**	**Phototoxic Potential**	**Toxicity probability**
CPZ	1.46 µg/ml	26.15 µg/ml	17.9	Yes	1.0
HCA	676.25 µg/ml	722.69 µg/ml	1.08	No	0.0

Table 14: Viability of HSE tissues after treatment with Chlorpromazine (CPZ) and Hydroxycinnamic acid (HCA) in the presence (UVA (+)) and absence (UVA (-)) of UVA irradiation.

Note: % decrease in viability indicates decrease in viability of the (UVA +) treated tissues as compared to the tissues kept in the dark.

CPZ		**HCA**	
Concentration (µg/ml)	**% decrease in viability**	**Concentration (µg/ml)**	**% decrease in viability**
3.16	22	3.16	-4
10	*54*	10	3
31.6	*61*	31.6	-10
100	*47*	100	-1

Table 15: *In vitro* skin penetration (A) and skin accumulation (B) of paraoxon through human cadaver skin after 6 hours of treatment in the presence and absence of SERPACWA and DEET.

	(A) Receptor Permeation after 6 h		
Treatment	**Flux ± S.E. (µg/cm^2/h)**	**Q_6 ± S.E. (µg/cm^2)**	**Retardation/Enhancement factor in Q_6 (b/a or c/a)**
Paraoxon only (a)	3.12±0.5	16.38± 2.8	
Paraoxon + SERPACWA (b)	2.44 ±0.3	4.74± 0.7	0.28 (Retardation)
Paraoxon + SERPACWA + DEET (c)	9.99 ±3.2	19.67± 5.9	1.2 (Enhancement)
	(B) Skin Accumulation after 6 h		
Treatment	**Amount (µg)**		**Retardation/Enhancement factor (b/a or c/a)**
Paraoxon only (a)	5340 ± 853		
Paraoxon + SERPACWA (b)	256 ± 56.9		0.047 (Retardation)
Paraoxon + SERPACWA + DEET (c)	1499 ± 685		0.28 (Retardation)

Table 16: *In vitro* skin penetration (A) and skin accumulation (B) of paraoxon through HSE after 6 hours of treatment in the presence and absence of SERPACWA and DEET.

	(A) Receptor Permeation after 6 h		
Treatment	**Flux ± S.E. (μg/cm^2/h)**	**Q_6 ± S.E. (μg/cm^2)**	**Retardation/Enhancement factor in Q_6 (b/a or c/a)**
Paraoxon only (a)	191.9±79.2	1094.7± 259.5	
Paraoxon + SERPACWA (b)	74.0 ±21.6	402.1± 121.3	0.36 (Retardation)
Paraoxon + SERPACWA + DEET (c)	262.2 ±105.5	1530.4± 661.7	1.39 (Enhancement)
	(B) Skin Accumulation after 6 h		
Treatment			**Retardation/Enhancement factor (b/a or c/a)**
Paraoxon only (a)	2383.9± 372		
Paraoxon + SERPACWA (b)	116.7 ± 37.5		0.048 (Retardation)
Paraoxon + SERPACWA + DEET (c)	1966.7 ± 725		0.82 (Retardation)

Table 17: Total Penetration Effect of NR (Mean ± S.E.) in the Human Skin Equivalent after treatment with various NR formulations for 24 h.

NR: Nile Red, PG: Propylene Glycol, NSP: Nanospheres, HPMC: HydroxyPropyl MethylCellulose.

Formulation	**Penetration Effect in all skin layers (Mean ± S.E.)**
NR in PG:Water	70.17 ± 12.04
NR in HPMC gel	108.59 ± 5.54
NR in HPMC gel + 0.2 M Azone	184.30 ± 7.9
NR-NSP aqueous dispersion	184.16 ± 6.49
NR-NSP + 0.2 M Azone aqueous dispersion	234.83 ± 7.83
NR-NSP in HPMC gel	189.6 ± 12.33
NR-NSP in HPMC gel + 0.2 M Azone	250.59 ± 17.77

11 Figures

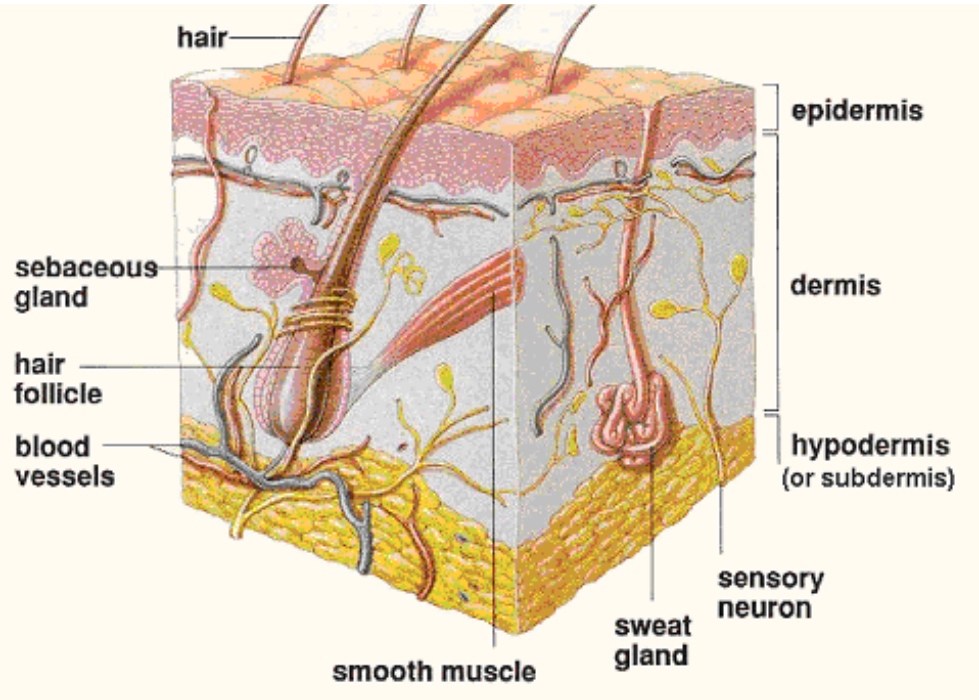

Figure 2.1: Structure of Skin

Various layers of the epidermis are depicted; the stratum corneum (the outermost horny layer, is about 10-20 µ thick and composed of flattened corneocytes (terminally differentiated keratinocytes) and intercellular lipid lamellae (secreted by the lamellar bodies). This brick and mortar structure presents a tortuous route that forms the main barrier to drug permeation. Figure adapted from Ref: (107).

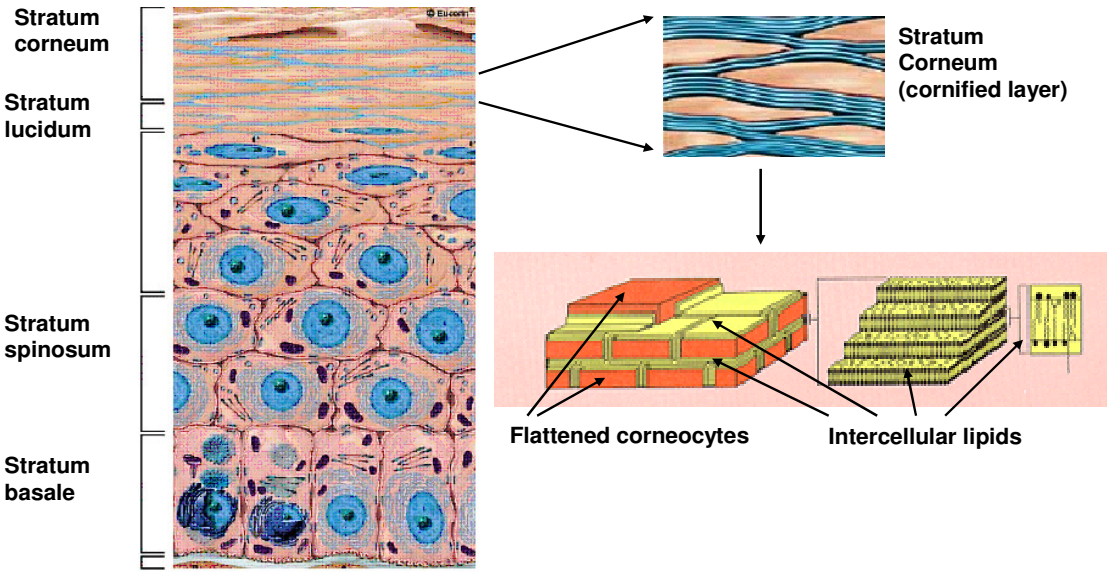

Figure 2.2: Cross-section of the epidermis depicting the epidermal layers of human skin and the composition of the stratum corneum barrier. Figure adapted from Ref: (108).

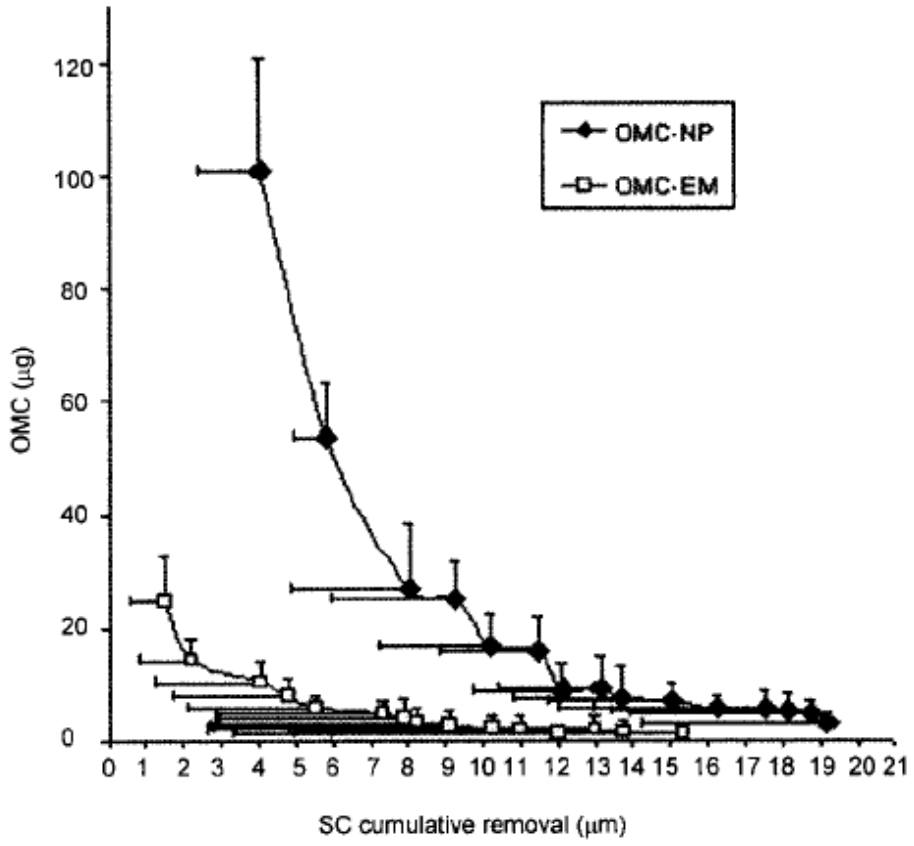

Figure 4.1: Concentration profiles of OMC (Octyl Methoxycinnamate) in porcine stratum corneum following delivery from an emulsion (OMC-EM) and from poly(ε - caprolactone) (MW: 10 000) nanoparticles (OMC-NP) following a 6-h application. Figure taken from Ref: (25).

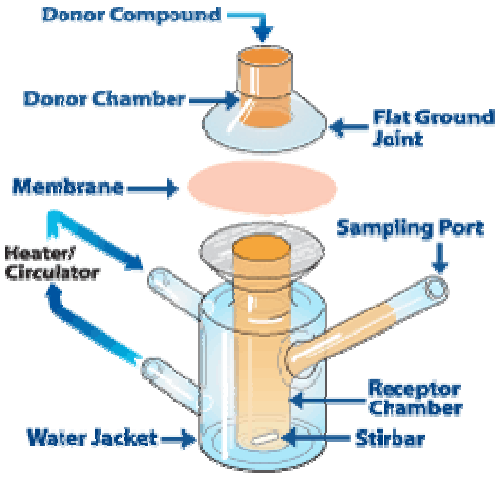

(A): Figure adapted from Ref: (109)

(B): Figure adapted from Ref: (110)

Figure 4.2: Diagrammatic representation (A) and actual image (B) of a vertical static Franz diffusion cell.

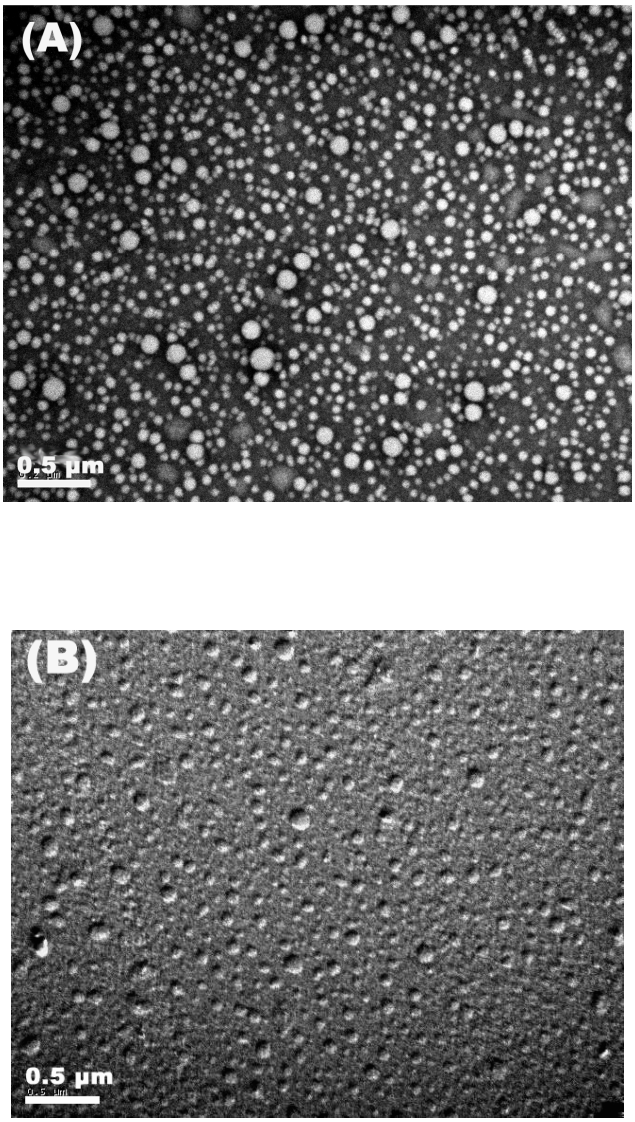

Figure 4.3: Transmission electron microscopy (TEM) images of Nanospheres (NSP) made from tyrosine based polymers in aqueous solution. (A): negative staining method (2% uranyl acetate); (B): Pt/C shadow method.

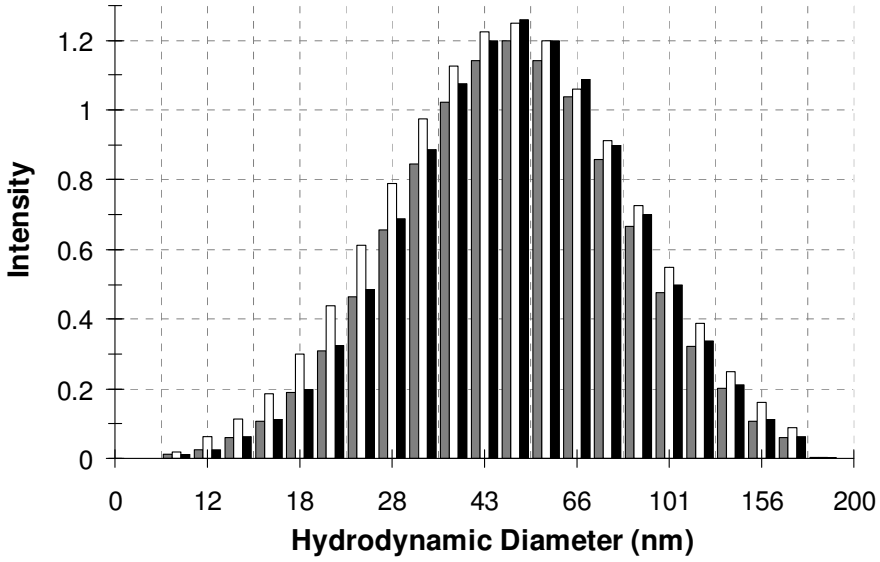

Figure 4.4: Size distribution of solute-nanosphere formulations as measured by dynamic light scattering. (Black) nanosphere-Nile Red; (Empty) nanosphere-DAF complexes; (Grey) nanosphere alone.

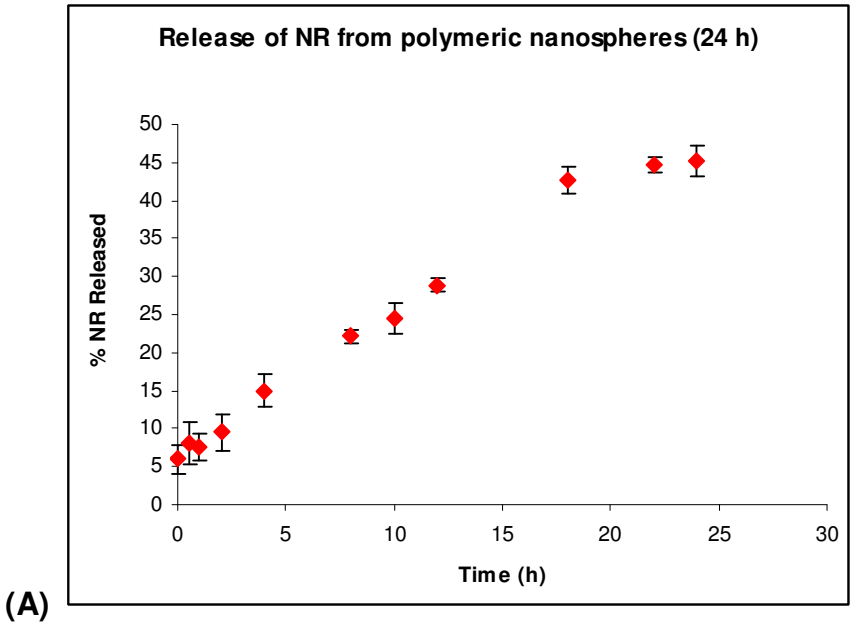

(A)

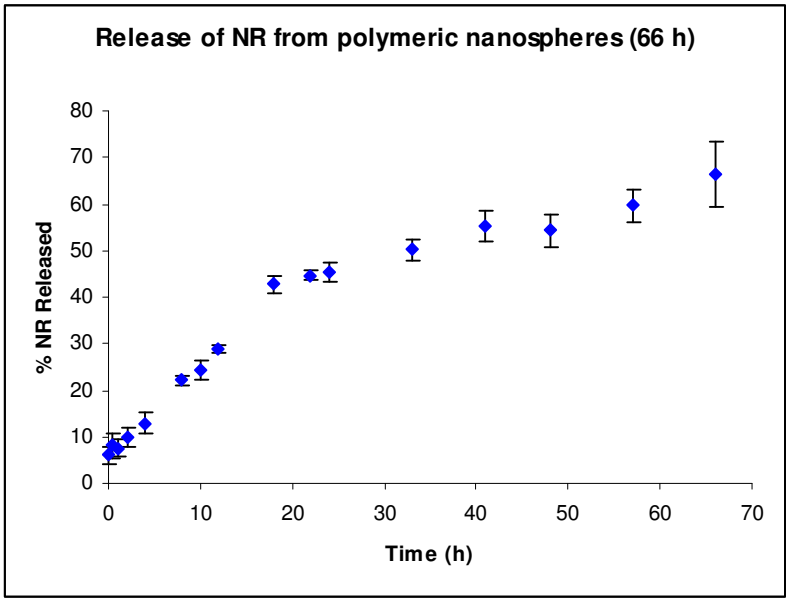

(B)

Figure 4.5: Release of Nile Red (NR) from tyrosine based polymeric nanospheres over (A) 24 h and (B) 66 h.

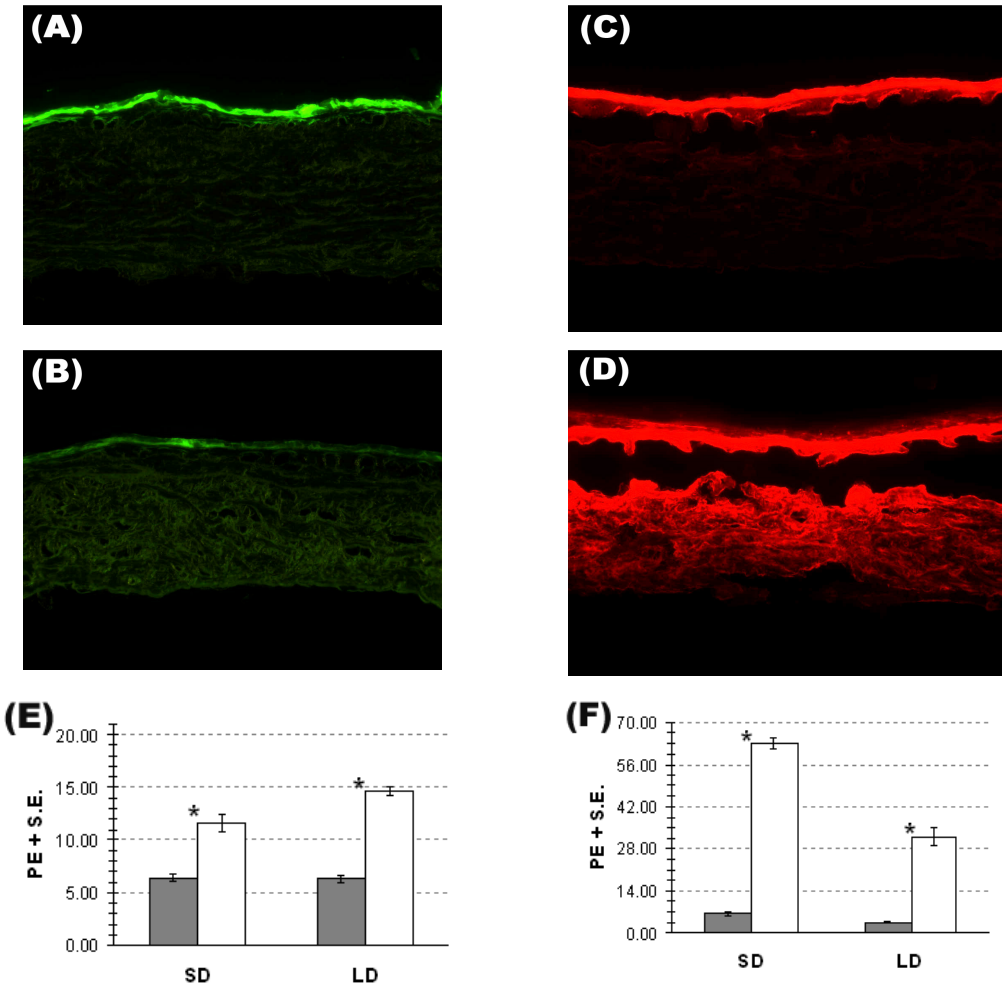

Figure 4.6: Cross-sectional images obtained following 24 h of passive permeation of fluorescent dyes via NSP through human skin *in vitro*. (A) PG-DAF; (B) NSP-DAF; (C) PG-NR; (D) NSP-NR.

Graphs show Penetration effect (P.E. ± S.E.) of NSP (empty box) with respect to PG (Grey box) after 24 h of passive permeation, (E) DAF; (F) NR.

Note: SD: superficial dermis; LD: lower dermis, $*p < 0.05$.

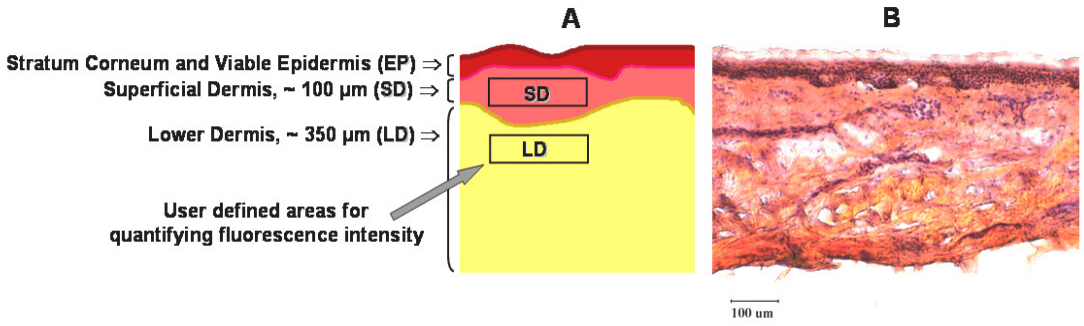

Figure 4.7: Schematic representation (A) and H&E staining (B) of cryo-sectioned human skin.

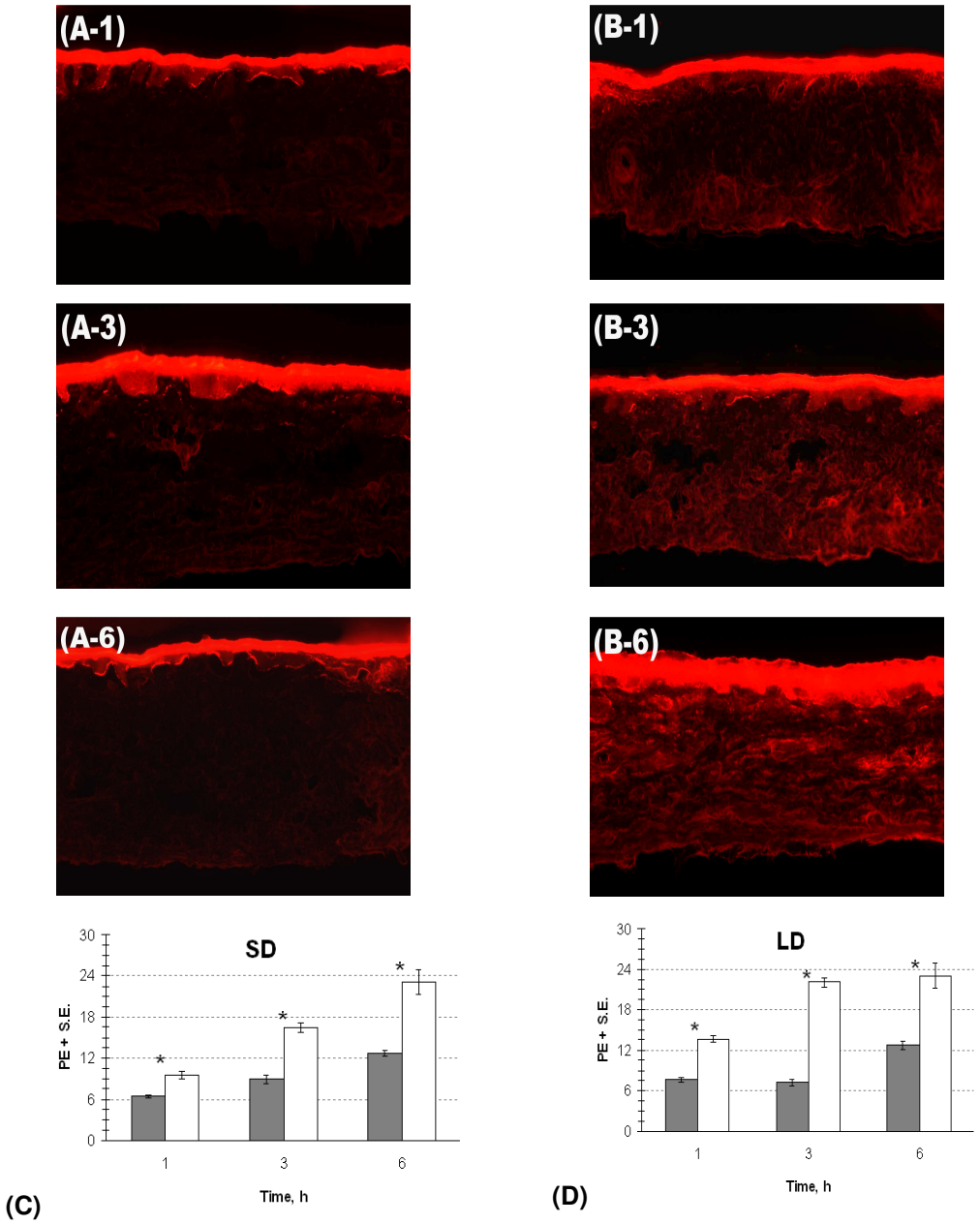

Figure 4.8: Cross-sectional images obtained following 1, 3 and 6 h of passive permeation of dyes via NSP through human skin *in vitro*. (A-1, 3, 6: PG-NR) and (B-1, 3, 6: NSP-NR). Graphs show Penetration effect (P.E.± S.E.) of NSP (empty box) with respect to PG (Grey box) after 1, 3, and 6 h of passive permeation. Note: SD: superficial dermis; LD: lower dermis, $*p < 0.05$.

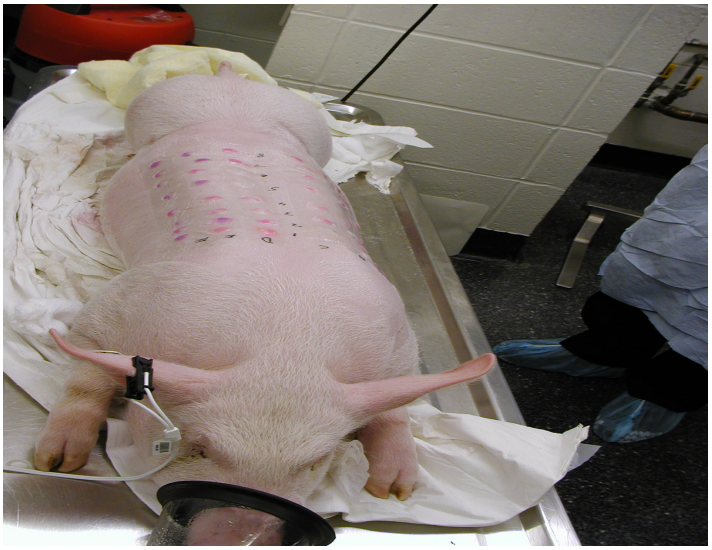

(A) Formulations applied on the domestic pig with the aid of Hill Top Chambers

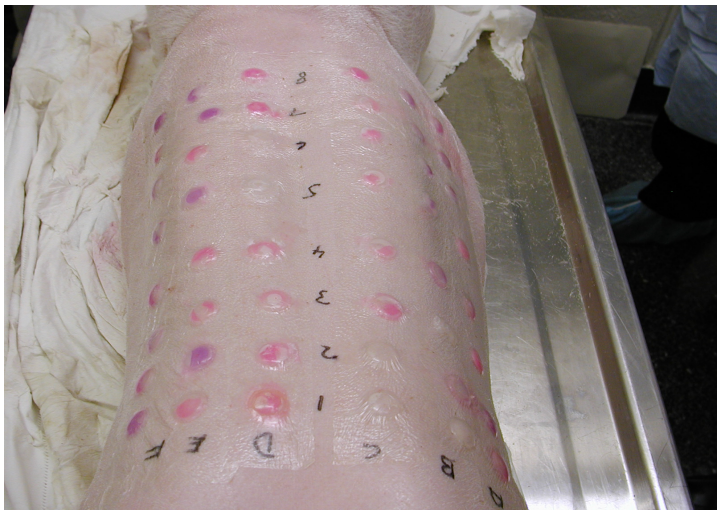

(B) Formulations (n=6/treatment) were randomized to sites on the back of the pig

Figure 5.1: *In vivo* skin penetration study for evaluation of skin delivery of NSP. Study was conducted in a single female domestic pig. The NR-NSP-HPMC gel and the control formulations were applied to the shaved back of the pig with the aid of Hill Top Chambers. The application of the formulations was randomized to different areas on the back to eliminate any site-specific bias.

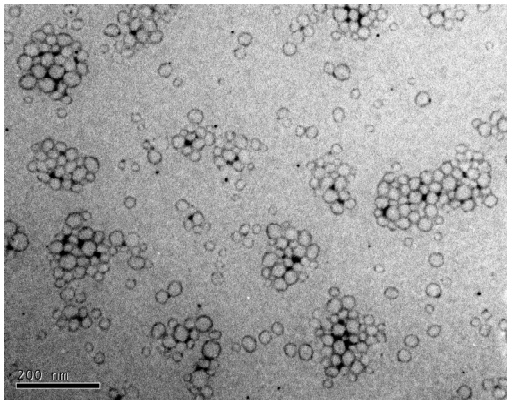

(A) NSP (10 mg/ml) in 1 % w/v HPMC

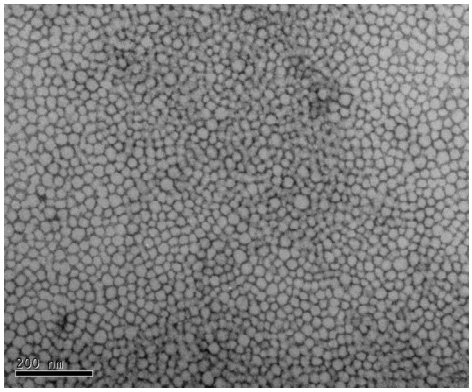

(B) NSP (10 mg/ml) in 1 % w/v carbopol 981NF

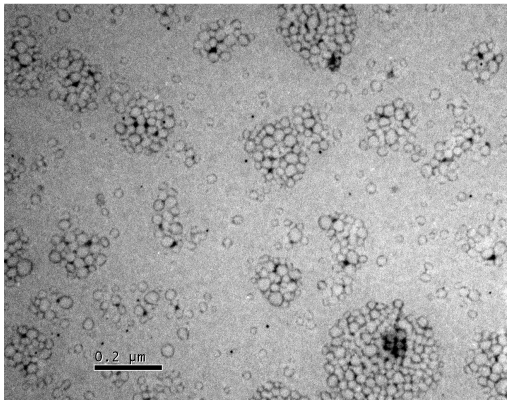

(C) NSP (10 mg/ml) in 1 % w/v HPMC with 0.2 M Azone

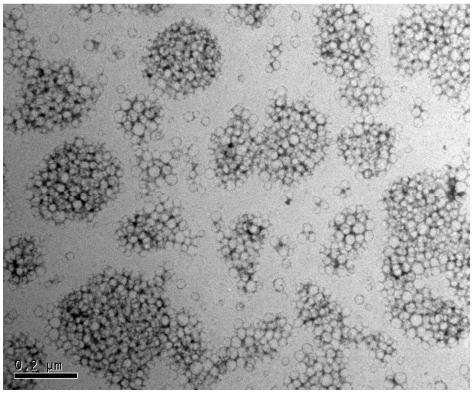

(D) NSP (10 mg/ml) in 1 % w/v HPMC with 2 % menthone

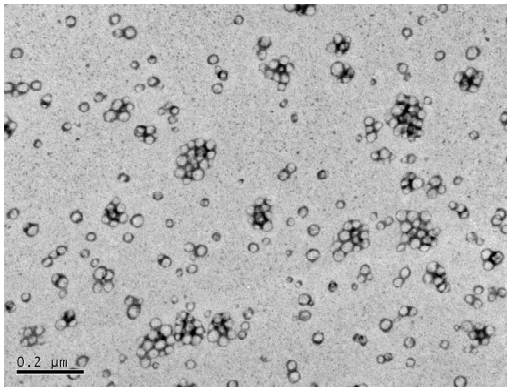

(E) NSP (3 mg/ml) in 1 % w/v HPMC

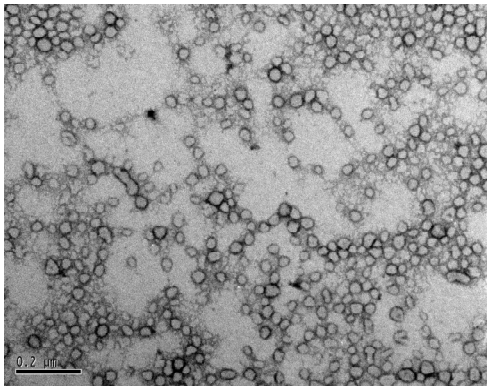

(F) NSP (3 mg/ml) in 1 % w/v carbopol 981NF

Figure 5.2: TEM images of polymeric NSP at various concentrations in hydrophilic gels in the presence and absence of chemical enhancers.

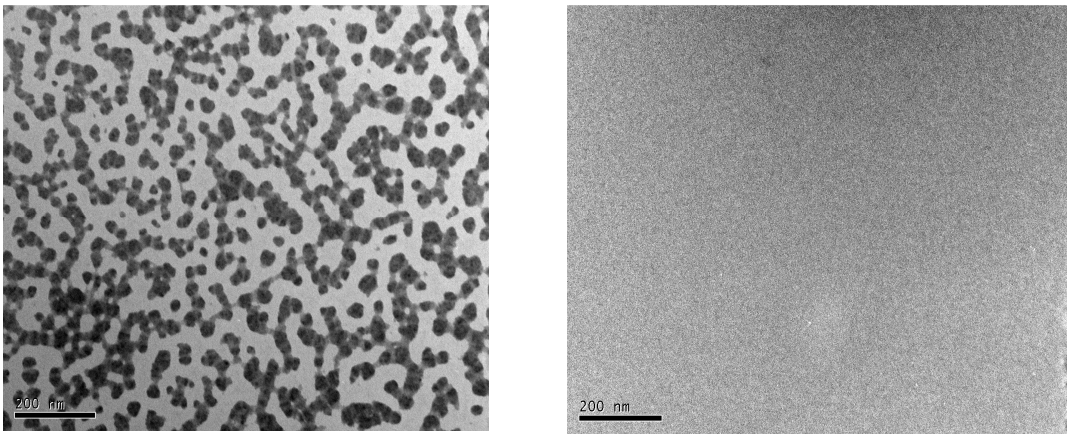

(A) TEM of 1 % w/v HPMC gel

(B) TEM of 1 % w/v carbopol 981NF gel

Figure 5.3: TEM images of HPMC and carbopol gels after negative staining.

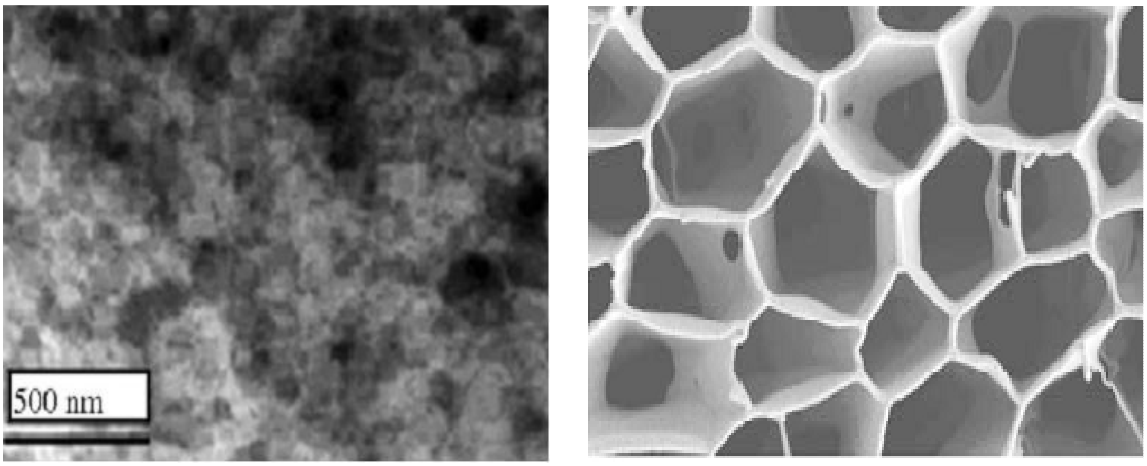

(A) TEM of Carbopol 940
Adapted from ref: (111)

(B) Cryo-SEM of 2 % Carbopol 941
Adapted from Ref: (112)

Figure 5.4: TEM and cryo-SEM images of carbopol gels depicting the nature of their network.

(A) 1% w/v HPMC gels with DS 1% and 2.5 % w/v

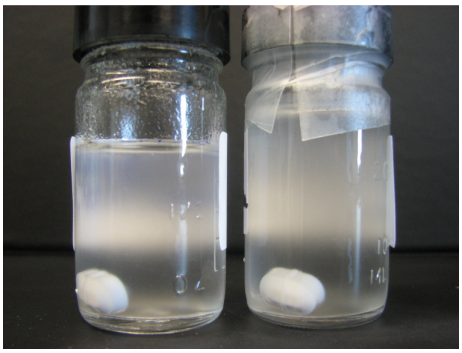

(B) 1% w/v HPMC gels with DS 1% and 2.5 % w/v

(C) 1% w/v carbopol 981 NF gels with DS 1% and 2.5 % w/v

(D) 1% w/v carbopol 981 NF gels with DS 1% and 2.5 % w/v

Figure 5.5: Images of 1% w/v HPMC (A, B) and carbopol 981 NF (C,D) gels with Diclofenac sodium (DS) 1% and 2.5% w/v. Images were taken after prepared gels were allowed to stabilize at room temperature for 48 h.

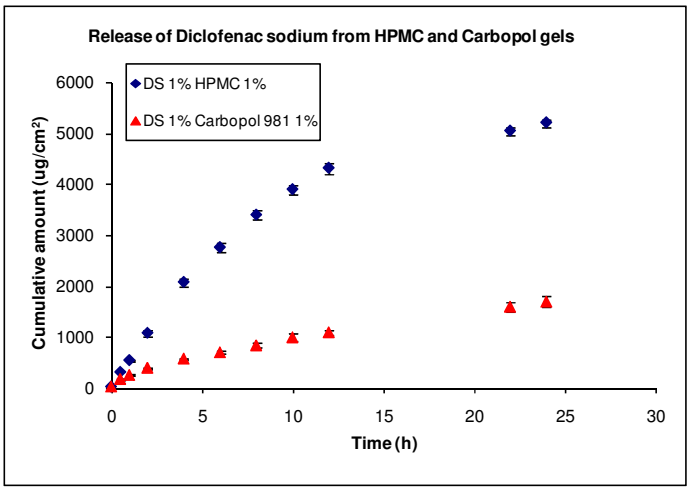

(A)

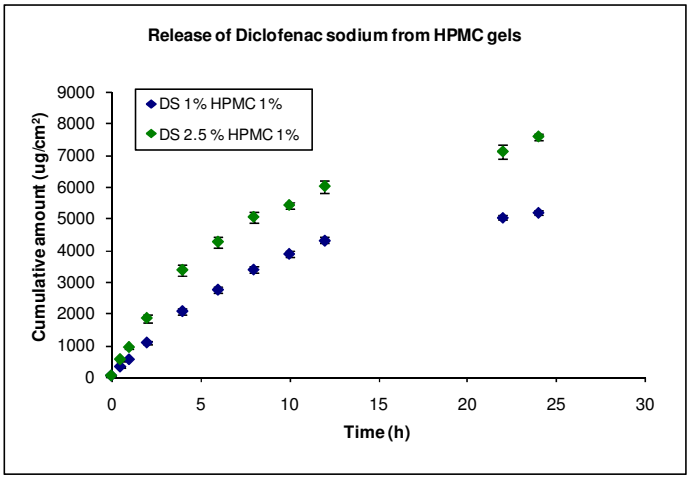

(B)

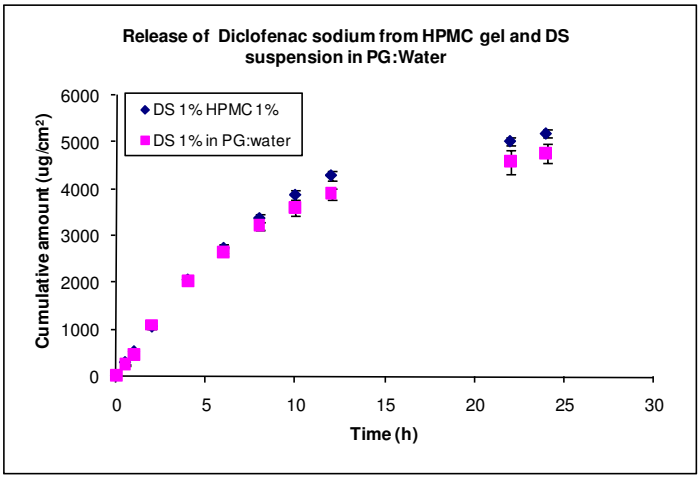

(C)

Figure 5.6: Effect of polymer type (A, C) and drug loading (B) on *in vitro* release of Diclofenac Sodium (DS) from formulations.

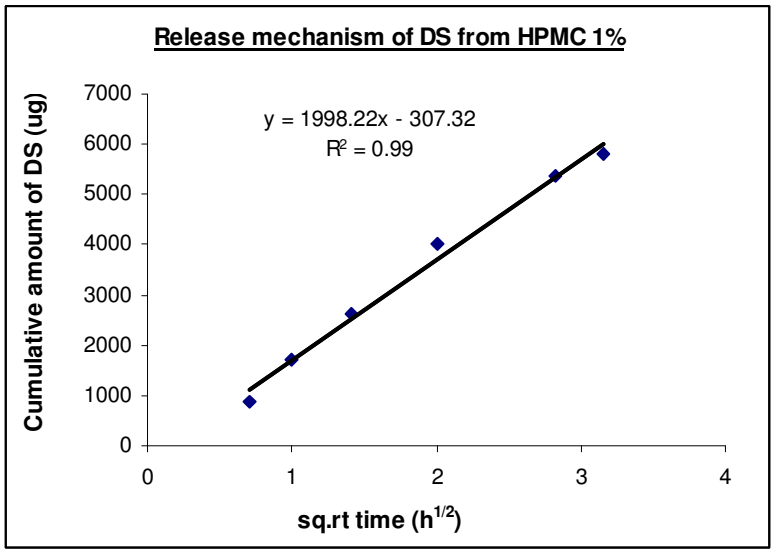

Figure 5.7: Release of Diclofenac Sodium (DS) from HPMC 1% w/v gel follows Fickian diffusion.

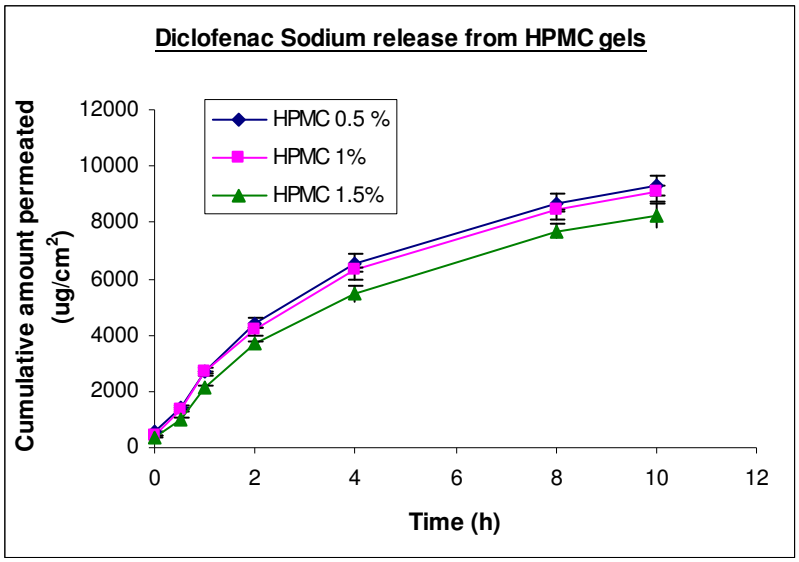

Figure 5.8: Release of Diclofenac Sodium (DS) from three concentrations of HPMC gels.

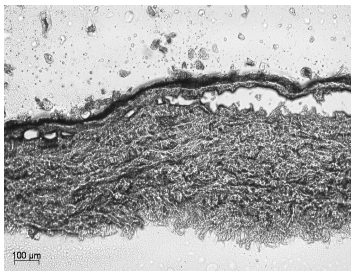

(A) Phase contrast (10 X)

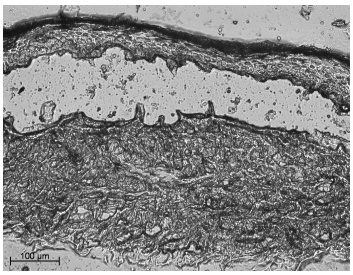

(B) Phase contrast (20 X)

(C) NSP only

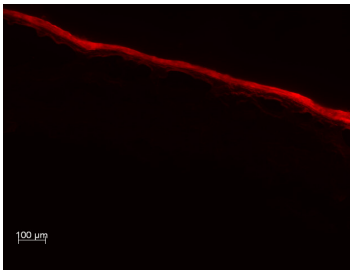

(D) NR in PG:H20 (10 X)

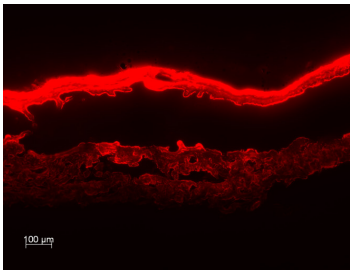

(E) NR-NSP-aqueous (10 X)

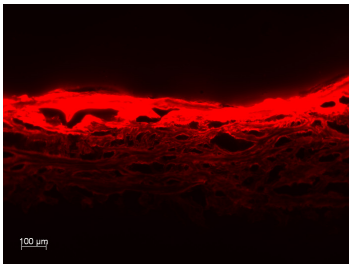

(F) NR-NSP-aqueous (20 X)

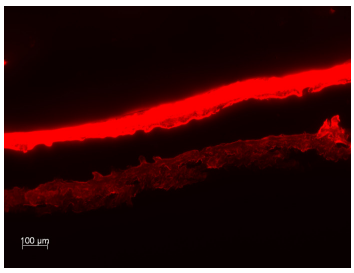

(G) NR-NSP-aqueous with 0.2 M Azone (10 X)

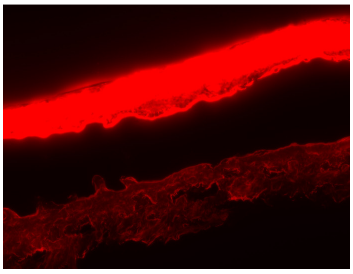

(H) NR-NSP-aqueous with 0.2 M Azone (20 X)

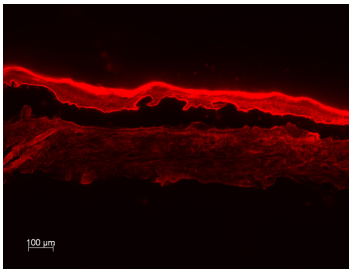

(I) NR-NSP-HPMC (10 X)

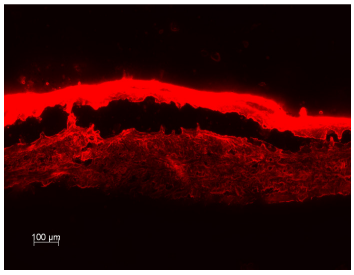

(J) NR-NSP-HPMC (20 X)

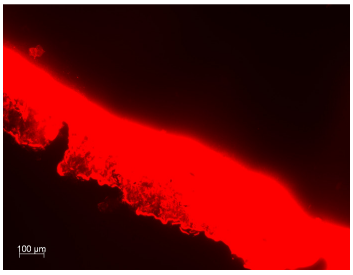

(K) NR-NSP-HPMC gel + Azone 0.2 M (10 x)

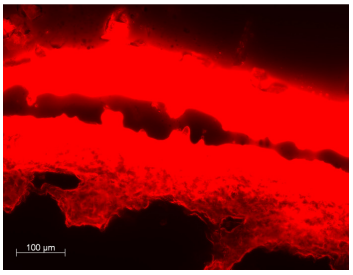

(L) NR-NSP-HPMC gel + Azone 0.2 M (20 x)

Figure 5.9: *In vitro* permeation of NR via NSP in HPMC gel and aqueous formulations through human skin. Pictures denote qualitative determination of NR penetration in different skin layers of cryo-sectioned (20 µm thickness) skin.

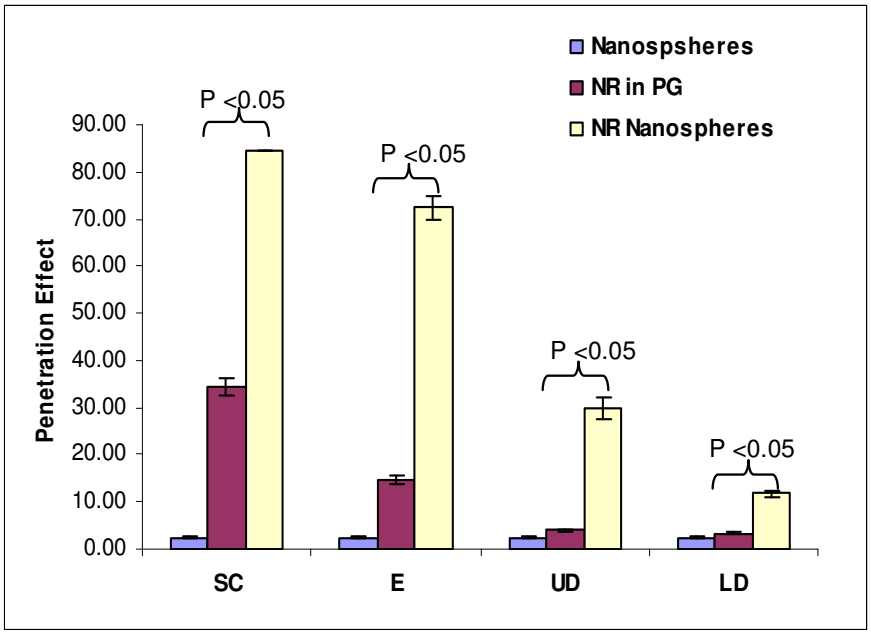

Figure 5.10 (A) Effect of Nanospheres (NSP) on the *in vitro* skin penetration of NR

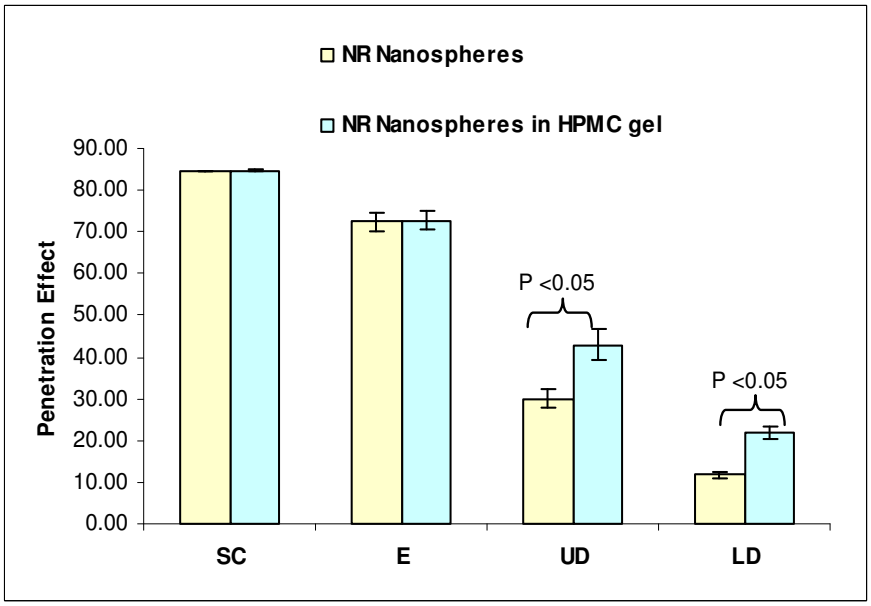

Figure 5.10 (B) Effect of NSP-HPMC gel on the *in vitro* skin penetration of NR

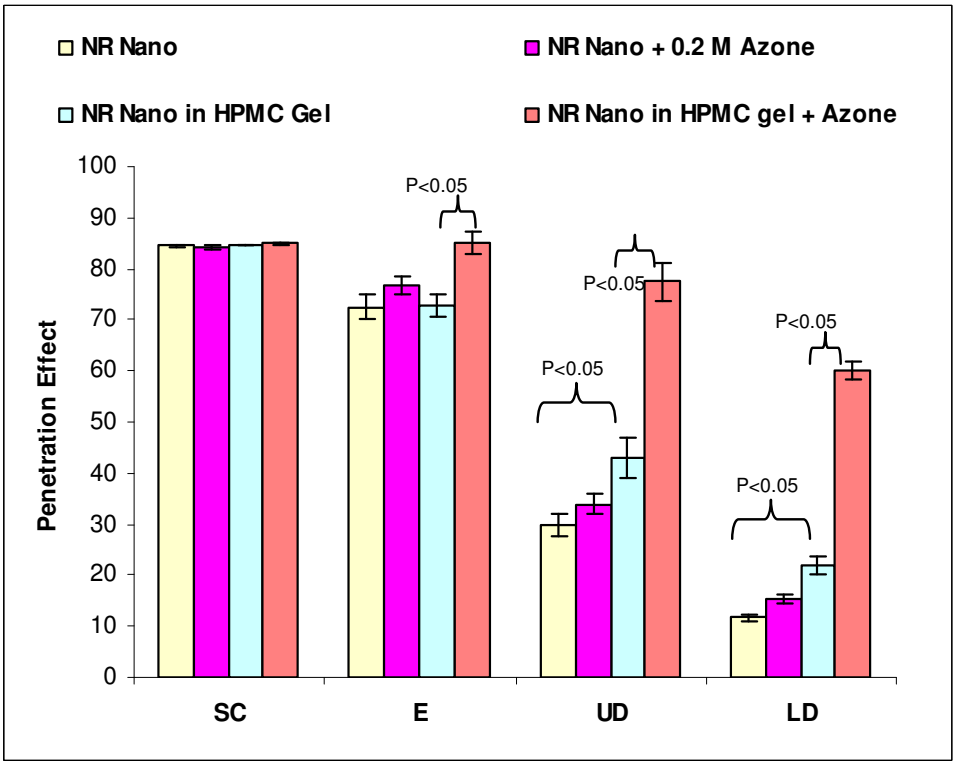

Figure 5.10 (C) Effect of Azone 0.2 M on the *in vitro* skin penetration of NR via NSP formulated as aqueous suspensions or HPMC gels.

Figure 5.10: Quantitative determination of *in vitro* skin permeation of NR via NSP in HPMC gel and aqueous formulations through human cadaver skin. Quantitation of the NR fluorescence was conducted with Image J software (NIH, USA) in terms of pixel intensities and converted to Penetration Effect (Arbitrary Units). Skin was histologically divided into four vertical sections representing different layers: a) 10 µm depth from top of skin: stratum corneum b) 100 µm from the SC: viable epidermis c) 100 µm depth from the viable epidermis: upper dermis d) 100 µm depth from the upper dermis: lower dermis. ANOVA ($p<0.05$) was used for statistical analysis.

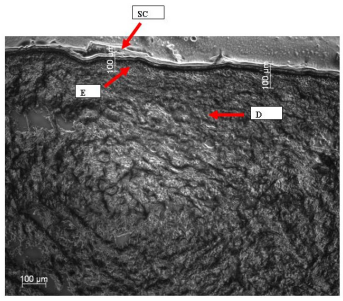

(A) Phase contrast

(B) NSP alone

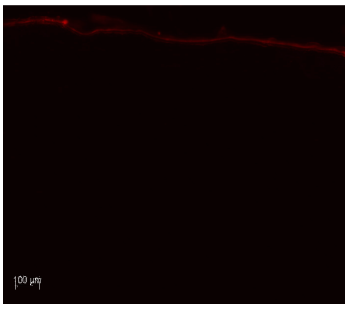

(C) NR in PG:Water

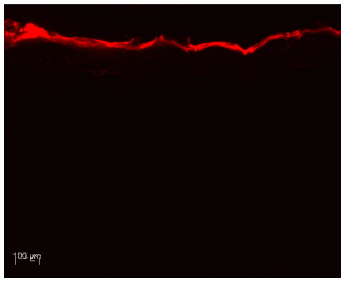

(D) NR-NSP-aqueous

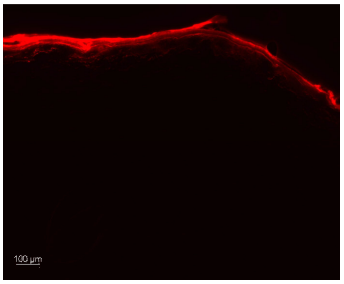

(E) NR-NSP-aqueous with 0.2 M Azone

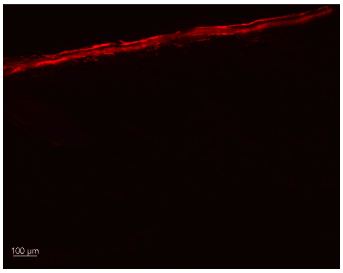

(F) NR-HPMC

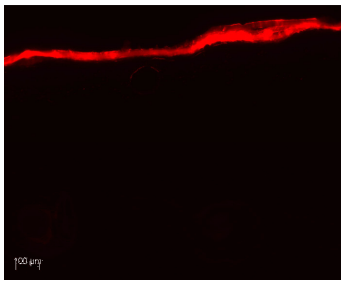

(G) NR-NSP-HPMC

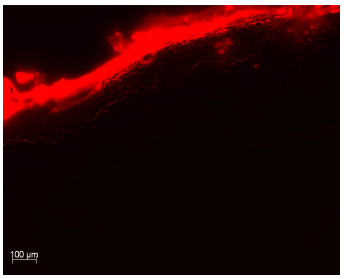

(H) NR-NSP-HPMC with 0.2 M Azone

Figure 5.11: *In vivo* skin permeation of NR via NSP in HPMC gel and aqueous formulations. Pictures denote qualitative determination of the extent of NR penetration in different skin layers. Skin pieces treated with NR in various formulations were cryo-sectioned (20 µ thickness) and observed by fluorescent microscopy. A phase contrast picture of pig skin has been shown for reference (A).

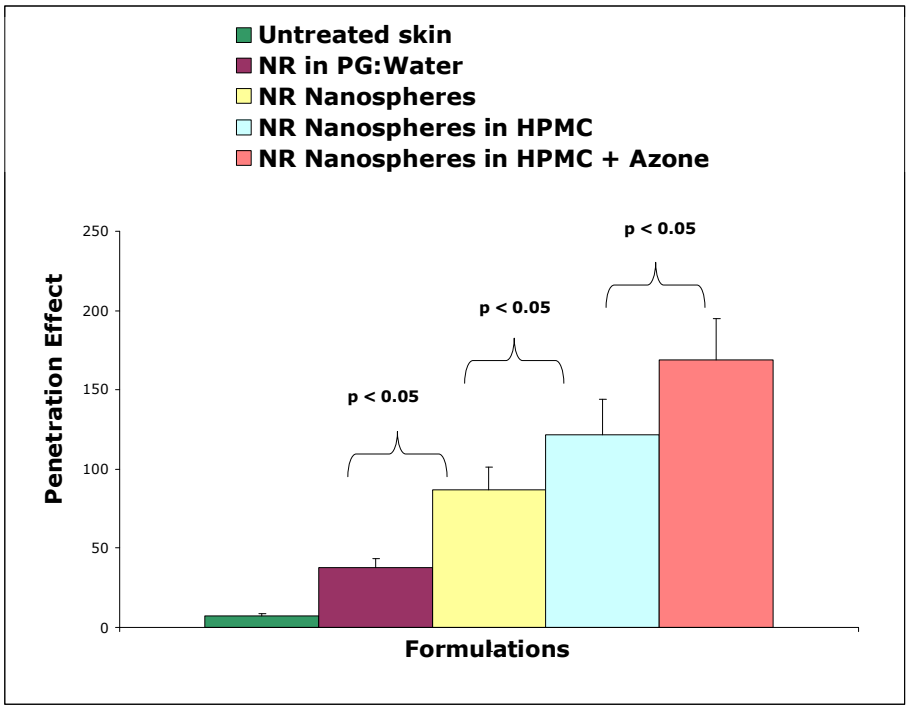

Figure 5.12: Quantitative determination of i*n vivo* skin permeation of NR via NSP in HPMC gel and aqueous formulations in the stratum corneum and epidermis of the domestic pig. Quantitation of the NR fluorescence was conducted with Image J software (NIH, USA) in terms of pixel intensities and converted to Penetration Effect (Arbitrary Units) ± S.E. ANOVA ($p<0.05$) was used for statistical analysis.

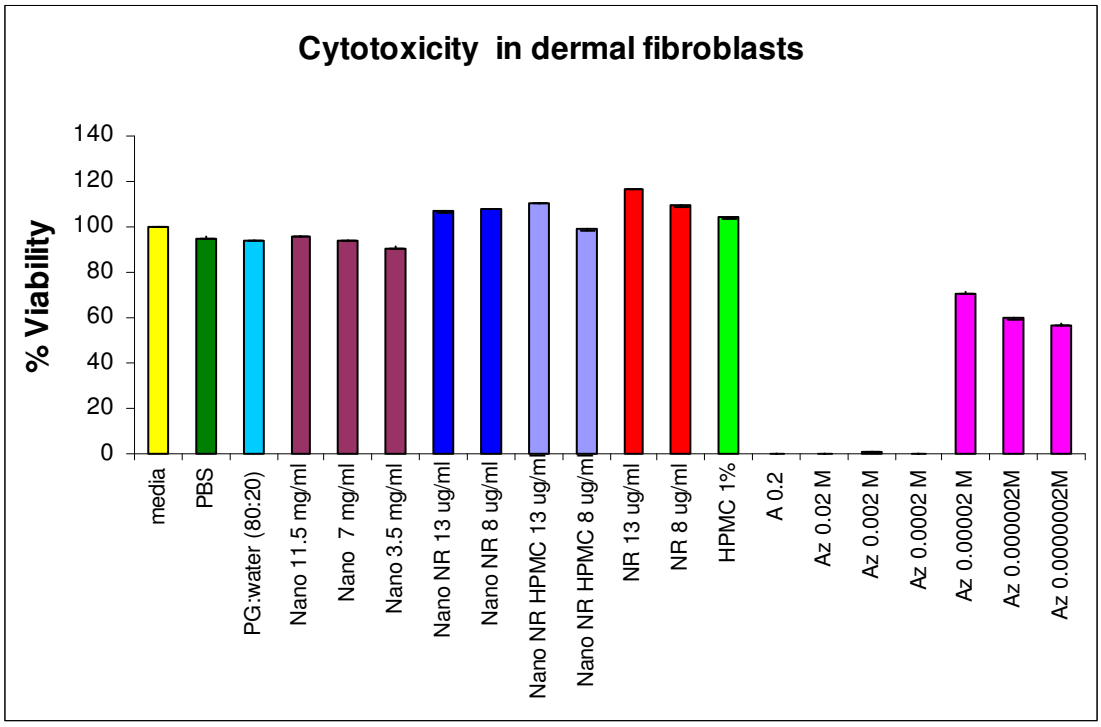

Figure 5.13: Cytotoxicity determination of NR-NSP formulations in human dermal fibroblasts. % viability of cells was determined by the MTS assay.

PBS: Phosphate Buffered Saline; PG: Propylene Glycol; Nano: Nanospheres, NR: Nile Red; Nano NR: NR in Nanospheres, Az: Azone; HPMC: HydroxyPropyl Methyl Cellulose

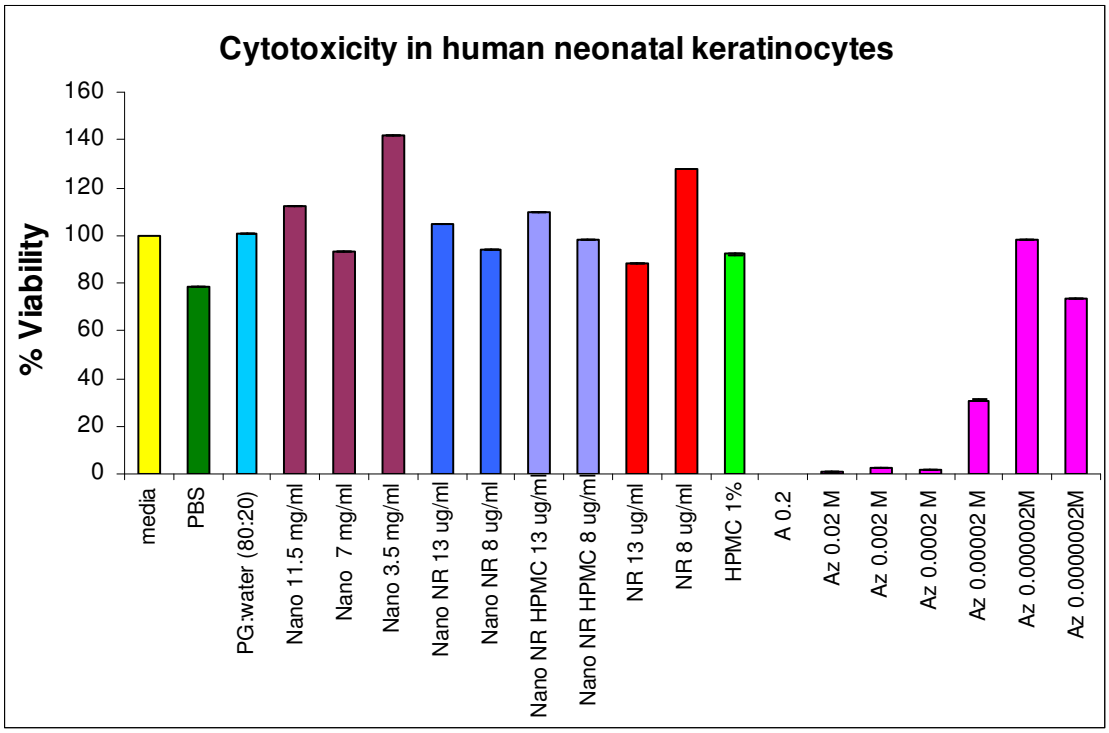

Figure 5.14: Cytotoxicity determination of NR-NSP formulations in neonatal keratinocytes. % viability of cells was determined by the MTS assay.

PBS: Phosphate Buffered Saline; PG: Propylene Glycol; Nano: Nanospheres, NR: Nile Red; Nano NR: NR in Nanospheres, Az: Azone; HPMC: HydroxyPropyl Methyl Cellulose.

Column A: Skin Surface **Column B: Skin cross section**

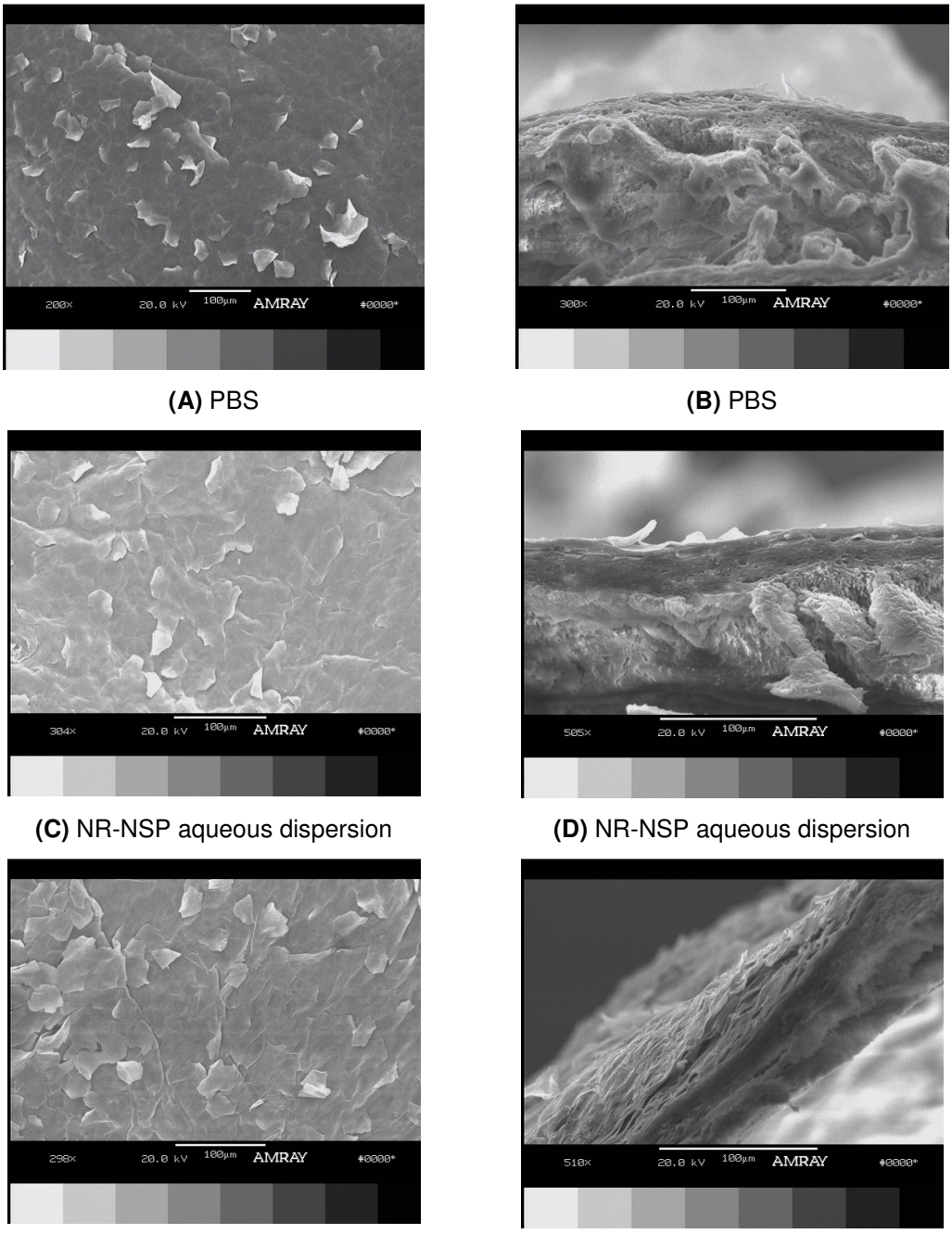

(A) PBS **(B)** PBS

(C) NR-NSP aqueous dispersion **(D)** NR-NSP aqueous dispersion

(E) NR in PG:water **(F)** NR in PG:water

Figure 5.15: Scanning Electron Microscopy (SEM) images of skin surface (column A) and skin cross-section (column B) treated with various aqueous and gel formulations of Nanospheres (NSP) for 24 h. NR: Nile Red.

Column A: Skin Surface | **Column B: Skin cross section**

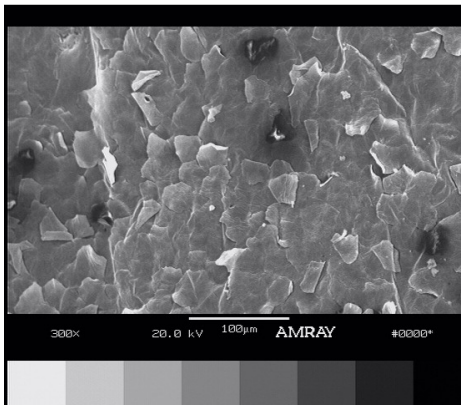

(G) NR-NSP in HPMC gel

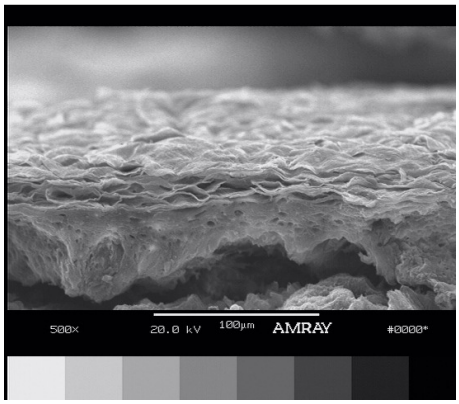

(H) NR-NSP in HPMC gel

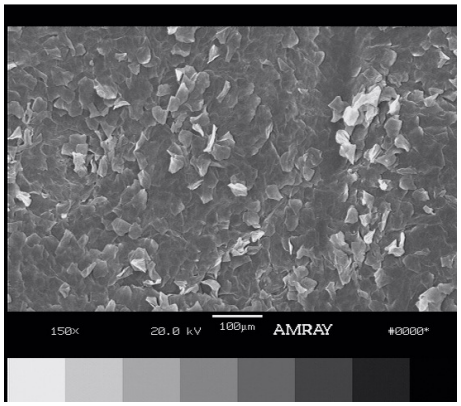

(I) NR-NSP in HPMC gel + 0.2 M Azone

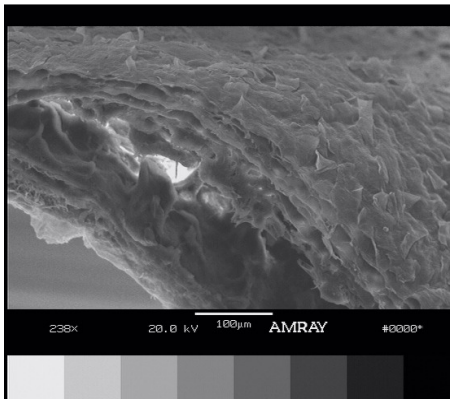

(J) NR-NSP in HPMC gel + 0.2 M Azone

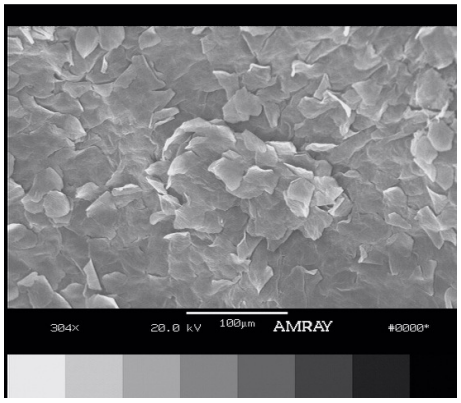

(K) NR-NSP in HPMC gel + 0.2 M Azone

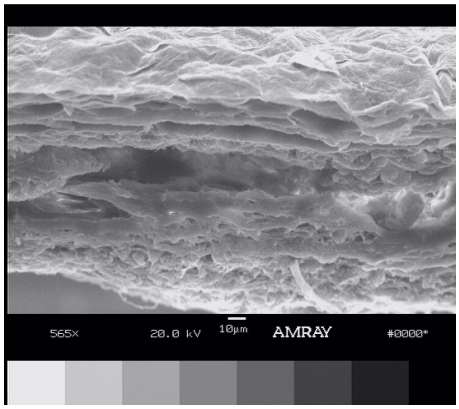

(L) NR-NSP in HPMC gel + 0.2 M Azone

Figure 5.15: Scanning Electron Microscopy (SEM) images of skin surface (column A) and cross section (column B) treated with various aqueous and gel formulations of Nanospheres (NSP) for 24 h. NR: Nile Red.

Column A: Skin Surface

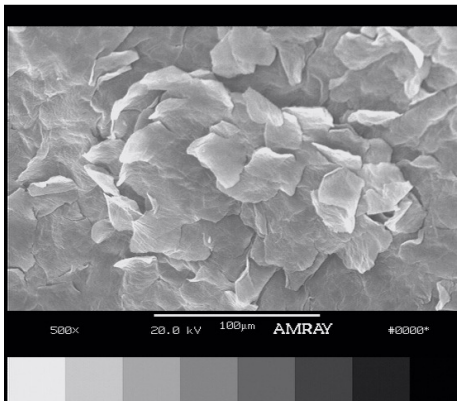

(M) NR-NSP in HPMC gel + 0.2 M Azone

Column B: Skin cross section

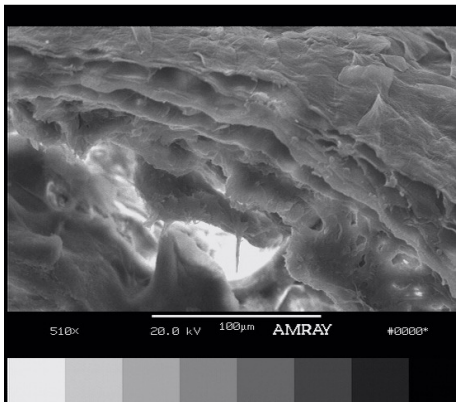

(N) NR-NSP in HPMC gel + 0.2 M Azone

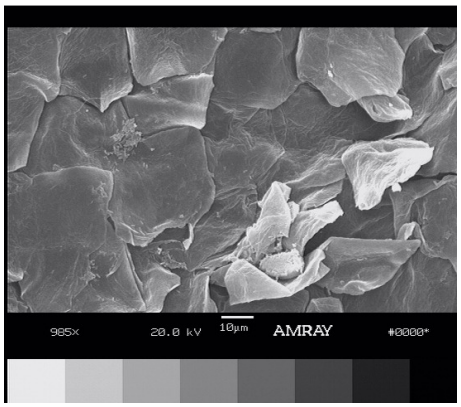

(O) NR-NSP in HPMC gel + 0.2 M Azone

Figure 5.15: Scanning Electron Microscopy (SEM) images of skin surface (column A) and cross section (column B) treated with various aqueous and gel formulations of Nanospheres (NSP) for 24 h. NR: Nile Red.

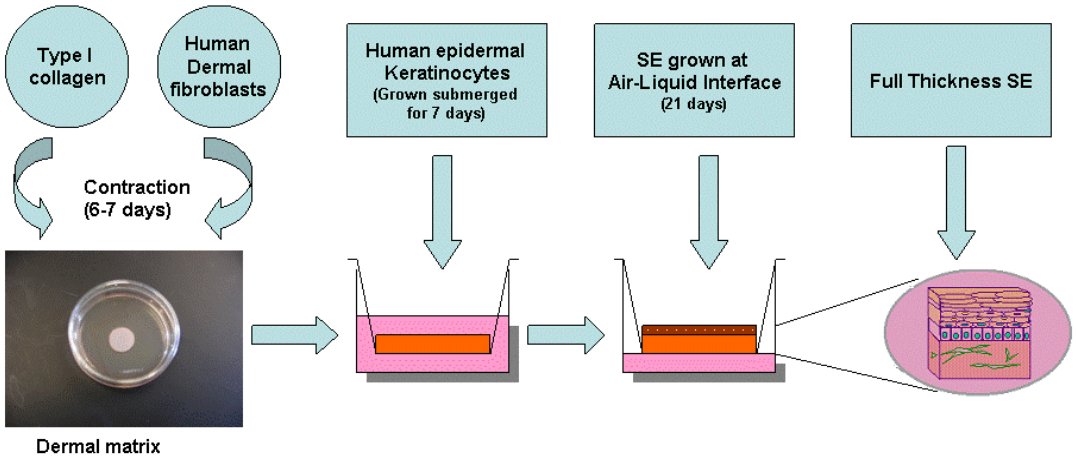

Figure 6.1: Preparation of the Human Skin Equivalent (HSE). The dermal matrix was made by contraction of bovine Type I collagen by human dermal fibroblasts. Neonatal keratinocytes (Passage 2–3) were seeded onto the dermis, where they proliferate and differentiate (when exposed to the ALI) leading to formation of a multilayered epidermis. SE: Skin Equivalent.

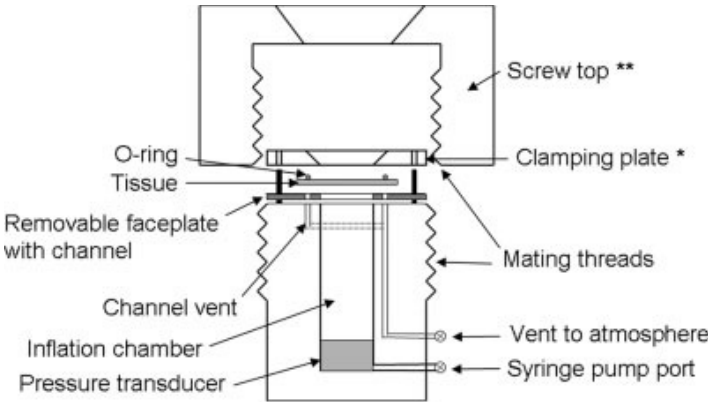

(A) Schematic representation of the inflation device

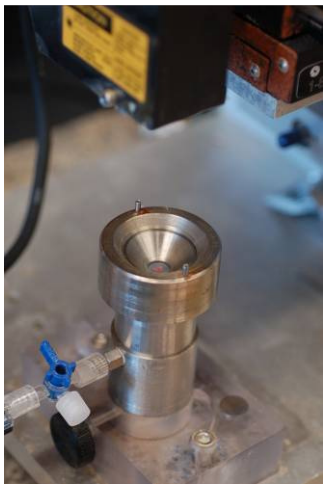

(B) Image of the inflation device

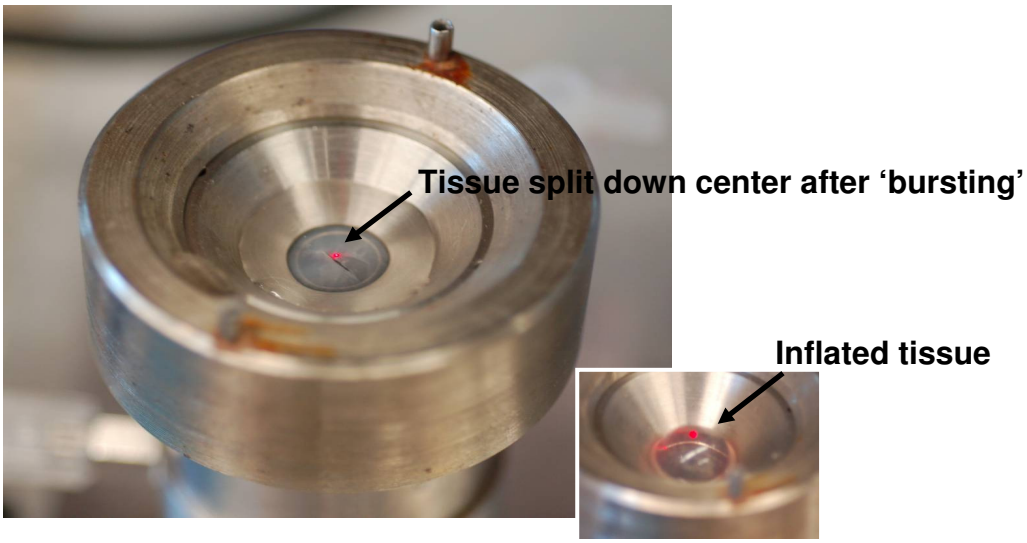

(C) Biaxial mechanical testing of tissue with the inflation device

Figure 6.2: Schematic representation (A) (74) and images of the inflation device (B and C) used for mechanical testing of the HSE and EpidermFT® tissues. Pictures B and C are courtesy of Kristen L. Billiar, Ph.D., Assistant Professor of Biomedical engineering, Worcester Polytechnic Institute.

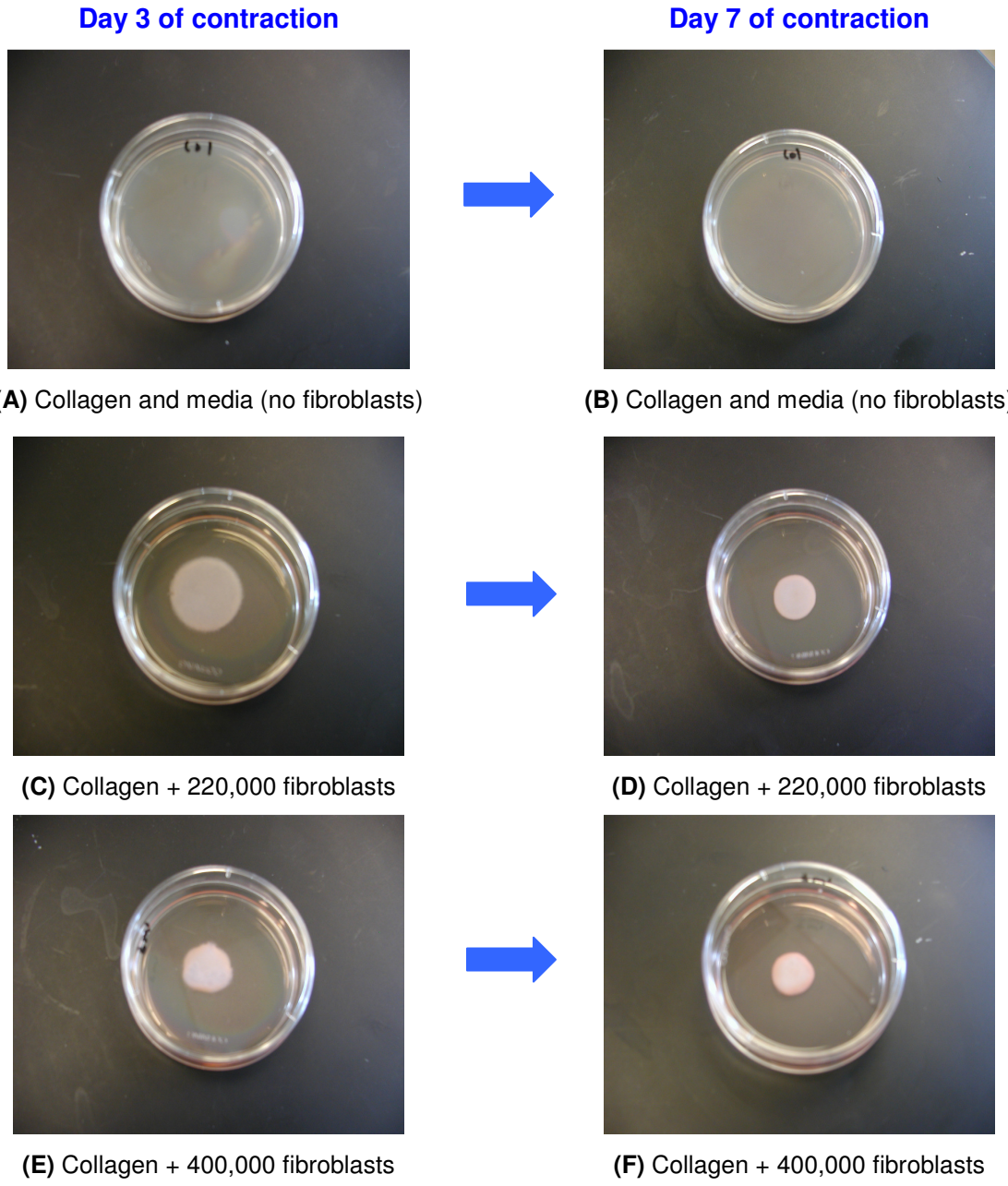

Figure 6.3: Contraction of dermal layers over 7 days of incubation at 10% CO_2 at 37℃ in a humidified incubator. Dermal layers were made from a mixture of 2X DMEM, FBS, 1 N NaOH, bovine type I collagen and human dermal fibroblasts. The contraction of the collagen matrix on the 3rd and the 7th day after mixing is shown in the presence of no fibroblasts (A and B), 220,000 fibroblasts (C and D) and 440,000 fibroblasts (E and F).

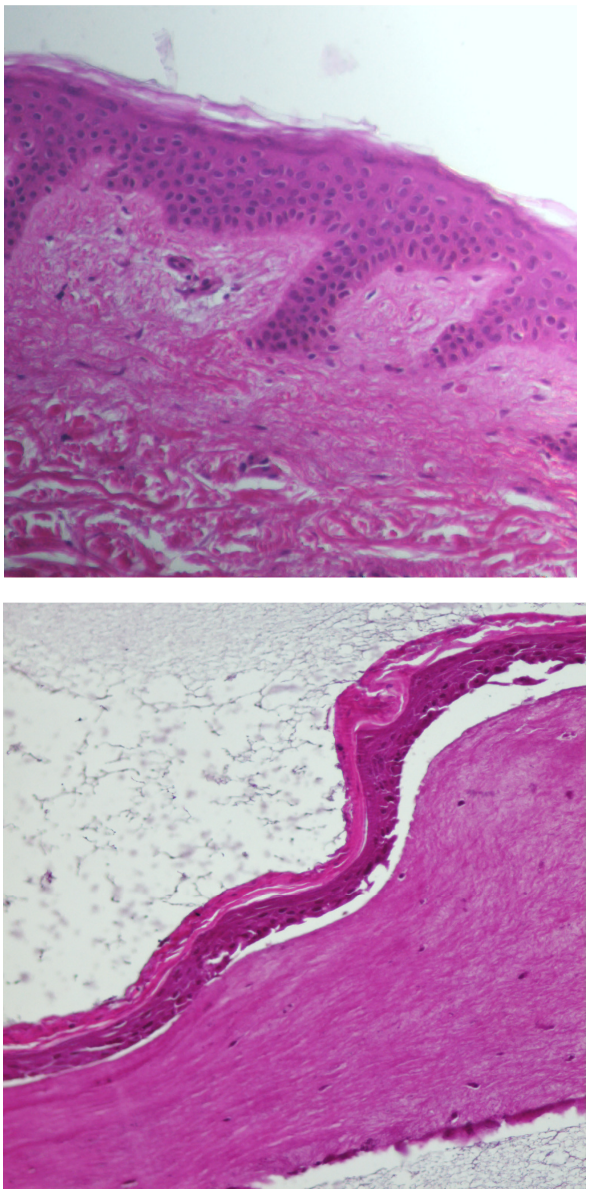

(A)

(B)

Figure 6.4: Histology of human skin (A) and of HSE at 7 days after exposure to ALI (B). Sections (6 µm) were stained with H &E and observed by light microscopy.

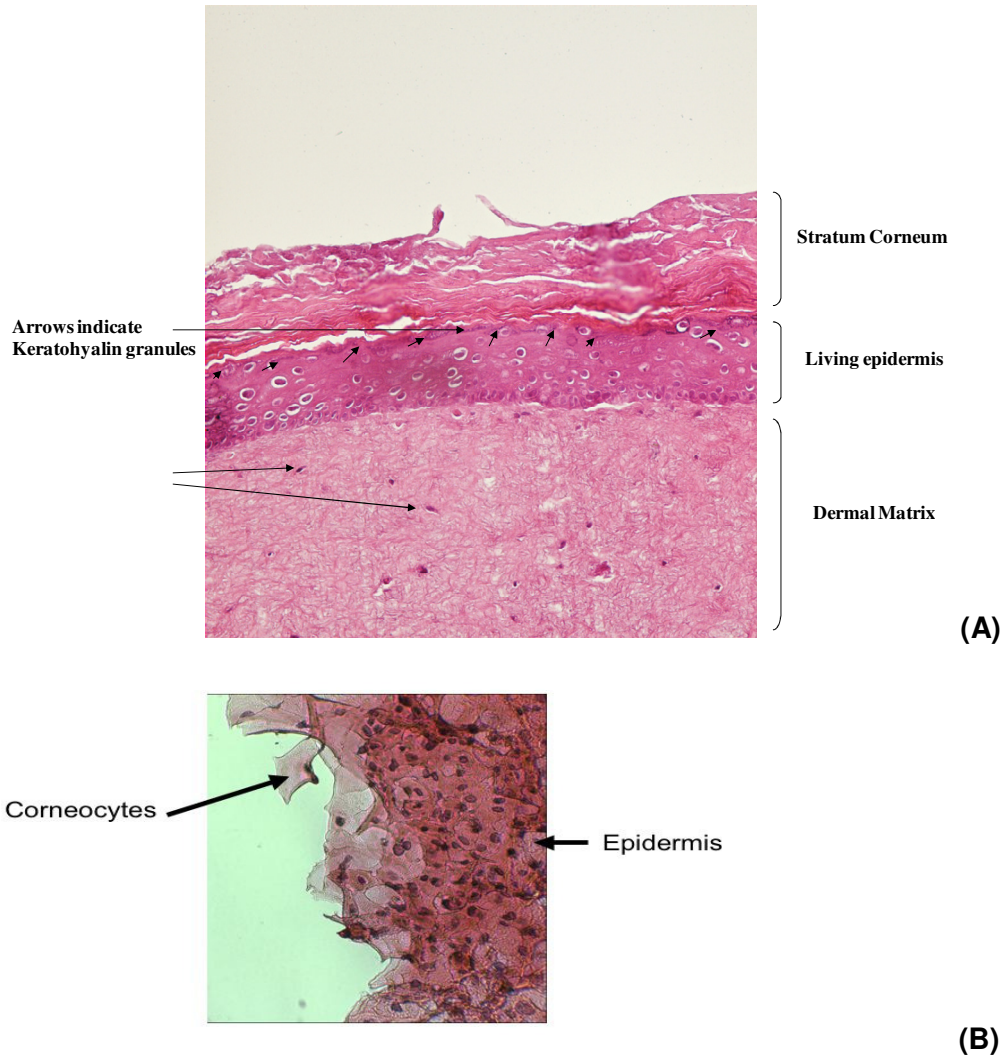

Figure 6.5: Vertical (cross-section) and horizontal (looking down from stratum corneum surface) histology of HSE at 21 days after exposure to ALI. Sections (6 µm) were stained with H & E and observed by light microscopy. The vertical cross-section (A) shows presence of abundant keratohyalin granules in the granular layer of epidermis. A horizontal (top-down) image of the HSE (B) after H &E staining shows the superficial anucleated corneocytes and the lower nucleated keratinocytes.

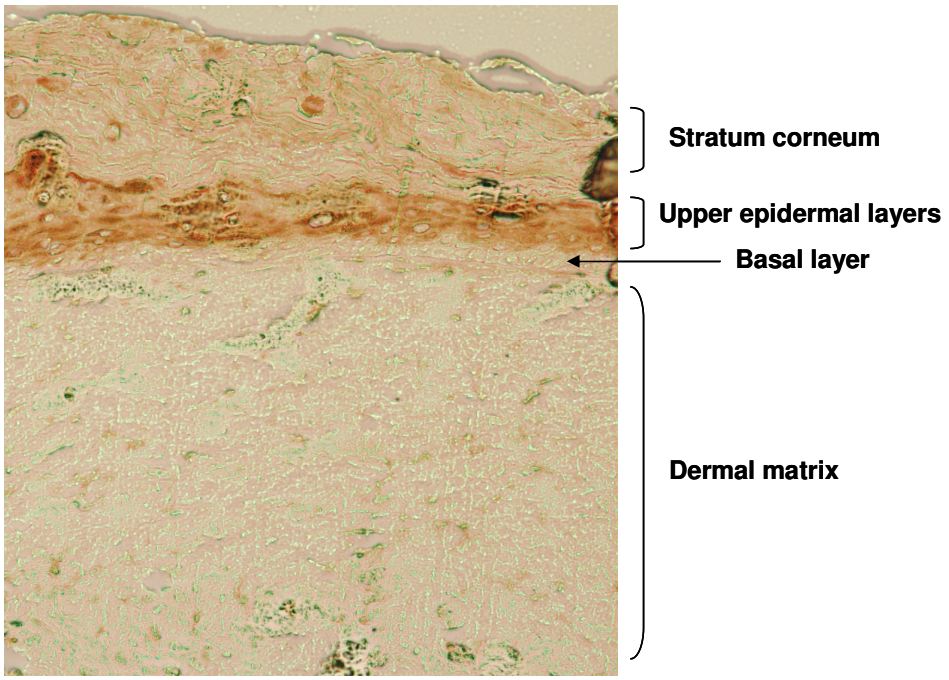

(A) Involucrin localization in HSE

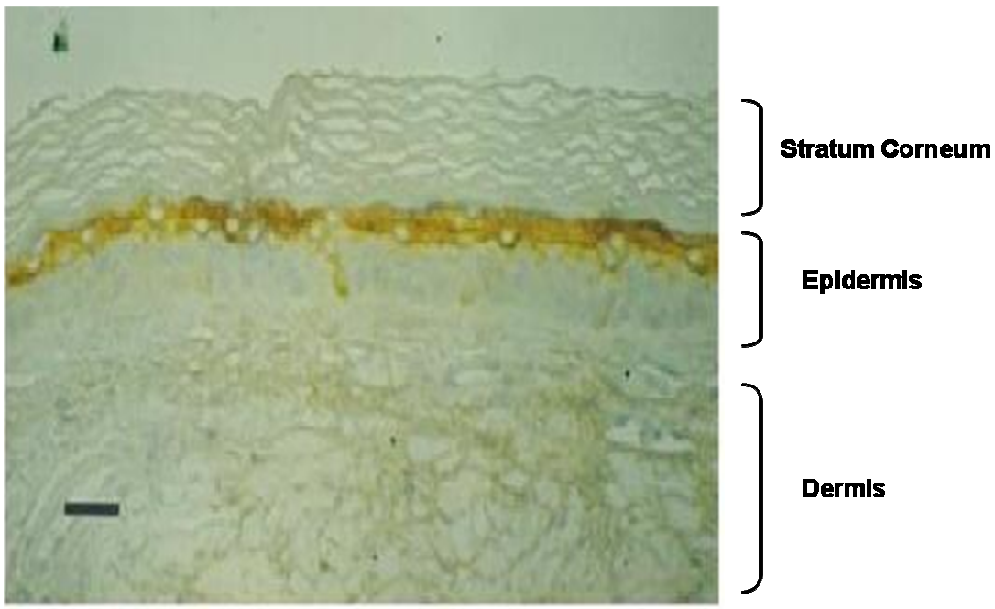

(B) Involucrin in human skin, picture adapted from Ref:(83)

Figure 6.6: Involucrin expression in HSE (A) and in human skin (B)

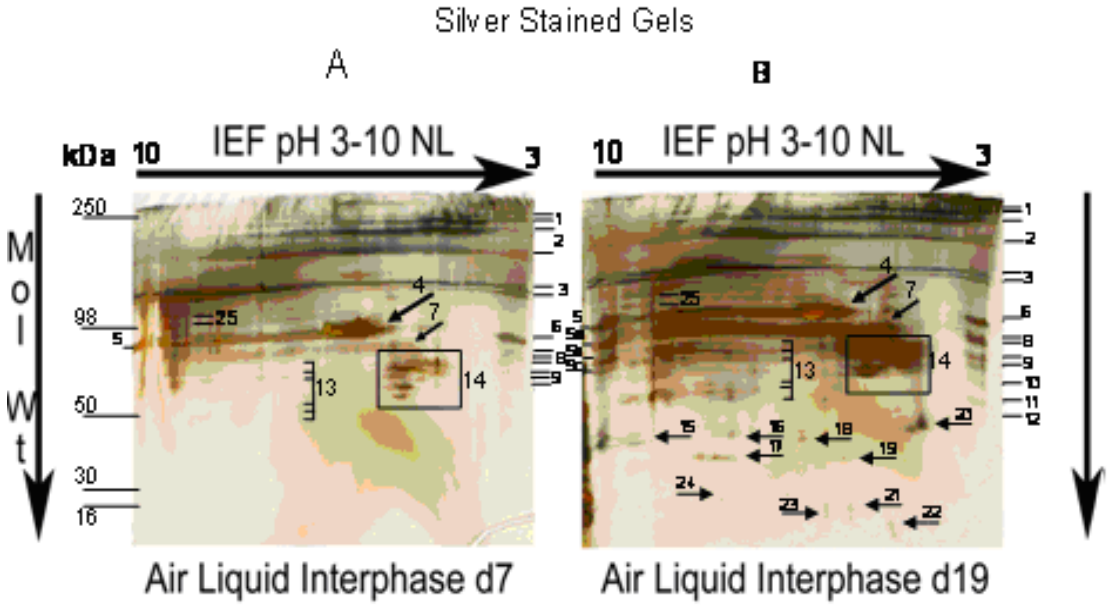

(A) **(B)**

Figure 6.7: Changes in protein expression in HSE after culture at 7 days at ALI (A) and 19 days at ALI (B) detected by 2 D Gel Electrophoresis.

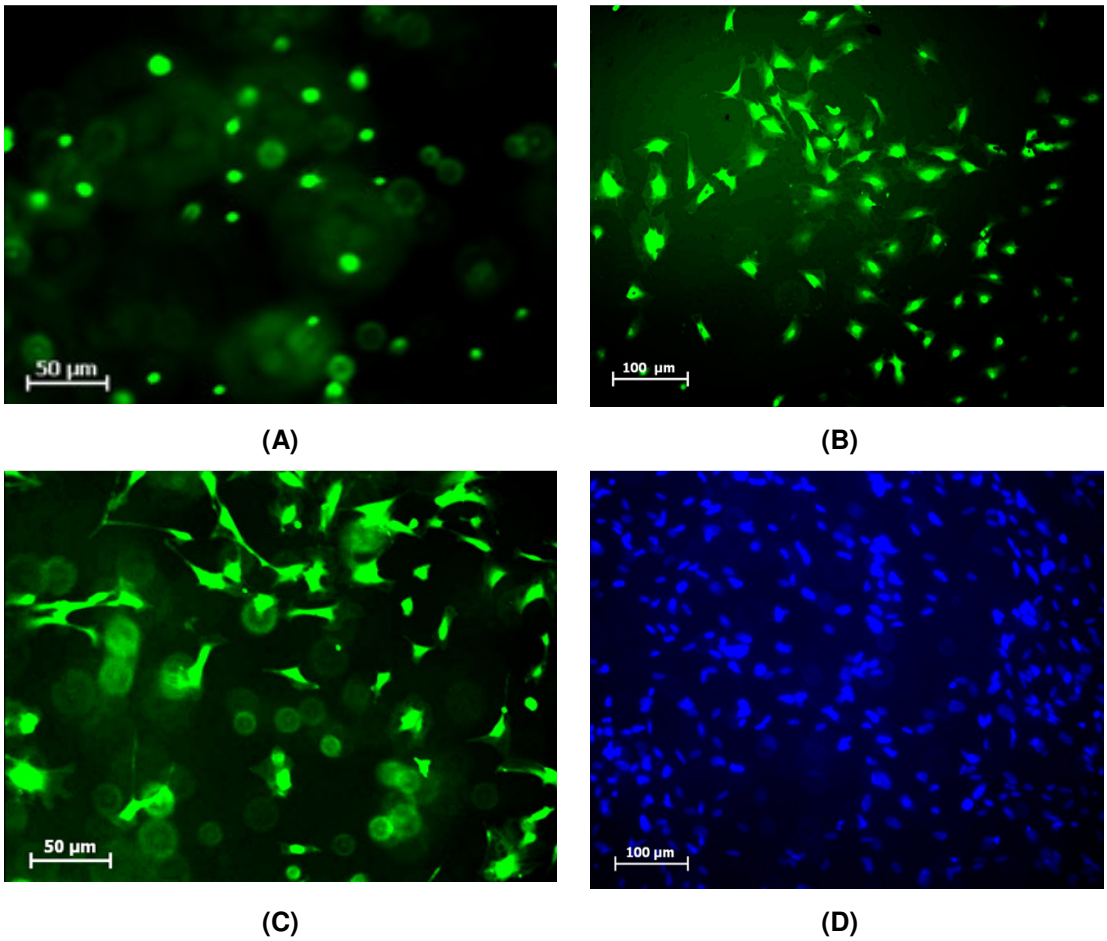

Figure 6.8: (A,B,C): Dermal layers made with GFP expressing fibroblasts. On day 1 (A), cells appear circular and homogenously distributed in the collagen matrix, circularity index: 0.86 (SD: 0.04) Image J software, NIH, USA. Cells are growing well and are fibrous on day 4 (B), circularity index: 0.43 (SD: 0.12) and on day 6 (C), circularity index: 0.22 (SD: 0.07) and appear to be proliferating in the matrix. (D): Nuclei of keratinocytes labeled with Hoechst 33342 dye seen attached on the surface of the fibroblast–collagen matrix. The attachment of keratinocytes is homogenous.

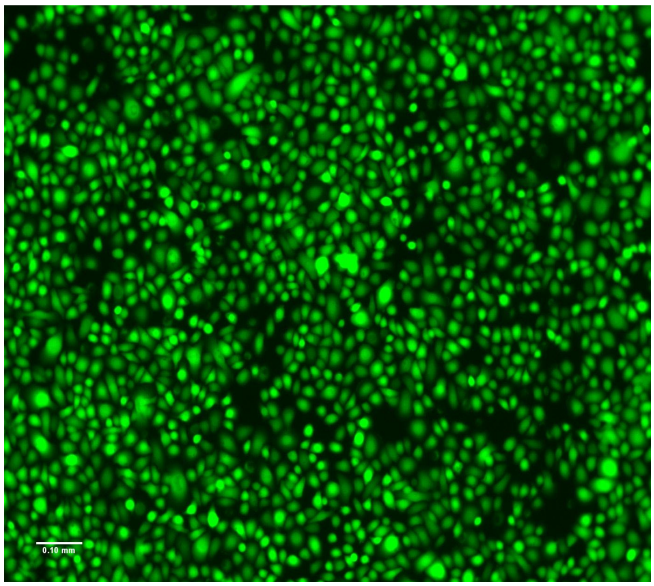

Figure 6.9: Keratinocytes labeled with 7.5 µM Calcein AM post 3 h of adhesion in wells of polycarbonate plates (10 X).

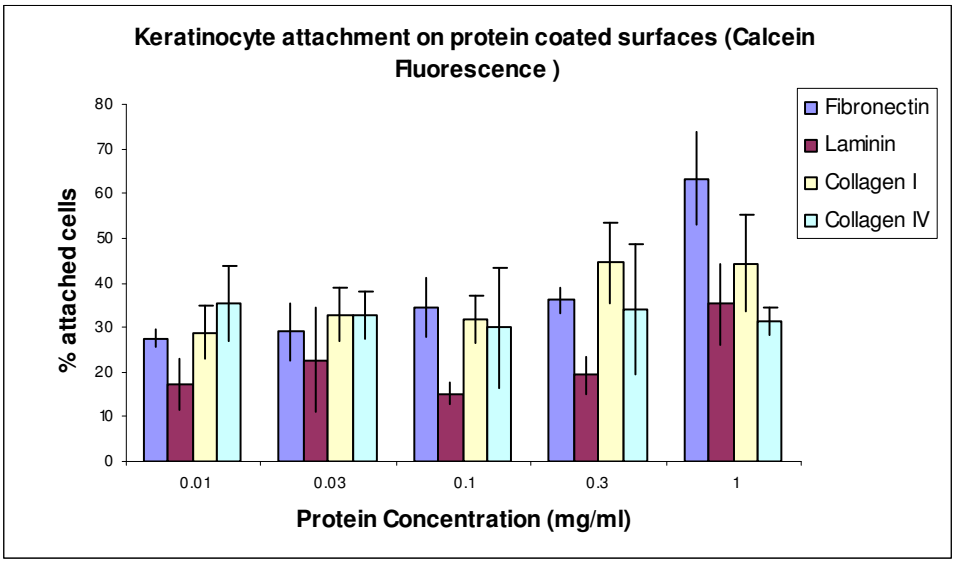

(A) % attachment of keratinocytes on individual ECM protein coated surfaces

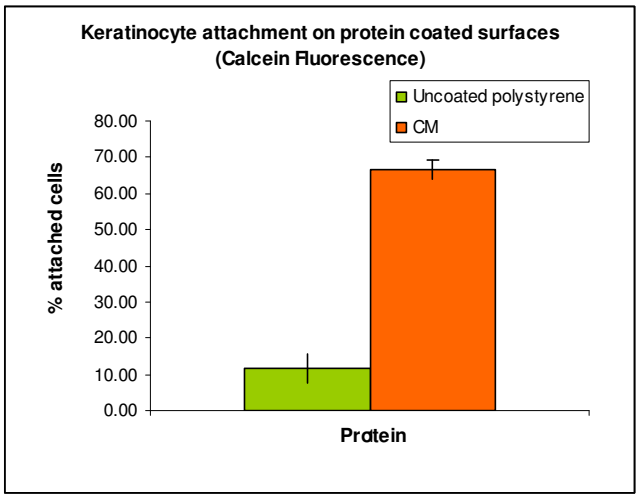

(B) % attachment of keratinocytes on Coating Matrix (CM) coated surfaces

Figure 6.10: Attachment of Calcein labeled keratinocytes on protein coated surfaces. Analysis was conducted by Calcein fluorescence determination after attachment. Coating matrix (CM) is a mixture of Type I and Type IV Collagen.

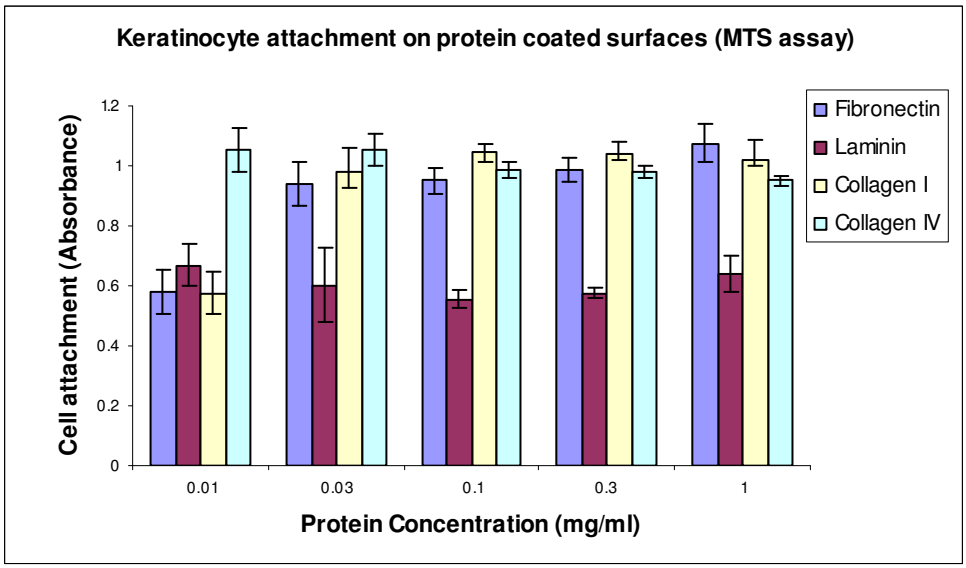

(A) % attachment of keratinocytes on individual ECM protein coated surfaces

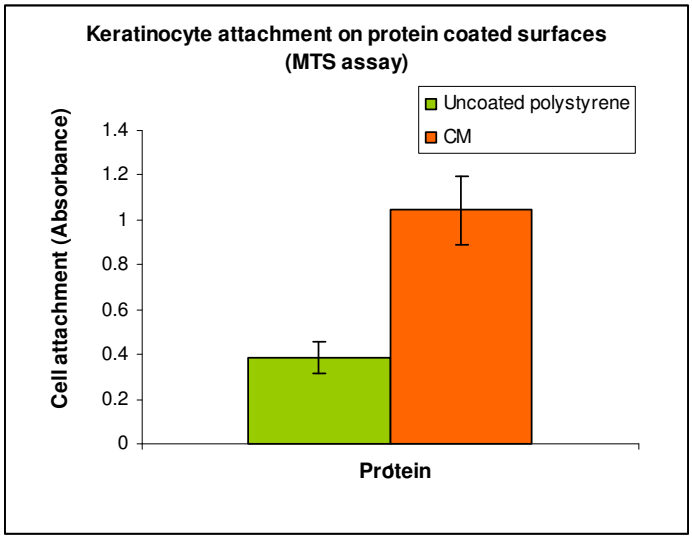

(B) % attachment of keratinocytes on Coating Matrix (CM) coated surfaces

Figure 6.11: Attachment of Calcein labeled keratinocytes to protein coated surface. Analysis was conducted by determination of cell viability (absorbance) using the MTS assay. Coating matrix (CM) is a mixture of Type I and Type IV Collagen.

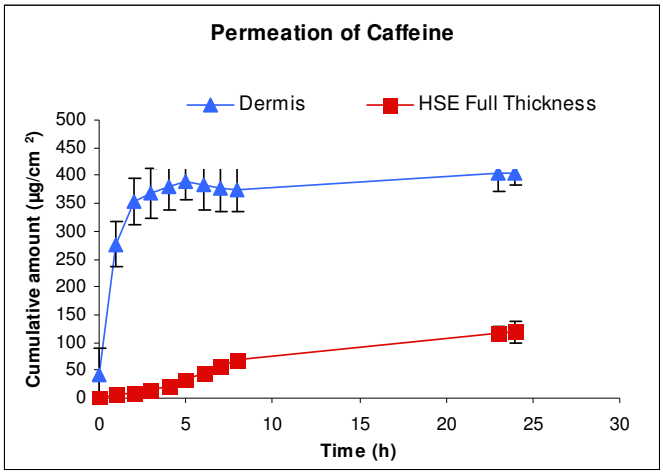

(A)

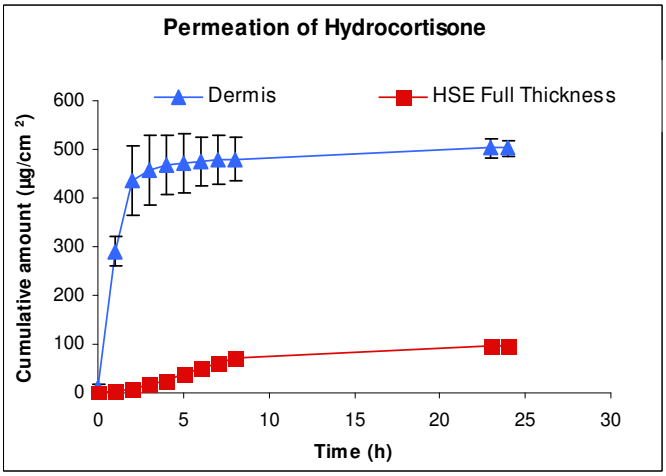

(B)

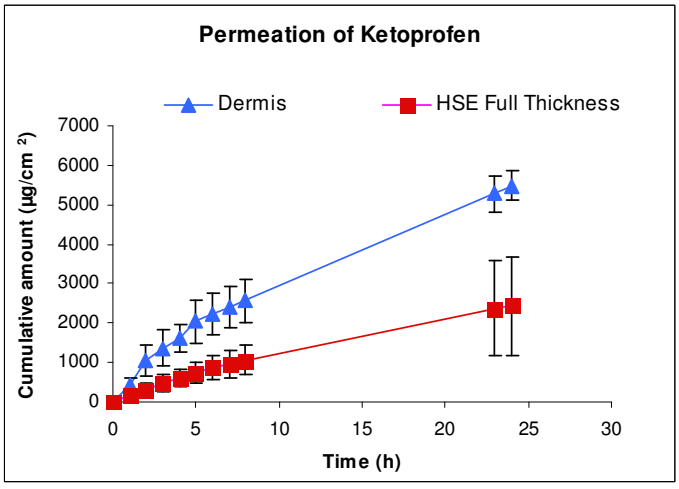

(C)

Figure 6.12: Permeation of caffeine (A), hydrocortisone (B) and ketoprofen (C) through the full thickness HSE and its dermal component.

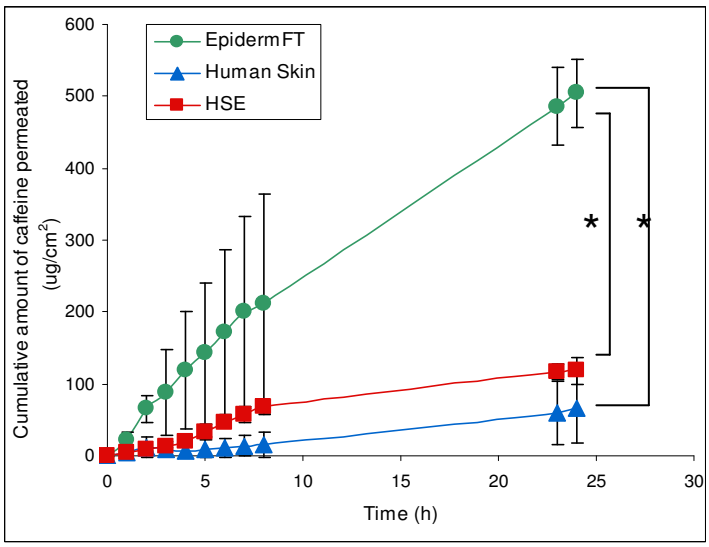

(A) Caffeine

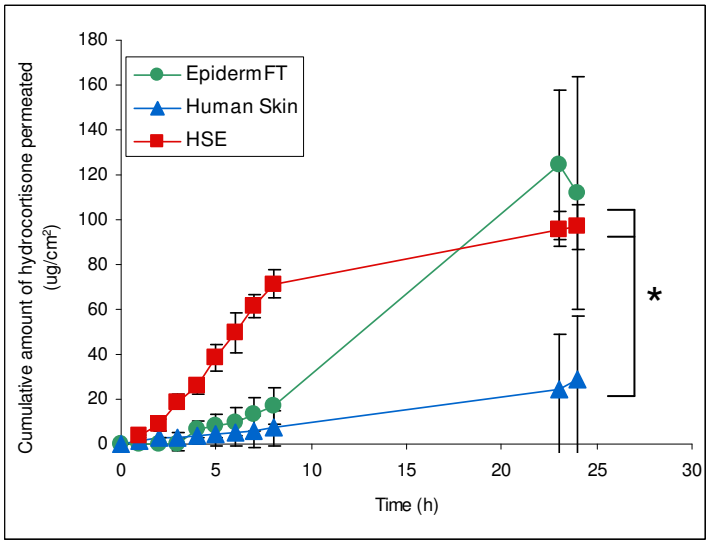

(B) Hydrocortisone

Figure 6.13: Permeability profiles of agents through HSE-OP, EpidermFT® and Human Skin

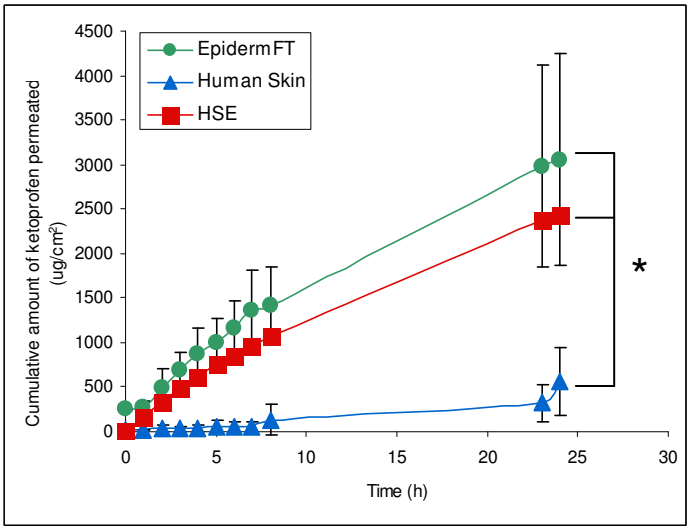

(C) Ketoprofen

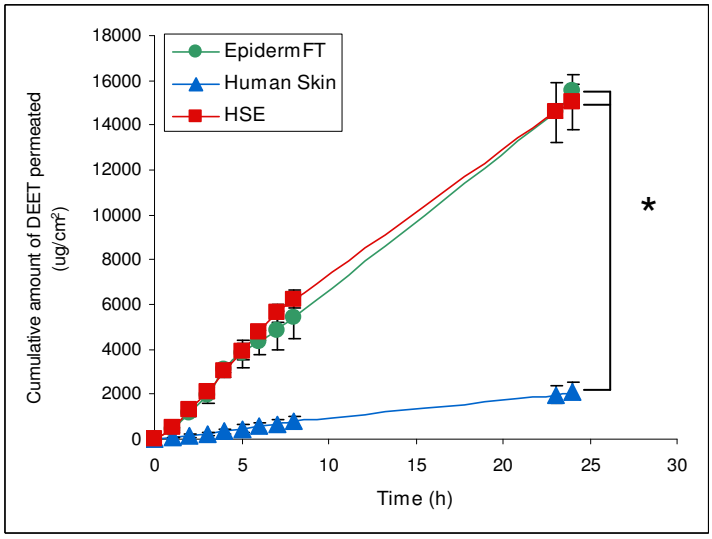

(D) DEET

Figure 6.13: Permeability profiles of agents through HSE-OP, EpidermFT® and Human Skin

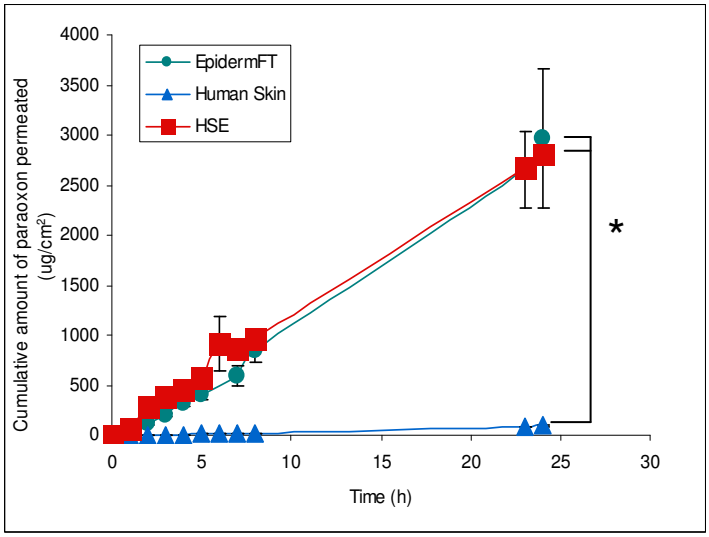

(E)Paraoxon

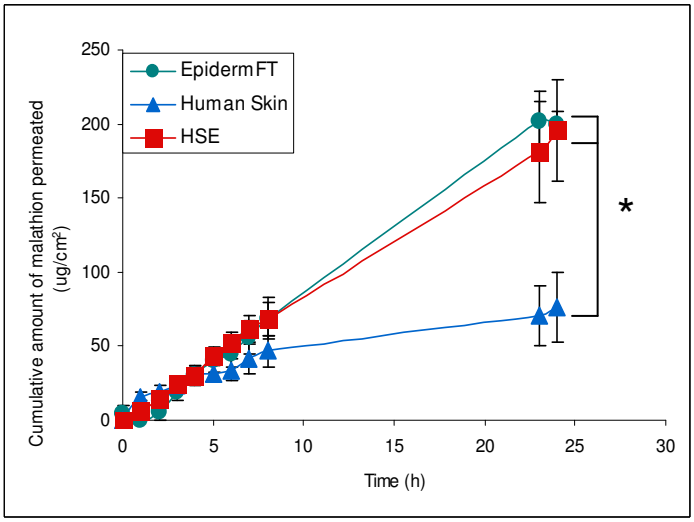

(F) Malathion

Figure 6.13: Permeability profiles of agents through HSE-OP, EpidermFT® and Human Skin.

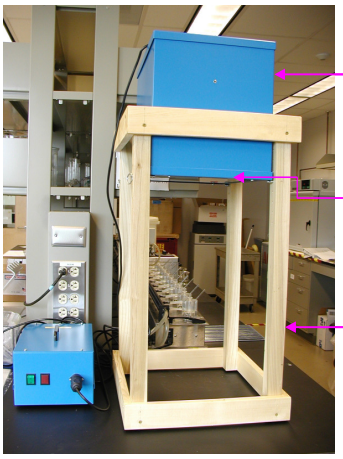

(A)

(B)

(C)

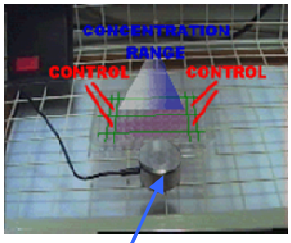

(D) Adapted from Ref: (113)

Figure 7.1: UVA irradiation source for the Phototoxicity experiments. The source consists of the solar simulator: an SOL 500 lamp (A), an adjustable platform to change the distance between the lamp and the sample (B), protective dark covering to focus irradiation on the sample (C), and a UVA meter (D) kept next to the sample to measure the exact incident irradiation.

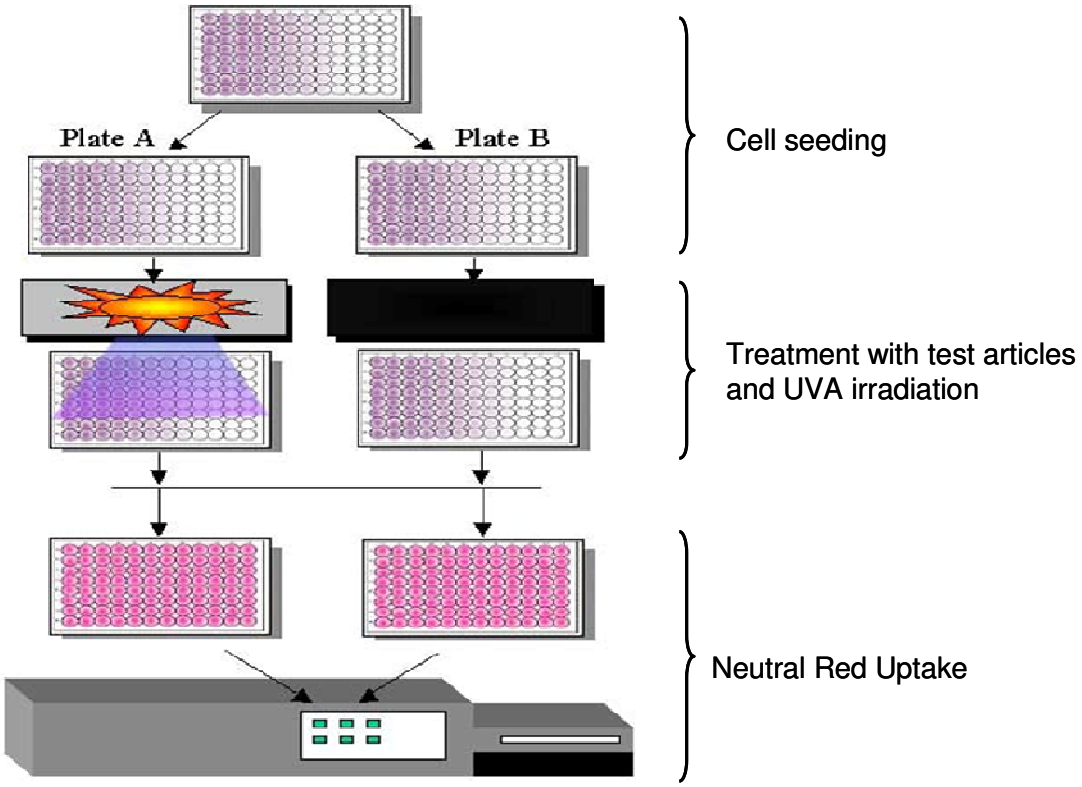

(A)

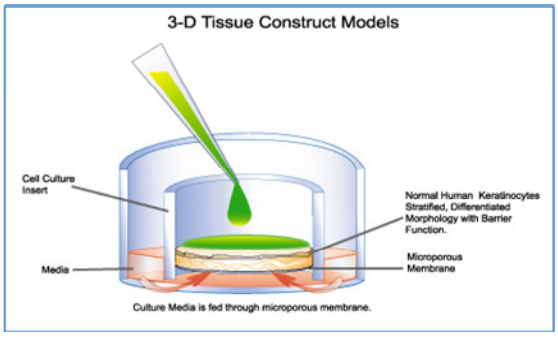

(B)

Figure 7.2: Schematic representation of evaluation of phototoxicity potential of agents in fibroblasts by the 3T3 Neutral Red Uptake assay (A) (Adapted from Ref: (114)) and in a skin equivalent (B) (Adapted from Ref: (115)).

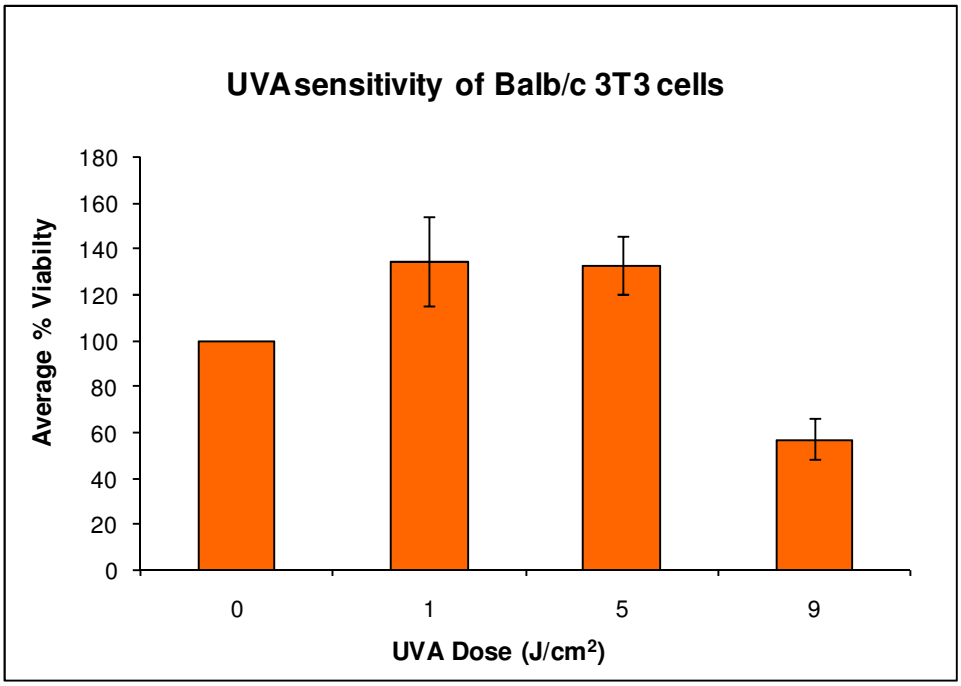

Figure 7.3: UVA sensitivity of Balb/c 3T3 fibroblasts.

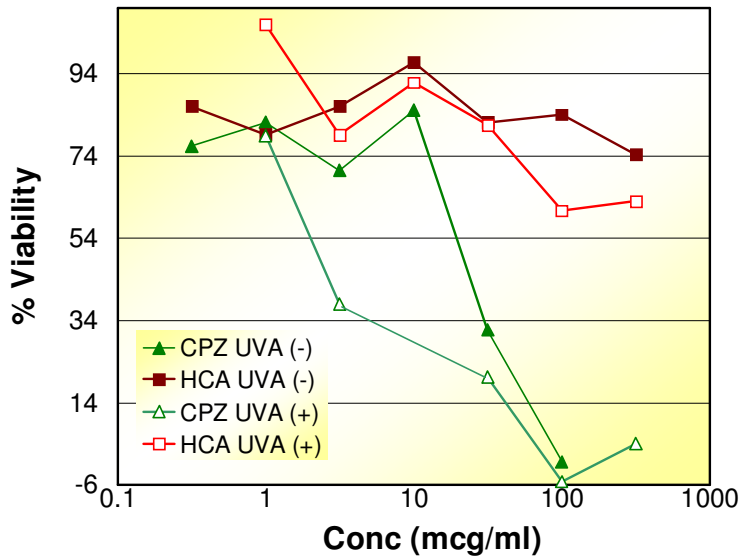

Figure 7.4: Dose Response Curves of Hydroxycinnamic Acid (HCA) and Chlorpromazine (CPZ) from the range finder 3T3 Neutral Red Uptake assay.

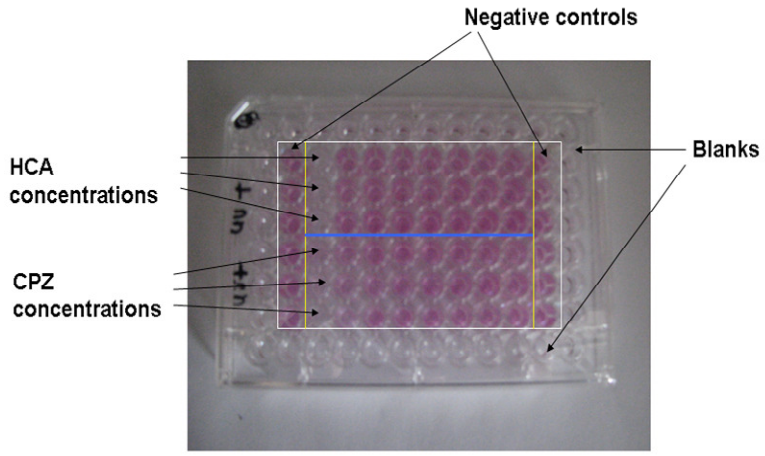

Neutral Red extracted from Balb/c 3T3 cells seeded in UVA (-) 96 well plate

Note: Concentrations from left to right range from highest to lowest

(A)

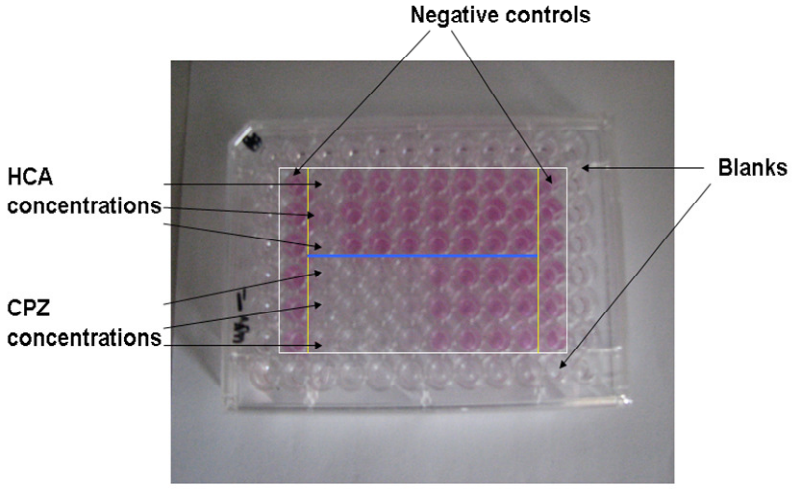

Neutral Red extracted from Balb/c 3T3 cells seeded in UVA (+) 96 well plate

Note: Concentrations from left to right range from highest to lowest

(B)

Figure 7.5: Neutral Red extracted from 3T3 fibroblasts after treatment with Chlorpromazine (CPZ) and Hydroxycinnamic Acid (HCA) in the absence (A) and presence (B) of UVA light (Main Experiment).

Note: Concentrations decrease from left to right.

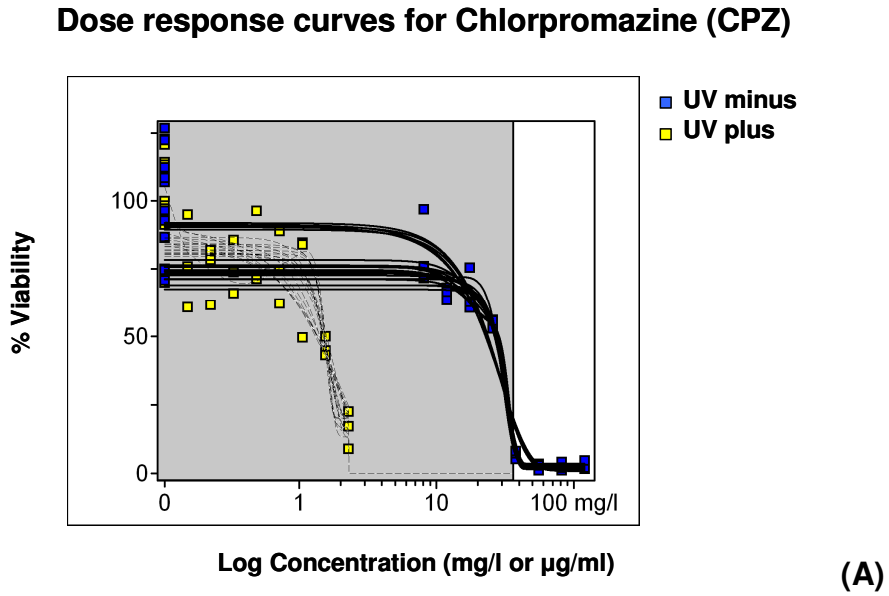

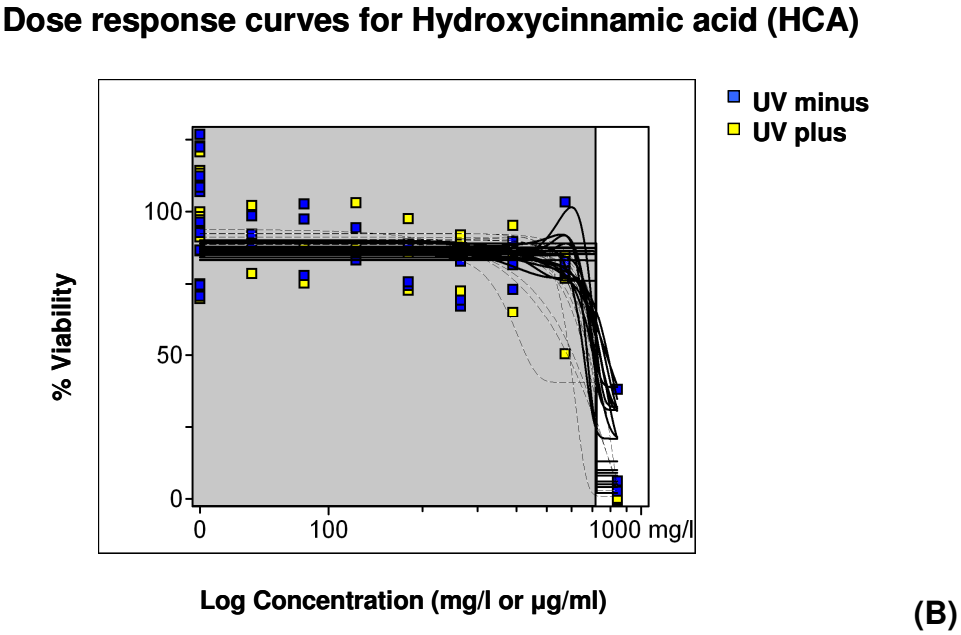

Figure 7.6: Dose Response Curves of Chlorpromazine (CPZ) (A) and Hydroxycinnamic Acid (HCA) (B) from main 3T3 Neutral Red Uptake assay.

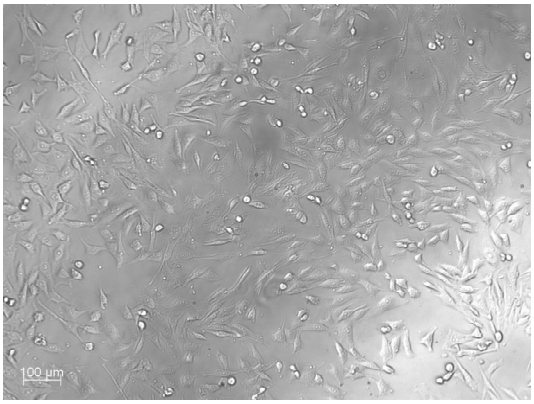

(A) Balb/c 3T3 cells –negative control (no treatment)

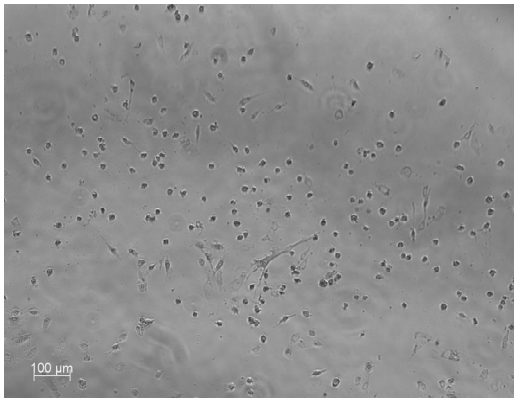

(B) Balb/c 3T3 cells –post treatment with CPZ (120.18 µg/ml) and UVA(+) irradiation

(C) Balb/c 3T3 cells – post treatment with HCA (390 µg/ml) and UVA (+) irradiation

Figure 7.7: Phase contrast images of Balb/c 3T3 cells after treatment with Hydroxycinnamic Acid (HCA) or Chlorpromazine (CPZ) and UVA irradiation.

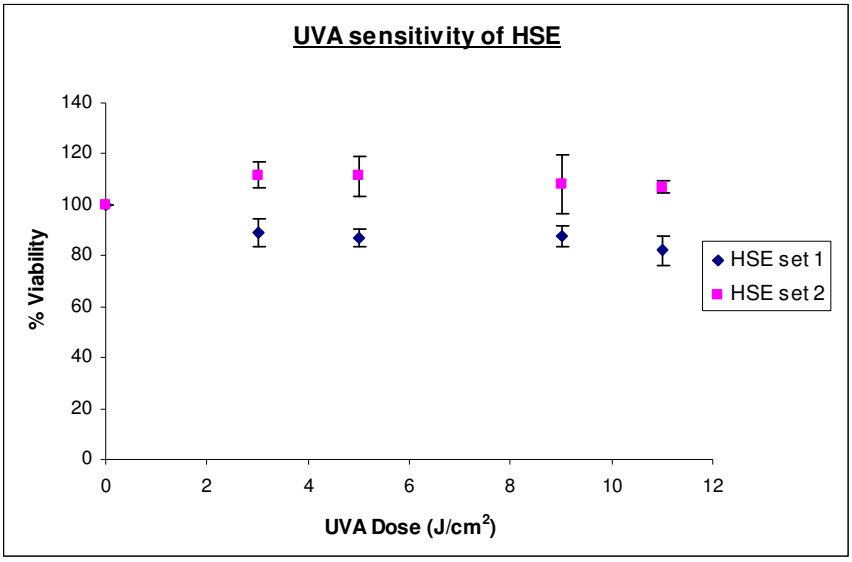

Figure 7.8: UVA sensitivity of HSE tissues

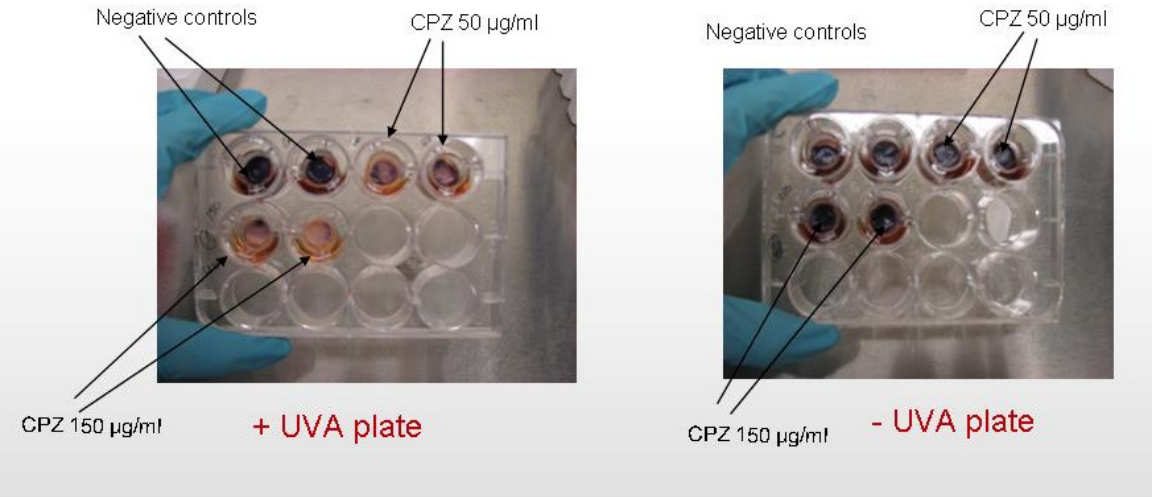

Figure 7.9: HSE after 3 h of incubation with MTS reagent 1mg/ml. Tissues were treated with Chlorpromazine (CPZ) concentrations 50 µg/ml and 150 µg/ml in the presence (A) and absence (B) of UVA light. Tissues stained purple indicate high viability, while clearer tissues indicate cytotoxicity.

CPZ: Chlorpromazine, HSE: Human Skin Equivalent

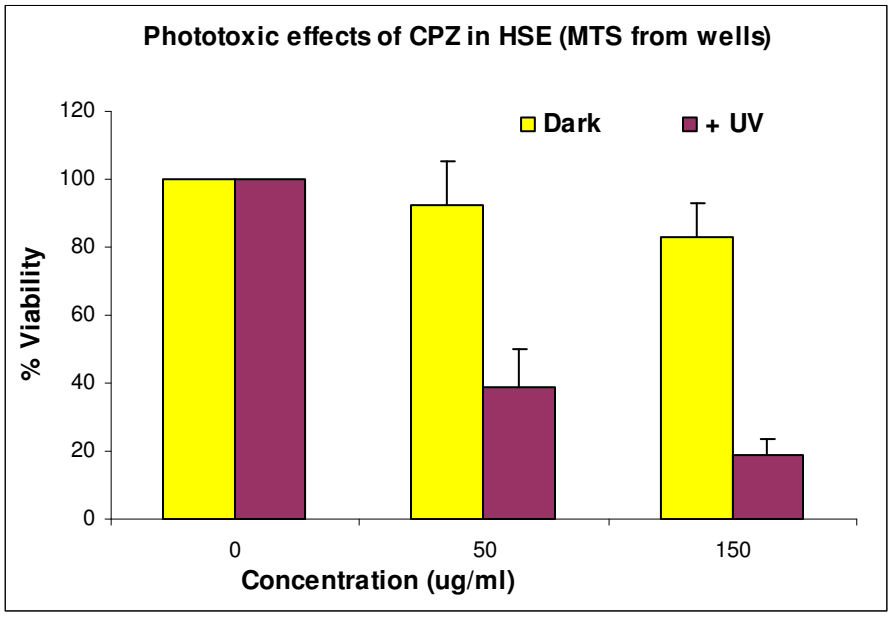

(A)

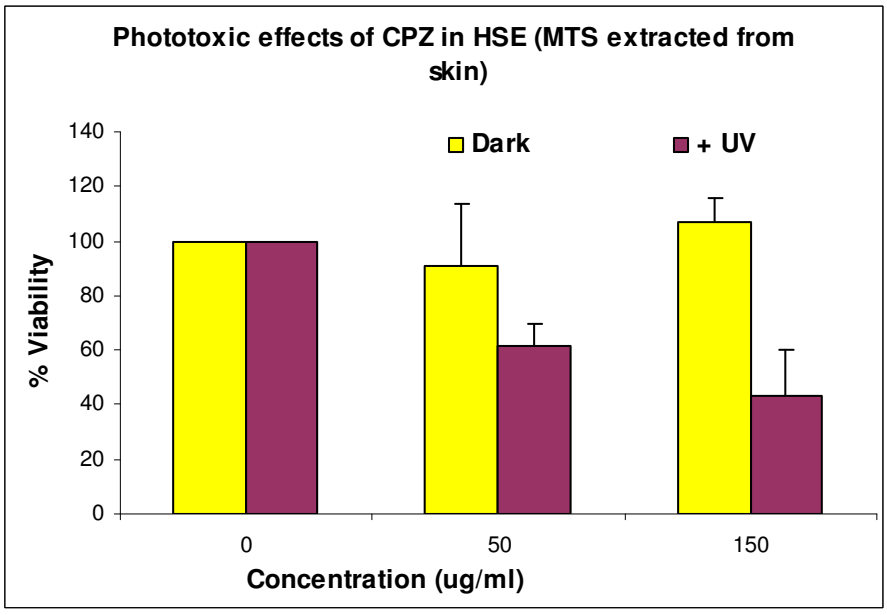

(B)

Figure 7.10: Quantitation of HSE viability after 3 h of incubation with MTS reagent 1mg/ml. Tissues were treated with CPZ concentrations 50 µg/ml and 150 µg/ml in the presence and absence of UVA light. MTS reagent extracted from well (A) or from HSE tissues (B) was used as a measure of tissue viability.

CPZ: Chlorpromazine, HSE: Human Skin Equivalent.

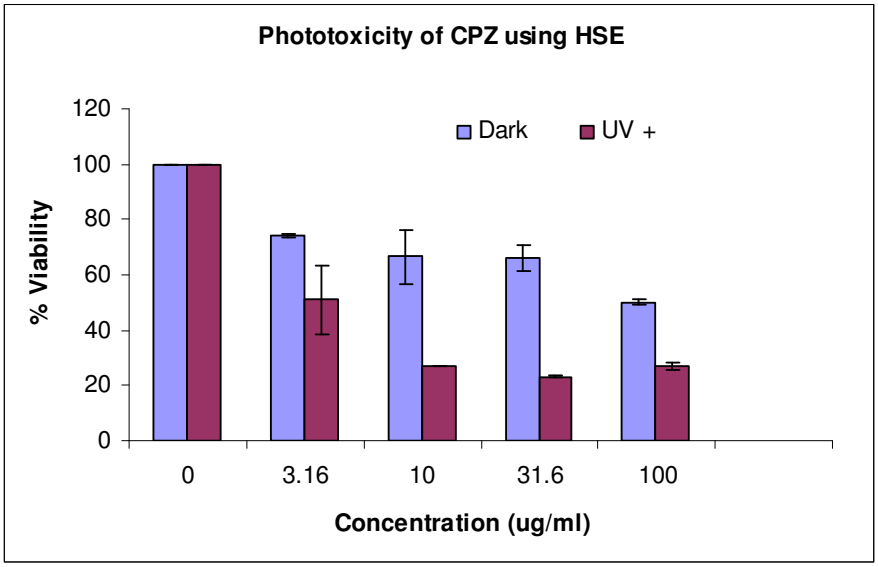

(A)

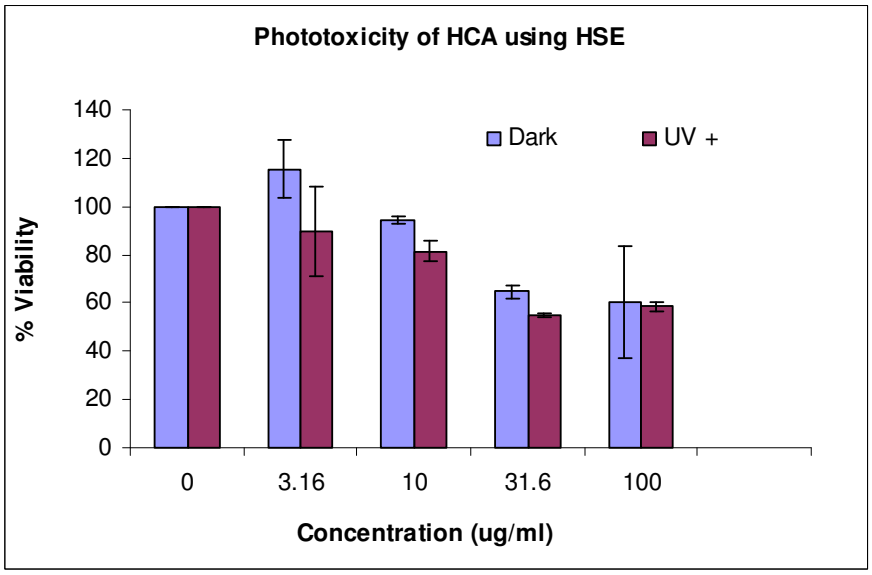

(B)

Figure 7.11: Evaluation of Phototoxicity of Hydroxycinnamic acid (HCA) in the HSE model. % Viability of HSE tissues after 3 h of incubation with MTS reagent 1mg/ml is shown. Tissues were treated with four CPZ (A) and HCA (B) concentrations in the presence and absence of UVA light and the percent viability was calculated by MTS assay (extracted from wells). CPZ: Chlorpromazine, HSE: Human Skin Equivalent.

Figure 8.1: Transwell inserts with cultured HSE mounted on vertical Franz diffusion cells (5.1 ml) for evaluation of the skin penetration potential of nanosphere formulations. The inserts were fixed on the receptor compartment of the cells with the aid of silicone grease.

HSE: Human Skin Equivalent.

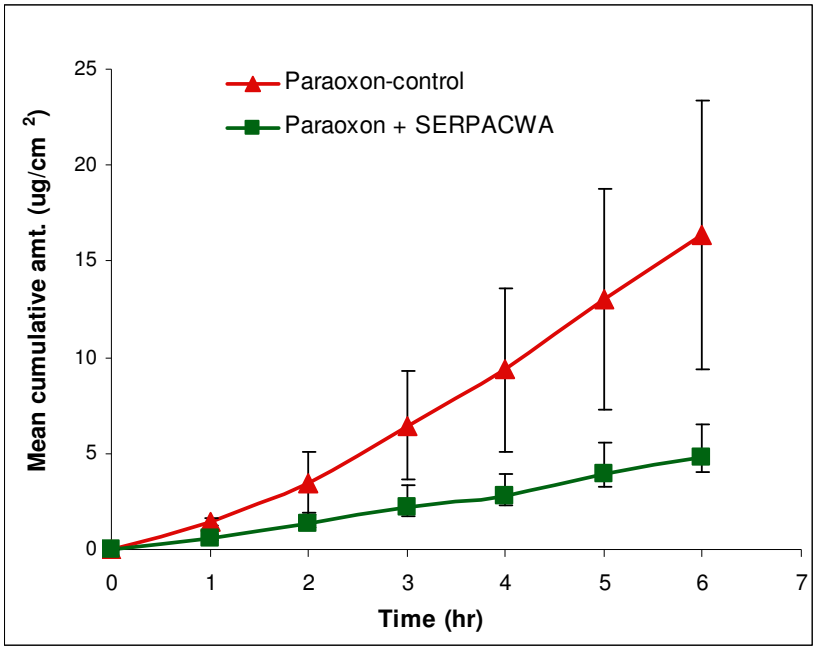

Figure 8.2: Mean cumulative amount (± S.E) of paraoxon permeated per cm^2 of human skin in the presence and absence of SERPACWA.

SERPACWA: Skin Exposure Reduction Paste Against Chemical Warfare Agents.

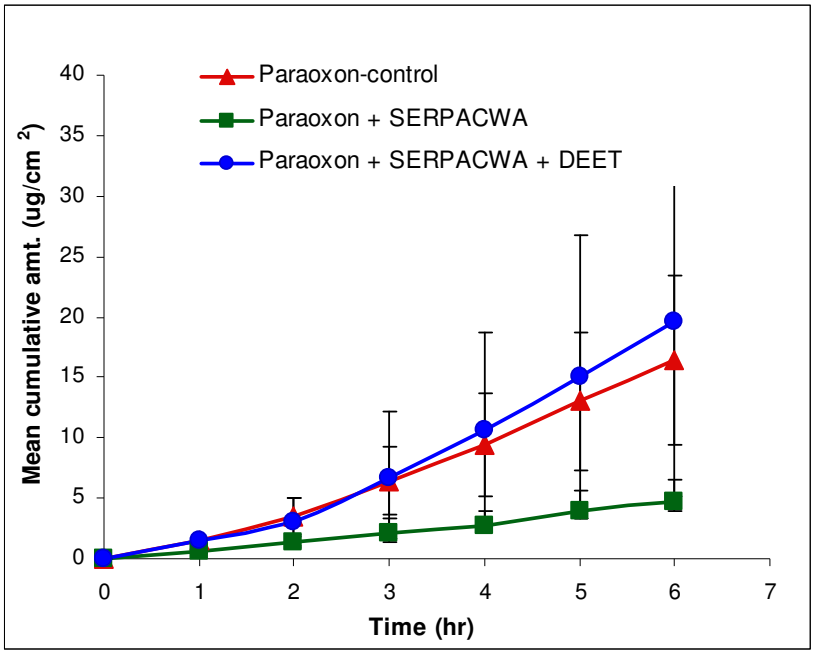

Figure 8.3: Mean cumulative amount (± S.E) of paraoxon permeated per cm^2 of human skin in the presence and absence of SERPACWA and DEET.

SERPACWA: Skin Exposure Reduction Paste Against Chemical Warfare Agents.

DEET: n,n, Diethyl-m-toluamide.

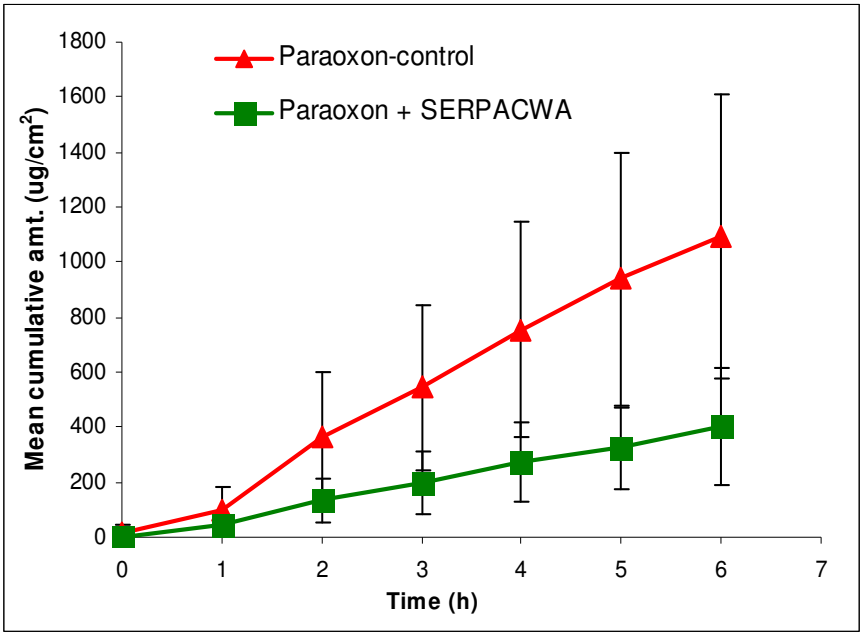

Figure 8.4: Mean cumulative amount (± S.E) of paraoxon permeated per cm^2 of HSE in the presence and absence of SERPACWA.

SERPACWA: Skin Exposure Reduction Paste Against Chemical Warfare Agents.

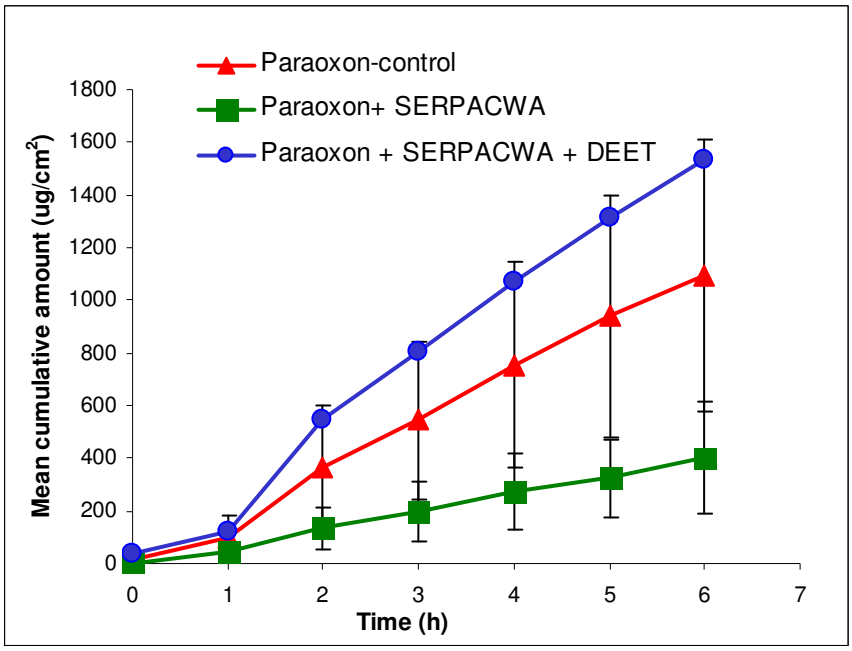

Figure 8.5: Mean cumulative amount (± S.E) of paraoxon permeated per cm^2 of HSE in the presence and absence of SERPACWA and DEET.

SERPACWA: Skin Exposure Reduction Paste Against Chemical Warfare Agents.

DEET: n,n, Diethyl-m-toluamide.

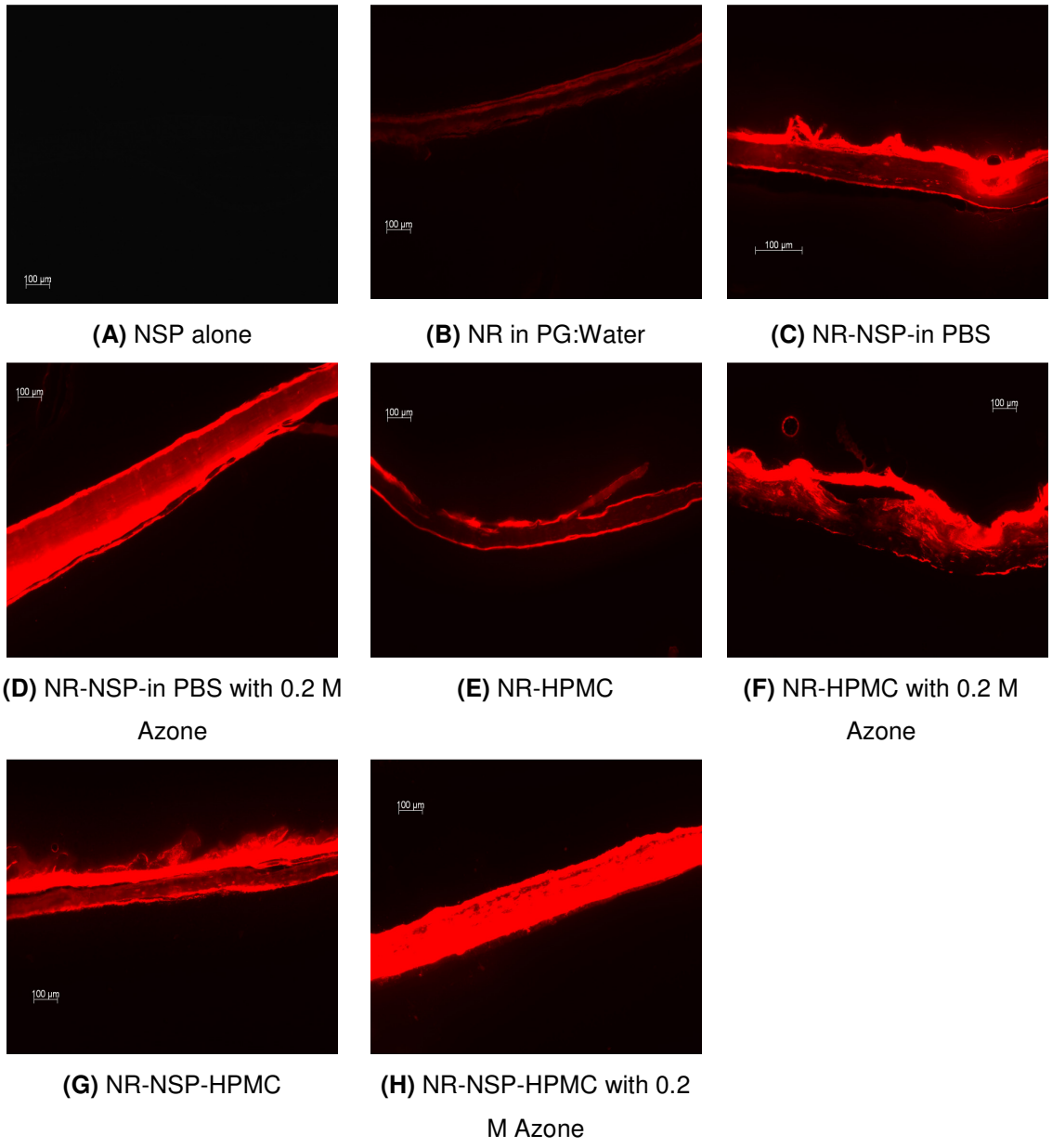

(A) NSP alone

(B) NR in PG:Water

(C) NR-NSP-in PBS

(D) NR-NSP-in PBS with 0.2 M Azone

(E) NR-HPMC

(F) NR-HPMC with 0.2 M Azone

(G) NR-NSP-HPMC

(H) NR-NSP-HPMC with 0.2 M Azone

Figure 8.6: *In vitro* skin permeation of NR via NSP in HPMC gel and aqueous formulations through the Human Skin Equivalent. Pictures denote qualitative determination of the extent of NR penetration in different skin layers. Skin pieces treated with various NR formulations were cryo-sectioned (6 µ thickness) and observed by fluorescent microscopy.

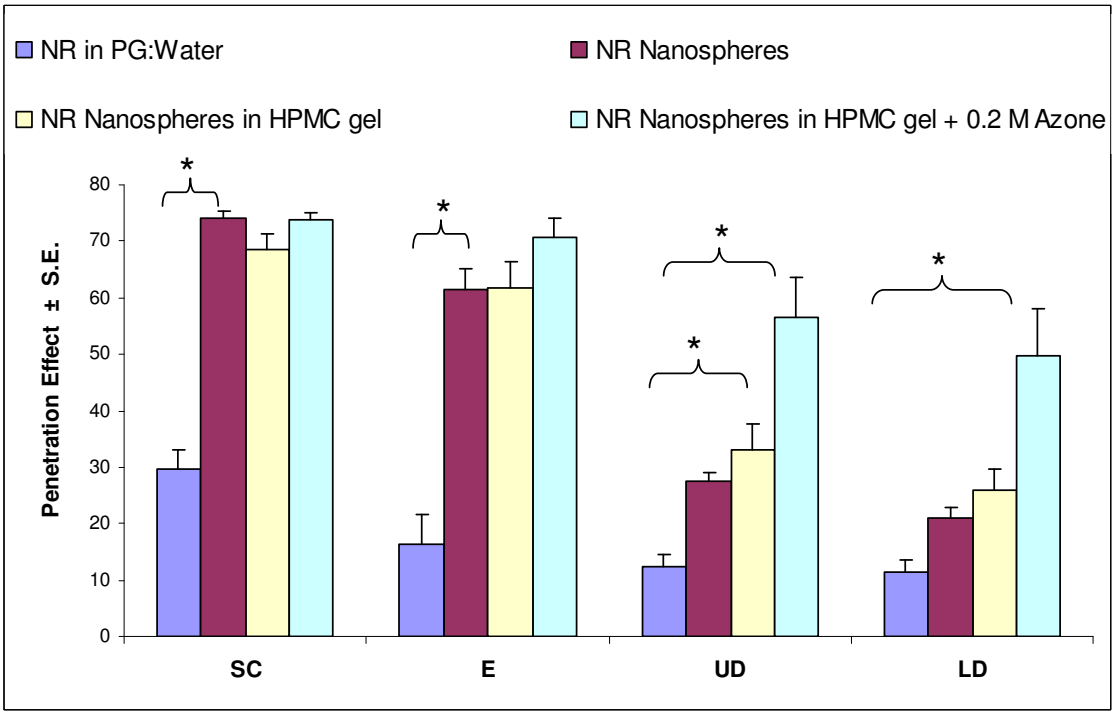

Figure 8.7: Quantitative determination of *in vitro* skin permeation of NR via NSP in HPMC gel and aqueous formulations through the Human Skin Equivalent. Quantitation of the NR fluorescence was conducted with Image J software (NIH, USA) in terms of pixel intensities and converted to Penetration Effect (Arbitrary Units).

SC: Stratum Corneum, E: Epidermis, UD: Upper Dermis, LD: Lower Dermis

Note: Selected statistical analyses are shown, and were conducted using the ANOVA test. * indicates a statistically significant difference with $p < 0.05$.

12 Structures

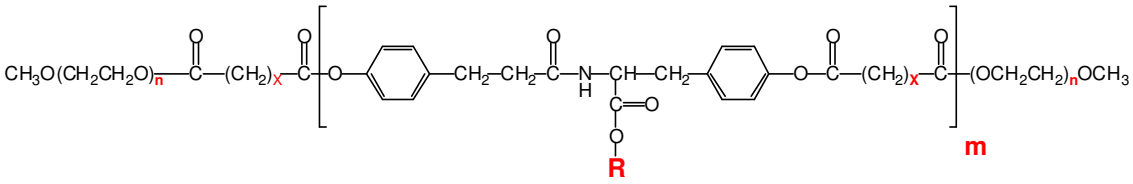

Structure 1: Structure of PEG-*b*-oligo(DTO-SA)-*b*-PEG triblock copolymer (ABA Triblock Copolymer). The Mw of PEG = 5000.

R= DTO (Octyl)

X= SA (Suberate)

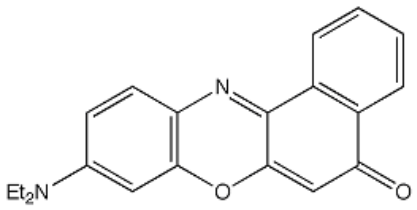

Nile Red (Log D 3.10)

Structure 2: Nile Red.

LogD values (pH 7) were obtained from (ACD/Labs software).

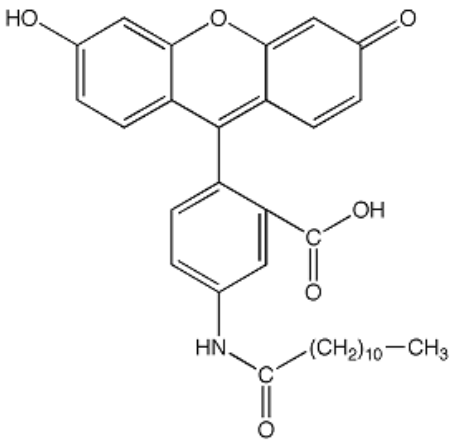

DAF (Log D 7.54)

Structure 3: 5-dodecanoylaminofluorescein (DAF)

LogD values (pH 7) were obtained from (ACD/Labs software).

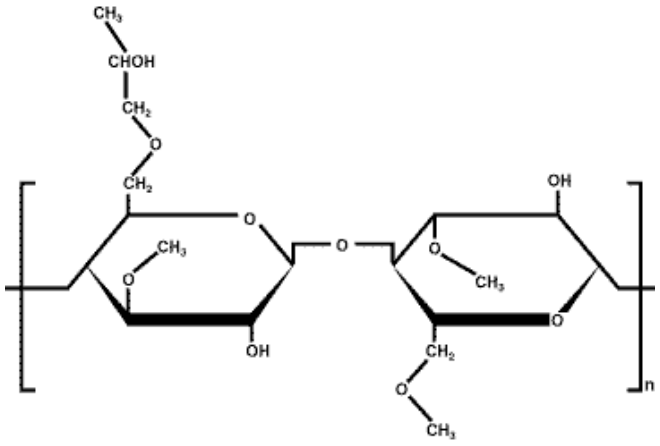

Structure 4: HydroxyPropyl MethylCellulose (HPMC) (Adapted from Ref: (116))

Chemical composition: $C_{56}H_{108}O_{30}$

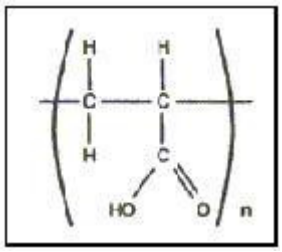

Structure 5: General Structure of Carbopol Polymers (Adapted from Ref: (117))

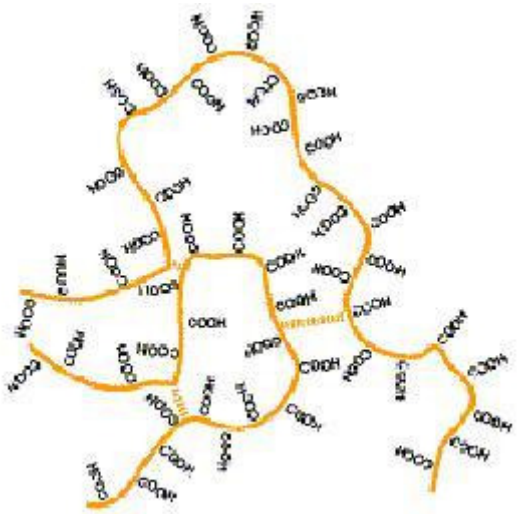

Structure 6: Schematic representation of a molecular segment of a cross-linked polyacrylic acid polymer (Adapted from Ref: (117))

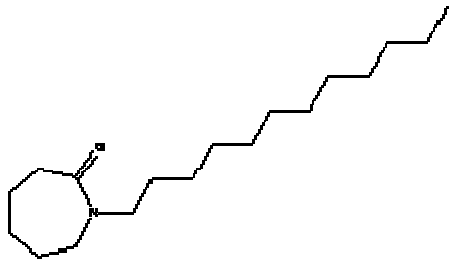

Structure 7: Azone (1-dodecylazacycloheptan-2-one or laurocapram) (Adapted from Ref:(118))

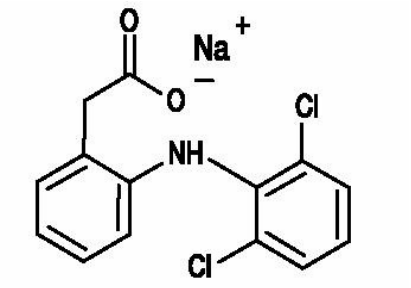

Structure 8: Diclofenac Sodium, Adapated from Ref: (119)

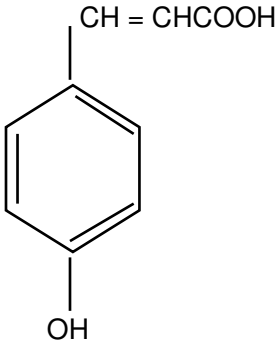

Structure 9: p-Hydroxycinnamic acid (HCA)

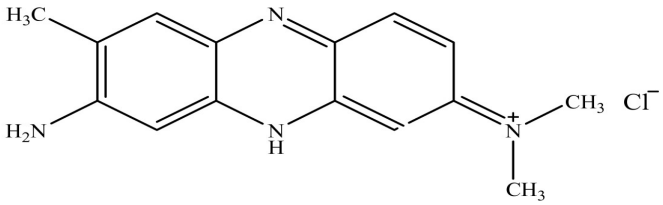

Structure 10: Neutral Red (3-amino-7-dimethylamino-2-methylphenazine hydrochloride)

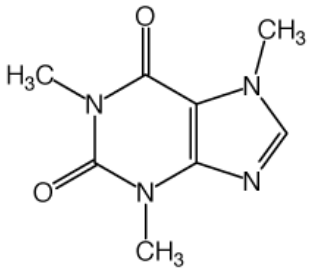

Structure 11: Caffeine

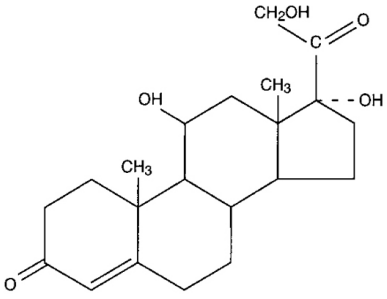

Structure 12: Hydrocortisone

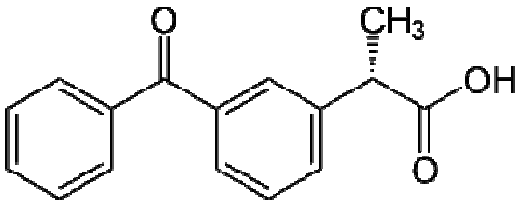

Structure 13: Ketoprofen

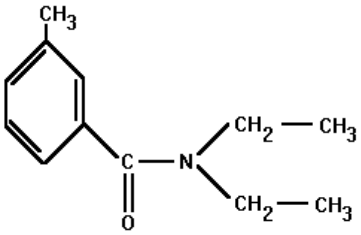

Structure 14: DEET

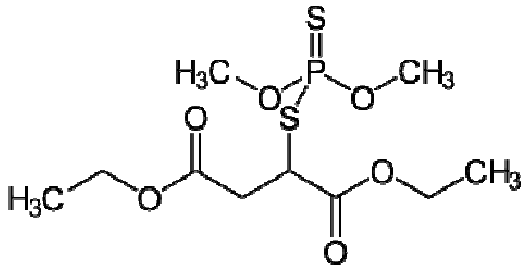

Structure 15: Malathion

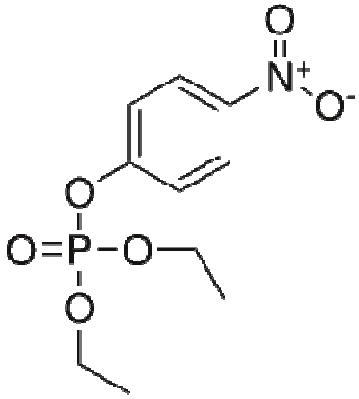

Structure 16: Paraoxon

13 Bibliography

1. C. Dubin. Transdermal delivery becoming more active. *Drug Delivery Technology* **8**: 38-43 (2008).

2. T. Tannerand R. Marks. Delivering drugs by the transdermal route: review and comment. *Skin Res Technol* **14**: 249-60 (2008).

3. A. Nanda, S. Nanda, and N. M. Ghilzai. Current developments using emerging transdermal technologies in physical enhancement methods. *Curr Drug Deliv* **3**: 233-42 (2006).

4. L. Sheihet, R. A. Dubin, D. Devore, and J. Kohn. Hydrophobic drug delivery by self-assembling triblock copolymer-derived nanospheres. *Biomacromolecules* **6**: 2726-31 (2005).

5. L. Sheihet, Kohn, J., Devore, D., Rubin, E.H., Gounder, M.K. Development of a Novel Biodegradable nanospheres-Paclitaxel Formulation as a Potential Anti-Cancer Agent: Evaluation of Toxicity and Efficacy in Comparison with Cremophor-Based Paclitaxel. *The Annual Retreat on Cancer Research in New Jersey, New Jersey.* (2007).

6. A. C. Williams. 'Structure and function of human skin' in Transdermal and Topical Drug Delivery: From theory to clinical practice. *Pharmaceutical Press* (2003).

7. G. L. Wilkes, I. A. Brown, and R. H. Wildnauer. The biomechanical properties of skin. *CRC Crit Rev Bioeng* **1**: 453-95 (1973).

8. E. Proksch, J. M. Brandner, and J. M. Jensen. The skin: an indispensable barrier. *Exp Dermatol* (2008).

9. P. W. Wertz, and Downing, P.T. Stratum corneum:biological and biochemical considerations. *in:Transdermal Drug Delivery:Developmental Issues and Research Initiatives, Marcel Dekker, NY, Hadgraft, J. and Guy, R.H. (Eds.)* 1-22 (1989).

10. B. W. Barry. Novel mechanisms and devices to enable successful transdermal drug delivery. *Eur J Pharm Sci* **14**: 101-14 (2001).

11. P. Karande, A. Jain, K. Ergun, V. Kispersky, and S. Mitragotri. Design principles of chemical penetration enhancers for transdermal drug delivery. *Proc Natl Acad Sci U S A* **102**: 4688-93 (2005).

12. M. Aqil, A. Ahad, Y. Sultana, and A. Ali. Status of terpenes as skin penetration enhancers. *Drug Discov Today* **12**: 1061-7 (2007).

13. H. A. Benson. Transdermal drug delivery: penetration enhancement techniques. *Curr Drug Deliv* **2**: 23-33 (2005).

14. S. M. Moghimiand H. M. Patel. Current progress and future prospects of liposomes in dermal drug delivery. *J Microencapsul* **10**: 155-62 (1993).

15. G. Cevc, Schatzlein A., Blume, G. Transdermal drug carriers: basic properties, optimization and transfer efficiency in the case of epicutaneously applied peptides. *Journal of controlled release* **36**: 3-16 (1995).

16. E. Touitou, N. Dayan, L. Bergelson, B. Godin, and M. Eliaz. Ethosomes - novel vesicular carriers for enhanced delivery: characterization and skin penetration properties. *J Control Release* **65**: 403-18 (2000).

17. S. M. Niemiec, C. Ramachandran, and N. Weiner. Influence of nonionic liposomal composition on topical delivery of peptide drugs into pilosebaceous units: an in vivo study using the hamster ear model. *Pharm Res* **12**: 1184-8 (1995).

18. S. D. Mandawgadeand V. B. Patravale. Development of SLNs from natural lipids: application to topical delivery of tretinoin. *Int J Pharm* **363**: 132-8 (2008).

19. V. Teeranachaideekul, P. Boonme, E. B. Souto, R. H. Muller, and V. B. Junyaprasert. Influence of oil content on physicochemical properties and skin distribution of Nile red-loaded NLC. *J Control Release* **128**: 134-41 (2008).

20. M. P. Alves, A. L. Scarrone, M. Santos, A. R. Pohlmann, and S. S. Guterres. Human skin penetration and distribution of nimesulide from hydrophilic gels containing nanocarriers. *Int J Pharm* **341**: 215-20 (2007).

21. J. Shim, H. Seok Kang, W. S. Park, S. H. Han, J. Kim, and I. S. Chang. Transdermal delivery of mixnoxidil with block copolymer nanoparticles. *J Control Release* **97**: 477-84 (2004).

22. J. Pardeike, A. Hommoss, and R. H. Muller. Lipid nanoparticles (SLN, NLC) in cosmetic and pharmaceutical dermal products. *Int J Pharm* **366**: 170-84 (2009).

23. S. Kuchler, M. R. Radowski, T. Blaschke, M. Dathe, J. Plendl, R. Haag, M. Schafer-Korting, and K. D. Kramer. Nanoparticles for skin penetration enhancement--a comparison of a dendritic core-multishell-nanotransporter and solid lipid nanoparticles. *Eur J Pharm Biopharm* **71**: 243-50 (2009).

24. R. Alvarez-Roman, G. Barre, R. H. Guy, and H. Fessi. Biodegradable polymer nanocapsules containing a sunscreen agent: preparation and photoprotection. *Eur J Pharm Biopharm* **52**: 191-5 (2001).

25. R. Alvarez-Roman, A. Naik, Y. N. Kalia, R. H. Guy, and H. Fessi. Enhancement of topical delivery from biodegradable nanoparticles. *Pharm Res* **21**: 1818-25 (2004).

26. J. Lademann, H. Richter, A. Teichmann, N. Otberg, U. Blume-Peytavi, J. Luengo, B. Weiss, U. F. Schaefer, C. M. Lehr, R. Wepf, and W. Sterry. Nanoparticles--an efficient carrier for drug delivery into the hair follicles. *Eur J Pharm Biopharm* **66**: 159-64 (2007).

27. B. Zavan, V. Vindigni, K. Vezzu, G. Zorzato, C. Luni, G. Abatangelo, N. Elvassore, and R. Cortivo. Hyaluronan based porous nano-particles enriched with growth factors for the treatment of ulcers: a placebo-controlled study. *J Mater Sci Mater Med* **20**: 235-47 (2009).

28. C. Colonna, B. Conti, P. Perugini, F. Pavanetto, T. Modena, R. Dorati, P. Iadarola, and I. Genta. Ex vivo evaluation of prolidase loaded chitosan nanoparticles for the enzyme replacement therapy. *Eur J Pharm Biopharm* **70**: 58-65 (2008).

29. P. W. Lee, S. F. Peng, C. J. Su, F. L. Mi, H. L. Chen, M. C. Wei, H. J. Lin, and H. W. Sung. The use of biodegradable polymeric nanoparticles in combination with a low-pressure gene gun for transdermal DNA delivery. *Biomaterials* **29**: 742-51 (2008).

30. C. Nardin, D. Bolikal, and J. Kohn. Nontoxic block copolymer nanospheres: design and characterization. *Langmuir* **20**: 11721-5 (2004).

31. G. T. Warnerand G. L. Plosker. Clindamycin/benzoyl peroxide gel: a review of its use in the management of acne. *Am J Clin Dermatol* **3**: 349-60 (2002).

32. F. Ocakand I. Agabeyoglu. Development of a membrane-controlled transdermal therapeutic system containing isosorbide dinitrate. *Int J Pharm* **180**: 177-83 (1999).

33. N. A. Peppas, P. Bures, W. Leobandung, and H. Ichikawa. Hydrogels in pharmaceutical formulations. *Eur J Pharm Biopharm* **50**: 27-46 (2000).

34. R. Panchagnula, K. Stemmer, and W. A. Ritschel. Animal models for transdermal drug delivery. *Methods Find Exp Clin Pharmacol* **19**: 335-41 (1997).

35. F. Cilurzo, P. Minghetti, and C. Sinico. Newborn pig skin as model membrane in in vitro drug permeation studies: a technical note. *AAPS PharmSciTech* **8**: E94 (2007).

36. P. G. Shakespeare. The role of skin substitutes in the treatment of burn injuries. *Clin Dermatol* **23**: 413-8 (2005).

37. D. M. Suppand S. T. Boyce. Engineered skin substitutes: practices and potentials. *Clin Dermatol* **23**: 403-12 (2005).

38. S. MacNeil. Progress and opportunities for tissue-engineered skin. *Nature* **445**: 874-80 (2007).

39. T. Welss, D. A. Basketter, and K. R. Schroder. In vitro skin irritation: facts and future. State of the art review of mechanisms and models. *Toxicol In Vitro* **18**: 231-43 (2004).

40. M. Ponecand J. Kempenaar. Use of human skin recombinants as an in vitro model for testing the irritation potential of cutaneous irritants. *Skin Pharmacol* **8**: 49-59 (1995).

41. F. Netzlaff, M. Kaca, U. Bock, E. Haltner-Ukomadu, P. Meiers, C. M. Lehr, and U. F. Schaefer. Permeability of the reconstructed human epidermis model Episkin in comparison to various human skin preparations. *Eur J Pharm Biopharm* **66**: 127-34 (2007).

42. M. A. Perkins, R. Osborne, F. R. Rana, A. Ghassemi, and M. K. Robinson. Comparison of in vitro and in vivo human skin responses to consumer products and ingredients with a range of irritancy potential. *Toxicol Sci* **48**: 218-29 (1999).

43. OECD. Test Guideline 431: In vitro skin corrosion: human skin model test. *Adopted on 13th April 2004, Paris, France* (2004).

44. J. Vicanova, E. Boelsma, A. M. Mommaas, J. A. Kempenaar, B. Forslind, J. Pallon, T. Egelrud, H. K. Koerten, and M. Ponec. Normalization of epidermal calcium distribution profile in reconstructed human epidermis is related to improvement of terminal differentiation and stratum corneum barrier formation. *J Invest Dermatol* **111**: 97-106 (1998).

45. M. Ponec, S. Gibbs, G. Pilgram, E. Boelsma, H. Koerten, J. Bouwstra, and M. Mommaas. Barrier function in reconstructed epidermis and its resemblance to native human skin. *Skin Pharmacol Appl Skin Physiol* **14 Suppl 1**: 63-71 (2001).

46. S. D. Roy, J. Fujiki, and J. S. Fleitman. Permeabilities of alkyl p-aminobenzoates through living skin equivalent and cadaver skin. *J Pharm Sci* **82**: 1266-8 (1993).

47. F. P. Schmook, J. G. Meingassner, and A. Billich. Comparison of human skin or epidermis models with human and animal skin in in-vitro percutaneous absorption. *Int J Pharm* **215**: 51-6 (2001).

48. www.oecd.org.

49. H. Spielmannand M. Liebsch. Lessons learned from validation of in vitro toxicity test: from failure to acceptance into regulatory practice. *Toxicol In Vitro* **15**: 585-90 (2001).

50. http://rsbweb.nih.gov/ij/.

51. C. Allen, Maysinger, D., and Eisenberg, A. Nano-engineering block copolymer aggregates for drug delivery. *Colloids and Surfaces B: Biointerfaces* **16**: 3-27 (1999).

52. K. Yamato, Y. Takahashi, H. Akiyama, K. Tsuji, H. Onishi, and Y. Machida. Effect of penetration enhancers on transdermal delivery of propofol. *Biol Pharm Bull* **32**: 677-83 (2009).

53. R. Gannu, Y. V. Vishnu, V. Kishan, and Y. M. Rao. In vitro permeation of carvedilol through porcine skin: effect of vehicles and penetration enhancers. *PDA J Pharm Sci Technol* **62**: 256-63 (2008).

54. J. Liu, W. Hu, H. Chen, Q. Ni, H. Xu, and X. Yang. Isotretinoin-loaded solid lipid nanoparticles with skin targeting for topical delivery. *Int J Pharm* **328**: 191-5 (2007).

55. G. Cevc, A. Schatzlein, and H. Richardsen. Ultradeformable lipid vesicles can penetrate the skin and other semi-permeable barriers unfragmented. Evidence from double label CLSM experiments and direct size measurements. *Biochim Biophys Acta* **1564**: 21-30 (2002).

56. G. Cevc. Lipid vesicles and other colloids as drug carriers on the skin. *Adv Drug Deliv Rev* **56**: 675-711 (2004).

57. A. Schatzleinand G. Cevc. Non-uniform cellular packing of the stratum corneum and permeability barrier function of intact skin: a high-resolution confocal laser scanning microscopy study using highly deformable vesicles (Transfersomes). *Br J Dermatol* **138**: 583-92 (1998).

58. L. Sheihet, P. Chandra, P. Batheja, D. Devore, J. Kohn, and B. Michniak. Tyrosine-derived nanospheres for enhanced topical skin penetration. *Int J Pharm* **350**: 312-9 (2008).

59. M. Glavas-Dodov, K. Goracinova, K. Mladenovska, and E. Fredro-Kumbaradzi. Release profile of lidocaine HCl from topical liposomal gel formulation. *Int J Pharm* **242**: 381-4 (2002).

60. P. V. Popleand K. K. Singh. Development and evaluation of topical formulation containing solid lipid nanoparticles of vitamin A. *AAPS PharmSciTech* **7**: 91 (2006).

61. H. Chen, X. Chang, D. Du, J. Li, H. Xu, and X. Yang. Microemulsion-based hydrogel formulation of ibuprofen for topical delivery. *Int J Pharm* **315**: 52-8 (2006).

62. K. Walters, Brian, K. Dermatological Formulation and Transdermal Systems, in: Dermatological and Transdermal Formulations, Marcels Dekker, NY, Eds: Walters, K. (2002).

63. S. Ramachandran, S. Chen, and F. Etzler. Rheological characterization of hydroxypropylcellulose gels. *Drug Dev Ind Pharm* **25**: 153-61 (1999).

64. http://www.hill-top.com/services/safety/hill-top-chambers.php.

65. A. Banga. In vitro experimental technique for Iontophoresis research in the laboratory. *Electrically assisted transdermal and topical drug delivery, Taylor & Francis.* (1998).

66. S. T. Boyceand M. L. Williams. Lipid supplemented medium induces lamellar bodies and precursors of barrier lipids in cultured analogues of human skin. *J Invest Dermatol* **101**: 180-4 (1993).

67. M. Ponec, A. Weerheim, J. Kempenaar, A. Mulder, G. S. Gooris, J. Bouwstra, and A. M. Mommaas. The formation of competent barrier lipids in reconstructed human epidermis requires the presence of vitamin C. *J Invest Dermatol* **109**: 348-55 (1997).

68. S. Pasonen-Seppanen, T. M. Suhonen, M. Kirjavainen, E. Suihko, A. Urtti, M. Miettinen, M. Hyttinen, M. Tammi, and R. Tammi. Vitamin C enhances differentiation of a continuous keratinocyte cell line (REK) into epidermis with normal stratum corneum ultrastructure and functional permeability barrier. *Histochem Cell Biol* **116**: 287-97 (2001).

69. M. Rivier, I. Safonova, P. Lebrun, C. E. Griffiths, G. Ailhaud, and S. Michel. Differential expression of peroxisome proliferator-activated receptor

subtypes during the differentiation of human keratinocytes. *J Invest Dermatol* **111**: 1116-21 (1998).

70. M. Q. Man, E. H. Choi, M. Schmuth, D. Crumrine, Y. Uchida, P. M. Elias, W. M. Holleran, and K. R. Feingold. Basis for improved permeability barrier homeostasis induced by PPAR and LXR activators: liposensors stimulate lipid synthesis, lamellar body secretion, and post-secretory lipid processing. *J Invest Dermatol* **126**: 386-92 (2006).

71. H. R. Choi, S. K. Kim, S. B. Kwon, and K. C. Park. The fixation of living skin equivalents. *Appl Immunohistochem Mol Morphol* **14**: 122-5 (2006).

72. H. J. Stark, M. Baur, D. Breitkreutz, N. Mirancea, and N. E. Fusenig. Organotypic keratinocyte cocultures in defined medium with regular epidermal morphogenesis and differentiation. *J Invest Dermatol* **112**: 681-91 (1999).

73. A. M. Throm, W. C. Liu, C. H. Lock, and K. L. Billiar. Development of a cell-derived matrix: Effects of epidermal growth factor in chemically defined culture. *J Biomed Mater Res A* (2009).

74. K. L. Billiar, A. M. Throm, and M. T. Frey. Biaxial failure properties of planar living tissue equivalents. *J Biomed Mater Res A* **73**: 182-91 (2005).

75. E. Bell, S. Sher, B. Hull, C. Merrill, S. Rosen, A. Chamson, D. Asselineau, L. Dubertret, B. Coulomb, C. Lapiere, B. Nusgens, and Y. Neveux. The reconstitution of living skin. *J Invest Dermatol* **81**: 2s-10s (1983).

76. H. Hennings, D. Michael, C. Cheng, P. Steinert, K. Holbrook, and S. H. Yuspa. Calcium regulation of growth and differentiation of mouse epidermal cells in culture. *Cell* **19**: 245-54 (1980).

77. S. T. Boyceand R. G. Ham. Calcium-regulated differentiation of normal human epidermal keratinocytes in chemically defined clonal culture and serum-free serial culture. *J Invest Dermatol* **81**: 33s-40s (1983).

78. M. Manabeand W. M. O'Guin. Keratohyalin, trichohyalin and keratohyalin-trichohyalin hybrid granules: an overview. *J Dermatol* **19**: 749-55 (1992).

79. R. L. Eckert, M. B. Yaffe, J. F. Crish, S. Murthy, E. A. Rorke, and J. F. Welter. Involucrin--structure and role in envelope assembly. *J Invest Dermatol* **100**: 613-7 (1993).

80. R. H. Riceand H. Green. Presence in human epidermal cells of a soluble protein precursor of the cross-linked envelope: activation of the cross-linking by calcium ions. *Cell* **18**: 681-94 (1979).

81. S. Banks-Schlegeland H. Green. Involucrin synthesis and tissue assembly by keratinocytes in natural and cultured human epithelia. *J Cell Biol* **90**: 732-7 (1981).

82. E. Boelsma, S. Gibbs, C. Faller, and M. Ponec. Characterization and comparison of reconstructed skin models: morphological and immunohistochemical evaluation. *Acta Derm Venereol* **80**: 82-8 (2000).

83. S. Ekanayake-Mudiyanselage, H. Aschauer, F. P. Schmook, J. M. Jensen, J. G. Meingassner, and E. Proksch. Expression of epidermal keratins and the cornified envelope protein involucrin is influenced by permeability barrier disruption. *J Invest Dermatol* **111**: 517-23 (1998).

84. K. A. Bush, B. R. Downing, S. E. Walsh, and G. D. Pins. Conjugation of extracellular matrix proteins to basal lamina analogs enhances keratinocyte attachment. *J Biomed Mater Res A* **80**: 444-52 (2007).

85. N. Segal, F. Andriani, L. Pfeiffer, P. Kamath, N. Lin, K. Satyamurthy, C. Egles, and J. A. Garlick. The basement membrane microenvironment directs the normalization and survival of bioengineered human skin equivalents. *Matrix Biol* **27**: 163-70 (2008).

86. C. Asbill, N. Kim, A. El-Kattan, K. Creek, P. Wertz, and B. Michniak. Evaluation of a human bio-engineered skin equivalent for drug permeation studies. *Pharm Res* **17**: 1092-7 (2000).

87. M. Schafer-Korting, U. Bock, A. Gamer, A. Haberland, E. Haltner-Ukomadu, M. Kaca, H. Kamp, M. Kietzmann, H. C. Korting, H. U. Krachter, C. M. Lehr, M. Liebsch, A. Mehling, F. Netzlaff, F. Niedorf, M. K. Rubbelke, U. Schafer, E. Schmidt, S. Schreiber, K. R. Schroder, H. Spielmann, and A. Vuia. Reconstructed human epidermis for skin absorption testing: results of the German prevalidation study. *Altern Lab Anim* **34**: 283-94 (2006).

88. S. Schreiber, A. Mahmoud, A. Vuia, M. K. Rubbelke, E. Schmidt, M. Schaller, H. Kandarova, A. Haberland, U. F. Schafer, U. Bock, H. C. Korting, M. Liebsch, and M. Schafer-Korting. Reconstructed epidermis versus human and animal skin in skin absorption studies. *Toxicol In Vitro* **19**: 813-22 (2005).

89. T. Fredriksson. Studies on the Percutaneous Absorption of Parathion and Paraoxon. Vi. In Vivo Decomposition of Paraoxon During the Epidermal Passage. *J Invest Dermatol* **42**: 37-40 (1964).

90. W. G. Reifenrath, G. S. Hawkins, and M. S. Kurtz. Percutaneous penetration and skin retention of topically applied compounds: an in vitro-in vivo study. *J Pharm Sci* **80**: 526-32 (1991).

91. K. Hanley, L. G. Komuves, N. M. Bass, S. S. He, Y. Jiang, D. Crumrine, R. Appel, M. Friedman, J. Bettencourt, K. Min, P. M. Elias, M. L. Williams, and K. R. Feingold. Fetal epidermal differentiation and barrier development In vivo is accelerated by nuclear hormone receptor activators. *J Invest Dermatol* **113**: 788-95 (1999).

92. L. G. Komuves, K. Hanley, M. Q. Man, P. M. Elias, M. L. Williams, and K. R. Feingold. Keratinocyte differentiation in hyperproliferative epidermis: topical application of PPARalpha activators restores tissue homeostasis. *J Invest Dermatol* **115**: 361-7 (2000).

93. S. Wright. Essential fatty acids and the skin. *Br J Dermatol* **125**: 503-15 (1991).

94. P. M. Elias, B. E. Brown, and V. A. Ziboh. The permeability barrier in essential fatty acid deficiency: evidence for a direct role for linoleic acid in barrier function. *J Invest Dermatol* **74**: 230-3 (1980).

95. Y. Uchida, M. Behne, D. Quiec, P. M. Elias, and W. M. Holleran. Vitamin C stimulates sphingolipid production and markers of barrier formation in submerged human keratinocyte cultures. *J Invest Dermatol* **117**: 1307-13 (2001).

96. C. Lotte, C. Patouillet, M. Zanini, A. Messager, and R. Roguet. Permeation and skin absorption: reproducibility of various industrial reconstructed human skin models. *Skin Pharmacol Appl Skin Physiol* **15 Suppl 1**: 18-30 (2002).

97. P. A. Jones, A. V. King, L. K. Earl, and R. S. Lawrence. An assessment of the phototoxic hazard of a personal product ingredient using in vitro assays. *Toxicol In Vitro* **17**: 471-80 (2003).

98. P. Portes, M. J. Pygmalion, E. Popovic, M. Cottin, and M. Mariani. Use of human reconstituted epidermis Episkin for assessment of weak phototoxic potential of chemical compounds. *Photodermatol Photoimmunol Photomed* **18**: 96-102 (2002).

99. M. Schafer-Korting, U. Bock, W. Diembeck, H. J. Dusing, A. Gamer, E. Haltner-Ukomadu, C. Hoffmann, M. Kaca, H. Kamp, S. Kersen, M. Kietzmann, H. C. Korting, H. U. Krachter, C. M. Lehr, M. Liebsch, A. Mehling, C. Muller-Goymann, F. Netzlaff, F. Niedorf, M. K. Rubbelke, U. Schafer, E. Schmidt, S. Schreiber, H. Spielmann, A. Vuia, and M. Weimer. The use of reconstructed human epidermis for skin absorption testing: Results of the validation study. *Altern Lab Anim* **36**: 161-87 (2008).

100. F. Dreher, F. Fouchard, C. Patouillet, M. Andrian, J. T. Simonnet, and F. Benech-Kieffer. Comparison of cutaneous bioavailability of cosmetic preparations containing caffeine or alpha-tocopherol applied on human skin models or human skin ex vivo at finite doses. *Skin Pharmacol Appl Skin Physiol* **15 Suppl 1**: 40-58 (2002).

101. D. A. Godwin, B. B. Michniak, and K. E. Creek. Evaluation of transdermal penetration enhancers using a novel skin alternative. *J Pharm Sci* **86**: 1001-5 (1997).

102. D. Braue E.B., B.F., Lumpkin, H.L., Hanssen, K.A., Stevenson, R.S., Deckert, R.R., Graham, J.S. Military perspectives in chemical penetration retardation, in: Percutaneous Penetration enhancers, Second edition, Editors: Smith, E.W. and Maibach, H.I. (2006).

103. R. Alvarez-Roman, A. Naik, Y. N. Kalia, R. H. Guy, and H. Fessi. Skin penetration and distribution of polymeric nanoparticles. *J Control Release* **99**: 53-62 (2004).

104. F. Rancan, D. Papakostas, S. Hadam, S. Hackbarth, T. Delair, C. Primard, B. Verrier, W. Sterry, U. Blume-Peytavi, and A. Vogt. Investigation of polylactic acid (PLA) nanoparticles as drug delivery systems for local dermatotherapy. *Pharm Res* **26**: 2027-36 (2009).

105. J. A. Bouwstra, G. S. Gooris, A. Weerheim, J. Kempenaar, and M. Ponec. Characterization of stratum corneum structure in reconstructed epidermis by X-ray diffraction. *J Lipid Res* **36**: 496-504 (1995).

106. P. Batheja, Y. Song, P. Wertz, and B. Michniak-Kohn. Effects of Growth Conditions on the Barrier Properties of a Human Skin Equivalent. *Pharm Res* (2009).

107. http://ww2.coastal.edu/kingw/psyc450/skin/skin.html. (last accessed: 2/23/2009).

108. www.eucerin.no.

109. www.permegear.com.

110. www.pracs.com.

111. H. Chen, D. Mou, D. Du, X. Chang, D. Zhu, J. Liu, H. Xu, and X. Yang. Hydrogel-thickened microemulsion for topical administration of drug molecule at an extremely low concentration. *Int J Pharm* **341**: 78-84 (2007).

112. J. Kim, Song, J., Lee, E., Park, S. Rheological properties and microstructures of Carbopol gel network system. *Colloids and Polymer Science* **281**: 614–623 (2003).

113. http://www.ib.amwaw.edu.pl/invittox/prot/78.htm.

114. www.3t3nru.mbresearchlabs.com/background.htm.

115. www.mbresearch.com/epiderm.htm.

116. http://www.herc.com/aqualon/personal_care/pc_prod_data/pc_primaflo.html.

117. A. Hosmani. Carbopol and its Pharmaceutical Significance: A Review. *Pharmainfo.net* **4**: (2006).

118. http://www.chemyq.com.

119. http://dailymed.nlm.nih.gov/.

14 Appendix

Skin penetration effects of a lamellar delivery system

Published as*:* Oleic acid induced skin penetration effects of a lamellar delivery system

Dayan, N., **Batheja, P**. and Michniak, B.

Cosmetics and Toiletries, 2007, 122 (9), pp: 73-82

Introduction

Skin serves as a tough barrier to penetration of compounds owing to the rigid 'brick and mortar' structure of the stratum corneum (SC). In the SC, dead corneocytes are cemented by intercellular lipids that have a unique composition of long chain ceramides, free fatty acids and cholesterol. These lipids are organized in the form of lamellar structures, existing mostly in their gel crystalline phase and parallel to the SC surface. The chemical composition and the lamellar nature of these lipids restrict the passage of most agents, making skin delivery difficult. Modulation of this rigid barrier will require perturbation or manipulation of these lipids without causing significant toxicity. To this effect, a unique delivery system was developed by Lipo Chemicals, Inc. (Paterson, NJ). This skin delivery system consists of a mixture of phospholipids, oleic acid, oil and water. The components of this system possess the capability to alter the structure and the

thermodynamic properties of the skin's lipid barrier, thereby enhancing skin delivery.

The physical properties and thermodynamic activity of the combination of soy lecithin, oleic acid, oil and water leads to their existence as fluid and flexible structures. TEM images of this delivery system at different ratios of their components show the presence of three different structures: intact vesicles, ruptured vesicles with non-uniform unilamellar membranes and lamellar sheets. While each formulation shows pre-dominance of one type of vesicle, all three systems exist in each formulation in different amounts. The formulation with 0% oleic acid shows the presence of droplets (like an emulsion) and increase in the oleic acid content increases the formation of lamellar-like structures (Figure 1). The phase change of the systems was confirmed by Differential Scanning Colorimetry (DSC) analysis, where a decrease in the Tm value of the formulation was observed with an elevation in oleic acid concentration.

The authors postulated that these lamellar delivery systems, due to their lipid-like composition and their dynamic nature, could fuse with the skin's barrier lipids and fluidize them, consequently delivering the enclosed agents to skin's layers. The action of fusion with the skin lipids has thought to be the primary skin delivery mechanism of many lipid based carriers, such as liposomes and ethosomes. In order to investigate the skin delivery capabilities of these systems, we incorporated a trace amount of radiolabeled oleic acid as a marker in these

formulations. The *in vitro* human skin deposition and penetration of this marker from the delivery systems after topical application was studied by tape stripping the skin layers and evaluating the amount of marker present in these layers.

Methods

Formulation preparation

Four formulations containing 0, 5, 10 and 15% oleic acid along with soy lecithin, oil and water were prepared at Lipo Chemicals Inc., Paterson, NJ. Samples were prepared by cold mixing soy lecithin (ALC, Oxford, CT), oleic acid (Cognis, Cincinnati, OH), and natural oils, such as Jojoba or Rice Bran oils (Lipo Chemicals, Paterson, NJ). This oil phase was then mixed with water in various ratios. The oil concentrations ranged between 15% to 20% w/w, and the soy lecithin from 10% to 20% w/w. 2 µl of tritiated oleic acid [9,10 (n) – 3H] with a specific activity of 60 Ci/mmol (MP Biomedicals, Irvine, CA) was added to the 20 grams of each formulation and mixed to achieve a uniform dispersion. When incorporated in such relative trace amounts, oleic acid was predicted to have no effect on the physical properties of the formulations.

Skin permeation

Skin permeation experiments were carried out on vertical Franz diffusion cells (Permegear, Inc., Bethlehem, PA) with a receptor volume of 5.1 ml and penetration surface area of 0.64 cm^2. The receptor chamber of the Franz

diffusion cell was filled with isotonic phosphate buffer (pH=7.4) containing 10% ethanol and was continuously stirred at 600 rpm. Samples of human cadaver skin (AlloSource, Englewood, CO) were mounted on top of the receptor chambers and clamped between the donor and the receptor, and the diffusion cells were maintained at 37℃ in order to achieve skin temperature of 32± 0.5℃. The skin was allowed to pre-hydrate for 1 hour, after which approximately 0.15 g accurately weighed quantity of each formulation (n=5) was added to the donor compartment with the aid of a glass rod. The donor compartments and the sampling ports were covered tightly with Parafilm® and receptor samples (300µl) were withdrawn every hour for up to 8 hours. The withdrawn volume was replaced by an equivalent amount of fresh receptor solution. After 8 hours, the skin was removed from the cells; the excess formulation was removed and added to the donor washings. The surface of the skin was washed with phosphate buffer (pH 7.4) and the skin pieces were labeled and stored at -80℃ for tape stripping. Ethanol (3ml) was used to collect the donor washings.

Tape stripping

Each piece of skin was weighed before tape stripping. Approximately one square inch pieces of Scotch Tape (810 Magic Tape™, 3M, St. Paul, MN) were cut and weighed. The tape was then pressed onto the skin with a constant weight, removed and weighed again. Each piece of skin was tape-stripped in a similar manner 7 times and the weights of the pieces of tape before and after stripping were recorded. Each tape stripped skin was then placed in a

scintillation vial. The remaining tissue (epidermis and dermis) was digested in 2 ml of 0.3 M NaOH for 12 hours at 80℃.

Detection of the radioactive marker in skin layers

Approximately 0.15g (accurate weights recorded) of the radioactive formulations were weighed and 10 ml of scintillation cocktail (Ecolite™, MP Biomedicals, Irvine, CA) was added to each. The radioactive counts obtained from these samples, in disintegrations per minute (dpm), were used to normalize the counts of radioactive formulations added to the donor compartments. Scintillation cocktail was added to all receptor samples, the tape strips, the digested epidermis and dermis and the donor washings. All samples were read in a scintillation counter (Tricarb 2750 TR/LL, Packard), and the radioactive counts in each sample were determined in terms of dpm. The radioactive counts (dpm) obtained from the receptor solutions, tape stripped skin, dermis and donor washings, were normalized to the counts (dpm) obtained from the formulations added to the donor compartments. These normalized counts were translated to the percentage of the radioactive marker retained in the stratum corneum and other skin layers.

Results and discussion

Tape stripping is a method widely used to examine the localization and distribution of substances within layers of the stratum corneum. Repeated

application of adhesive tapes with a constant and validated pressure sequentially removes layers of the SC which can be analyzed for content of the applied agent. We used tape stripping to evaluate the skin deposition of the added radioactive marker (tritiated oleic acid) from various delivery systems. Figure 2 shows that the weight of skin (corresponding to the corneocytes removed) and the amount of radioactive marker decreased progressively with increasing tape strips. This shows that the presence of the marker was higher in the top layers of the SC and decreased with deeper layers. This may have also occurred because larger amount of SC layers are detached in the first few tape strips, a phenomenon observed in most tape strip experiments.[1] Figures 3, 4 and 5 demonstrate the penetration and deposition of the radiolabeled oleic acid in different layers of the skin. The presence of the amount of marker in various skin layers is indicative of its delivery from the four different systems. The formulation containing 15% oleic acid showed significantly higher deposition in the SC as compared to the other three systems. A different behavior was observed when the target of interest was the live epidermis and the dermis, where the 5% oleic acid system created the highest deposition. Analysis of the amount of product that remained on the skin surface and in the donor shows that the systems containing oleic acid allow for significantly better penetration of the marker when compared with the control. Thus, the control formulation with 0% oleic acid showed the highest retention of the marker on the skin surface (Figure 5).

Oleic acid is an unsaturated fatty acid and has been shown to act as a skin penetration enhancer. At high levels (10 -15%), oleic acid can induce dramatic changes to the lamellar lipid structures and increase their fluidity. Thus the presence of oleic acid at these levels in the delivery system would serve to fluidize the SC intercellular lipids after the fusion of the lamellar systems in the applied formulation with those in the SC. This action may be responsible for enhancement of delivery of the marker and the higher skin deposition. The fluidization effects of oleic acid on the lipids are postulated to be a result of the double bond and the chain length of its molecular structure. While the chain length helps in the intercalation of oleic acid between the tightly packed lipid chains in the SC, the cis-double bond produces a further 'kink' in the lipid chains, both effects leading to lipid structure disruption.

Conclusion

The combination of oleic acid, phospholipids, oil and water in different ratios produced systems with different physical structures and thermodynamic properties. Although the exact transition point was not identified, increase in the amount of oleic acid from 0 to 15% led to formation of varying lipid structures in these systems. Although one structure existed pre-dominantly in a system, all structures co-existed in all three systems with oleic acid. While the formulation with no oleic acid showed typical o/w emulsion structure, adding oleic acid produced "flexible" structures ranging from vesicles at 5% oleic acid to lamellar sheets at 15% oleic acid. The composition changes in the formulations resulted

in different actions on the skin lipids and thereby different penetration profiles, assessed by the deposition of the radiolabeled compound with which it was marked. The system containing predominantly lamellar sheets targeted the marker to the stratum corneum, while the soft vesicles allowed for further penetration and deposition in the live epidermis and dermis. Thus, varying the formulation composition of these formulations can produce delivery systems for targeting different skin layers for specific diseases or for administration of personal care agents.

Note: *The authors would like to thank Dr. Nava Dayan and Lipo Chemicals Inc. (Paterson, NJ) for providing us with the opportunity and funding to contribute to this project.*

References

1. Escobar-Chavez, J. et al. The tape-stripping technique as a method for drug quantification in skin, J Pharm Pharm Sci, 2008, 11(1): pp: 104-30

Figures for Appendix

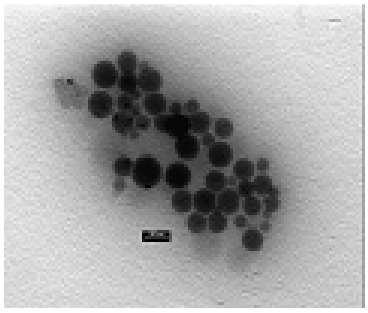

(A) 5% oleic acid
(Intact Vesicles)

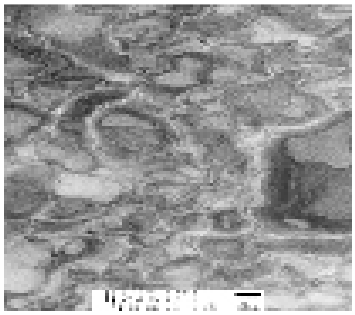

(B) 10% oleic acid
(Ruptured vesicles with non-uniform lamellar structures)

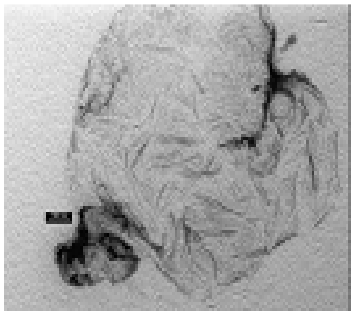

(C) 15% oleic acid
(Lamellar sheets)

Figure 1: TEM images obtained after negative staining of delivery systems with varying compositions of oleic acid.

Images were obtained courtesy of Dr. Nava Dayan, at Lipo Chemicals Inc., Paterson, NJ.

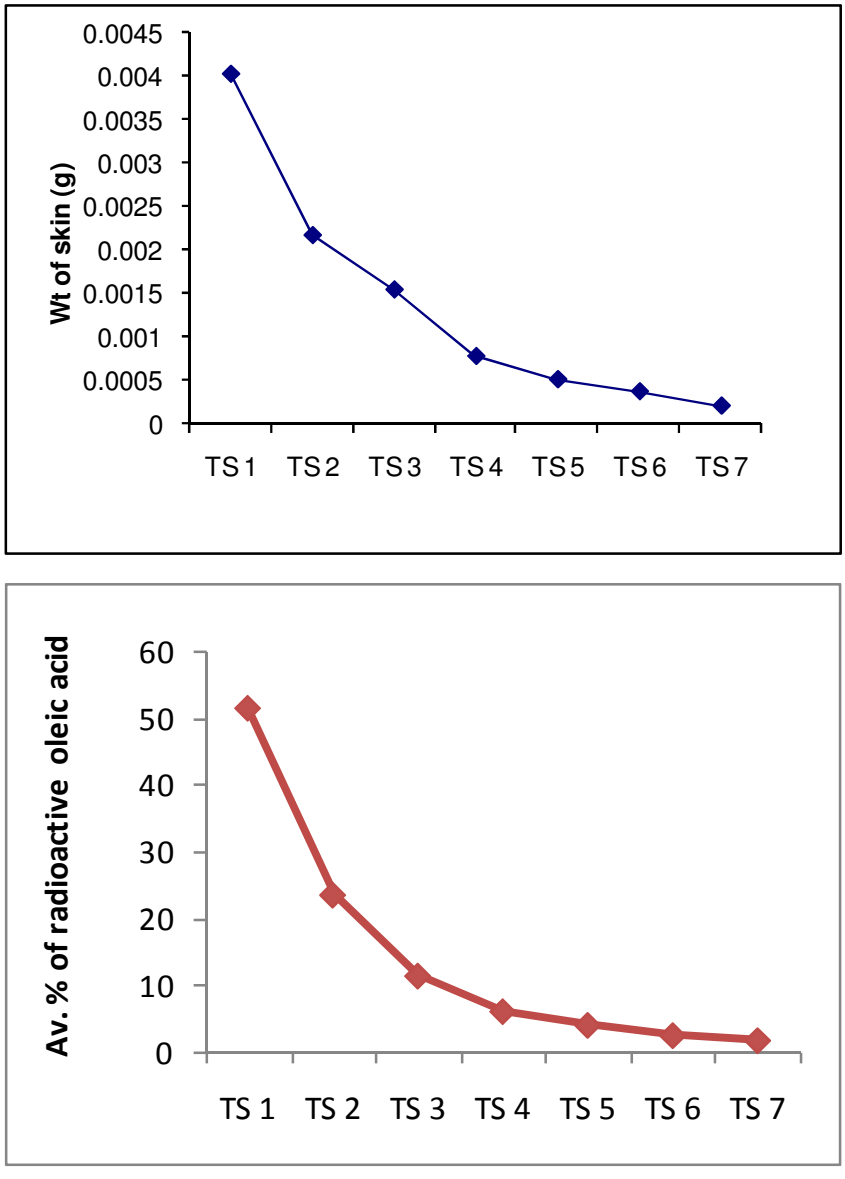

Figure 2: Weight of skin (A) and the % of radioactive oleic acid (B) obtained in each of seven tape strips obtained after tape stripping human skin treated with a lamellar delivery vehicle.

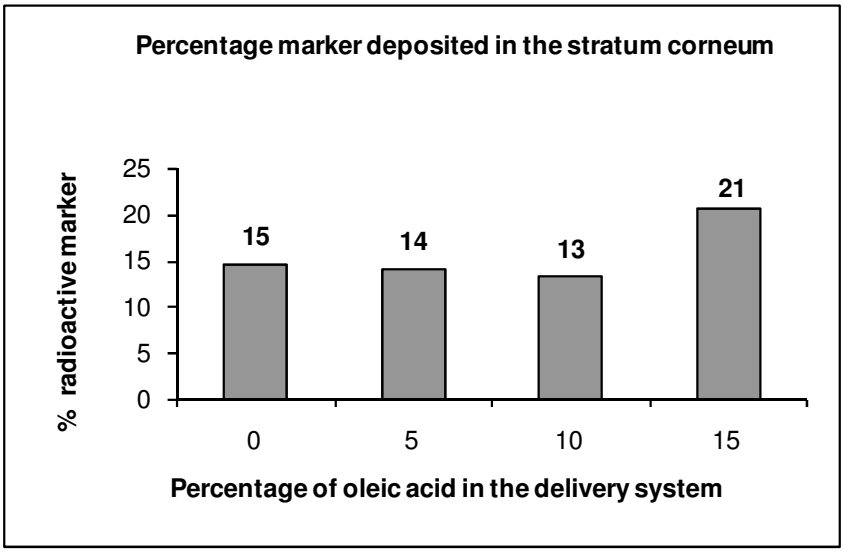

Figure 3: Percentage of radioactive oleic acid deposited in the stratum corneum from four delivery systems after 8 h application.

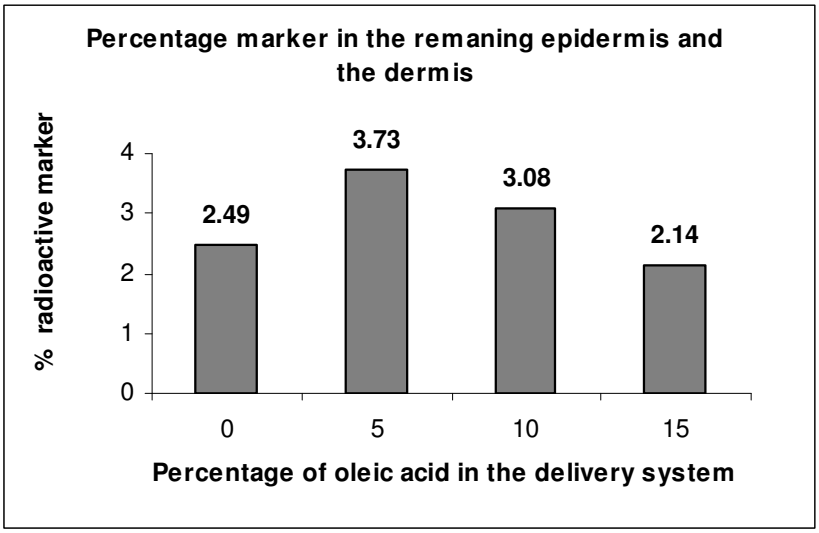

Figure 4: Percentage of radioactive oleic acid deposited in the epidermis and the dermis from four delivery systems after 8 h application.

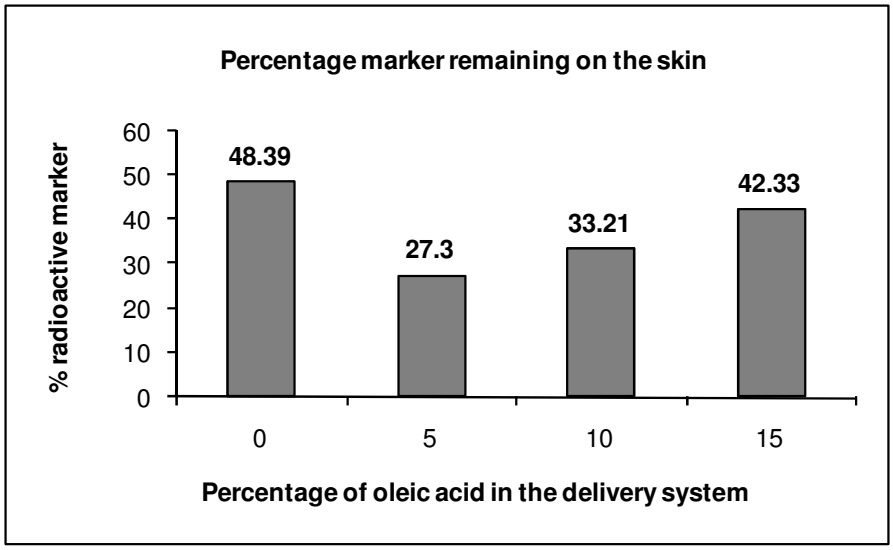

Figure 5: Percentage of radioactive oleic acid remaining on the skin surface from four delivery systems after 8 h application.

15 Curriculum Vita

Priya Batheja

EDUCATION

- Ph.D in Pharmaceutical Sciences: Rutgers -The State University of New Jersey, New Jersey (January 2010).
- Masters in Business Administration (MBA): K.J. Somaiya Institute of Management Studies and Research, University of Mumbai, India (May 2000).
- Bachelor of Pharmacy (B. Pharm): Principal K. M. Kundnani College of Pharmacy, University of Mumbai, India (May 1997).

PROFESSIONAL EXPERIENCE

- (Laboratory for Drug Delivery), Rutgers-The State University of New Jersey (September 2004 – present): Research Assistant
- Novartis Pharmaceuticals Corporation (May 2009 - August 2009): Intern - Pharmaceutical development
- GlaxoSmithKline Pharmaceuticals India Ltd., Mumbai, India (June 2000 - April 2002): Assistant Manager
- Nicholas Piramal India Ltd. (August 1997 - March 1998): R & D executive

PUBLICATIONS

1. **Batheja P**., Polymeric nanospheres for skin penetration enhancement: *in vitro* and *in vivo* assessment in skin models, Doctoral Dissertation
2. **Batheja, P.,** Sheihet, L., Saloman, S., Kohn, J. and Michniak, B. Formulation development of Polymeric Nanospheres for Enhanced Skin Delivery, *to be submitted in January 2010*

3. **Batheja, P.**, Song, Y. Wertz, P. and Michniak, B., Effects of growth conditions on the barrier properties of a human skin equivalent, *Pharm Res,* 2009; 26(7), p: 689-700.
4. Sheihet, L., Chandra, P., **Batheja, P.**, Devore, D., Kohn, J., Michniak, B., Tyrosine-derived nanospheres for enhanced topical skin penetration, *Int J Pharm*, 2008; 350 (1-2), p: 312-319.
5. Dayan, N., **Batheja, P.**, Michniak, B., Oleic acid-induced skin penetration effects of a lamellar drug delivery system, *Cosmetics and Toiletries*, 2007; 122 (9), p: 73-82.
6. Hu, L., **Batheja**, **P**., Meidan, V. and Michniak, B., Iontophoretic Transdermal Drug Delivery, in the book titled *'Handbook of Non-Invasive Drug Delivery Systems',* Elsevier Inc., to be published in January 2010.
7. Kaushik, D., **Batheja, P.**, Kilfolyle, B., Rai, V., Michniak, B., Percutaneous permeation modifiers: enhancement versus retardation, *Expert Opin Drug Deliv*, 2008; 5 (5), p: 517-529.
8. **Batheja, P.**, Thakur, R., Michniak, B., Basic Biopharmaceutics of Buccal and Sublingual Absorption, in the book titled "Enhancement in Drug Delivery" 2007; Touitou, E. and Barry, B. (Eds.) CRC Press.
9. **Batheja, P.**, Thakur, R., Michniak, B., Transdermal iontophoresis, *Expert Opin Drug Deliv*, 2006; (1), p: 127- 138.
10. Thakur, R., **Batheja, P.**, Kaushik, D., Michniak, B., Structural and Biochemical Changes in Aging Skin and their Implications on Skin Permeability Barrier, in: *Skin Aging Handbook*: An Integrated Approach to Biochemistry and Product Development, Nava Dayan (Ed.), William Andrew Publishing, 2008.
11. **Batheja, P.**, Kaushik, D., Hu, L., and Michniak, B., Transdermal Iontophoresis, *Drug Delivery,* 2007; touch briefings.
12. **Batheja, P.**, Kydonieus, A., Michniak, B., "Transdermal Patent Watch" in the *Controlled Release Society (CRS) newsletters* (CRS Vol 22-No 2-2005, CRS Vol 22 No. 3-2005, CRS Vol 23-No 2-2006).
13. **Batheja, P.**, Song, Y., Michniak, B., A bioengineered Human Skin Equivalent (HSE) for the evaluation of protectants**,** *25th Army Science Conference proceedings*, 2006.